Investigation of the Effects of IGF-1 Slow Release on Human Neuromuscular Junctions Formation and Functions

I KARIM

PhD 2020

Investigation of the Effects of IGF-1 Slow Release on Human Neuromuscular Junctions Formation and Functions

Ikbal Karim

A thesis submitted in partial fulfilment of the requirements of the Manchester Metropolitan University for the degree of Doctor of Philosophy

School of Healthcare Science
Faculty of Science and Engineering
Manchester Metropolitan University

2020

Table of Contents

Acknowledgements

Firstly, I would like to thank my director of studies Dr Nasser Al-Shanti for the opportunity to further my academic career and to express how incredibly grateful I am for all the insightful support and guidance he has given me throughout this project. Working together has been an extraordinary experience and it is one I will treasure.

I would like to thank my supervisors Dr Debra Whitehead and Dr Michele Edge for their help in the beginning of this project and also I would like to thank all the technicians and colleagues in both the Chemistry and Biology departments that helped me in the lab during my project.

Most importantly, thank you to my father (Kadum Karim), mother (Jalila Hassan) and sister (Mariam Karim) for their unconditional love and continuous support.

Special thanks to my wonderful children, Saleh Albaghdady and Shahad Albaghdady for their incredible patience and for inspiring me to strive for excellence in all aspects of my life. I would not have been able to do this without their love and support.

List of abbreviations

α-BTX	α-bungarotoxin
αFF	fast-twitch fatigable motor neurons
αFR	fast-twitch fatigue-resistant motor neurons
αMN(s)	alpha motor neuron(s)
αS	slow-twitch fatigue resistant motor neurons
β-III-tubulin	class III β-tubulin
βMN(s)	beta motor neuron(s)
γMN(s)	gamma motor neuron(s)
AP(s)	action potential(s)
ACh	acetylcholine
AChR(s)	acetylcholine receptor(s)
ADP	adenosine diphosphate
ALS	amyotrophic lateral sclerosis
AR	aspect ratio
ATM	37°C with a 5% CO2 atmosphere
ATP	adenosine triphosphate
BDNF	brain-derived neurotrophic factor
bHLH	basic helix–loop–helix
C25	25-year-old immortalised human myoblasts
Ca2+	calcium ions
CF	contraction frequency
ChAT	choline acetyltransferase
CMS	congenital myasthenic syndrome
CNS	central nervous system
DAPI	4′,6-Diamidine-2′-phenylindole dihydrochloride
DHPR	dihydropyridine receptor
DM	differentiation media
DMEM	Dulbecco's modified eagle medium
DMSO	Dimethyl sulfoxide
DPBS	Dulbecco's phosphate buffered saline 1X
DRG(s)	dorsal root ganglion(s)
DS	donkey serum

ECM	extracellular matrix
ED	embryonic development day
EGF(s)	epidermal growth factor(s)
EPP	endplate potential
FBS	fetal bovine serum
FGF-7	fibroblast growth factor 7
FGF(s)	fibroblast growth factor(s)
FGFb	basic fibroblast growth factor
FI	fusion index
GDNF	glial-cell-line-derived neurotrophic factor
GFAP	glial fibrillary acidic protein
GM	complete growth media
GS	goat serum
HBSS	Hanks' balanced salt solution
hESC(s)	human embryonic stem cell(s)
HGF(s)	Hepatocyte growth factor(s)
hiPSC(s)	human induced pluripotent stem cell(s)
HMC(s)	hypaxial motor column(s)
HS	horse serum
ICC	immunocytochemistry
IGF-1	insulin-like growth factor 1
IGFBP(s)	insulin-like growth factor-binding protein(s)
IP	inorganic phosphate
LEMS	Lambert-Eaton myasthenic syndrome
L-Glut	L-glutamic acid
MSNP	Mesoporous Silica Nanoparticles
MA	myotube area
MEP(s)	motor endplate(s)
MMC(s)	medial motor column(s)
MN(s)	motor neuron(s)
MNT(s)	motor neuron terminal(s)
MHC	myosin heavy chain
MRF4	myogenic regulatory factor 4
MRF(s)	myogenic regulatory factor(s)

MuSK	muscle-specific tyrosine kinase
Myf5	myogenic factor 5
NPs	Nanoparticles
Na+	sodium ions
ND	neurodegenerative
NFH	neurofilament heavy
NGF	nerve growth factor
NM	neuromuscular
NMJ(s)	neuromuscular junction(s)
Pax3	paired box protein 3
Pax7	paired box protein 7
Pen/Strep	penicillin-streptomycin
PGC	preganglionic column
PlGF	placental growth factor
PMC	phrenic motor column
PWB	Prem/Wash buffer
Rapsyn	43 kDa receptor-associated protein of the synapse
RyR	ryanodine receptor
SC(s)	satellite cell(s)
± SD	plus/minus standard deviation
SkM	skeletal muscle
SkMC(s)	skeletal muscle cell(s)
SMN1	survival motor neuron 1
SMN2	survival motor neuron 2
SOD1	superoxide dismutase 1
SR	sarcoplasmic reticulum
Sty1	synaptotagmin 1
TGFβ	transforming growth factor beta
TX100	Triton X-100
VAChT	vesicular acetylcholine transporter
VEGF	vascular endothelial growth factor

List of Figures

List of Tables

Abstract

Insulin-like growth factor 1 (IGF-1) plays central roles in neuromuscular junction (NMJ) development, skeletal muscle and motor neurons growth. The NMJ is the interface between the nerve and muscle fibre, and thus they may receive (patho) physiological input from both the muscle and the motor neuron. Several conditions including ageing, disuse, neurodegenerative diseases, diabetes, and cancer are associated with NMJ dysfunctions which lead to profound muscle wasting and impaired NMJ function. Recent attention has focused on the use of anabolic growth factors such as IGF-1 in preventing muscle atrophy associated with NMJ dysfunction, however, difficulties in isolating and extracting functional NMJs, low bioavailability and potential side effects such as hypoglycaemia appear to limit the usefulness of IGF-1 for clinical treatment of muscle wasting conditions linked with NMJs degeneration. Therefore, there is a need for a simplified and reproducible system of engineered *in vitro* NMJs to facilitate the investigation of sustained slow release of IGF-1 on NMJs function. The aim of this thesis was to fabricate mesoporous silica nanoparticles (MSNPs) loaded with IGF-1 to manipulate the function of NMJ using physiologically relevant human *in vitro* NMJ model. MSNPs were generated using the Stöber method and fully characterised using different techniques (dynamic light scattering, scanning electron microscopy, powder X-ray diffraction and nitrogen adsorption) and then loaded with IGF-1. Human *in vitro* co-culture model of NMJ was engineered using human immortalised myoblast and human embryonic stem cells (hESCs)-derived neural progenitor cells (NPCs). In the co-culture, myoblasts differentiated into aligned myotubes and NPCs differentiated spontaneously into cholinergic motor neurons sprouted axons that branched to form multiple NMJ innervation sites along myotubes, which showed extensive spontaneous contractile activity. The NMJ model was characterised using pre- and postsynaptic markers and functional assessment was verified using agonist and antagonist to NMJ. Finally, the NMJ platform was treated with IGF-1 loaded MSNPs for 7 days. The data showed that the slow IGF-1 release enhanced the formation and the functions of NMJs significantly compared with exogenous IGF-1. Furthermore, the slow release of IGF-1 enhanced the bi-directional communications between motor neurons and muscle cells through the elevation of endogenously secreted essential neural growth factors providing regenerative niche for NMJ formation and function. The outcome of this project may provide a breakthrough approach to enable research in designing new therapeutic treatments using IGF-1 for muscle wasting linked with NMJ deterioration.

Chapter 1: Introduction

1.1 Skeletal muscle

The body mass of a healthy adult constitutes of between 40% and 50% skeletal muscle. This muscle is extremely metabolic in nature and is important for the stability and movement of the body. The muscle provides storage for around 80% of glycogen found in the body; making it an important reservoir for protein. This is in addition to being a primary provider of the requirements of metabolism and in the process, making a contribution to thermoregulation (Yin et al., 2013). According to Pedersen and Toft (2000), skeletal muscle responds strongly to stimuli, a good example is the way it responds to a workout or inactivity, which could lead to synthesis or degradation, respectively. Muscle contraction increases the risk of injury or muscle tissue damage due to its mechanical forces and its anatomical superficial location; furthermore, the danger of muscle tissue damage increases over periods of deconditioning associated with disease and in elderly people, with reduced regenerative ability (Price et al., 2015).

In contemporary times, the muscle wasting is a current public health problem, originating from numerous life threatening disorders like heart disease and cancer cachexia. Ageing is linked to decreased muscle mass; individuals aged between 40 and 70 years lose 10 to 25% of their body mass and the elderly over 80 years lose 40% of their mass (McPhee et al., 2013). It is estimated that after the age of 50, healthy persons lose around 1% of their skeletal muscle mass per annum (Marzetti et al., 2010). Added to the comparatively slow advanced degeneration arising due to natural ageing, a varied range of chronic diseases that are seen in elderly people regularly result in secondary muscle wasting, which happens at a moderately rapid level (Aoyagi et al., 2015). This results in the dysfunction of the muscle, which can be seen through the typical process of ageing, referred to as sarcopenia (Dodds et al., 2015). It is for this reason why it is important to discover the reasons behind muscle wasting with the aim of determining what could be done to mitigate the challenge so that people could maintain a healthy muscle mass through ageing and disease.

Discoveries from recent studies suggest that as people age, the ability for their systems to restore skeletal muscle becomes reduced. The moderated capability of muscle reparation and revival with ageing is caused by drop in skeletal muscle stem cells (satellite cells), a definite population of muscle precursor cells. Equally, in ageing, there is a noticeable failure in immune function. For example, in the case of an injury, immune cells donate to the local situation that can impact on the reformative procedure of skeletal muscle cells. Muscle injury is supplemented by the encouragement of precursor satellite cells by the infiltration of immune cells, which in turn discharge cytokines that affect muscle

restoration and regeneration (Tidball, 2005). This is the reason why a reduced capacity among older people is linked to a reduction in immune reaction (Dumke & Lees, 2011).

Human and animals depend on skeletal muscle to do almost everything. It is common for people to take everyday tasks such as dressing, getting up from bed, chewing food, and managing personal hygiene for granted. However, a close analysis shows that it is these seemingly easy exercises that necessitate institutional care for many people. Even though there are certain cases where a precise reason behind weakness can be identified, like a neurological disease, one of the factors that are inevitable is the process of ageing. Hence, it is with old age that the biggest loss of ability to do things is observed (Mitchell et al., 2012; Moore, 1965). This leads to a loss of independence for around 25 percent of people over the age of 90 in the UK; often sending them to nursing, residential, or hospital care (Bajekal et al., 2006; Office of Fair Trading, 2005). Mitchell et al. (2012) report that a compromised muscle function has been observed to be a way that can be used for predicting whether an individual ends up with a disability or hospitalization.

Muscle wasting is characterised by a slowing down of rehabilitation after a person has been immobilised due to fractures or undergoing surgery. When mobilising the elderly is delayed after surgery, the result could be a rapid loss of muscle. This could eventually degenerate into a spiral leading to pneumonia which can end in death. According to Argiles et al (2003), muscle wasting can accompany a number of other diseases such as cancer cachexia, arthritis, diabetes, and cardiovascular disease. Lynch et al (2007) note that the problem of muscle wasting is usually associated with ageing and loss of the ability to function independently. This could lead to a reduced quality of life especially when one considers the statistics made available by the Office of National Statistics (Office for National Statistics) which reports that in the last 30 years, there has been an increase of 3 percent in the proportion of people above the age of 65 and this is estimated to increase by another 7 percent by 2031.

The decline of the neuromuscular system, linked to age, has been identified as the basis of the loss of independence among the elderly that results from a weakening in physical performance (Baumgartner et al., 1999). Several studies, especially within the last ten years, have placed their attention on causal factors for impairment in old age.

1.1.0 The structure of the skeletal muscle

According to Yin et al. (2013), skeletal muscle (SkM) is responsible for around half of the total mass of a healthy human being. The same author notes that there could be around 650 designated muscles in the human body; making it the biggest metabolically active muscle in the body of a human being. SkM is different from the other main types of muscle (smooth and cardiac) in that its regulation happens through the somatic nervous system. This is the reason why its function can be managed by humans. This is a view also noted by Biswal et al. (1995) who report that the processes of Preparation, regulation, and implementation of voluntary locomotion of the body is regulated in the motor cortex region of the brain. The motor neurons of the upper side deliver information from the brain's motor cortex via the spinal cord to the lower motor neurons. Notwithstanding the fact that the main job of the SkM is to facilitate movement, another vital job done by SKM is the regulation of metabolism through the macronutrient storage, with substrate oxidation replenishing the adenosine triphosphate stores (ATP) (Leto & Saltiel, 2012) which keep depleting. Added to this, Pedersen and Febbraio (2008) report that the SkM also performs important roles in respiration and endocrine functions. The body's systematic and local environments are also subject to the influence of growth factors, cytokines, and myokines discharged into the ECM by SKM fibres (Pedersen, 2011).

The SkM development is a process that includes the synthesis of myoblasts to create multinucleated fibres which are referred to as myotubes, which will later mature into myofibers. A motor neuron is responsible for triggering these SkM singular contractile cells. According to Sherrington (1925), the name given to this organisation of MN and the other muscle fibres, which that same neuron innervates, is called the functional motor unit. The endomysium draws the separate myofibers unto bundles, referred to as muscle fascicle. They are kept together by a perimysium. This is followed by the wrapping and encapsulation of the fascicles by a connecting tissue called epimysium. This is how the whole tissue is produced, as is represented in Figure 1.0. There are several motor units located inside the tissue (Light & Champion, 1984; Mc Comas et al., 1971).

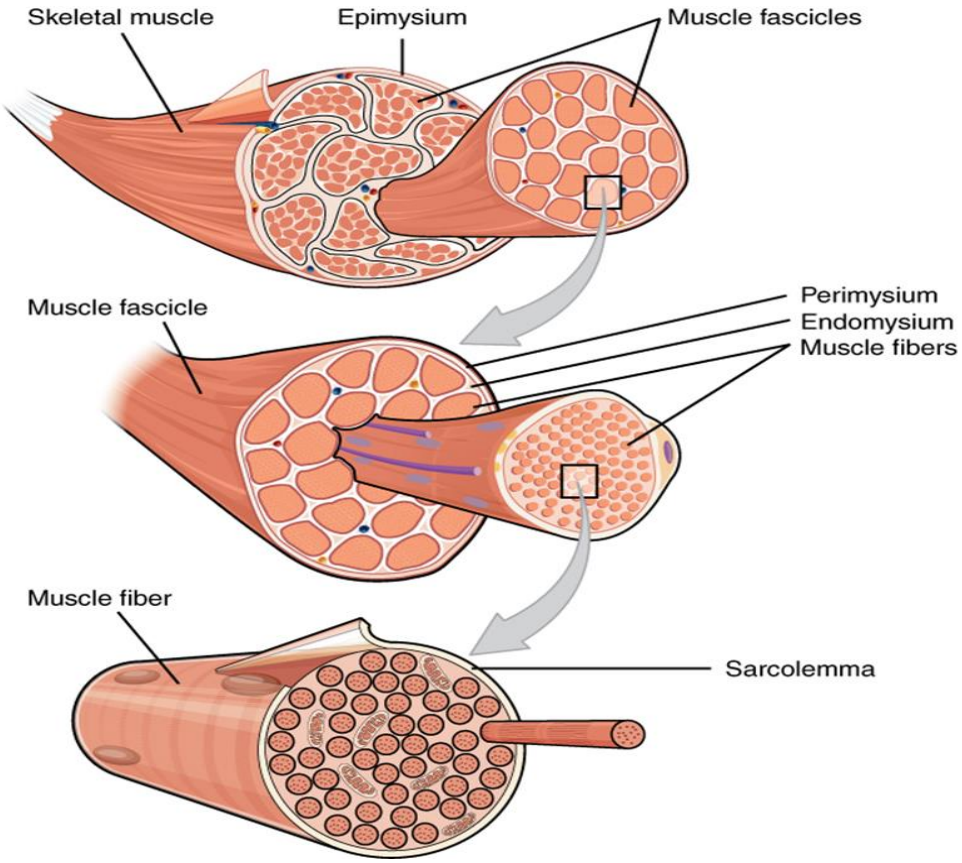

Figure 1.0: Gross anatomy of a skeletal muscle belly. The separate skeletal muscle fibres are enclosed inside the dedicated cell membrane known as the sarcolemma. A fine coating of connective tissue, known as the endomysium, plays the role of binding the fibres together. The same tissue also plays the role of delivering nerve axons, oxygen, and other nutrients through the lymphatic vessels and the blood. These bound muscle fibres are held together by a perimysium. This is a thin fibrous layer of connected tissue that splits the muscle belly into fascicles. The epimysium then forms an envelope on top of the thick fibrous epimysium and in the process builds the complete SkM (Image "1007_Muscle_Fibes_ (large).jpg" available for free public reuse at OpenStax CNX (https://cnx.org/contents/FPtK1zmh@12.8:bfiqsxdB@6/Skeletal-Muscle), licenced under Attribution 4.0 International (CC BY 4.0) (https://creativecommons.org/licenses/by/4.0/).

1.1.1 Fibres in the skeletal muscle

Mature myofibres are comprised of structures of myofibrils, which include among them thin filaments protein actin and thick filaments protein myosin (Rayment et al., 1993), with titin providing support. The term sarcomeres is used to denote the iterative organisation of such proteins within the myofibrils (Figure 1.1), expressing as striations on the myofibres. The actin molecules, found on the edges of a sarcomere, are attached to a place known as Z-discs, which form the distinct boundaries between the sarcomeres. The actin, which is attached to the Z-disc on one end, projects in the direction of the M-line in the middle. The Myosin filaments interfacing with the actin filaments that are static is found in the centre of the M-line, with the end of the myosin filament are carefully attached by titin to the Z-disks. If nervous input prompts them, the result is a creation of a cross-bridge while the actin filaments are also triggered and move along the myosin filaments, a process that results in the sarcomere becoming shorter and triggering a myofiber contraction (Denoth et al., 2002).

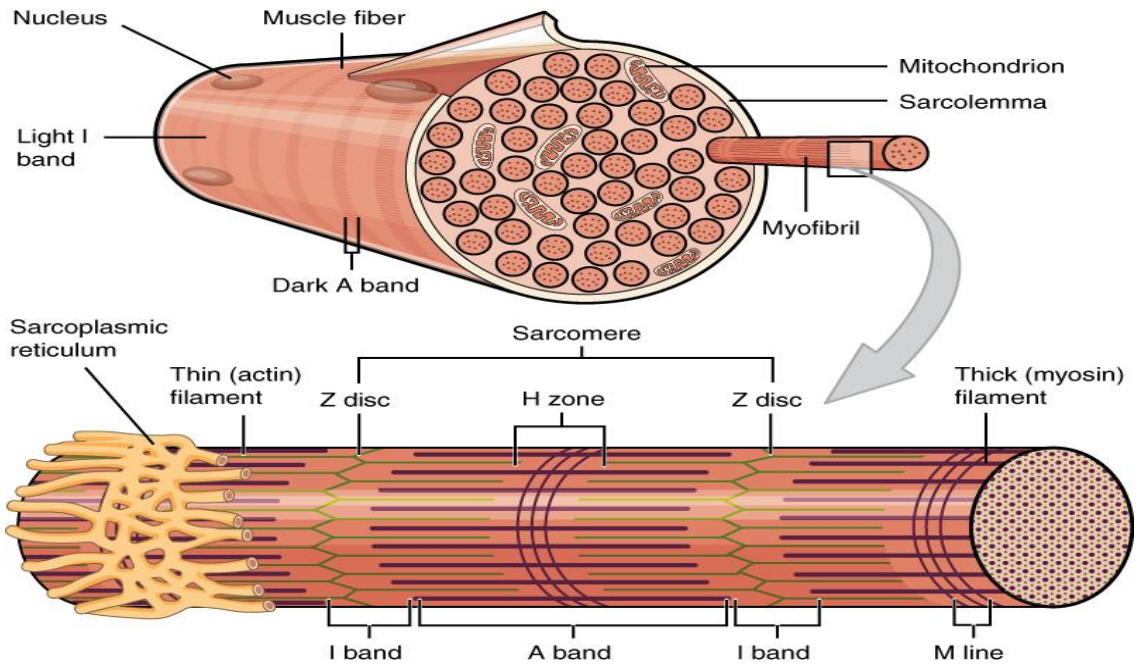

Figure 1.1: Structures of a myofibril. Myofibrils fill a myofiber, composed of distinct sarcomeres connected in a sequence. A distinct sarcomere is found between a set of Z-disks, creating a distinctive contractile unit, which is made up of a dense (myosin) filament and thin (actin) filament. The sarcomere's I-band is the zone where the myosin is not overlapping the actin, providing the muscle fibre with its lightened appearance. Since it has anisotropic myosin protein, the A-band has a darker appearance on the muscle fibre. The different banding provides muscle fibres with the ridges appearance. Structural stability is provided by the M-line which is located at the centre inside the H-zone. (Image "1022_Muscle_Fibers_(small).jpg" available for free public reuse at OpenStax CNX (https://cnx.org/contents/FPtK1zmh@12.8:bfiqsxdB@6/Skeletal-Muscle), licenced under Attribution 4.0 International (CC BY 4.0) (https://creativecommons.org/licenses/by/4.0/.

1.1.2 Myogenesis and satellite cells

With the exclusion of muscle cells in the head, skeletal muscle cells are initiated from forthcoming mesodermal precursor cells, created from somites. Within the vertebrate embryo that is still in a state of change, the somites develop into three practical cellular categories which would eventually turn into vertebrae (sclerotome), dermis (dermatome), and skeletal muscle (myotome) (Parker et al., 2003; Buckingham, 2006). The construction of the skeletal muscle starts in the embryonic myogenesis and is finally concluded in the utero (Bentzinger et al., 2012). The myogenic precursors, developed in the mesoderm, appear within the somite and turn into embryonic satellite cells (muscle stem cells) which later develop into myoblasts (Chen & Goldhamer, 2003). The embryonic satellite cells are reproduce significantly in the embryonic myogenesis primary stages until the maximum for myofibrils protein synthesis is obtained (Bentzinger et al., 2012). Once the satellite cells arrive at the myoblasts, they depart from the cell lining and sequence to create multinucleated cells which are called myotubes. Eventually, the myotubes will turn into myofibres, the skeletal muscles' distinct contractile unit (LeGrand & Rudnicki, 2007). The distribution of the satellite cells created within the embryonic myogenesis move to a state where they are inactive; remaining inactive until they are triggered at a time when muscle repair or growth is needed. After that, the terminally distinct microfibers are unable to proliferate because of embryonic myogenesis. This is the reason why the quantity of microfibers an individual has at birth and afterwards is likely to diminish as old age and disease degrade muscle fibres (Carosio et al., 2011).

A rationally consistent procedure is skeletal muscle renewal after birth. Myofibre damage results in the inflammatory response, which can be seen through the interruption of muscle tissue by populations of inflammatory cells which follows (Tidball, 2005; Carosio et al., 2011). This response is attained through a renewal platform whose origins are in the inactive satellite cell stimulation. Skeletal muscle renewal can happen if there is a stimulation of the mitotically inactive satellite cells so that they turn into myoblasts (Siegel et al., 2011; Turner & Badylak, 2012). Once stimulated, the satellite cells quickly permeate the cell system once more and begin the reproduction process (Sousa-Victor et al., 2015). Once the propagation limit has been reached, a group of satellite cells will undergo a process of renewal and then become dormant so that they can join the muscle renewal process when required (Relaix & Zammit, 2012). The myoblasts, waiting to be used, move near the area that is damaged and start coming together to create myotubes. As the myotubes expand, they interface with the existing central myofibres, repairing the damage caused to the muscle (Simionescu & Pavlath, 2011). Research has also concluded that a decline in the quality, processes, and stimulation

of satellite cells is associated with the dilapidation of muscle mass which can be observed among the elderly (Shefer et al., 2006; Brack et al., 2007; Brack et al., 2005; Tajbakhsh, 2013).

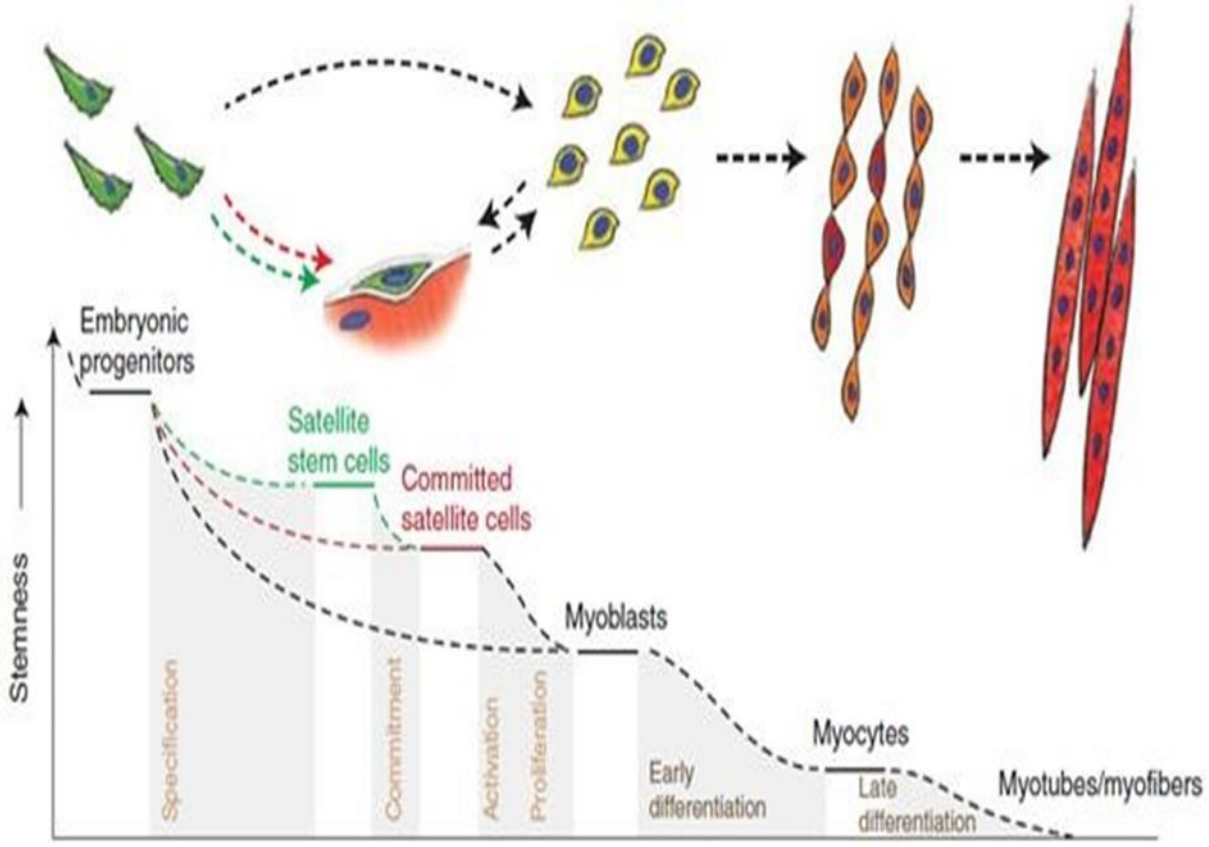

Figure 1.2: Myogenesis. The development of embryonic progenitors into mature muscle fibres (Bentzinger et al., 2012).

1.2 Motor Neurons

Motor neurons (MNs) can be defined as neuronal cells which emanate from the central nervous system (CNS) and then assign the axons into the margins to create synapses with the tissue that is targeted. Whether one is thinking about people or other vertebrates, a system which transmits signals is important for such important tasks as locomotion and breathing. Even though the MNs are often described as homogenous cells, these cells have great diversity with regards to the expression of genes, molecular profiles, and target muscles which are also varied. Their diverse character permits for separated innervation of the many separate SkM groups in the body of the vertebrate (Kanning et al., 2010). For instance, in humans there are over 600 SkM throughout the body with most muscles making up one part of an identical bilateral pair found on both sides, resulting in approximately 300 pairs of muscles (Frontera & Ochala, 2015). This is the reason why the transmission of CNS signals in the direction of the MN and MN outputs to the SkM targeted should be strictly regulated. This strict regulation seeks to organise and refine motor control, as is seen in advanced motor behaviours. Results from several studies show that the MNs innervation sequence and the link to the target SkM are regulated by the MN subtype identity (Landmesser, 2001; Milner & Landmesser, 1999). It is for this reason that MN subtype diversity requires further exploration so that the role of MNs and their motor units are fully understood.

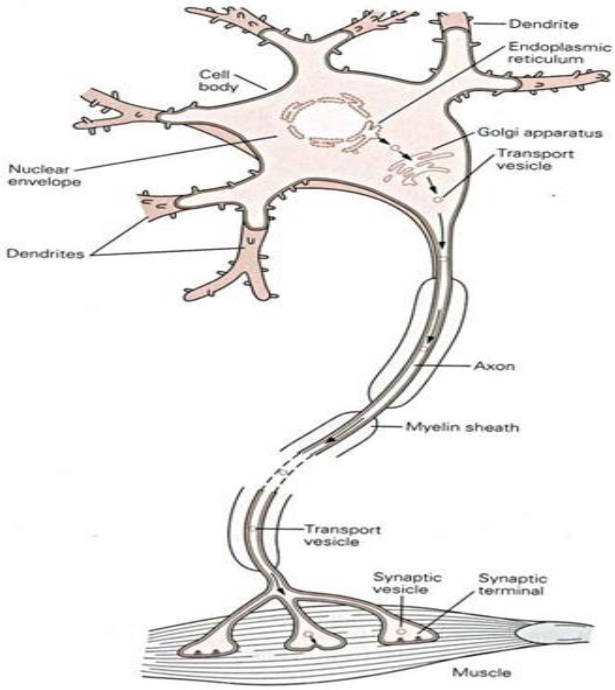

Figure 1.3: Diagram of a spinal motor neuron, showing both the cell body and synapse to a muscle (Kandel et al., 2000).

1.3 The Neuromuscular Junction

The neuromuscular junction (NMJ) is a dedicated site that connects a motor neuron's axon's terminal to skeletal muscle. As the structure that makes it possible for a neuron to transmit a chemical or electrical signal to another neuron, the integrity of the NMJ is vital for moving the motor neuron signals which trigger the contraction of the skeletal muscle. The majority of diseases and the ageing of the skeletal muscle can be connected to the impairment in NMJ function and the connected wasting of the muscle (Liu & Chakkalakal, 2018).

The NMJ constitutes the ultimate element in the process of control of skeletal muscle contraction. Hence, the NMJ plays the role of being the access for back and forth communication between the muscle fibres and motoneurons. An important feature of neuromotor control is the practical match existing between the characteristics of the motoneuron and the muscle fibres it innervates.

The NMJ forms the structure responsible for the transmission of the nerve impulse to the muscle, which triggers muscle contraction. On its way to the muscle, the axon splits into a linkage of terminal branches. Every one of the muscle fibres has one neuromuscular junction, providing a way through which the neuron's axon connects to the fibre. The end where the axon terminates is located adjacent to the endplate of the motor, an area of the muscle cell membrane or sarcolemma. A space known as the synaptic cleft separates the plate and the nerve, which are not in direct contact. Chemical transmission is, therefore, the method through which muscle activation takes place. In the axon, is located the transmitter acetylcholine, which binds to the motor endplates' receptors as soon as it is released (Rodger Laurent, 2010). This is an action that leads to the depolarization of the sarcolemma and the action potential is dispersed through the sarcolemma and travels through the transverse tubules, making its way to the triads inside the cell. The discharge of the calcium and the muscle contraction that follows is triggered by the potential stimulus. The acetylcholine effect does not last long because this zone has a lot of enzyme acetylcholinesterase, which quickly leads to the destruction of the acetylcholine. At the NMJ, certain drugs can have the effect of facilitating such processes. An example of such drugs is curare which races against acetylcholine for access to endplate receptors. A depolarization block is, on the other hand, produced by suxamethonium (Laurent, 2010).

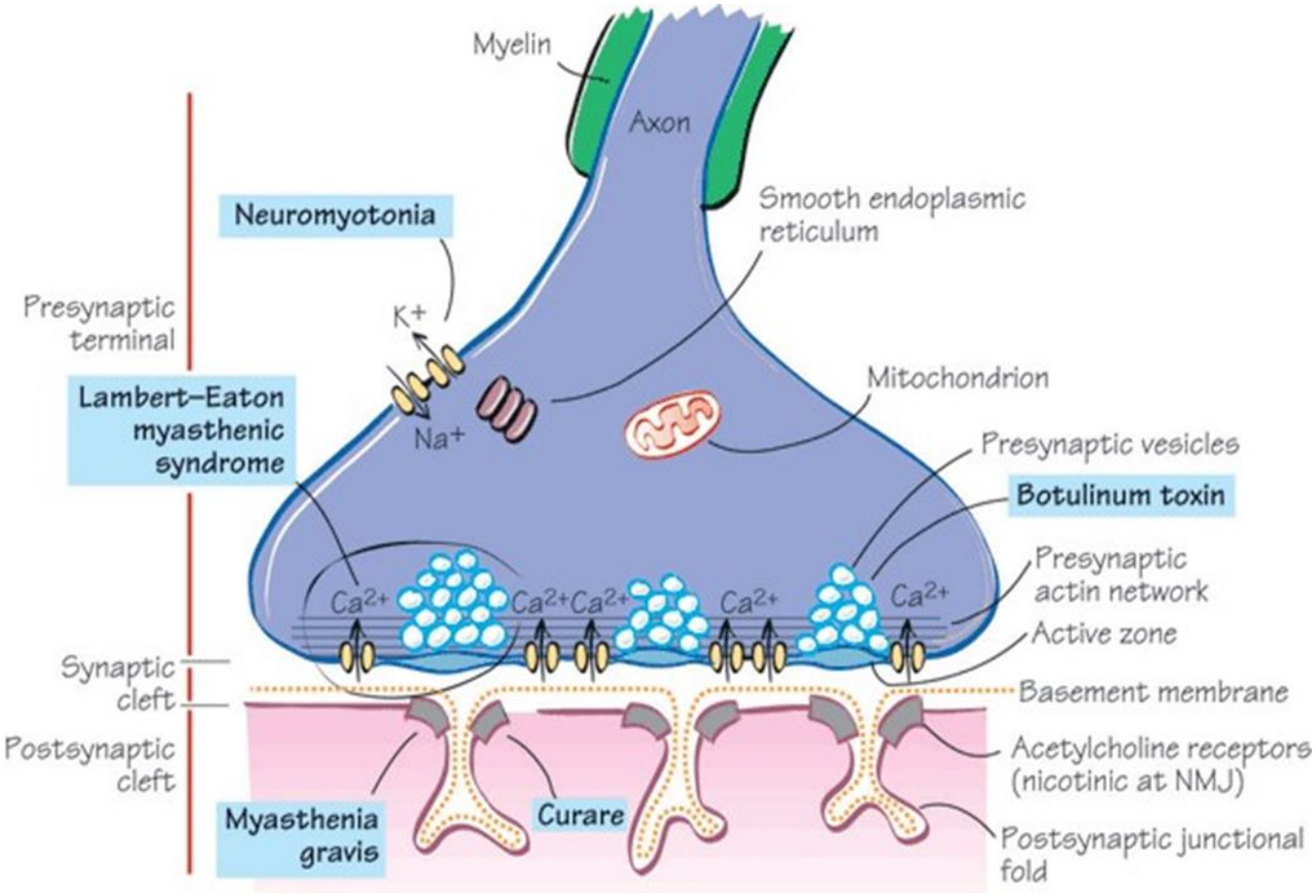

Figure 1.4: Neuromuscular junction. It is possible that action leads to the release of Neurotransmitters over the synaptic left, resulting in muscle contraction (Scicurious, 2010).

Motor neurons are responsible for transporting signals for the SkM to contract; making the voluntary movement in humans possible. Each skeletal muscle fibre is innervated by a single motor neuron, so it is vital that the nerve-muscle connection is maintained to avoid muscle fibre degeneration and movement impairment. Neuromuscular Junctions also play the role of being a platform for the skeletal muscle and nerves to interact. The NMJ contains a presynaptic motor neuron terminal, a postsynaptic motor endplate, and a synaptic cleft. The structure for the formation and maintenance of NMJs relies on the back and forth molecular interface between the motor neuron and muscle (Zahavi et al., 2015). In the event that there is a disruption in communication, the consequence is a degradation of the NMJ, including the degeneration of the axon, disruption of the synapse, a reduction in NMJ transmission, and degradation of the muscle fibre (Gonzalez-Freire et al., 2014). All this leads to the proliferation of chances for other conditions such as muscle wasting, neuromuscular diseases myopathy peripheral neuropathy and myopathy (Zhou et al., 2014).

Even though most of the investigations into NMJ function make use of animals, its function and structure have been well characterised, although the vast majority of investigations utilised animal models (reviewed in Wu, Xiong, & Mei (2010). Which do not sufficiently reflect disease progression in humans (Van der Worp et al. 2010). To date, some progress has been achieved through development of *in vitro* co-culture models employing human (Thomson et al.,2012 & Berry et al.,2015]; cross-species models (Vilmont et al.,2016; Arnold, Christe, & Handschin 2012); mouse (Umbach et al., 2012); human embryonic stem cells (hESC) (Happe et al.,2017; Guo et al.,2014); human primary myoblasts (Guo et al.,2017; Demestre et al., 2015); or rats (Smith et al.,2013). Available *in vitro* skeletal muscle and motor neuron arrangements often need complicated neural growth media which consists of cocktails and serum of about 15 neural growth factors (of which some originate from animals). This is a factor that makes the discovery of drugs and the ability to conduct toxicology studies challenging because of the potential novel compound cross-communication with the factors existing in the media which is added; providing a possible explanation as to why most of the promising therapies never make their way into clinics. The other challenge with models that currently exist is that contraction is triggered by applied chemical or electrical stimulation, which fails to duplicate the innate physiological stimulation needed for the muscle to contract (Guo et al., 2011; Umbach et al., 2012; Guo et al., 2010).

From the discussion above, it is a clear that there is a requirement for NMJ models that use human nerve and muscle cells types for which the contraction of the skeletal muscle does not need external input (chemical or electrical). Inventions introduced in recent times connected to the employment of iPSCs delivers possibilities for deriving of motor neurons and myoblasts for developing an NMJ model in vitro. Nonetheless, iPSCs-derived cells could show genetic modification and inconsistency, which could make their use limited (Chin et al., 2009). Primary cells such as surgical samples or muscle biopsy can be used for obtaining human skeletal myoblasts, but that challenge is that their lifespan is limited, which hampers effective experimentation because of the need for a repeated supply of such cells (Webster & Blau 1990; Mouly et al.,2005). Another challenge is that primary cells tend to be inconstant when it comes to purity. Also, when such cells expand, they go through phenotypic changes; making primary myoblasts a challenging choice when one wants a reliable co-culture system which can be produced over and over (Webster & Blau 1990; Mouly et al.,2005).

1.4 Insulin-Like Growth Factor-1 (IGF-1)

Insulin-Like Growth Factor-1 (IGF-1), which is originally referred to as somatomedin C, can be defined as a 70-amino acid polypeptide hormone programmed by a chromosome 12q22–23 localised gene. It has a molecular weight of 7.6 K Daltons. IGF1 is the primary moderator of both the prenatal and postnatal growth. It is mainly manufactured in the liver and takes the role of the endocrine (also an autocrine and paracrine) hormone which moderates the GH action in marginal tissues such as muscle, lungs, cartilage, skin, bone, nerves, kidney, and the liver itself. Within the circulation system, the IGF1 is present together with an acid-labile subunit (ALS) and IGF binding protein 3 (IGFBP3) (Alan Lap-Yin Pang, 2009).

The IGF-1 is also a key moderator of the effects of growth hormone (GH). Inside the pituitary gland is where the growth hormone is manufactured, before its release into the bloodstream, and then triggering the liver to start the process of making IGF-1. Organised blood growth is then stimulated by IGF-1. It also has the capacity to trigger growth in almost any body cell, particularly the cells in the skeletal muscle, lung, cartilage, hematopoietic, bone, skin, liver, nerve, and kidney cells. Apart from IGF1's insulin-like effects, it also has the capability to the synthesis of cellular DNA (Yaker et al., 2002).

When IGF-1 is absent, the result is the autosomal recessive mode of transmission. Currently, four IGF-1 transformations which lead to negative or extremely low IGF-1 expression have been defined (Pang & Chan, 2010). One of IGF-1's features is that its pleiotropic growth factor has many characters that present in numerous properties of compulsive and standard differentiation and propagation. The IGF-1 receptor (IGF1R) is responsible for facilitating the IGF1's natural activities. There is a structural and functional relationship between the insulin receptor and the cell-surface heterotetramer.

The outcomes of IGF-1 are moderated by the intimate binding proteins (IGFBPs) that transmit the ligand in the motion and extracellular fluids. IGF-1 is widely expressed in the central nervous system (CNS) where it facilitates the propagation, presence, and differentiation of non-neuronal and neuronal cells. Also, IGF-1 is a potent neurotrophic factor which can save neurons from apoptosis and develop neuronal growth and myelination. Again, IGF-1's signalling conduit plays an important role in the proliferation of cancer. Currently, attempts are being made to prompt this pathway for healing purposes.

An appreciation of how the IGF-1 system functions and how it transmits instructions will be important for both clinical and basic application (Bentov & Werner, 2013). Added to this, comprehending the comparative roles of peptide hormones in the regulation of receptiveness to insulin comes with the

fact that the growth hormone IGF-1 in the insulin system is flexible. Variations in insulin and glucose discharge result in counter controlling reactions, and adjustments in growth hormone and IGF-1 occupation modify insulin's ability to maintain normal carbohydrate homeostasis (Clemmons, 2004).

An autosomal recessive mode of transmission is followed by a deficiency of IGF-1. This can be a consequence of molecular defects which impact any of the GHRH-GH-IGF1 axis and the IGF-1's upstream components. At the moment, there are only four IGF-1 mutations which have been described. The homozygous deletion of 181 nucleotides constitutes the first case. Included are IGF-1's Exons 4 and 5. IGF-1's translated product is completely absent in patients with short stature. The other case was observed in a patient circulating IGF1 was low. At the 3'UTR of IGF1, a homozygous T→A trans-version was discovered. The consensus sequence of the mRNA polyadenylation is disrupted by the mutation, leading to the alteration of the IGF-1 precursor, which is vital for the maturation of the IGF. The V44M mutant indicates an extremely lessened attraction to the IGF receptor. The other mutant that has a homozygous Arg-to-Gln substitution at the C domain shows only a limited loss of attracting for the receptor (Pang et al., 2009).

IGF-1 binds to at least two cell surface receptor tyrosine kinases: the insulin receptor and the IGF-1 receptor (IGF1R). The main action of the IGF-1 is regulated by the act of binding IGF-1 to IGF1R, its specific receptor. IGF1R can be found on the external walls of many types of cells within cell tissues. The process of intracellular signalling is initiated by the binding to the IGF1R. In the AKT transmission conduit, IGF-1 is one of the strongest natural activators. The AKT signalling pathway is a trigger for cell proliferation and growth, and a vital mechanism for stopping the involuntary death of cells (Peruzzi et al., 1999).

It looks like the IGF-1 receptor seems to be the "physiologic" receptor because it binds IGF-1 with significantly higher affinity than insulin receptor does. Specifically, IGF-1 receptor binds at around 0.1 times better than insulin. The IGF1R/Insulin receptor heterodimers may provide a conduit for part of the signalling. The reason why there is a certain level of confusion has to do with the fact that binding research indicates that IGF-1 binds the insulin receptor 100 times weaker than insulin when it binds. However, this is not consistent with the IGF-1's actual potency in vivo with regards to the induction of the insulin receptor's phosphorylation and hypoglycaemia. There are several pathways for signalling for the IGF-1R and the other tyrosine kinase growth factor receptors. The phosphatidylinositol-3 kinase (PI3K), working with its other downstream partner, the mammalian target of rapamycin (mTOR), regulate an important pathway: Rapamycins complex with FKBPP12 to constrain the mTORC1 complex. The mTORC2 is not impacted on, and its response happens through the upregulation of Akt, moving the signals via the mTORC1, which is inhibited. The 4EBP's capacity to inhibit if-4E and slow down metabolism is itself inhibited by the phosphorylation of

eukaryotic initiation factor 4e (eif-4E) [4EBP] by mTOR. It has been observed that the Insulin-like growth factor 1 binds and interfaces with all the seven IGF-1 binding proteins (IGFBPs): IGFBP1, IGFBP2, IGFBP3, IGFBP4, IGFBP5, IGFBP6, and IGFBP7. Certain IGFBPs have inhibiting characteristics. For instance, both IGFBP-5 and IGFBP-2 have the capacity to bind IGF-1 with a more robust attraction than what it has when binding its receptor. Hence, the reduction in IGF-1 activity corresponds with an escalation in levels of serum in these two IGFBPs (Peruzzi et al., 1999). IGF-1 is unique growth factors which is the only factor induces proliferation and differentiation. At high concentrations (>20ng/ml), IGF-1 induces proliferation whereas at low concentration (<20ng/ml) in induces differentiation (Zanou and Gailly, 2013).

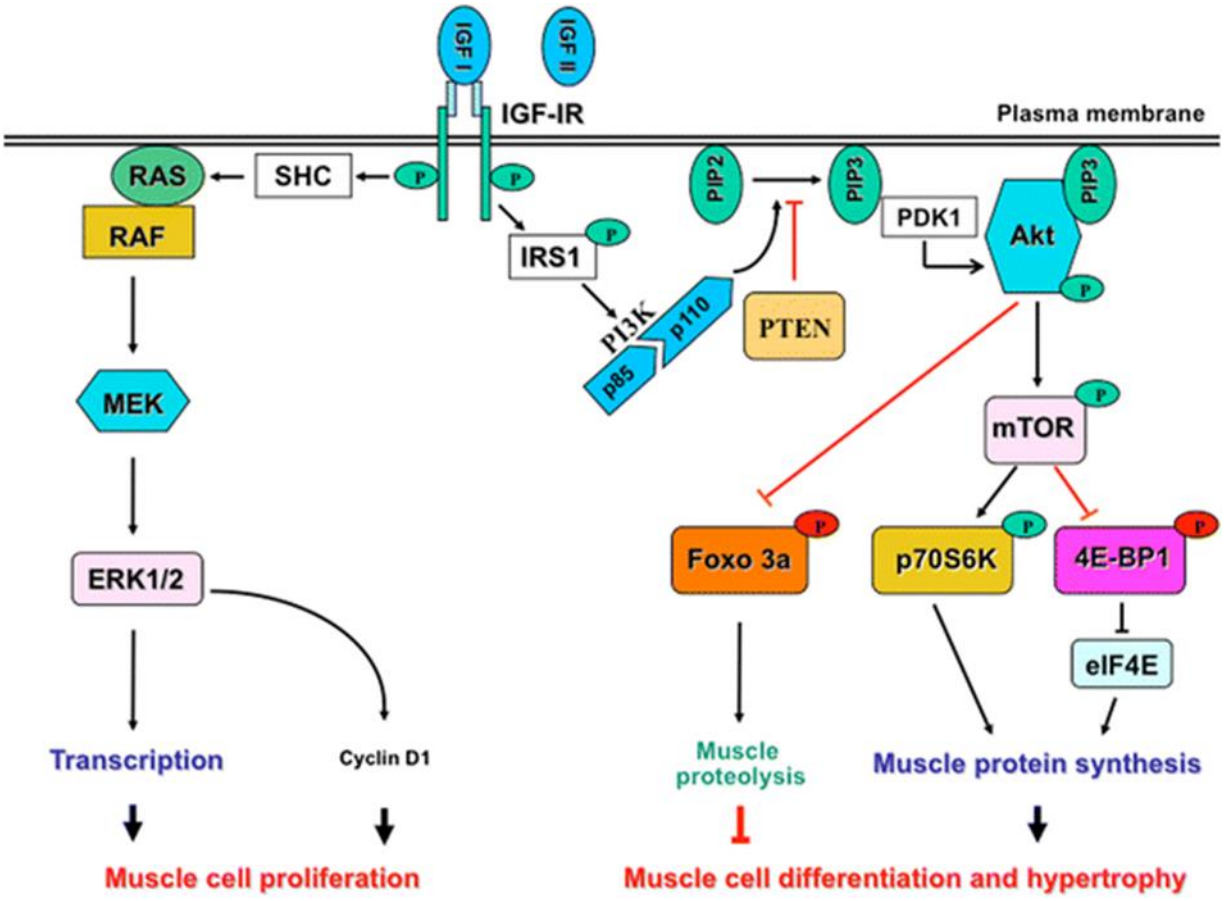

Figure 1.5: Diagram of a skeletal muscle hypertrophy and regeneration, showing interplay between the myogenic regulatory factors and insulin-like growth factors pathways (Zanou and Gailly, 2013).

There is a close relationship between IGF-1 and a protein which also binds to the IGF receptor; known as "IGF-2". However, on its own IGF-2 binds a receptor known as “IGF-2 receptor" (Sometimes called mannose-6 phosphate receptor). The insulin-like growth factor-II receptor (IGF2R) does not have the signal transduction capacity. It has the primary task of being an IGF-2's sink; making lower quantities of IGF-2 available for binding with IGF-1R. As is denoted b the name “insulin-like growth factor 1”, there is a structural relationship between insulin and IGF-1, and even has the capacity to bind the insulin receptor, even though this happens at affinity levels that are lower than those of insulin (Peruzzi et al., 1999).

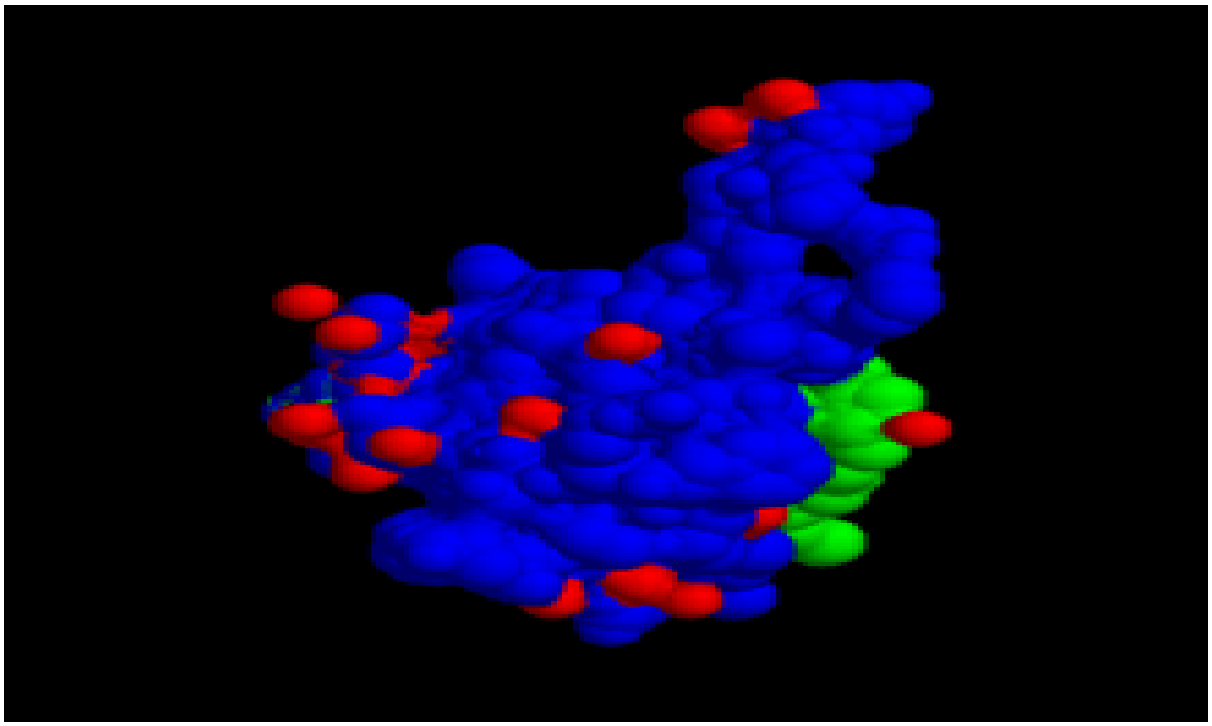

Figure 1.6: Shows 3D model of IGF-1 (https://en.wikipedia.org/wiki/Insulin-like_growth_factor_1).

1.4.0 IGF-1 and Neuromuscular Junction (NMJ) disorders

According to Lewis et al. (1993), the Insulin-like growth factor-I (IGF-1) has a role to play in the development and preservation of neurons. It has also been noted that impaired IGF-1 signalling plays a role in numerous neurological conditions such as stroke. Disorders linked to motor neurons like the loss of motor neurons in the spinal cord in amyotrophic lateral sclerosis or the deterioration of spinal cord motor neuron axons in particular outlying neuropathies, present a distinctive opening for the use of neurotrophic proteins for therapeutic intervention. Typically, these kinds of proteins would not cross the brain-blood barrier. However, nerve terminals and neuron axons lie outside the barrier, which makes it possible for them to be the target of the general administration of protein growth factors (Lewis et al., 1993). Within the spinal cord, Insulin-like growth factor-I (IGFI) receptors can be found. Just like affiliates of the neurotrophin receptor clan, IGF-1 receptors intermediate the transduction of signals through a tyrosine kinase domain. It has been noted that IGF-1 inhibits the loss of choline acetyltransferase activity in embryonic spinal cord cultures and also leads to a reduction of the programmed cell death of motor neurons in vivo in the process of typical development or after axotomy or spinal transection.

In line with prior reports, which indicate that IGF-1 boosts neuronal sprouting in vivo, focusing on subcutaneous administration of IGF-1 increases muscle endplate size in rats (Lewis et al., 1993; Chen et al., 2005), it can be noted that IGF-1 injections also result in an acceleration of functional recovery after sciatic nerve crush in mice. It has also been observed to weaken the marginal motor neuropathy triggered by the administration of chronic cancer chemotherapeutic agent vincristine in mice. IGF-1 doses which make a recovery to happen faster after sciatic nerve crush in mice leads to raised serum levels of IGF-1; comparable to the ones attained after formulated recombinant human IGF-1 (Myotrophin) injections in normal human subjects. Using such conclusions as a basis and the proof of safety in humans and animals, clinical trials of recombinant human IGF-1 are now being administered in patients who have peripheral neuropathies induced by chemotherapy (Lewis et al., 1993; Borasio et al., 1998; Chen et al., 2005).

1.4.1 Neuromuscular dysfunction in Type 2 Diabetes

When compared to non-diabetic patients, diabetic patients have an increased risk of developing physical disabilities. In the majority of cases, these physical disabilities are related, even if partly, to a malfunction of the muscles (Orlando et al., 2016). A number of studies have come to the conclusion that lessened muscle strength under statistic or dynamic conditions happens in both the lower and upper limbs of patients with Type 2 Diabetes. Other effects associated with diabetes include reduced muscle mass which is also accompanied by changes in the composition of muscle fibre. However, it needs to be noted that the data linked to these parameters are conflicting (Orlando et al., 2016).

Diabetes' impact on neuromuscular function has been linked to the presence of long-term complications. It has been observed that peripheral neuropathy affects muscles, damaging the nerve condition. The declining strength of the muscle may also be attributed to vascular complications. However, muscle dysfunction happens much earlier in the progression of diabetes and may also have an impact on the upper limbs. What this implies is that it could develop without the aid of micro and macrovascular disease (Orlando et al., 2016). Increasingly, evidence is indicating the possibility of hyperglycaemia causing changes in the muscle's intrinsic properties with regards to the generation of force through the use of numerous mechanisms. In recent studies, it has been proved that resistance exercise can be an effective way of countering the dilapidation of muscle performance. It has also been noted that the greater the intensity of the exercise, the more the benefits. On the other hand, the impact of power training is still to be determined (Orlando et al., 2016).

1.4.2 Amyotrophic Lateral Sclerosis (ALS) and Motor Neuron Disease

There has been an extensive examination of the potential of IGF-1 to deal with neuronal loss and muscle weakness of ALS (Sullivan et al., 2008). This is because of the positive effects it has shown on both motor neurons and muscle. When it comes to human patients who either have motor neuron disease or not, the immunoreactivity is detected in Schwann cells, motor neurons, skeletal muscle, and astrocytes. In the same kinds of cells, IGF-II immunoreactivity is also identified to a lesser degree. Dore et al. report increased binding of the IGF-1 and –II in the spinal cords of all patients with ALS, implying increased IGF-1R expression. On the other hand the western blotting of post-mortem human spinal cervical spinal cord study showed no change in the total IGF-1 levels between healthy patients and ALS patients. Nonetheless, free IGF-1 was reduced by 53% in ALS patients (Sullivan et al., 2008). The concept of free IGF-1 denotes the IGF-1 which is available for binding with IGF-1R, which is not complexed with IGFBPs. For this study, there was a significant up-regulation of IGFBP-2 and -5, a situation which implies that there was a possible change in the bioavailability of IGF-1(Sullivan et al., 2008 ; Sakowski & Feldman, 2012). However, in this study the levels of IGF-1 were taken post-mortem so perhaps could factor into why the IGF-1 levels decreased.

1.4.3 The need for IGF-1 in Central Nervous System Axonal Regeneration

One of modern medicine's biggest challenges is the functional repair of the adult central nervous system (CNS). Whether it is the traumatic injuries of the CNS or neurodegenerative diseases, it has been shown that the result is irreparable motor and cognitive functions, which are linked to permanent disability. The dendritic or axonal regeneration is a primary condition for functional recovery, for the neuronal connections to be re-establish so that the CNS can operate normally again. In the past, the thinking was that it was impossible for the axonal revival of the adult CNS (Goldberg & Barres, 2000). However, Dupraz et al. (2013) note that prevailing knowledge of external and internal factors regulating axonal renewal and construction of new synapses has led to a shift in such a view. Proposals have been advanced to the effect that the processes which constitute an axonal renewal of adult CNS has several features which make them comparable to those that are vital in the development of the CNS (Cui Q, 2006). Nonetheless, a number of characteristics of axonal renewal are still not known, particularly the ones regarding directing the new axon sprouting by extracellular cues (Harel & Strittmatter, 2006). The majority of CNS neurons fail to regenerate after a lesion (Rossi, Gianola, & Corvetti, 2007).

An understanding of how the axonal outgrowth and specification is regulated during the development of extracellular factors is beginning to be possible. The established model for the examination of such events in culture are the pyramidal cells acquired from the embryonic hippocampus. An important reflection is that a specifically early event in those neurons that are not yet showing obvious axon (perceived as the second stage of differentiation) (Sosa et al. 2006), involves the isolation of activatable IGF-1 receptors (IGF-1R) to one single neurite. This is followed by the accumulation of phosphatidylinositol-3 kinase (PI3K) and PIP_3. This accumulation takes place in the growth cone and distal zone of that particular neurite, coupled with IGF-1R. These are important events with regards to the outgrowth of the future axon (Shi, Jan & Jan 2003). Definitely, the axon designation needs the IGF-1R to activate P13K (Sosa et al. 2006). For the renewal of the adult peripheral nervous system, a similar arrangement is involved (Dupraz et al., 2013).

On the other hand, no information can be found about the potential involvement of the IGF1R-PI3K pathway in the regeneration of CNS neurons in adult mammals. For purposes of dealing with this question, as a model for experimentation, they employed retinal ganglion cells (RGC). The reason why RGCs were used is that it has been observed that they have the ability to survive and rejuvenate neurites *in vitro* (Luo X et al., 2001). Also, both IGF-1R and IGF-1 exist extensively in various mammalian retinal cells, including humans (Lambooij et al., 2003; Cha et al, 2013).

From the results we obtained, it can be seen that IGF-1R expression is substantially higher in cultured adult RGC than it is in freshly disaggregated adult retina cells. The results also show that the variant of IGF-1R that contains bipolar cells is enriched at the third distal axon. Experiments dealing with the loss of function which employ a process of blocking the IGF-1R antibody or the use of shRNA directed against IGF-1R, and also the pharmacological inhibition of PI3K signalling, resulted in the repression of axonal renewal. The use of a constitutively active type of PI3K, used in the co-transfection of cells suppressed with IGF-1R was observed to rescue the phenotype with the outgrowth of a single axon or more (Dupraz et al., 2013).

Physical exercise's neurobiological effects are many and include a broad array of interconnected effects on the cognition, and brain structure and function (Erickson, Hillman & Kramer, 2015). In part, these effects may be regulated by the discharging of peptides, referred to as myokines, from the muscles that are contracting. A huge amount of research using humans has shown that people involved in steady aerobic exercise of around half an hour every day, results in clear improvements in cognitive functions, healthy changes in the brain's gene expression, and other desirable types of behavioural plasticity and neuroplasticity. Other effects that will be observed in the long term include augmented growth of neurons, better intellectual regulation of behaviour, boosted neurological activity, improvements with regards to coping with stress, improved spatial, declarative, and working memory, and functional and structural advances in brain pathways and structures linked to memory and cognitive control (Erickson, Hillman, & Kramer, 2015).

The impact of exercise on cognition has vital implications with regards to boosting academic performance in both children and students in college, boosting productivity for adults, maintaining cognitive function in old age, averting or treating particular neurological disorders, and leading to improvements in the overall quality of life (Erickson, Hillman, & Kramer, 2015). When it comes to adults who are healthy, it has been observed that aerobic exercise leads to temporary effects with regards to cognition after one session of exercise. However, for regular exercise, results from studies show lingering effects over a period of several months (Cox et al., 2016). It has also been concluded that individuals who are regularly involved in aerobic exercise such as running, cycling, walking fast, jogging, and swimming, tend to have higher scores neuropsychological function and performance tests measuring particular cognitive functions. Examples of such tests include declarative memory, attentional control, speed of information processing, inhibitory control, spatial memory, working memory capacity, and updating (Cox et al., 2016).

The temporary effect of exercise on cognition include enhancements in the majority of executive functions such as attention, making decisions, working memory, solving problems, cognitive flexibility, and inhibitory control. It has also been observed that there are improvements in the speed of information processing for a period of about 120 minutes following an exercise session (Erickson, Hillman, & Kramer, 2015).

Both short and long-term effects on emotional states and mood can be induced by aerobic exercise. This has the impact of promoting long and short-term positive effect, preventing negative effect, and lessening the biological response to severe psychological stress. In the short-term aerobic exercise can play the role of both a euphoriant and antidepressant, while physical exercise done on an ongoing basis has the effect of boosting self-esteem and mood (Basso & Suzuki, 2017).

When done on a regular basis, aerobic exercise results in improvements in symptoms linked to several disorders linked to the central nervous system and could play the role of being an adjunct therapy for such conditions. Evidence of exercise treatment effectiveness is available when it comes to the attention deficit hyperactivity disorder and other major depressive orders (Schuch et al., 2016). The American Academy of Neurology's clinical practice guideline for mild cognitive impairment advises clinicians to recommend that patients who have been diagnosed with this condition are involved in physical exercise at least twice every week (Petersen et al., 2018). Other reviews of clinical evidence are consistent with the idea that exercise can be effective as an adjunct therapy for particular neurodegenerative conditions, especially Parkinson’s disease and Alzheimer’s disease. Exercise done on a regular basis has also been linked to a lowered risk of developing neurodegenerative conditions. A huge body of emerging clinical evidence and preclinical evidence provides support to the employment of exercise therapy for both the prevention and treatment of the development addiction to drugs (Cormie et al., 2015).

1.4.4 The effects of IGF-1 on the neuromuscular junction associated with sarcopenia

The declining skeletal strength and mass which happens as a result of ageing, known as sarcopenia can be attributed to several factors, including a lack of balance between the synthesis of protein and its degradation, alterations in hormonal/metabolic status, and the levels of inflammatory mediators in circulation (Ascenzi et al, 2019). For this reason, the factors that lead to an increase in muscle mass while also boosting anabolic pathways may be useful in counteracting sarcopenia therapy. Among such the growth factor-1 (IGF-1) is associated with numerous skeletal muscle pathways.

Insulin-like growth factor 1 is a pleiotropic growth factor that plays several roles, including fortification from oxidative stress, neurotrophic effect, preservation of muscle strength and mass, and advancement of motor neuron existence (Gonzalez-Freire et al., 2014.). Numerous studies have arrived at the conclusion that levels of circulating IGF-1 deteriorate with age. This deterioration may lead to motor unit denervation and neuromuscular junction degeneration (Messi & Delbono, 2003; Delbono, 2003). In keeping with this hypothesis, in mouse models, when muscle-specific IGF-1 is overexpressed, sarcopenia can be reversed (Musaro et al., 2001). This inhibits the decrease in type IIB and escalation of type IIA fibres which are linked to age (Messi & Delbono, 2003). It also results in enhanced nerve renewal through its action on axons, the NMJ, and Schwann cells. When IGF-1 is administered systemically, the result is a decrease in the death of motor neuron cells. It promotes the muscle re-innervation following injury in animals that are still young. This implies that declining levels of IGF-1 as individuals age could weaken the ability to repair and preserve NMJ's integrity (Vergani et al., 1998). It is possible that IGF-1 sensitivity does not decrease as individual age, implying that IGF-1 may still have the capacity to facilitate rejuvenation after an injury to the nerve in individuals who are older. In mice, overexpression of IGF-1 may increase the NMJ size without extensive alteration in muscle fibre size, implying that the maintenance of a precise force in aged animals overexpressing IGF-1 in muscle is attained, partly, by improved motor neurons-muscle coupling (Payne et al., 2006).

The problem of muscle wasting is that it can only be partly mitigated by making changes to the diet and engaging in physical exercise however, these are long-term strategies that do not usually solve the problem when a patient requires to be mobilised after being in a forced state of immobility, in which a short term pharmaceutical mediation could be the most viable solution. Whether targeted or sustained, the administration of insulin-like growth-1 (IGF-1) could be helpful for both normal growth, development, and skeletal growth of muscle. What makes IGF-1 unique is that it triggers both proliferation and differentiation of the cells in the muscle after the activation of its receptor and the following phosphorylation of the insulin receptor substrate-1 (IRS-1) and the downstream

signalling molecules. There are reports that both differentiation and proliferation include the phosphorylation and stimulation of extracellular signal-regulated Kinases 1/2 (ERK1/2), PI3K/Akt (Coolican et al., 1997), together with their downstream targets that have in previous cases been associated with the activation of the synthesis of protein (Glass, 2005).

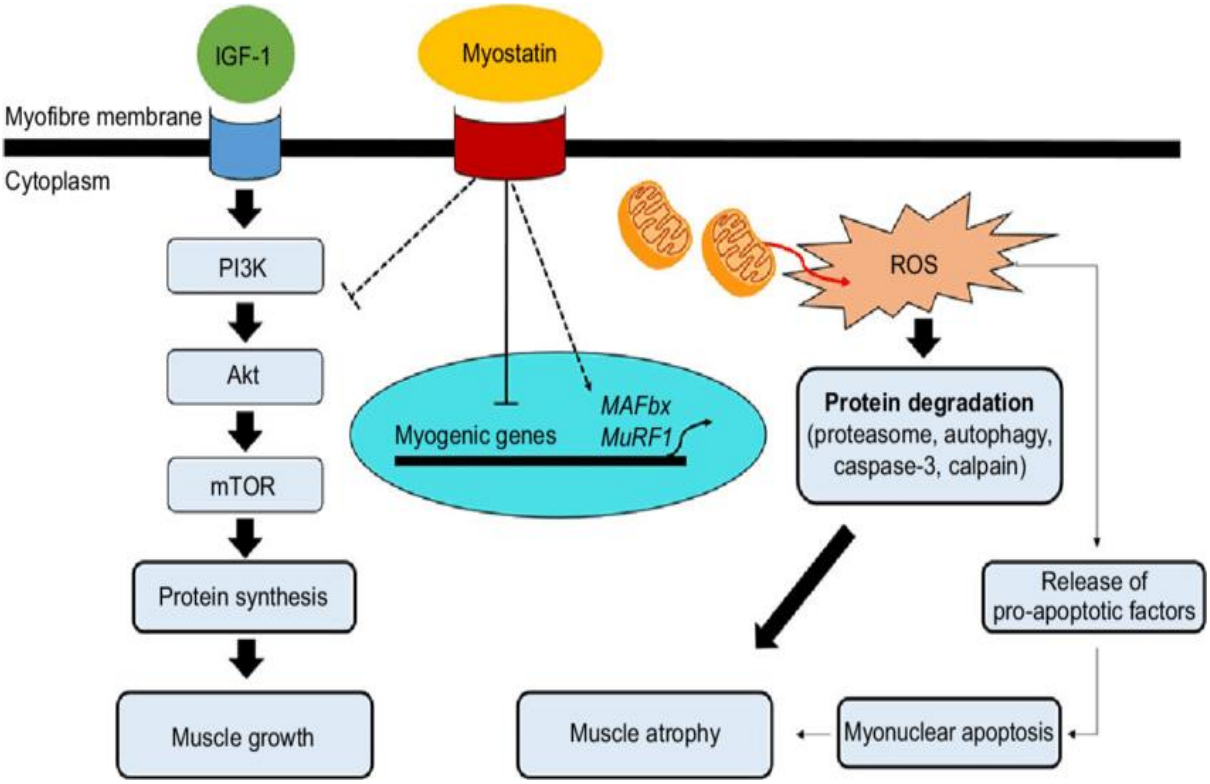

Figure 1.7: Signalling pathways associated with muscle growth and muscle disuse atrophy (Reilly and Franklin, 2006).

According to Lai et al (1997) and Sorenson et al (2008), investigations are currently in progress on using IGF-1 as a possible solution for muscle wasting (Lai et al. 1997, and Sorenson et al., 2008). Coolican et al (1997) note that the reason behind the trials on IGF-1 as a treatment solution has to do with its effectiveness and capacity to promote both muscle survival and growth in cell culture in both human beings (Borasio et al. 1998) and animals (Svanberg et al. 2000). Apart from targeting this anabolic growth factor in stopping the wasting of muscle as a result of catabolic conditions (Borasio et al. 1998; Williams et al. 2008), contemporary applications have also been investigating how it can be applied to improve cardiac function in the context of chronic heart failure (Perkel et al. 2012).

Another area where it is also being applied is identified by Chernausek et al. (2007) as disorders of growth in children.

Even though IGF-1 is seen as a possible solution to the challenge of muscle wastage, authors like Yakar et al. (2002) see some practical challenges such as the fact that it is low in bioavailability and its rate of clearance is rapid. Others such as Metzger et al. (2011) refer to the side effects which include the suppression of growth hormones (GH) and hypoglycaemia. Added to this Takahashi et al (2003) observes that the gene transfer therapy of IGF-1 in human beings is still not yet properly defined with regards to treating muscle wasting. Moreover the IGF-1 bioactivity is poor hence it has short half-live (Kempen et al., 2015). IGF-1 circulates bound to an IGF binding protein (IGFBP) in blood. The binding protein is responsible for the long plasma half-life of IGF. IGF-1 half-life is approximately 12 hours (Lammers et al., 1989; Ursø et al, 1999). This challenge is related to the potential for insertional mutagenesis and maintaining of therapeutic levels through methodical delivery. For this reason coming up with new safe delivery methods is something that is required.

1.5 Nanoparticles (NP)

Nanotechnology is a multidisciplinary scientific endeavour which involves the development and use of materials, systems, or devices on the nanometer scale. Currently, the area of nanotechnology is undergoing changes on different fronts. It is expected that the technology will result in innovations and will also have a profound role to play in numerous biomedical applications, not just in the area of drug delivery but also in biomarkers, molecular imaging, and biosensors. Target-specific drug therapy and techniques to facilitate early diagnosis of pathologies are the main areas of study where nanotechnology is expected to have a huge role to play. In this review, several nanotechnology-based drug imaging and delivery approaches, and their economic impact on the biomedical and pharmaceutical industries are considered (Sahoo, 2003).

Nanotechnology can be defined as the comprehension and regulation of matter which is generally within the 1–100 nm dimension range. Its application in the field of medicine, which is referred to nanomedicine, is concerned with the employment of specifically engineered materials, at this length scale, to create innovative diagnostic and therapeutic modalities (Zhang et al., 2008). Nanomaterials possess distinct physicochemical characteristics like ultra-small size, large surface area to mass ratio, and high reactivity. These differ from bulk materials of similar composition. These are the characteristics that can be taken advantage of to deal with some of the limitations which have been identified in standard diagnostic and therapeutic agents (Zhang et al., 2008).

Often, NPs have a vital role to play as carriers, even though they also have the capacity to directly play the role of therapeutic agents. Based on conclusions from previous studies, NPs can be grouped into numerous types, even though it is not all types that can be used in combination with growth factors (GFs) (Kalantarian et al., 2018). Concerning the IGFs/NPs conjugation, they conducted an examination of some novel and classical models of exterior and interior patterns. The majority of the patterns were used effectively in the modulation of the release of drugs in a spatiotemporal way (Zhang et al., 2008; Kalantarian et al., 2018).

Within the IGFs/NPs arrangement, other than the synergistic effects of NPs combined with growth factors, it has been noted that nanoparticles also exert specific effects. In the past, the focus was mainly given to stem cells and inductive growth factors in tissue engineering. However, several nano-materials like perovskite nanoparticles, hydroxyapatite (HA), and Nano fibrin have also shown to have explicit effects in facilitating the renewal of tissue (Zhang et al., 2008; Kalantarian et al., 2018).

1.5.0 Nanoparticles and Therapy

Even though NPs/GFs applications are many, the diversity and specificity of GFs could best be represented in the advancement of the differentiation of progenitor cells or stem cells. Some of the cells that are most used in the NP/GF applications are identified by Kim et al. (2013): the adipose-derived stem cells (ASCs), human mesenchymal stem cells (hMSCs), urine-derived stem cells (USCs), bone marrow stem cells (BMSCs).

According to Kim et al. (2013) numerous GFs, including basic fibroblast growth factors (bFGF), bone morphogenic proteins (BMPs), and transforming growth factor b (TGF-b), can be added into PLGA nanosphere coated microspheres and trigger adipogenesis, osteogenesis, and chondrogenesis in hMSCs, respectively. In comparable studies, the human-derived dermal fibroblasts were transfected with TGF-b3, insulin-like growth factor (IGF)/bFGF, and BMP-2 genes coated on PLGA-NPs, and chondrogenesis, adipogenesis and osteogenesis were induced, respectively (Kurakhmaeva et al., 2009). What can be inferred from the information above is that various growth factors can lead to varying effects. Hence, it can be argued that the selection of appropriate GFs based on what the experiment requires is extremely vital (Kurakhmaeva et al., 2009; Saboktakin, 2017).

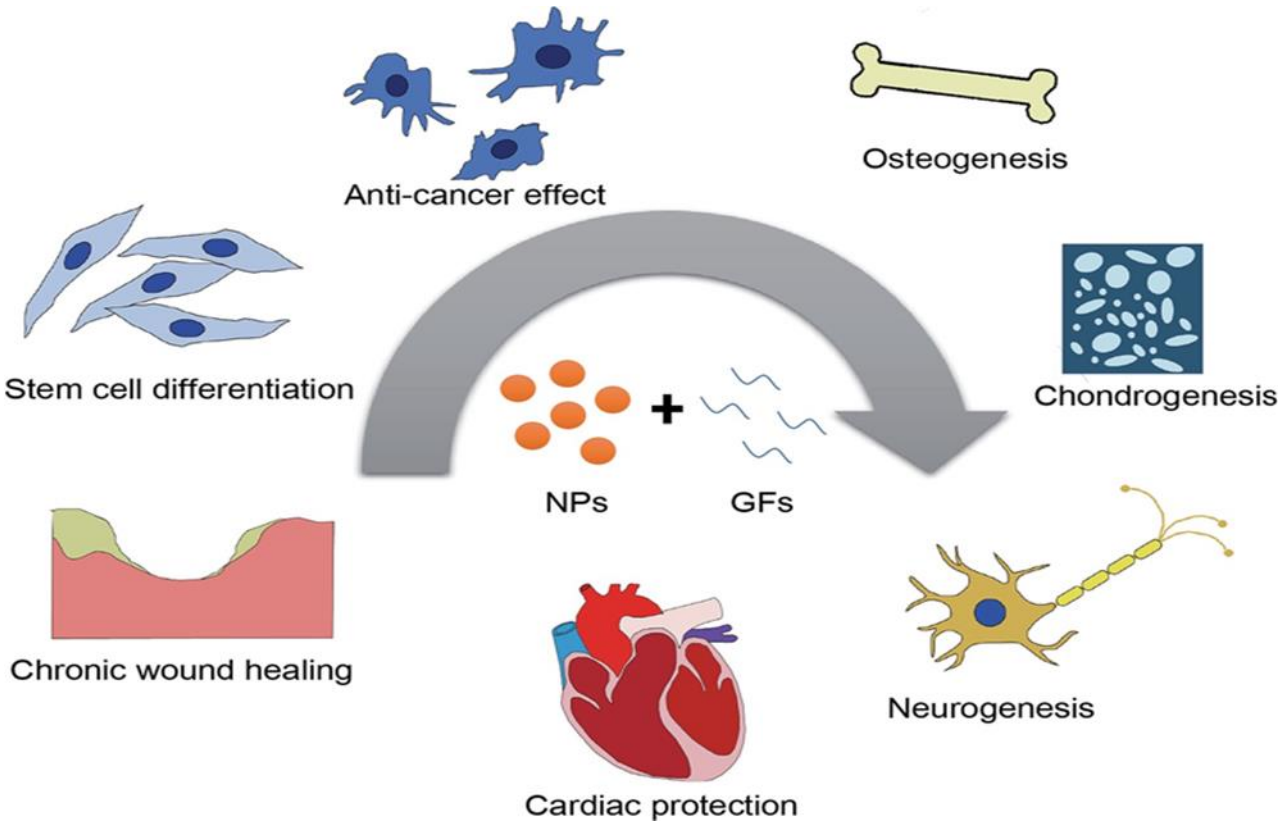

Figure 1.8: NPs/GFs function and application. GFs and a section of NPs can impact signal transduction pathways. GFs can also interface with various sites across the body. This characteristic has a contribution to their wide range of functions in various processes such as stem cell differentiation, healing of chronic wounds, osteogenesis, anti-cancer effects, chondrogenesis, cardiac protection, angiogenesis, and neurogenesis (Nanoparticles combined with growth factors: recent progress and application, RSC Advances, 2016, 6, 90856).

1.5.1 Nanoparticles and IGF-1 discharge

Within both the nervous system and the peripheral nervous system (PNS), neural tissue repair can be promoted by NPs/GFs. In the CNS, the repairing of brain tissue is a more complicated process when compared to bone renewal. This is because the degree of tissue differentiation in the brain is higher, and there is also a presence of a blood-brain barrier (BBB). Some research paid attention to the use of NPs for the treatment of neurodegenerative disorders (Kurakhmaeva et al., 2009). The main focus of such studies has been determining in vivo and in vitro delivery methods. Based on a clear comprehension of the challenges linked to in vivo NP delivery, studies conducted in recent times have paid their attention to BBB and blood and brain circulation isolation by either chemical or physical means. In healthy organisms, the BBB is a requirement for ensuring that the brain is protected from the majority of pathogens and toxins. Unfortunately, it is this barrier that makes it impossible to deliver the majority of drugs in pathological settings; an arguable position (Kurakhmaeva et al., 2009).

Standard systems of delivery like an intravenous injection of low-dose drugs do not have the capability to permeate BBB. Even though drugs administered in high doses can, to a certain degree, go past the BBB and enter the brain, they also have the potential to result in undesirable cytotoxicity (Pardridge & NeuroRx, 2005).

It is good to note, however, that in the last few years, there has been a gradual exploration of improved delivery methods. An example of such methods is intranasal delivery which is a non-invasive technique for the treatment of numerous disorders/conditions of the CNS (Pardridge, & NeuroRx, 2005). The leading limitations linked to intranasal delivery is that the nasal epithelium has limited capacity to absorb and the nasal cavity also has a short residence time (Pardridge & NeuroRx, 2005). To deal with the limitations, a few approaches have been embraced. Previously, it has been reported that NPs conjugated with Solanum tuberosum lectin (STL) can entrap bFGF, which has the capability to selectively bind to the nasal epithelial membrane in the treatment of Alzheimer's disease (Kurakhmaeva et al., 2009).

Added to growing the nasal epithelium affinity, the other approach involves a further enhancement of the penetration via BBB. Because they are compatible with biomembranes, Gelatin-nanostructured lipid carriers (GNLs) that encapsulate bFGF (GNLs/bFGFs) can be delivered to the brain effectively. Hence, GNLs/bFGFs have turned into an innovative carrier for conveyance via BBB. Based on their opinion, lipid nano-carriers present the best promise for applicable NPs because they have the

potential to penetrate the BBB through combining with the biological membrane, and they can also be functionally and structurally infused with other materials (Kurakhmaeva et al., 2009).

It is not only in the brain that the repair of the CNS can occur but also in the spinal cord. For instance, scaffolds attained through the interface between fibrinogen and thrombin-conjugated g-Fe2O3 magnetic NPs have been implemented to injuries of the spinal cord via the nasal olfactory mucosa cells (Kurakhmaeva et al., 2009). They also came to the realisation that the peripheral nerve's functional recovery after an injury usually needs numerous GFs; especially NGF, because of its synergistic effects. Self-assembled cubic lipid-based crystalline nanoparticles were developed by Bu et al. with the aim of boosting the internal ear bioavailability of bioactive NGF through a round membrane route. The NGF-loaded reservoirs substantially triggered the growth of neurons. Generally, studies on the implementation of IGFs/NPs still pay most of their attention to diseases of the brain (Kurakhmaeva et al., 2009).

Since mesoporous silica was discovered in the later years of the 1970s, it has attracted a lot of attention. The reason for this attention can be attributed to their distinct properties like ordered pore structure, extremely high specific surface areas, and their potential fusion in a broad range of morphologies like discs, spheres, and powders. Mesoporous silica is different from traditional silica in that it displays remarkably ordered pores. This can be attributed to the nano-templating approach implemented during the material's synthesis. In the last three decades, a broad range of mesoporous silica (SBA 15, SBA 16, MCM 41, MCM 48), with pore geometries and particles morphologies coming in a broad range, have been synthesised. The porous silica spheres present as spherical particles with porosity that is quasi ordered (Coleman et al., 2001).

Current developments in the production of mesoporous silica, permitting manufacturing at large scale, has made it possible for them to transit from research-based in laboratories to more sophisticated implementation in driven studies. Currently, there is widespread employment of MS with tailorable and uniform pore dimensions with high surface areas in numerous applications. Such applications include the remediation of waste water, cleaning of indoor air, improvement of pervaporation membrane, catalysis, preparation of the bio-analytical sample, the capture of oxygen, delivery of drugs, and catalysis. MS also play the role of being templates that control the nanowires and quantum-confined nanoparticles' aspect ratio. In current years, nanomedicine has developed at the forefront of nanotechnology, generating great expectations in the biomedical field. Researchers are using novel nanoparticles for both treatment purposes and diagnostic applications using imaging technology through drug delivery. Between all the available nanoparticles, inorganic mesoporous silica nanoparticles are the newcomers to the field, contributing with their unique and excellent properties (Manzano and Vallet-Regí, 2020).

Nanoparticles and nano-mesoporous silicate particles are employed as potential drug delivery systems. This is attributed to their synthetic pore arrangement, large surface areas, and the fact that they are simple to chemically modify. In the biotechnology area, these particles are used broadly because of their distinct mesoporous arrangement (Lopez et al., 2006). Their structure allows for the absorption of drugs and proteins, because of their narrow and straight channels, large internal volumes, and high surface areas. Over a period of time, the absorbed proteins and drugs are diffused contingent on the chemical composition, the size, the morphology and size of particles, release medium, size of pores, and surface functionalization of the drugs (Tang et al., 2006). The factors controlling the release of drugs that happens over minutes, hours, or days include heat, chemicals, pH, magnetism, ultrasound, and light (Vallet-Ragi et al., 2004; Vallet-Regi et al., 2001). Considering that nanoparticles employed in drug delivery are required to appropriate pore size, and a narrow structure and channel, Santa Barbara Amorphous (SBA) are considered to be appropriate for this study. SBA-15 is substantial mesoporous silica that has significant and limited properties of mesopores that are well organised. Its wall is thick and hydrothermally stable, has a huge surface area, and the volume of its pores is large (Rahmat et al., 2010). The pore size of SBA-15 is 7.2- 9.9 nm. It also consists of pore sizes that are regularly ordered spheres (100 – 150 nm) and rods (700 – 800 nm) respectively. The main application of SBA- 15 is in biorefinery production (Rahmat et al., 2010).

Kim et al (2011) discuss one developing application of nanotechnology medicine which deploys nanoparticles for the transmission of drugs, and other substances to specific types of cells and tissues. According to Yin et al. (2013), one of the reasons why nanoparticles are preferred when compared to standard methods of delivering drugs has to do with the fact that their exterior surfaces can be conjugated to proteins for example cytokines and antibodies so that they can be delivered to a specific location in the body. For in vivo application, porous silica nanoparticle has indicated considerable possibilities (Tasciotti et al. 2008; Low et al. 2009; Gu et al. 2013).

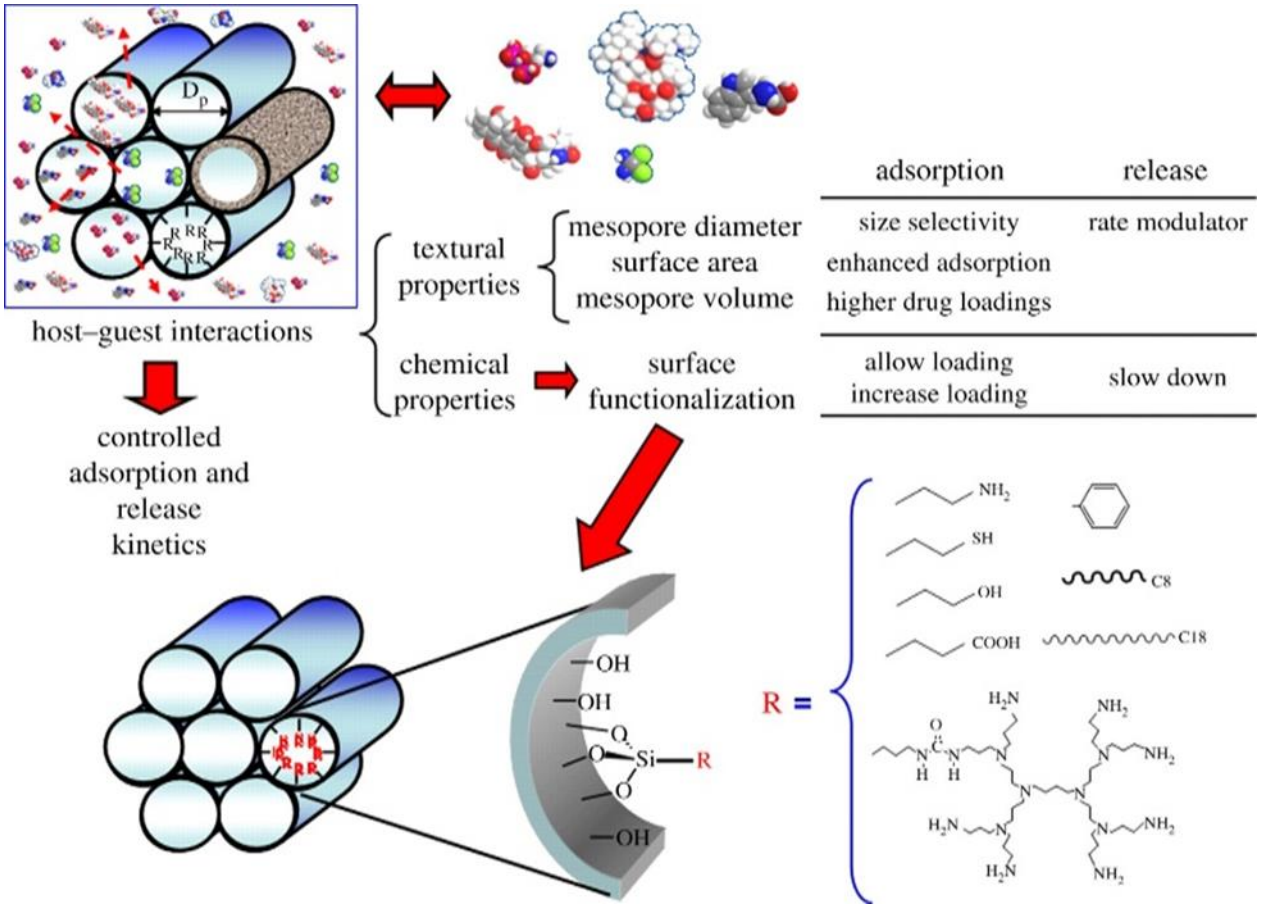

Figure 1.9: Parameters that govern the loading and release rate of drug molecules in silica-based ordered mesoporous materials. Functionalization of mesoporous materials with functional alkoxysilanes (R is the organic group). https://royalsocietypublishing.org/doi/10.1098/rsta.2011.0258 ((Vallet-Regi et al., 2012).

According to Vallet-Regi et al., 2007 and Vallet-Regi et al., 2012, mesoporous silica nanoparticles (MSNPs) are composed of channels that are ordered and packed close to each other, permitting the nanoparticles to play the role of a nanocontainer figure 1.9. The molecules adsorbed into the pores come out under constrained diffusion from the entrance of the pore. According to Al-Shanti & Aldahoodi (2006) nanoparticles can be used for drug delivery in slow release because they can be manipulated to have surface to volume ratios that are very high. Since they were discovered, different kinds of Mesoporous such as SBA-15, MCM-41, MCM-51 and MCM-48, have been developed.

However, for purposes of clinical applications, the SBA-15 is seen as the most suitable controlled drug delivery method (Izquierdo-Barba et al. 2009; Vavsari et al. 2015).

The administering of IGF-1 inside loaded MSNPs does not only have the possibility of prolonging the accessibility of bioactive IGF-1; but also comes with the extra benefit of slow release on a continuous basis. The benefit of this it could be the delivery of doses of IGF-1 which are higher without the risk associated with marked hypoglycaemia (Cheetham et al. 1997).

1.6 Aims and Objectives

The overarching aim of the PhD project was to develop a novel approach to manipulate NMJ formation and function using simplified bioengineered entirely NMJ platform. This was achieved through chemical and biological objectives:

Chemical objectives

1. Fabricate of mesoporous silica nanoparticles (MSNPs) SBA-15 and MCM-41.
2. Characterise MSNPs SBA-15.
3. Optimise the non-toxic concentration of SBA-15.

Biological objectives

1. Investigate the effects of slow release of IGF-1 on muscle (drug release study).
2. Generate and characterise human NMJ platform.
3. Investigate the impact of slow release of IGF-1 on NMJ formation and function.
4. Investigate the effects of slow release of IGF-1 on the bi-directional communications between motor neuron and muscle and endogenously secreted neural growth factors.

Chapter 2: Materials and Methods

2.0 Materials

All materials were purchased from Sigma Aldrich and used as received, unless otherwise noted. Tetraethoxysilane (TEOS), cetyltrimethylammonium bromide (CTAB), ethanol, methanol, hydrochloric acid (37%), sodium hydroxide, sodium chloride, potassium chloride, magnesium sulphate, calcium chloride, trimethylbenzene (TMB), human insulin, hydrocortisone, carboxymethylcellulose (medium viscosity), glutaraldehyde, and Pluronic P123 were all obtained from Sigma. All cell and tissue culture media and supplements were purchased as sterile. Heat-inactivated (HI), foetal bovine serum (FBS), and HI new born calf serum (NCS) were purchased from Gibco (Paisley, Scotland); HI horse serum (HS) was from TCS Biosciences (Corby, England); penstrep (penicillin and streptomycin) and trypsin from Bio Whittaker (Wokingham, England); L-glutamine from BDH (Poole, England), gelatine from Sigma (St Louis, MO, USA). Glassware, distilled water (dH2O) and phosphate buffered saline (PBS; Oxoid, Hampshire, England) were autoclaved prior to use. Sterile plasticware was purchased from Greiner Bio-one (Kremsmunster, Austria) unless otherwise stated. Recombinant human IGF-1 was obtained from Calbiochem (Nottingham, England).

2.1 Methods

2.1.0 Synthesis of dye labelled Mesoporous Silica Nanoparticles (MCM-41, small pore size)

Stöber methods, was used to fabricate the MCM-41. N-cetyltrimethylammonium bromide (CTAB) 1.0 g (2.7 x 10^{-3} mol) was dissolved in deionised water 480 ml. Sodium hydroxide 3.5 ml (2.0 M) was added to the solution and stirred vigorously at 80°C. Tetraethyl orthosilicate (TEOS) 5.0 ml (2.6 x 10^{-3} mol) and fluorescein isothiocyanate FITC-APS was added dropwise to the solution containing CTAB. This mixture was stirred for 2 hours at 80°C, giving rise to white precipitates (MSNs). The round bottom flask from condenser was removed and the decanted equally into two 240 ml centrifuge bottles (Weighing was done to ensure equal distribution) and then centrifuged at 6000rpm for 15 minutes. The supernatant was then removed and stored in a large brown bottle or a clear bottle wrapped in foil. This product was filtered and then washed with deionized water and methanol. Next, the surfactant template (CTAB) needed to be removed. This was done by acid extraction. A suspension of 1.0 g of the product was in static condition left overnight at 50°C in methanol solution 100 ml and concentrated HCl 1ml. The template removed solid product and was centrifuged and dried at 60°C in the oven for 1-2 hours (Trewyn et al., 2007).

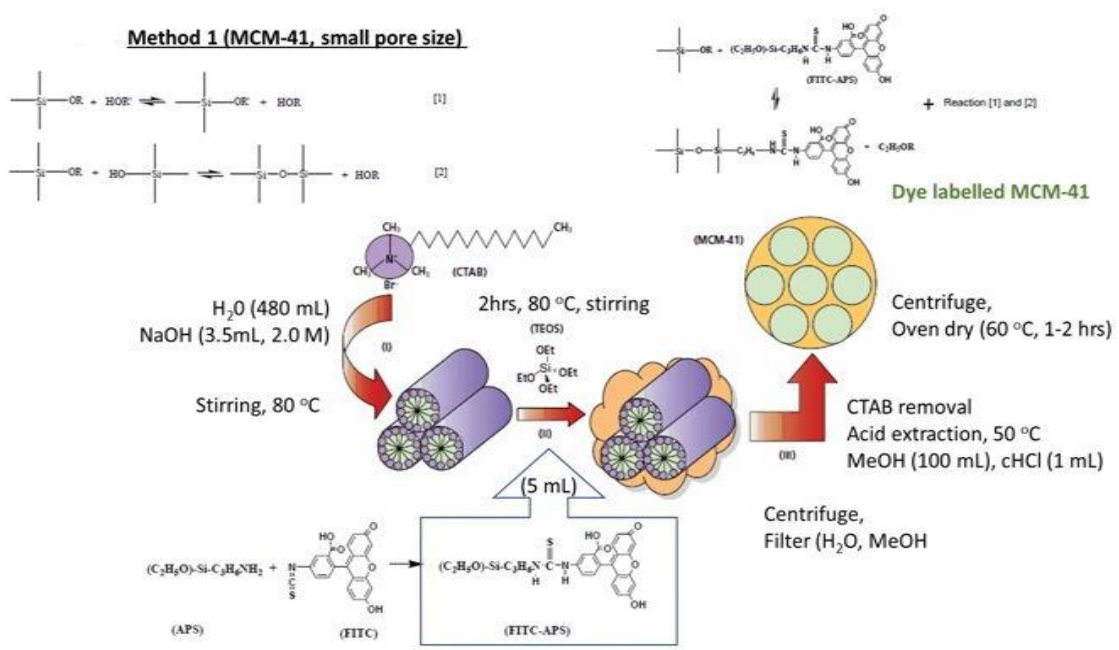

Figure 2.0: Explain method 1, which is a synthesis of dye labelled Mesoporous Silica Nanoparticles (MCM-41, small pore size).

2.1.1 Synthesis of dye labelled Mesoporous Silica Nanoparticles (MCM-41, large pore size)

N-cetyltrimethylammonium bromide (CTAB) 1.0 g (2.7 x 10^{-3} mol) was dissolved in deionised water measuring 480 ml and sodium hydroxide measuring 3.5 ml (2.0 M). Mesitylene 7.0 ml (48.8 mmol) was then added to the solution and stirred vigorously at 80 °C for 2 hours. Tetraethyl orthosilicate (TEOS) 5.0 ml (2.6 x 10^{-3} mol) was added dropwise to the solution containing CTAB. This mixture was stirred for another 2 hours at 80°C, giving rise to white precipitates (MSNs). This product was centrifuged at 6000rpm for 15 minutes. Next, the surfactant template CTAB and mesitylene molecules were removed by acidic extraction. A suspension of 1.0 g of the product was in a static condition and left overnight at 50°C in methanol solution 100 ml with concentrated HCl 1ml. The template removed solid product and was centrifuged and dried at 60°C in the oven for 1-2 hours (Slowing,Trewyn, and Lin., 2007).

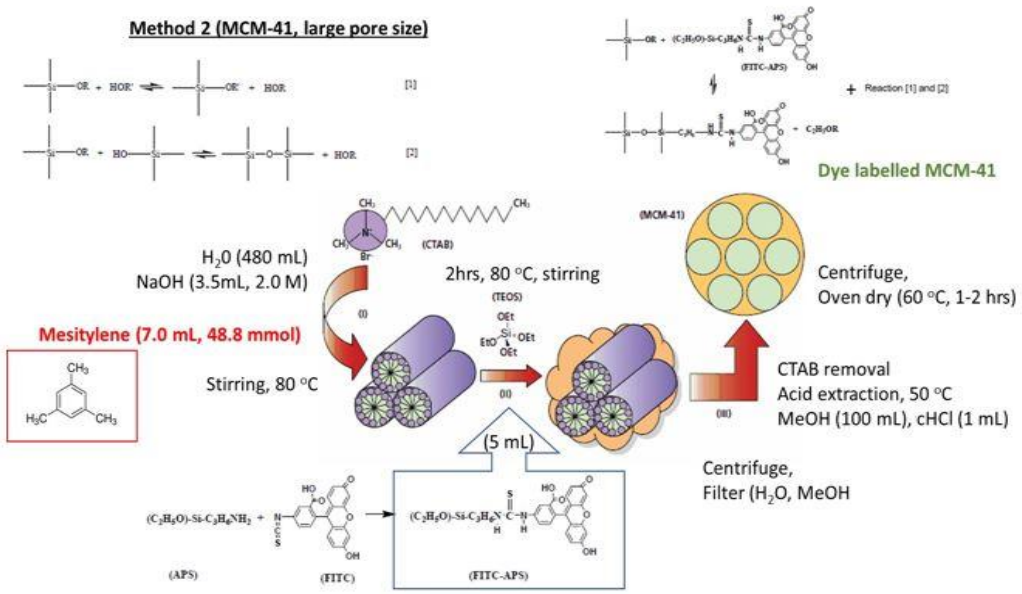

Figure 2.1: Explain method 2, which is a synthesis of dye labelled Mesoporous Silica Nanoparticles (MCM-41, large pore size).

2.1.2 Synthesis of dye labelled Mesoporous Silica Nanoparticles (SBA-15, small pore size)

SBA-15, with the average pore size of 9 nm, was prepared with a hydrothermal synthesis using Pluronic P123 (a PEG-PPG-PEG block copolymer, Aldrich) as a structure directing agent and tetraethyl orthosilicate (98% TEOS, Aldrich) as a silica precursor. First Pluronic P123 (2 g) was dissolved in a mixture of distilled water 50g and hydrochloric acid 12g (37% HCl, Aldrich) at 24 C under magnetic stirring. After 3 hours, the Pluronic P123 solution was placed in an oil bath at 24^{o}C .TEOS 4.25g was added drop-wise under vigorous stirring and prepared dye 505 µl (FITC-APS (0.002 g) + Ethanol anhydrous instead of DMF) was added. After 10 min, the mixture was kept under static conditions at 39^{o}C and left there for 20 hours. In the next day, the silica suspension was transferred into a Teflon-lined autoclave and placed in an oven for hydrothermal treatment at 100^{o}C for 24 hours. A suspension of 2g of the product, in a static condition, was left overnight at 59°C in methanol solution 100 ml with concentrated HCl 1ml. The template removed solid product which was centrifuged at 6000rpm for 15 minutes and dried at 60°C in the oven for 1-2 hours (Ukmar at al. 2011).

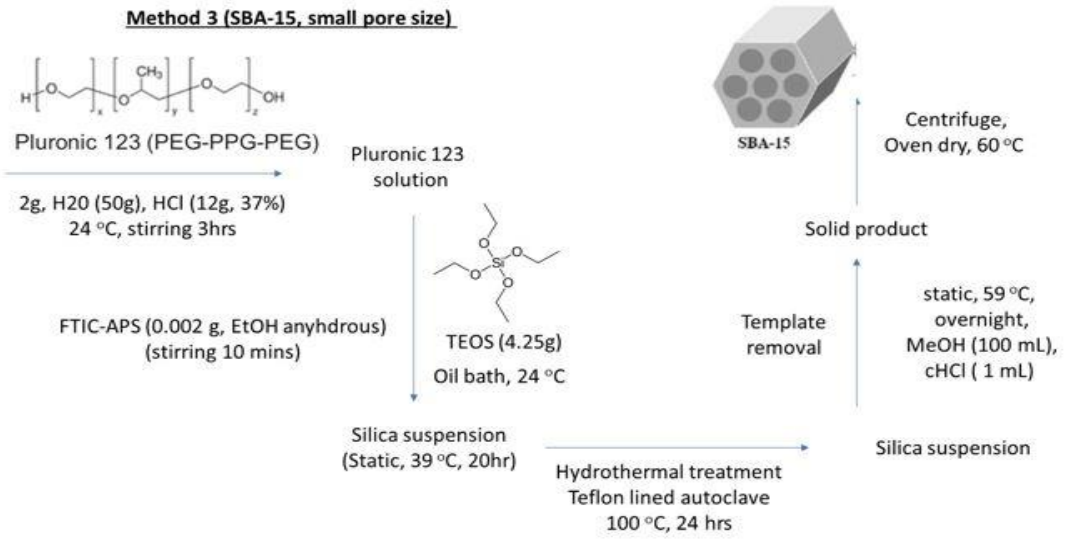

Figure 2.2: Explain method 3, which is a Synthesis of dye labelled Mesoporous Silica Nanoparticles (SBA-15, small pore size).

2.1.3 Synthesis of dye labelled Mesoporous Silica Nanoparticles (SBA-15, large pore size)

Conventional mesoporous SBA-15 materials were synthesized using Pluronic P123 triblock copolymer as a template and TEOS as a silica source. In a typical synthesis, P123 1.0g was added to a mixture of HCl 7.50g (2M) and H_2O 30g aqueous solution in a Teflon-lined container, which was stirred at 35^oC. Then TEOS 2.10g and FITC-APS was added to this solution under vigorous stirring. The reactant composition was P123 : TEOS : HCl : H_2O (Scheme 1: Schematic illustration of the two methods for the synthesis of large pore mesoporous silica nanoparticles and the coordinate bond based pH-responsive drug delivery system). The SBA-15 particles were selectively functionalized with amino groups on the mesoporous surface and quaternary ammonium groups on the particle surface via the post-synthesis and co condensation methods. The mixture was kept static at 35^oC for 24 h, and then sealed in a polypropylene bottle at 100^oC under static conditions for another 24 h. A suspension of 1.0g of the product was in static condition and left overnight at 50°C in methanol solution (100ml with concentrated HCl 1ml). The template removed the solid product which was centrifuged at 6000 rpm for 15 minutes and dried at 60°C in the oven for 1-2 hours (Zheng, Huang, and Che, 2012).

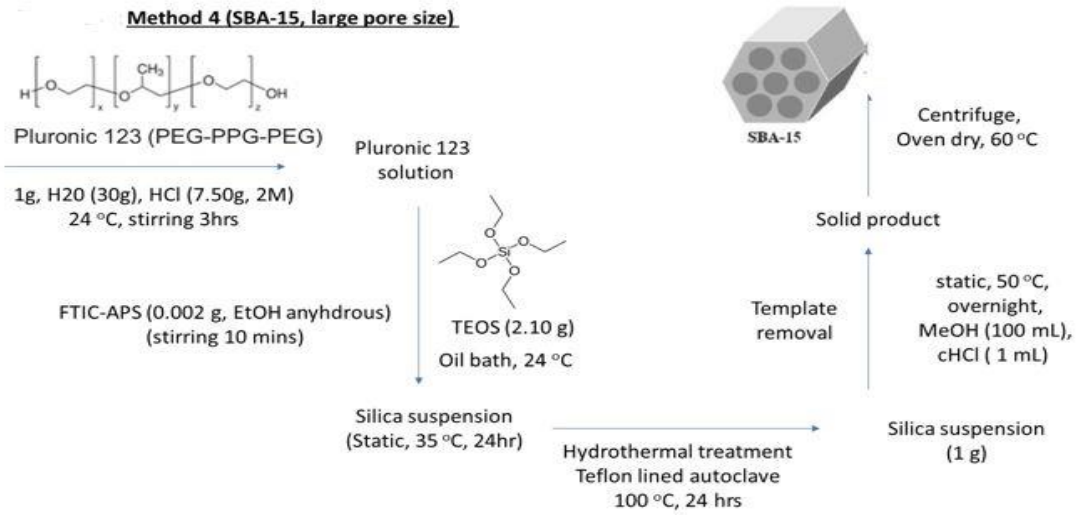

Figure 2.3: Explain method 4, which is a Synthesis of dye labelled Mesoporous Silica Nanoparticles (SBA-15, large pore size).

2.1.4 Fabrication of the dye Fluorescein isothiocyanate (FITC)

FITC-APS was prepared by placing fluorescein isothiocyanate (FITC, 0.002 g) into Eppendorf. This was followed by mixing anhydrous dimethyl formamide (DMF, 5 ml) with 3-amino propyl trimethoxy silane (APS, 50 µl). The next process involved taking 505 µl from the mixture solution of DMF with APS and adding it to the dye. The Eppendorf was then wrapped with foil, to prevent photo degradation. This mixture was stirred under nitrogen for two hours (Li et al., 2011).

2.1.5 Characterisation of the Mesoporous Silica Nanoparticles

2.1.6 Electron microscopy

2.1.7 SEM:

Scanning electron microscopy was conducted using a FEI/Philips XL30 FEG ESEM. Samples were dried and ground before SEM analysis. SEM images were analysed using Gatan Digital Micrograph Version 3.6.5. It gives information about the sample structure and can produce very high-resolution images of a sample surface, revealing details less than 1 nm in size (Argast and Tennis, 2004).

2.1.8 TEM:

Samples were pre-treated by sonication and vortexing for 2 hours. Transmission electron microscopy was conducted using a JEOL JEM 200CX or a JEOL JEM 2010 electron microscope operated at an accelerating voltage of 200 kV. The powder was suspended in ethanol and placed directly on a carbon-coated copper grid (Hettler et al., 2016).

2.1.9 Nitrogen adsorption

Nitrogen gas physisorption isotherms were measured in a Micromeritics Flowsorb apparatus. Surface area calculations were carried out using the Brunauer-Emmett- Teller (BET) method. Pore size distributions were calculated using the KJS adjustment of the thermodynamic-based Barrett-Joyner-Halenda (BJH) method (Li et al., 2021).

2.1.10 Size and zeta potential measurements

The particle size and zeta-potential measurement (surface charge) of the MSNs were measured using a Malvern Zetasizer NanoZS. Zeta-potential was calculated by Laser Doppler Electrophoresis (LDE) and size by dynamic light scattering (DLS). Samples were pre-treated by sonication and vortexing for 2 hours (Anuj et al., 2019).

2.1.11 Thermogravimetric analysis

The organic content on the different samples before and after protein adsorption was quantified by thermogravimetric analysis in a Mettler- Toledo TGA/SDTA851e apparatus (Wellisz et al., 2008).

2.1.12 X-ray diffraction

Powder X-ray diffraction data was obtained on a Philips X'pert diffractometer using Ni filtered Cu KR radiation with λ=1.54 Å. Samples were analysed from 0.3° to 70° 2θ. An endotoxin assay was conducted using the QCL-1000® test kit from Cambrex – samples were mixed with the LAL reagent and chromogenic substrate reagent over a short incubation period (16 minutes), and the absorbance was read at 408 nm. Using established protocols, which are already available within the chemistry division (Argast and Tennis, 2004).

2.1.13 FTIR

Spectra were obtained with a potassium bromide (KBr) disc of each mesoporous particle. This was performed upon a Thermo Scientific Nicolet 380 FT-IR spectrometer equipped with a Smart iTR diamond ATR device within the range 500-4000 cm^{-1} (Berthomieu and Hienerwadel, 2009).

2.1.14 Immortalized human myoblast

Our collaborating partners from the Institute of Myology made available the human myoblasts of 25 years SkMC (Mamchaoui et al., 2011). For purposes of preserving the cells, 10% dimethyl sulfoxide (DMSO) and 90% foetal bovine serum (FBS) were used. The cells were then stored in at a density of $1x10^6$ cells in 1 ml on frozen vial. For the proliferation, the cells in the vial were defrosted before being moved into a conical tube of 9 ml growth media (GM) (Table2.0).

Table 2.0: Growth media for SkMC proliferation

Growth media components	Concentration
Dulbecco's Modified Eagle's Media (DMEM) from Lonza (Nottingham, UK)	60% (v/v)
Medium 199 with Earle's BSS from Lonza (Nottingham, UK)	20% (v/v)
Heat inactivated foetal bovine serum (FBS) from Gibo (Loughborough, UK)	20% (v/v)
L-glutamine from Lonza (Nottingham, UK)	1% (v/v)
Fetuin from foetal bovine serum from Sigma-Aldrich (Dorset, UK)	25µg/ml
Recombinant human fibroblast growth factor-basic (FGFb) from Gibco (Loughborough, UK)	0.5ng/ml
Recombinant human epidermal growth factor (EGF) from Gibco (Loughborough, UK)	5ng/ml
Recombinant human hepatocyte growth factor (HGF) from Sino Biological Inc. (Suffolk, UK)	2.5ng/ml
Recombinant human insulin from Sigma-Aldrich (Dorset, UK)	5µg/ml
Dexamethasone from Sigma-Aldrich (Dorset, UK)	0.2µg/ml
Penicillin/Streptomycin (Sigma, UK)	1% (v/v)
Plasmocin (InvivoGen, UK)	1:1000 (50 µl)

2.1.15 Human skeletal myoblast cultures

In different flasks, the 25-year-old cells (C25) were plated. Each flask contained 10ml growth media (Table 2.0). The flasks with the C25 were kept at a temperatures of 37ºC and 5% CO_2 until the density of the cells was between 70% and 80% (the percentage of the covered area within the total area of view). Once the 70% to 80% of confluence was reached, Dulbecco's Phosphate Buffered Saline (DPBS) (Lonza, Nottingham, UK) was used to wash the cells twice, when the GM had been taken out of the flask. This was followed by the application of the Gibco-obtained 2 ml of TrypLE™ Express Enzyme (Loughborough, UK) and incubated in a temperature of 37°C in 5% CO2 over 5 minutes so that the cells could detach. Following this, the cell suspension was transferred into a conical 15 ml tube with 8 ml GM and centrifuged for 5 minutes at 1200xg. Using 5 ml GM, the pellet was re-suspended, and through cell count, the viable cells were measured.

2.1.16 Haemocytometer

A cell count was achieved using a haemocytometer. The process involved 1:1 ratio, mixing a 20 µl Trypan blue stain (0.4%) and 20 µl of cell suspension solution, all obtained from Lonza (Nottingham, UK). A pipette was used to apply the cells into the haemocytometer chambers. Using a microscope light, the cell was counted in each chamber's four large corner squares (16 squares) (as illustrated by the blue colour in Figure2.5). The only cells that were counted were the ones which were visible. The visibility of the cells was achieved by the Trypan blue as it is a crucial stain that is removed from cells that are live. A hand tally counter (Figures 2.4-2.6) was used for counting the cells in all eight corner squares. Once the cells in each square had been counted, the next task involved the calculation of the cell concentration. This was achieved using the equation: *average amount of live cells within 1 large corner square x dilution element x conversion factor* (10^4) = *cell concentration per ml*. A ratio of 1:1 was used. This leads to the dilution factor being equal to 2. A single large square's volume equals $1mm^2$ with the conversion factor equalling 10^4. On the other hand, the cell suspension layer equals 0.1mm; consequently 1mm2 x 0.1mm = 0.1cm x 0.1cm x 0.01cm =$10^{-4}cm^3$ = 10^{-4}ml, according to the illustration in Figure 2.5 (Public Health England – Culture Collections, 2013).

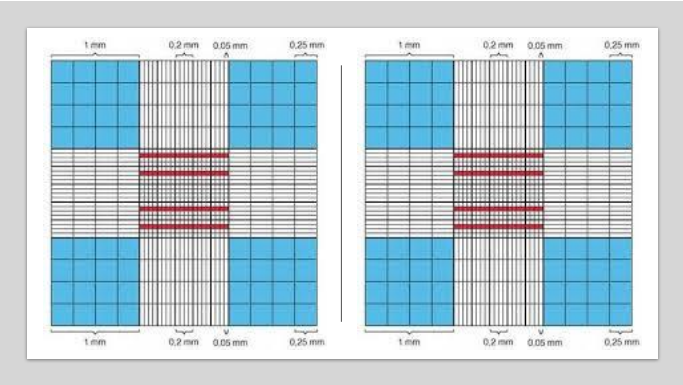

Figure 2.4: Schematic representation of the haemocytometer as visualised under a microscope; all eight squares highlighted in blue were counted (Khan& Khan, 2012).

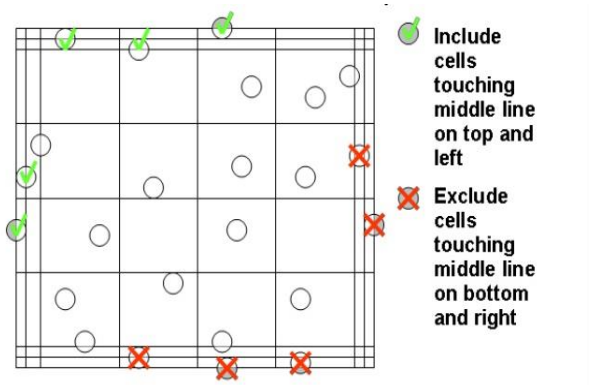

Figure 2.5: Shows one of the squares shown in blue in Figure 2.4. To ensure accuracy and consistency the counting method adapted from Sigma Aldrich (2018) was used.

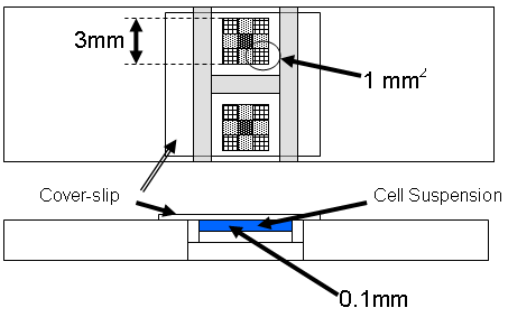

Figure 2.6: Dimensions of the haemocytometer; retrieved from (Public Health England – Culture Collections, 2013).

2.1.17 IGF-1 loading and release

DyLight 488 was used for IGF release. It is recommended by the manufacturer to mix DyLight with IGF in a 16-molar ratio. 1 mg of IGF was reconstituted in 1 ml distilled water. Thereafter, 100 µl (100µg) was taken from the 1 mg/mL IGF solution (7500 MW) and mixed with 13 µL of DyLight 488 NHS Ester (10 mg/mL) and the solution was incubated for 1 hour. After 1 hour of dialysis, a tube was used to clean unbound DyLight. Subsequently, 113 µl of labelled IGF was mixed with 900 µl PBS (pH 7.2). Thereafter, 1 ml of labelled IGF was added to 1.5mg of MSNs and left for incubation for 4 hours. After this period the sample was spun down and the supernatant was removed so that the fluorescence can be measured. Then, 1 ml of fresh PBS (pH 7.2) was added to a nanoparticles (NPs) pellet, and the release study was started. The sample was regularly centrifuged over certain time periods, namely 2 hours, 4 hours, 8 hours, 16 hours, 24 hours, 48 hours and 72 hours. Next, the fluorescence of the supernatant was measured to estimate the release of the labelled IGF-488 from the MSN (Kempen et al. 2015). In addition to uploading study, ELISA was performed. Then, 0.75mg of nanoparticles was added to 1ml of PBS and mixed together for 15 minutes in the rotator. Thereafter, 12.5µL of IGF-1 was added to the mix (NP+PBS+IGF). The substances were mixed together and placed in the rotator for 4hrs. After 4 hours, the mixture was centrifuged (speed 6000rpm for 5 minutes) and the supernatant was discarded. Thereafter, 5ml of DM was added to the nanoparticles and the solution was transferred to be added to SkMC (C25).

2.1.18 Uploading IGF-1Study

A total of 50µg (50 µl) of IGF was used: 25µg for uploading study and 25µg for standard curve (25µg dissolved in 1ml PBS). NPs (1.5mg) was dissolved in 1ml PBS with 25µg, rotated for 4hrs at room temperature with standard tube IGF uploading, 100 µl /well.

Standard curve plotting: 25µg/ml, serial dilution (1:1) was applied as follow (6 tubes): 25µg; 12.5µg; 6.25µg; 3.12µg; 1.56µg and 0.78 µg.

BCA protein kit was used. Reagent A (50 part) mixed with reagent B (1 part), then BCA reagent and sample mixed with ration 1:1 (100 µl of BCA reagent + 100 µl samples or standard).

2.1.19 Cell treatment

At a concentration of $1.5x10^5$ cell/ml in GM, the C25 was seeded in a 0.5% gelatine pre-coated 12-well plate. Over a period of 24 hours, the incubation of the cells was done in an environment with 5% CO_2 and a temperature of 37°C. This was followed by a process were DPBS was used to rinse the cells two times after the GM was extracted. After adding the differentiation media, DM (Table 2.1), to each well, the cells were incubated in an environment of 5% CO_2 and a temperature of 37°C for 96 hours. Contract microscopy was used for phenotypic differentiation for alignment, fusion, and elongation. The process of comparing the control's differentiation parameters and for the various conditions in cell treatment was achieved using immunofluorescence microscopy.

Confluence at specific intervals was measured using ImageJ software. This was achieved by adding together the whole myoblast area (MA). To complete this, the whole myoblast area over the total image x 100 was counted (Ricotti et al., 2011; Ren et al., 2008). For the assessment, five fields of view at a magnification of 10 times were selected. For each treatment, an aspect ratio was applied through dividing the length of the myotube by its width, for the differentiation parameter. This was in addition to the fusion index, a process involving taking the aggregate of the myotubes within a field and dividing it by the cumulative area of the field x 100. Table 2.2 presents the equations.

2.1.20 Cell treatment with IGF

Once the 0.5% gelatine was used for pre-coating the 12-well plate, at a concentration of $1.5x10^5$ cell/ml, the C25 was seeded in GM. This was followed by incubation in an environment of 5% CO2 and a temperature of 37°C for 24 hours. This was followed by the process of using DPBS to rinse the cells twice after the GM had been removed. To each cell, differentiation media was introduced. The IGF-1 concentrations of the differentiation media in each cell were different. The cells were then incubated in an environment of 5% CO_2 in temperatures of 37°C over 96 hours. The concentrations of IGF-1 used were 5 ng, 10 ng, 20 ng, 40 ng, 80 ng and 160 ng. In all studies, the incubation happened in an environment of 5% CO_2, a temperature of 37°C, over a period of 96 hours. Varying concentrations were used with the aim of determining if they boosted differentiation and proliferation. Hence, for this study, the proliferation marker Ki67 was used together with MHC and DAPI. Red dots were used to denote that Ki67 marker. From each condition, five images were selected. From each image, the total of red dots was counted, and eventually, the average number was employed in statistical analysis (ANOVA), to identify noteworthy variances. For purposes of comparison,

differentiation parameters were applied to each condition. The same technique was employed for five images from five experiments, and the average number was employed for statistical analysis.

2.1.21 Cell treatment with IGF-1 and nanoparticles

Mesoporous silica nanoparticles (0.75mg + 1ml PBS) were used for cell treatment together with IGF-1 after loading, and a release study 10 ng of IGF-1 was used; hence, for this concentration more differentiation was observed than proliferation. A pre-coated 0.5% gelatine 12-well plate was seeded with $1.5x10^5$ cell/ml in GM for the human SkMC (C25). The treatment was then incubated in an environment of 5% CO_2 at a temperature of 37°C for 24 hours. This was followed by the extraction of the GM and the rinsing of the cells twice using DPBS. To each well, DM was added with uploaded IGF-1 with MSNPs and then incubated in an environment with 5% CO_2 and a temperature of 37°C. The IGF-1 size was 3 nm, and the pore size for SBA-15 was 9nm, a situation that permitted the upload of IGF-1. Using DAPI, Ki67, and MHC, together with immunohistochemistry, differentiation parameters were applied.

Table 2.1: Differentiation media

Differentiation media components	Concentration
Dulbecco's Modified Eagle's Media (DMEM) from Lonza (Nottingham, UK)	500 ml
L-glutamine from Lonza (Nottingham, UK)	1% (v/v)
Recombinant human insulin from Sigma-Aldrich (Dorset, UK)	10 µg/ml
Penicillin/Streptomycin (Sigma, UK)	1% (v/v)
Plasmocin (InvivoGen, UK)	1:1000 (50 µl)

Table 2.2: Parameters of differentiation

Differentiation parameters	Formula
Aspect ratio (AR)	(myotube length) / (myotube width)
Fusion index (FI)	(nuclei in each myotubes in a field) / (total nuclei of the field) (100)
Myotube area (MA)	(total area of myotubes in a field) / (total area of the field) (100)

2.1.22 Expansion of Neural progenitor cells (NPCs)

The Neural progenitor cells (NPCs) used were derived from human embryonic stem cells (hESCs) and transfected with green fluorescent protein (GFP)-reporter lentivirus system, donated by the Skeletal Muscle Group at Manchester Metropolitan University (Abd Al Samid et al., 2018). NPCs, therefore, visually appeared green under a fluorescent microscope. A 1ml cryovial containing $0.5x10^6$ green fluorescent protein (GFP) transfected NPCs suspended in 90% fetal bovine serum (FBS) and 10% (v/v) dimethyl sulfoxide (DMSO) was thawed and transferred onto a laminin coated T25 flask (prepared 72 hours earlier) and incubated at 37°C in a 5% CO2 environment. Prior to the transfer, NPCs were integrated with 4ml neural expansion media (NEM) to initiate NPC expansion (Table 2.3). The NPC medium was renewed every 2 days for 6 days with 5ml NEM until a cell confluence of 80% was attained.

Table 2.3: Neural Expansion Medium (NEM)

NEM components	Volume/concentration
Dulbecco's Modified Eagles Media (DMEM)- F12 (1:1) from Lonza (Nottingham, UK)	48.5 ml
MEM Non-essential amino acids (NEAA) (Life Technologies, UK)	0.5ml (1x)
Penicillin/Streptomycin (Sigma, UK) (100x)	0.5 ml (1x)
bFGF (R&D systems, UK) (100 µg/ml)	10 µl (20ng/ml)
N2 supplement (Life Technologies, UK) (100x)	0.5 ml (1x)
Heparin (Sigma, UK) (2mg/ml)	50 µl (2 µg/ml)
B27 supplement (Life Technologies, UK) (50x)	1ml (1x)

2.1.23 Measurement of axonal growth in co-culture (nerve-muscle)

The NPCs with a GFP-reporter lentivirus in the *in vitro* co-culture model were imaged under the fluorescent microscope (Leica CTR 6000), over the 7 days of culture with different treatments like NPs, IGF-1, IGF-1/NPs and DM only as control. The axonal length of the differentiating motor neurons were measured over 7 days *in vitro* using Image J (procedure illustrate in figure 2.7), assessed at X20 magnification (at least five random fields of view selected).

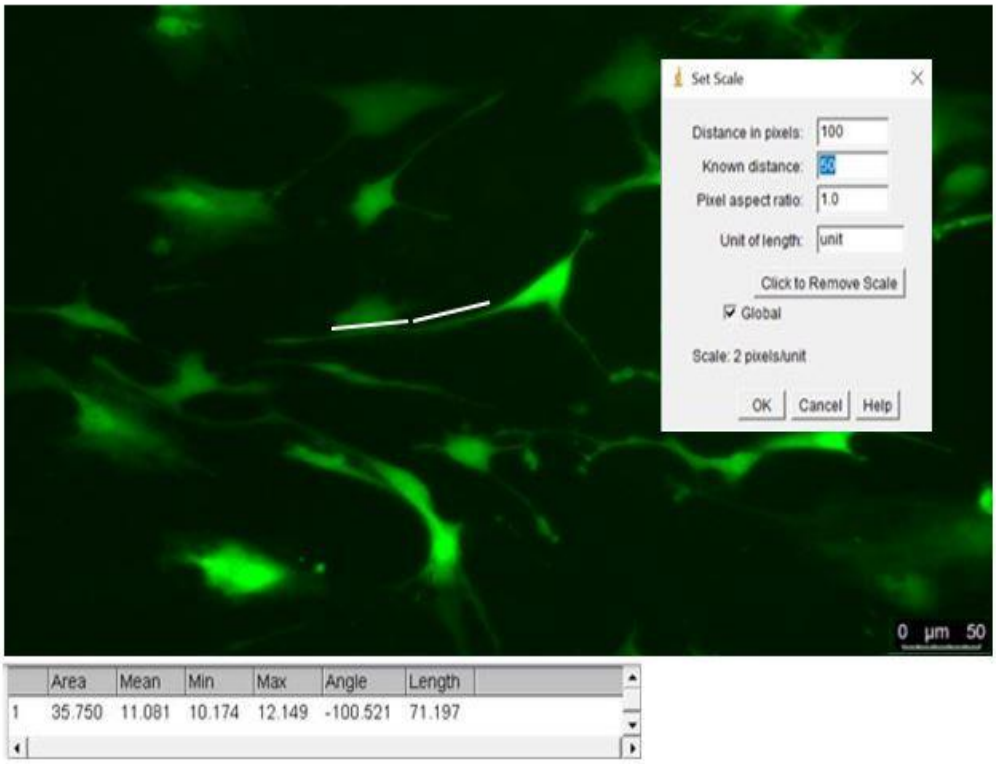

Figure 2.7: Axonal length measurement of motor neurons using Image J software. Images were measured using fluorescent microscope (Leica CTR 6000), over the 7 days of culture with different treatments like NPs, IGF-1, IGF-1/NPs and DM only as control. The axonal length was measured using Image J software and using "analyse→tools→ROl manger" function tab and the same procedure was used for all the images. These were assessed at X20 magnification (at least five random fields of view selected).

2.1.24 Immunocytochemistry

Cells were washed two times with DPBS at 96 hours. At a temperature of 21°C, 4% paraformaldehyde was used to fix the cells for 10 minutes. Using DPBS, the fixed cells were washed two times. This was followed by the process of permeabilising the cells using a 1x perm/wash buffer (BD Biosciences, Oxford, UK). Soon after, the cells were incubated at a temperature of 21°C for 30 minutes. The cells were then washed two times using DPBS for the final time. This was followed by adding a blocking solution of 0.2% Triton X-100 with 10% normal goat serum (GS) or horse serum (both obtained from Sigma-Aldrich (Dorset, UK)) before the cells were incubated for 60 minutes. Using DPBS, the cells were washed once more when the blocking solution had been removed. In the main antibody solution, there was 3% goat serum or horse serum with 0.05% Tween-20 (Sigma-Aldrich, UK). Before being incubated at a temperature of 4°C for 24 hours, Ki67's primary antibodies were added to the cells. Using DBPS, the primary antibodies were washed twice followed by incubation with matching secondary bodies after 24 hours. The incubation happened for one hour in an environment that also had 2 ng/ml 4′, 6-Diamidine-2′-phenylindole dihydrochloride (DAPI) from Sigma-Aldrich (Dorset, UK) and 5 μg/ml Anti-Myosin Heavy Chain Alexa Fluor® 488 from eBioscience (Hatfield, UK), at a temperature of 21°C. The Leica DMI6000 B inverted microscope obtained from Leica Microsystems (Milton Keynes, UK) was used for the confirmation of innervation for fluorescent microscopy. The qualification of the differentiation parameters was achieved through the use of ImageJ (Table 2.2).

2.1.25 Human Growth Factor Array

In parallel experiments were conducted to compare the concentration of 40 human growth factors (Table 2.4). One ELISA-based microarray standard glass slide is spotted with 16 wells of identical growth factor antibody arrays (Human Growth Factor Antibody, Cambridge Bioscience, UK). Each well was spotted with different controls: positive control spot (a control for the amount of biotinylated antibody printed onto the array), negative control spot (buffer printed, to measure the baseline responses) and a blank spot (nothing printed, to measure the background response). Each antibody was arrayed in quadruplicate. The ELISA-based microarray analysis of the growth/neurotrophic factor concentration was used to determine whether the slow release of IGF-1 impacts the secretion of growth/neurotrophic factors in co-cultured conditions (untreated co-culture, co-culture with NPs, co-culture with IGF-1 and co-culture with IGF-1/NPs). Supernatant samples were collected from each condition for assessment using a human growth factor array kit on day 7, when spontaneous myotube contractions were first observed contracting in unison as a motor unit. Total protein concentrations was determined in all collected supernatant to ensure adding equal amount of the protein to microarray slide (0.5µg/µml). Preparation of standards and reagents in the array kit were completed using manufacturer guidelines. Subsequently, 100 µl of sample diluent from the array kit was added to each well and incubated at 23°C for 30 minutes to block slides. The wells were then decanted and 100 µl of standards, controls and supernatant samples were added to the individually assigned wells. The slides were sealed and incubated for 24 hours at 4°C on microplate shaker fixed to 500 rpm. Following incubation, the samples were decanted from the wells and the slides were washed 5 times for 5 minutes each time with 150 µl of 1X wash buffer 1, then washed 2 times for 5 minutes each time with 150 µl of 1X wash buffer 2. Next, 80 µl of detection antibody cocktail was added to each well and the slides incubated for 1.5 hours at 23°C. The detection antibody cocktail was aspirated from the wells and the wash steps with wash buffer 1 and wash buffer 2 were repeated once again. After washing slides, 80 µl of Cy3 equivalent dye-conjugated streptavidin was added to each well then sealed and incubated in darkness for 1 hour at 23°C. Following incubation, the wash steps were repeated once again. The slides were then separated from the well gaskets and placed into the provided slide washer/dryer tube. The tube was then filled with 30 mL of 1X wash buffer 1 to completely cover the slides and shaken gently for 15 minutes. The 1X wash buffer 1 was removed from the tube and 30 mL of 1X wash buffer 2 was added to completely cover the slides and gently shaken for 5 minutes. The slides were removed from the washer/dryer tube and dried with compressed air to remove residual buffer solution. Subsequently, the array was visualised with a GenePix 4000B laser scanner at 532nm wavelength. Raw data from the visualised array images was generated and processed with the GenePix Pro 4.1 Microarray Acquisition & Analysis Software, further statistical

analysis of the data was performed with the Ray Biotech Q-Analyser® tool Software for QAH-GF-1.

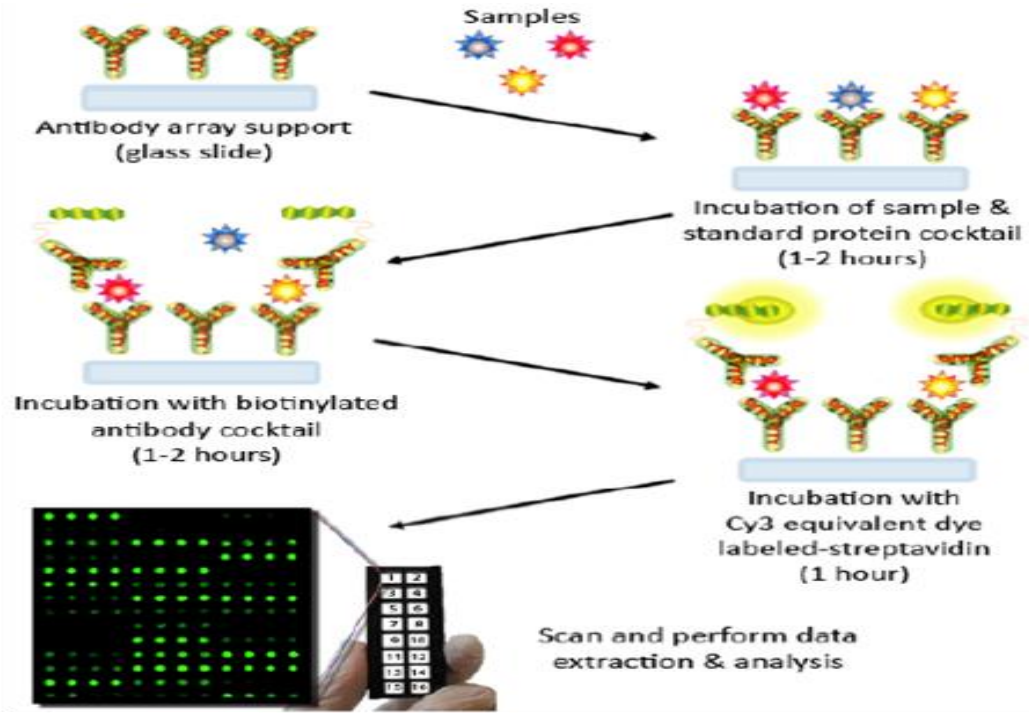

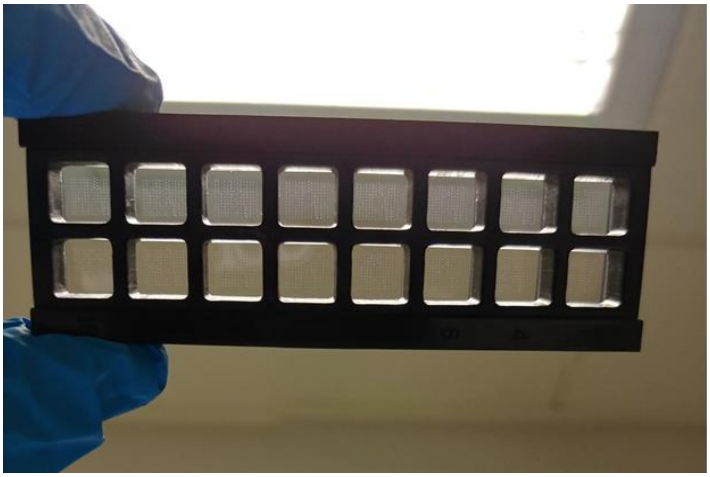

Figure 2.8: An illustration of the process of enumerating the growth /neurotrophic factors in the supernatant of (untreated co-culture, co-culture with NPs, co-culture with IGF-1 and co-culture with IGF-1/NPs). Using human growth /neutrophic factor microarray (adapted from Raybiotech, 2016).

Table 2.4: Descriptions of the human growth factors and neurotrophins quantified in aneural myotube cultures and co-cultured myotube supernatant.

Amphiregulin (AR) (Colorectum cell-derived growth factor) (CRDGF)
Brain-derived neurotrophic factor (BDNF) (Abrineurin)
Fibroblast growth factor 2 (FGF-2) (Basic fibroblast growth factor) (bFGF) (Heparin-binding growth factor 2) (HBGF-2)
Bone morphogenetic protein 4 (BMP-4) (Bone morphogenetic protein 2B) (BMP-2B)
Bone morphogenetic protein 5 (BMP-5)
Bone morphogenetic protein 7 (BMP-7) (Osteogenic protein 1) (OP-1) (Eptotermin alfa)
Beta-nerve growth factor (Beta-NGF)
Pro-epidermal growth factor (EGF) [Cleaved into: Epidermal growth factor (Urogastrone)]
Epidermal growth factor receptor (EC 2.7.10.1) (Proto-oncogene c-ErbB-1) (Receptor tyrosine-protein kinase erbB-1)
Prokineticin-1 (Endocrine-gland-derived vascular endothelial growth factor) (EG-VEGF) (Mambakine)
Fibroblast growth factor 4 (FGF-4) (Heparin secretory-transforming protein 1) (HST) (HST-1) (HSTF-1) (Heparin-binding growth factor 4) (HBGF-4) (Transforming protein KS3)
Fibroblast growth factor 7 (FGF-7) (Heparin-binding growth factor 7) (HBGF-7) (Keratinocyte growth factor)
Growth/differentiation factor 15 (GDF-15) (Macrophage inhibitory cytokine 1) (MIC-1) (NSAID-activated gene 1 protein) (NAG-1) (NSAID-regulated gene 1 protein) (NRG-1)
Glial cell line-derived neurotrophic factor (hGDNF) (Astrocyte-derived trophic factor) (ATF)
Somatotropin (Growth hormone) (GH) (GH-N) (Growth hormone 1) (Pituitary growth hormone)
Proheparin-binding EGF-like growth factor [Cleaved into: Heparin-binding EGF-like growth factor (HB-EGF) (HBEGF) (Diphtheria toxin receptor) (DT-R)]
Hepatocyte growth factor (Hepatopoietin-A) (Scatter factor) (SF) [Cleaved into: Hepatocyte growth factor alpha chain; Hepatocyte growth factor beta chain]
Insulin-like growth factor-binding protein 1 (IBP-1) (IGF-binding protein 1) (IGFBP-1) (Placental protein 12) (PP12)
Insulin-like growth factor-binding protein 2 (IBP-2) (IGF-binding protein 2) (IGFBP-2)
Insulin-like growth factor-binding protein 3 (IBP-3) (IGF-binding protein 3) (IGFBP-3)
Insulin-like growth factor-binding protein 4 (IBP-4) (IGF-binding protein 4) (IGFBP-4)
Insulin-like growth factor-binding protein 6 (IBP-6) (IGF-binding protein 6) (IGFBP-6)
Insulin-like growth factor I (IGF-I) (Mechano growth factor) (MGF) (Somatomedin-C)
Insulin [Cleaved into: Insulin B chain; Insulin A chain]
Macrophage colony-stimulating factor 1 receptor (CSF-1 receptor) (CSF-1-R) (CSF-1R) (M-CSF-R) (EC 2.7.10.1) (Proto-oncogene c-Fms) (CD antigen CD115)
Tumor necrosis factor receptor superfamily member 16 (Gp80-LNGFR) (Low affinity neurotrophin receptor p75NTR) (Low-affinity nerve growth factor receptor) (NGF receptor) (p75 ICD)
Neurotrophin-3 (NT-3) (HDNF) (Nerve growth factor 2) (NGF-2) (Neurotrophic factor)
Neurotrophin-4 (NT-4) (Neurotrophin-5) (NT-5) (Neutrophic factor 4)
Tumor necrosis factor receptor superfamily member 11B (Osteoclastogenesis inhibitory factor) (Osteoprotegerin)
Platelet-derived growth factor subunit A (PDGF subunit A) (PDGF-1) (Platelet-derived growth factor A chain) (Platelet-derived growth factor alpha polypeptide)
Placenta growth factor (PlGF)
Kit ligand (Mast cell growth factor) (MGF) (Stem cell factor) (SCF) (c-Kit ligand) [Cleaved into: Soluble KIT ligand (sKITLG)]
Mast/stem cell growth factor receptor Kit (SCFR) (EC 2.7.10.1) (Piebald trait protein) (PBT) (Proto-oncogene c-Kit) (Tyrosine-protein kinase Kit) (p145 c-kit)
Protransforming growth factor alpha [Cleaved into: Transforming growth factor alpha (TGF-alpha) (EGF-like TGF) (ETGF) (TGF type 1)]
Transforming growth factor beta-1 (TGF-beta-1) [Cleaved into: Latency-associated peptide (LAP)]
Transforming growth factor beta-3 (TGF-beta-3) [Cleaved into: Latency-associated peptide (LAP)]
Vascular endothelial growth factor A (VEGF-A) (Vascular permeability factor) (VPF)
Vascular endothelial growth factor receptor 2 (VEGFR-2) (EC 2.7.10.1) (Fetal liver kinase 1) (FLK-1) (Kinase insert domain receptor) (KDR)
Vascular endothelial growth factor receptor 3 (VEGFR-3) (EC 2.7.10.1) (Fms-like tyrosine kinase 4) (FLT-4) (Tyrosine-protein kinase receptor FLT4)
Vascular endothelial growth factor D (VEGF-D) (c-Fos-induced growth factor) (FIGF)

2.1.26 Functional Assessment of Neuromuscular Junction Formation

Co-cultures were functionally evaluated to validate the formation of NMJs via live phase contrast video analysis of myotube CF in response to agonist/antagonist treatments (Table 2.5). On Day 7, the co-cultured cell dishes were positioned onto an inverted microscope stage, which was enclosed by an incubation chamber to maintain atmospheric conditions of 37°C with 5% CO_2. Following 5 minutes of live observation of uninterrupted spontaneous myotube contractile activity, the co-cultures were treated with cholinergic antagonists to block AChRs at the NMJ.

Table 2.5: Treatments to inhibit or augment myotube contraction frequency via NMJ signal transmission.

Drug	**Concentration**
L-Glutamic acid (L-Glut)	400 µM
α-Bungarotoxin (α-BTX)	10 nM

The co-cultures were also treated with the glutamatergic receptor agonists to stimulate glutamate receptor on the motor neurons (MNs). The specified concentrations where selected based on previously established studies (Guo et al., 2011; Borodinsky and Spitzer, 2007; Das et al., 2007). The myotube CF was measured 30 seconds before the application of the treatments to the cells, to establish a baseline spontaneous CF. Subsequently, agonist or antagonist treatments were added to the dishes at the centre of the field of view. Modulation of CF was measured immediately upon application of the treatment to the cells. Live measurement of CF in response to treatment were also conducted again after 10 minutes, 15 minutes, 20 minutes, 30 minutes, 45 minutes 1 hour and 1hour 30 minutes. Following 1 hour and 35 minutes after treatment, the cells were washed three times with 500 µL of DPBS then fresh untreated DM was added to the cells. The dishes were placed back onto the microscope stage in the incubation chamber and CF was immediately measured again following the washout and resupply of DM. The CF was measured once again at 2 hours and 24 hours after the initial treatments. Live video analysis was conducted at 24 frames per second with phase contrast microscopy using the DMI6000 B inverted microscope with an N Plan 10x/0.25na Ph1 objective. Myotube CF was expressed as a mean ± SD.

2.1.27 Statistical analysis

Firstly, a normality test has been carried out using a Shapiro-Wilk test to determine if the data is normally distributed or not. If it's normally distributed then there will be a bell curve (Gaussian distribution) this means that it's parametric data and one-way ANOVA will be used. However, if the data is not-normally distributed data that means it's non-parametric and Kruskal-Wallis test will be used. Parametric tests are those that make assumptions about the parameters of the population distribution from which the sample is drawn. This is often the assumption that the population data is normally distributed. After that the GraphPad Prism software was employed in the analysis of results. The demonstration of the results is on the mean and standard deviation (±SD) of the mean. The Bonferroni's Multiple Comparison T-test and one way ANOVA were used for statistical analysis and the comparison of more than two means. At a level of 5% ($P<0.05$), the results were statistically significant. * denotes $P<0.01$, ** denotes $P<0.001$*** denotes $P < 0.0001$. The Bonferroni test is a type of multiple comparisons test used in statistical analysis. When performing a hypothesis test with multiple comparisons, eventually a result could occur that appears to demonstrate statistical significance in the dependent variable, even when there is none. Furthermore this statistical test is used to reduce the instance of a false positive. In addition, Bonferroni designed an adjustment to prevent data from incorrectly appearing to be statistically significant. The main limitation of Bonferroni correction is that it may lead analysts to mix actual true results (Hayes, 2020). Another analysis was used in this project which is the one-way analysis of variance (ANOVA) which is used to determine whether there are any statistically significant differences between the means of two or more independent groups and determining which of these groups differ from each other is important. In addition, a significant *P* value of this test refers to multiple comparison tests to identify the significant pairs (Mishra, et al., 2019) then in this test one continuous dependent variable and one categorical independent variable are used, where categorical variable has at least three categories. In Practical Statistics Software, SPSS (Analyze–compare means–one-way ANOVA) (Mishra, et al., 2019).

Chapter 3: Fabrication and Characterisation of Mesoporous Silica Nanoparticles (MSNPs)

3.0 Background

3.0.0 Introduction

Sometimes, because there is a lack of solubility and specification of drug molecules, patients remain with no option but to take drugs in high doses to get the required effects in disease treatment. In an attempt to deal with these challenges, several drug carriers are found in pharmaceuticals, which are employed in the delivery of therapeutic agents to a specific sit in the body (Bharti et al., 2015). A promising agent for dealing with the problems mentioned above is mesoporous silica materials, which have the ability to deliver effects in a way that is both controllable and sustainable. Specifically, mesoporous silica nanoparticles (MSNPs) are broadly employed as a delivery reagent since silica has some desirable chemical properties; it is biocompatible and thermally stable (Bharti et al., 2015). Silica's distinctive mesoporous construction enables drugs to be loaded effectively and eventually released in a controlled manner to the target site. It is possible to change the mesoporous properties such as the size of the pore, properties of the surface, porosity, and high drug loading. This ability depends on the preparation of the MSNPs. The active surface plays the role of facilitating functionalization to the changed surface and linked therapeutic molecules. MSNs are widely employed in the biomedical field in the areas of delivery of target drugs, diagnosis, cellular uptake, and bio-sensing. It is the aim of this review to deliver the prevailing knowledge about mesoporous nanoparticles that contain silica and how it is applied in different biomedical fields (Bharti et al., 2015). In recent times, the combination of MSNs with liposomes has been reported, leading to unique nanocarriers denoted as “protocells” (Butler et al, 2016) and this nanosystem shows the robustness and high loading and controlled release capability of MSNs with the low toxicity and immunogenicity of liposomes. Protocells open up novel expectations in the drug delivery development due to their potential to tackle multiple challenges, such as stability, specificity and high loading capacity for diverse loads (Villegas et al, 2018). For example a liposome was used as a drug delivery vehicle for administration of nutrients and pharmaceutical drugs, for instance lipid nanoparticles in mRNA vaccines and DNA vaccines (Li et al, 2019).

In the last ten or so years, several nanomaterials like mesoporous silica (Wang et al., 2015) have been used in the biomedical area for purposes of improving therapeutic results. In recent times, scholars have started to focus on exploring how stem cells are affected by biomaterials, in the process showing that the employment of biomaterials could present an effective alternative for c-kit-positive CSC

proliferation and migration. The mesoporous silica materials are among the biomaterials that have received the bulk of the attention as a drug release career for several biomedical uses. The reason behind this popularity has to do with its properties: the diameter of its pores, biocompatibility, and multifunctional surface features (Li et al., 2012). It is these features that place mesoporous silica materials among the effective careers for sustained IGF-1 discharge to lengthen the half-life (Yang et al., 2012; Chen et al., 2013).

3.0.1 Aims

The initial aim of this study is to use nanotechnology, mesoporous silica nanoparticles (MSNPs) as a system for delivering drugs in a safe, regulated, and slow discharge of IGF-1, in a manner that will lengthen the bioavailability of IGF-1 (half-life of serum IGF-1) while boosting its effectiveness. On this basis, the specific aims of the study are listed below.

- Fabricate mesoporous nanoparticles (MSNPs)
- Characterise mesoporous nanoparticles (MSNPs)
- Upload the IGF-1 into the mesoporous nanoparticles (MSNPs)
- Investigate the IGF-1 release from MSNPs (Drug release study)

3.1 Results

3.1.0 Fabricate mesoporous silica nanoparticles (MSNPs)

With the aim of examining if it is possible to fabricate MSNPs (MCM-41 & SBA-15), a succession of initial experiments has been carried out. Experiments have also been done to determine the cellular uptake and cytotoxic influence of mesoporous particles on cells. The researcher also examined if the MSNPs' pore size was big enough to permit for loading, into the MSNPs, the IGF-1 affinity and IGF-1. Considering that the cell surface is the area where the IGF-1 receptor is found, there is no need for MSNPs uptake. Hence, to facilitate my suggested project, the synthesis of MCM-41 & SBA-15 monodispersed mesoporous silica particles was conducted using the normal surfactant templating technique (Kresge et al. 1992). Template molecule selection and reaction concentration conditions are the techniques employed in regulating the diameter and porosity. The application of configuration was done as soon as the particles were formed. This happened before acid extraction was used to remove the surfactant molecules, with the results being a well-organised and regular porous arrangement.

MCM-41 MSNPs was fabricated and characterised carefully. This resulted in an even organisation of cylinder-shaped mesoporous, which create a pore system that is one dimensional (Reichinger, 2007). It consists of a pore diameter that can be adjusted independently, a distribution of pores that is sharp, this means a pore size distribution can be calculated easily, a big surface area measuring 1199m2/g and a big pore volume measuring in the range of 2.6 and 3.8nm, as is represented in Figure 3.7. It is easy to adjust the distribution of the pores (Silaghi et al., 2014).

Hydrothermally, MCM-41 NPs did not show stability. This was the result of the high levels of silicate units cross-linking so that they could attain a pore diameter which is defined. In the synthesis solution, surfactants are employed for purposes of forming micelles. From these, stencils that assist in building up the mesoporous structure are produced. Cetyltrimethylammonium bromide (CTAB) is used mostly for MCM-41.

Following the adding of silica species which cover the rod, micelles that look like the rods are initially produced by the surfactant. These rod-like micelles then organise into hexagonal arrays. After this, acid extraction was used to remove the template with Cetyltrimethylammonium bromide (CTAB). To accomplish this, there is a need for an adequate heat for 24 hours.

For this study, the synthesis of SBA-15 MSNPs took place as mentioned. The analysis of SEM indicated matching nanotube of SBA-15 MSNPs. Analysing the TEM showed that the SBA-15 MSNPs size could be about 800 nm to 1µm with the straight channel pores organised into a highly organised hexagonal shape as is indicated in Figure 3.5 (a, b). An analysis of the nitrogen

adsorption/desorption isotherm's sharp step shows clearly the well-arranged mesoporous structure of SBA-15 material. This is as a result of the nitrogen gas' capillary condensation/evaporation in the mesoporous at varying pressure levels. This depends on the size of the pore (in this case, 5-9 nm). Its surface area is also large (at 940 m^2/g), as is depicted in Figure 3.7.

3.1.1 Mesoporous silica nanoparticles (MSNPs) Characterisation

Producing mesoporous nanoparticles was done with the aim of creating arrangements of different particle porosity and size. A synthesis of 19 samples was done. They were completely characterised in both techniques SBA-15 and MCM-4. Around six samples were employed in this study for the purpose of confirming biodegradability, cytotoxicity, and the correct NP size to be employed for the uploading and release study.

From Table 3.0, below, can be seen the characteristics of the NPs: diameter, composition, porosity, and surface charge. With the aim of measuring the zeta potential and size, deionised water was used to re-centrifuge and dilute samples 1 to 7.

Table 3.0: MSNPs synthesised using Methods 1-4 Characteristics.

Sample No.	1	2	3	4	5	6	7
sample Name	MCM-41	MCM-41	MCM-41	MCM-41	MCM-41	SBA-15	SBA-15
production date	15/04/2013	17/04/2013	21/05/2013	28/05/2013	11/07/2013	19/06/2013	02/07/2013
weight (g)	1.1349	1.1821	0.124	0.4156	4.6944	0.55	0.4722
FITC-APS	yes	yes	no	no	yes	yes	yes
Mesitylene	no	no	no	no	no	no	no
Shape	sphere	sphere	sphere	sphere	sphere	rod	rod
size (nm)	240.5	312.6	611.7	248	405.2	1302	1651
zeta potential (mV)	-40.6	-36.8	-31.3	-53.1	9.63	-23.4	-0.8

Sample No.	8	9	10	11	12	13
Sample Name	SBA- 15	MCM-41	MCM-41	MCM-41	SBA-15	SBA-15
Production date	01/05/2014	12/10/2016	13/10/2016	19/10/2016	19/10/2016	20/10/2016
weight (g)	0.588	0.175	0.411	0.289	2.298	15.5
FITC	yes	no	yes	yes	yes	yes
Mesitylene	no	no	no	no	no	no
Shape	rod	sphere	sphere	sphere	rod	rod
size (nm)	1681	agglomerated	agglomerated	1000-3000	1000-2000	1000-2000
zeta potential (mV)	8.32	-27	12	-5	0	0

Sample No.	14	15	16	17	18	19
Sample Name	SBA-15	SBA-15	SBA-15	SBA-15	MCM-41	SBA-15
Production date	03/02/2017	17/02/2017	17/02/2017	27/02/2017	27/02/2017	27/02/2017
weight (g)	0.68	0.67	0.55	2.16	0.97	3.2
FITC	yes	yes	yes	yes	yes	yes
Mesitylene	no	no	no	no	yes	no
Shape	rod	rod	rod	rod	sphere	rod
size (nm)	1220	2526	2953	1167	356	1186
zeta potential (mV)	-6	38.8	19.8	5.4	32.9	11.4

3.1.2 Scanning Electron microscopy (SEM) and Transmission Electron microscopy (TEM) analysis

3.1.3 Scanning Electron microscopy (SEM)

With the aim of determining the morphology and size of the samples, SEM analysis was done. The figures presented below were examined in varying levels of magnification so that it could be confirmed that their shape was spherical and has sizes ranging between 200 and 300 nm.

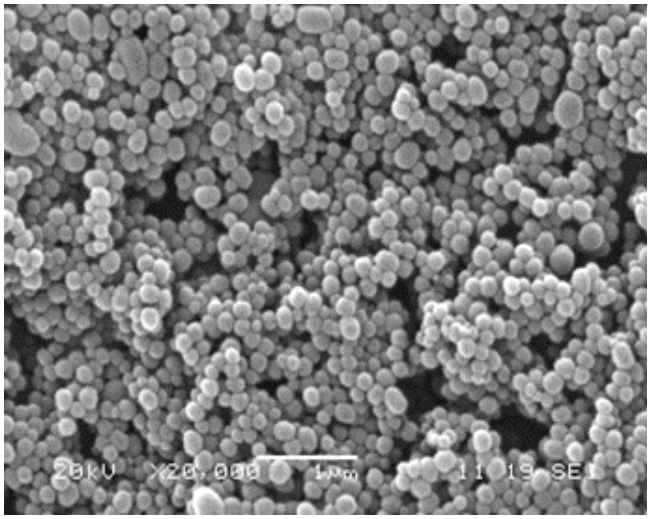

(a) SEM in 1μm scale, magnification x20.000

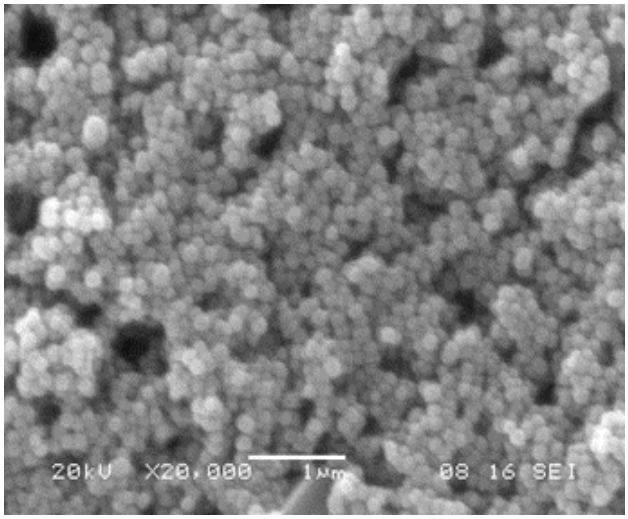

(b) SEM in 1μm scale, magnification x20.000

Figure 3.0 (a, b): SEM image of Sample 1 & 2 (MCM-41 technique). This analysis confirms the size and shapes of the sample following the acid extraction. All images were captures at 1μm scale, magnification X20.000.

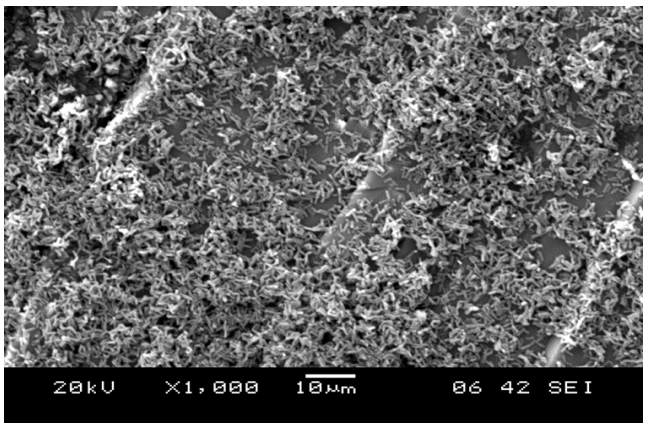

(a) SEM in 10µm scale, magnification X1000

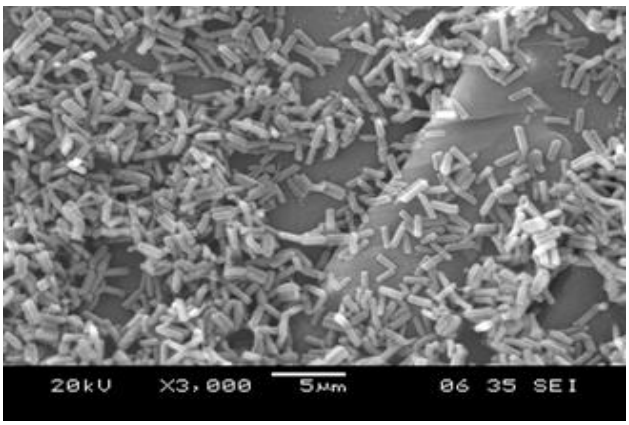

(b) SEM in 5µm scale, magnification X3000

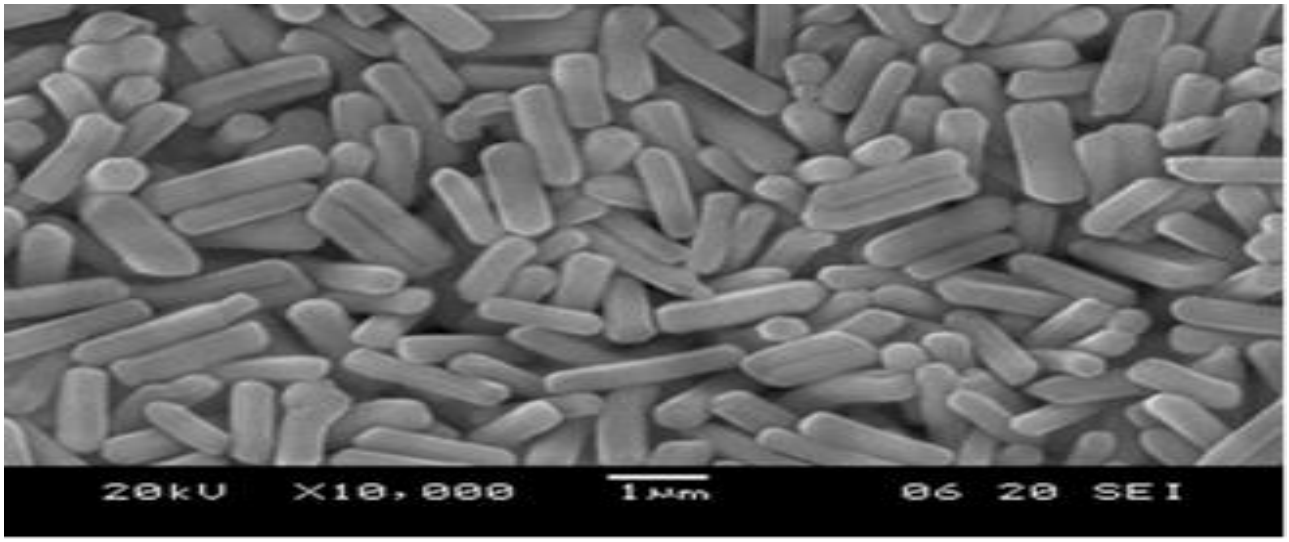

(c) SEM in 1µm scale, magnification X10.000

Figure 3.1 (a, b, c): Illustrates SEM images of Sample 6 (SBA-15). All images were captured in diverse magnifications and scales. They are rod-shaped, and their sizes ranged between 600 and 1µm.

For the above images, the sample was taken after 48 hours of the reaction in a Teflon bottle. For the entire 48 hours, the sample was in a static condition. Between zero and 24 hours, the temperature was maintained at 35^{o}C. Between 24 and 48 hours, the temperature was increased to 100^{o}C. The product was then centrifuged and kept in methanol. Observing the sample shows a rod shape with sizes ranging from between 600 and 1 µm. For further analysis, the sample is diluted and preserved in methanol.

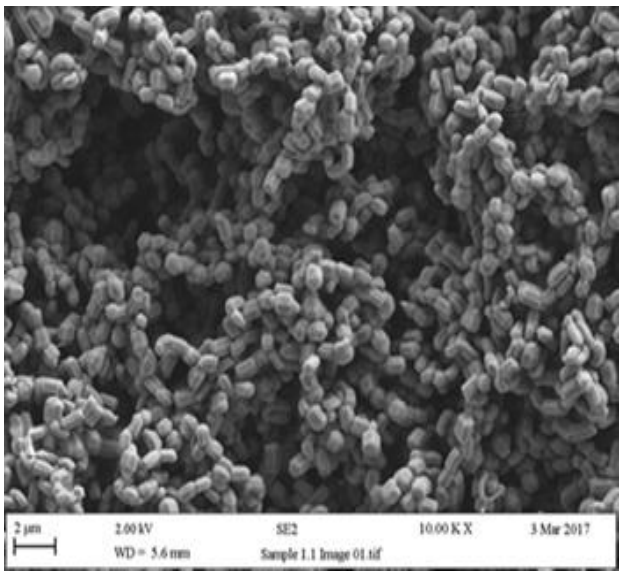

(a) SEM in 2µm scale, magnification x10.00

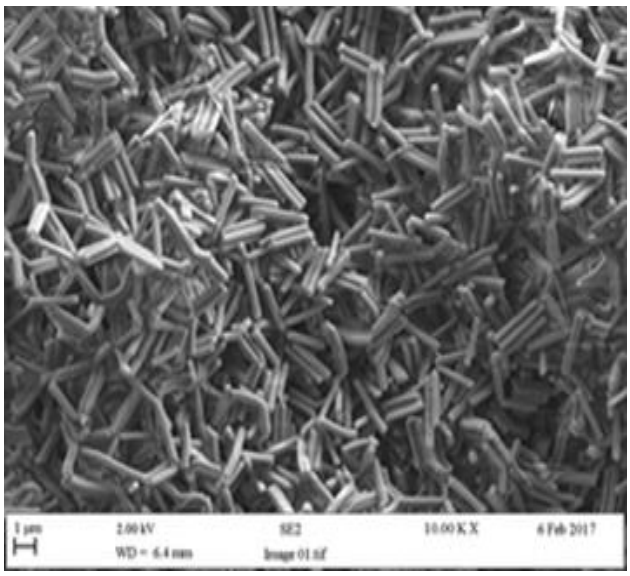

(b) SEM in 1µm scale, magnification x10.000

Figure 3.2 (a, b): SEM images of Sample 8 and 17 from SBA-15 technique following acid extraction. These images were captured in different magnifications and scales. They are rod-shaped, and their size was around 600-800 nm.

3.1.4 Transmission Electron microscopy (TEM)

When the SEM analysis was complete, Transmission Electron Microscope (TEM), obtained from the University of Manchester's specialist laboratory was used for the analysis and confirmation of the sample's porosity and its surface area. When TEM analysis is done in varying magnification, the Mesoporous Nanoparticles (MNPs) can be seen, and the surface area, shape, and porosity of the sample is confirmed. This analysis has the capability to image resolutions that are higher as a result of the small de Broglie wavelength of electrons interacting with the specimen when it passes through. The images presented below are focused on mesoporous nanoparticles with a round shape and numerous pores.

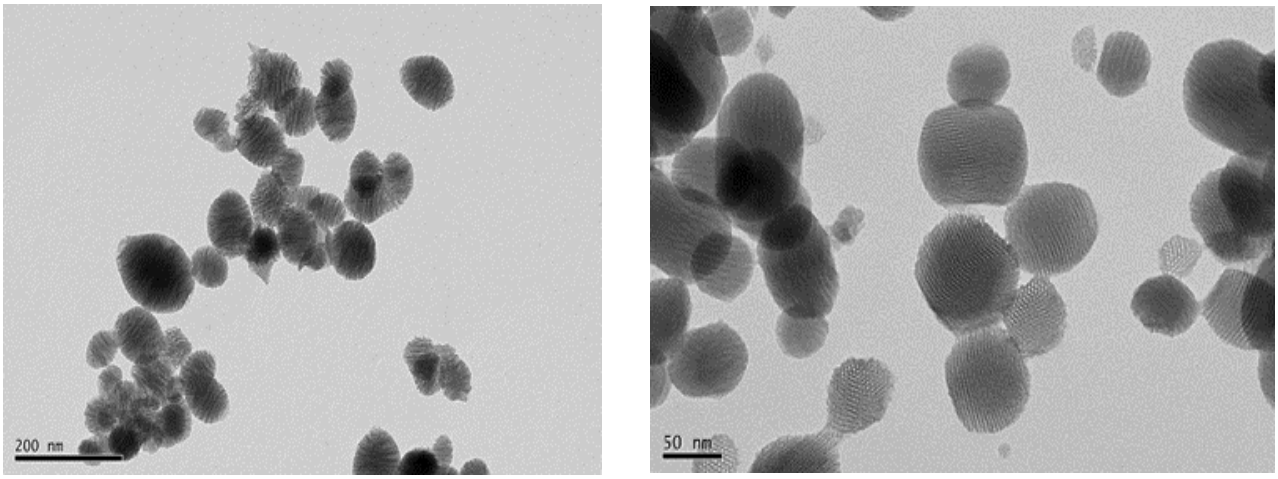

(a) TEM in 200 nm scale, magnification x23000 (b) TEM in 50 nm scale, magnification x49000

Figure 3.3 (a, b): TEM analysis for Sample 1 (MCM-41) and Sample 18 (MCM-41 with Mesitylene). Indicates that the samples' surface area and porosity are good. They also confirm the shape of the samples. These images were captured in varying magnifications and scales.

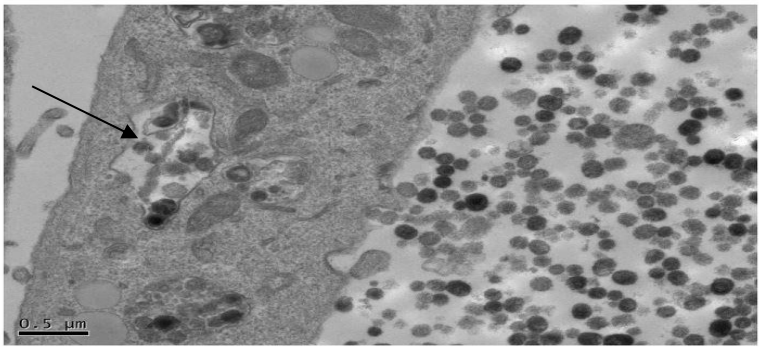

Figure 3.4: Representative TEM image of myotubes incubated with MCM-41 for 7 days, which did show internalisation of MCM-41.Scale 0.5µM.

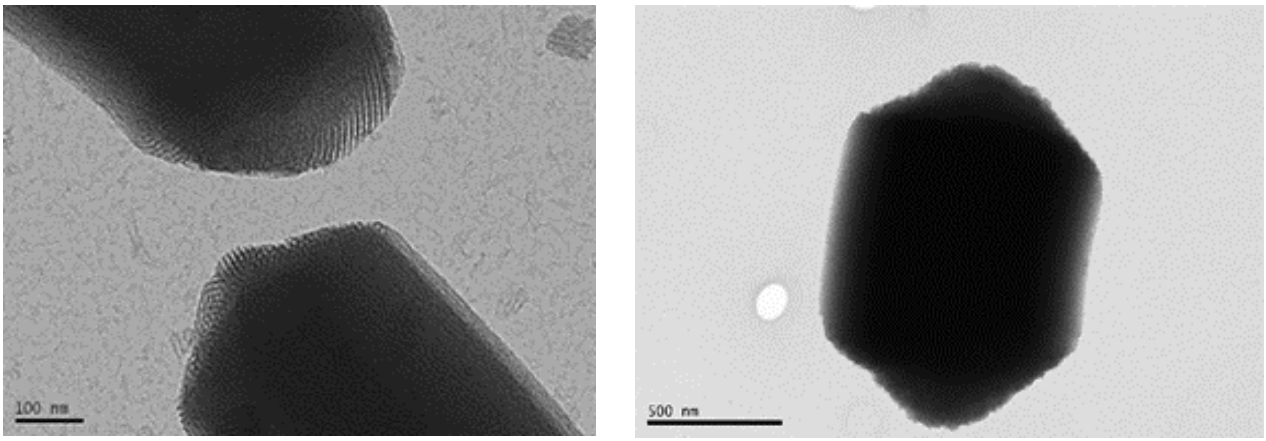

(a) TEM in 100 nm scale, magnification x30000 (b) TEM in 500 nm scale, magnification x11000

Figure 3.5 (a, b): **TEM images of Sample 6 (SBA-15, large size) and Sample 17 (SBA-15, small size)**. These images were captured in varying magnifications and scales. They illustrated an individual mesoporous nanoparticle at a higher resolution. It can be seen that they are rod hexagonal shaped, and the porosity with the surface area of the samples is confirmed.

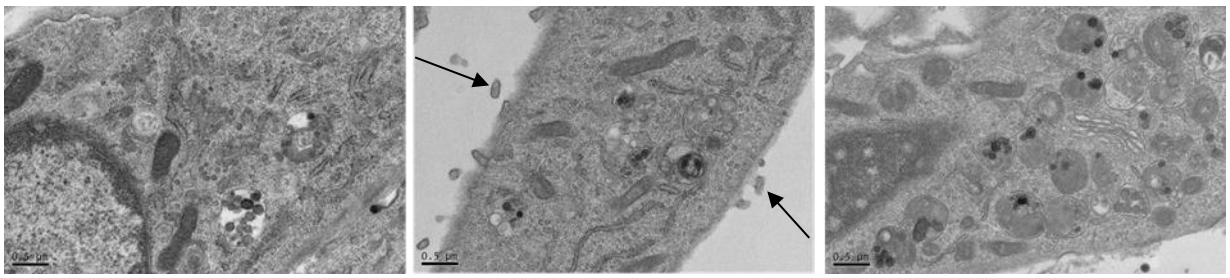

Figure 3.6: Representative TEM images of different sections of myotubes incubated with SBA-15 for 7 days, which did not show internalisation of SBA-15 which is desirable for this study as IGF1 receptor exist on the cell membrane of myotubes. Scale 0.5µM.

3.1.5 Nitrogen adsorption

The analysis of the nanoparticle was done through an evaluation of the surface area and pores by nitrogen gas desorption and adsorption. The significance of this is that it is not possible for the blocked pores in the template to be loaded with the drug. Analysis of the surface area makes it possible to calculate the pore's area and the amounts they can absorb. In the graphs below, the adsorption of the sample/desorption from SBA-15 and MCM-41 techniques is indicated. In this study, the adsorption confirmed that the gas had attached into the nanoparticles' surface. Simultaneously, the adsorption conducted an analysis of the gas discharge from the nanoparticles. For Sample 1(MCM-41), adsorption and desorption result was 1199 m^2/g, and for Sample 6 (SBA-15) it was 940 m^2 /g. For Sample 1 (MCM-41), the pore size was 2.6-3.8 nm, and for Sample 6 (SBA-15) it was 5-9.

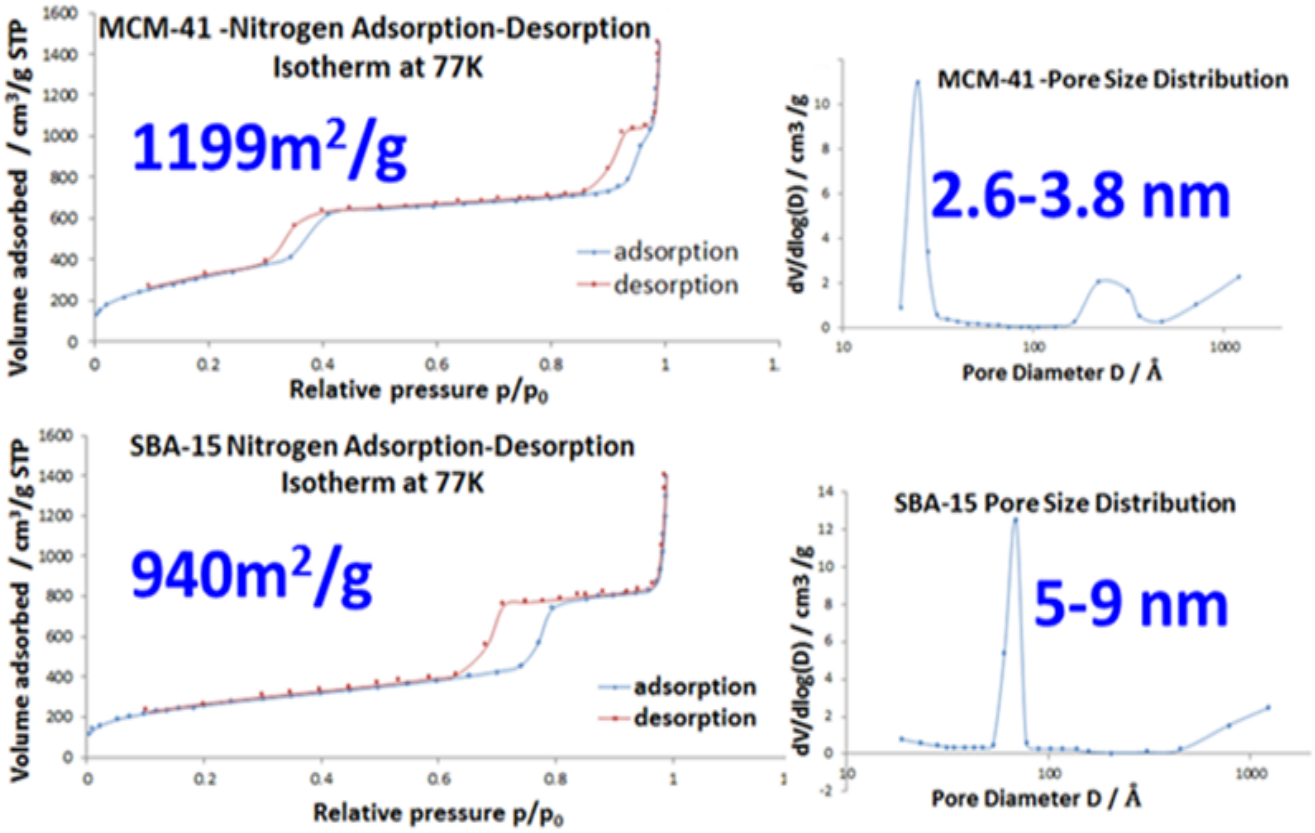

Figure 3.7: The graphs illustrate the surface area and the pore size distribution analysis of the mesoporous nanoparticles MCM-41 & SBA-15.

3.1.6 Size and zeta potential measurements (by Dynamic Light Scattering (DLS)

Figure 3.8 (a & b) below illustrate the zeta potential and size of Sample 2 (MCM-41). Water was used to dilute the sample. The high poyldispersion index (>0.7) shows particle aggregation. The average aggregate size is 256 nm. The zeta potential of Sample 2 is indicated in Graph B. In order for a colloidal solution to attain stability, the zeta potential has to be >+30 or <-30. For this sample, the zeta potential is -21, which shows a slight degree of particle instability. The light scattering result is confirmation of such particle instability.

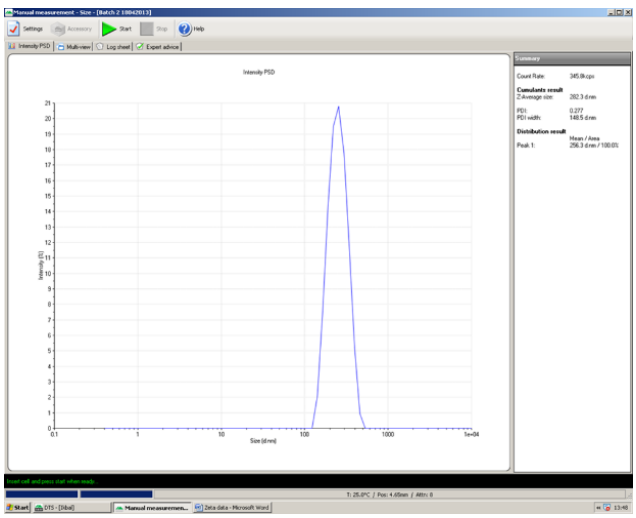

(a) Sample 2(MCM-41), the size was 256 nm

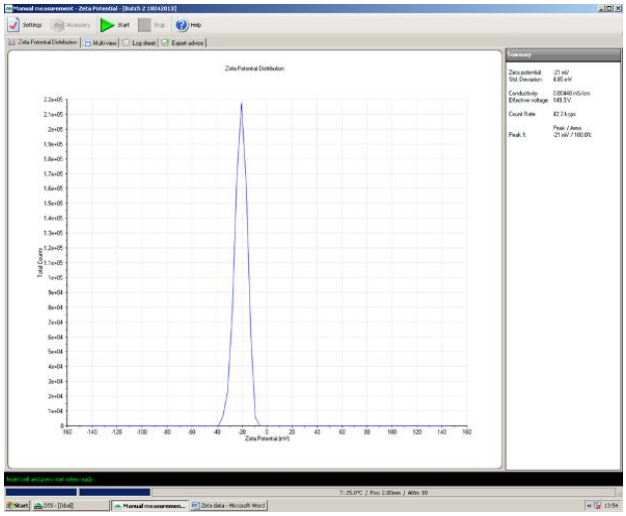

(b) Sample 2(MCM-41), the Zeta potential was -21mv

Figure 3.8 (a, b): Shows the size and the zeta potential of Sample 2 (MCM-41). This is measured by DLS (a). The size was 256 nm. (b)The zeta potential was -21 mv.

Figure 3.9 (a, b, c, and d) represents the results for Samples 6 and 8 (SBA-15). It shows that the size measured by DLS was in the region of 623 nm and 1681 nm. Methanol was used to dilute the samples. Nano-porous rods samples 6 and 8's zeta potentials for graphs b and d were measured. The results were -27 mv and 8.2 mv.

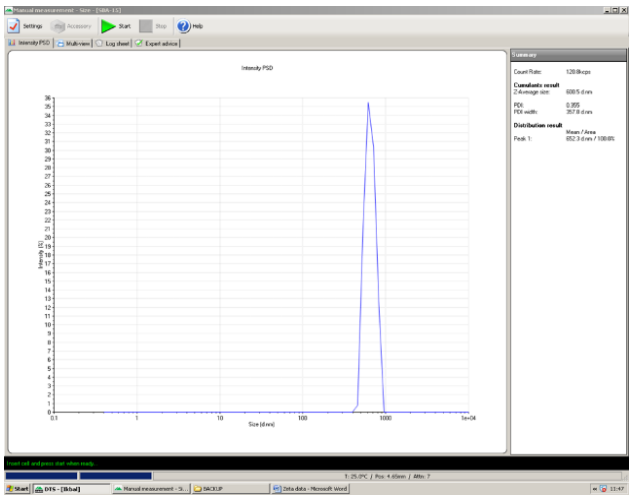

(a)Sample 6 (SBA-15) Size was around 623 nm

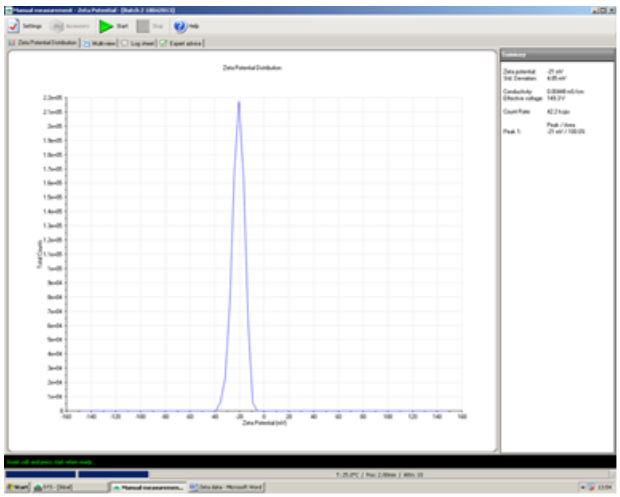

(b) Sample 6(SBA-15) Zeta potential was around -27 mv

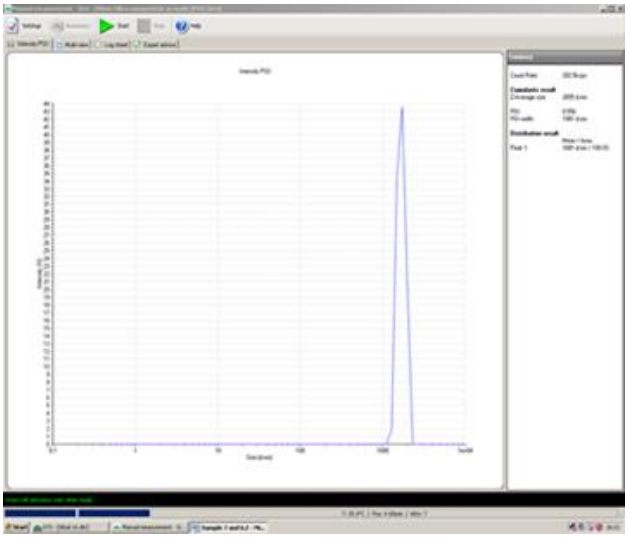

(c) Sample 8 (SBA-15) the size was 1681 nm

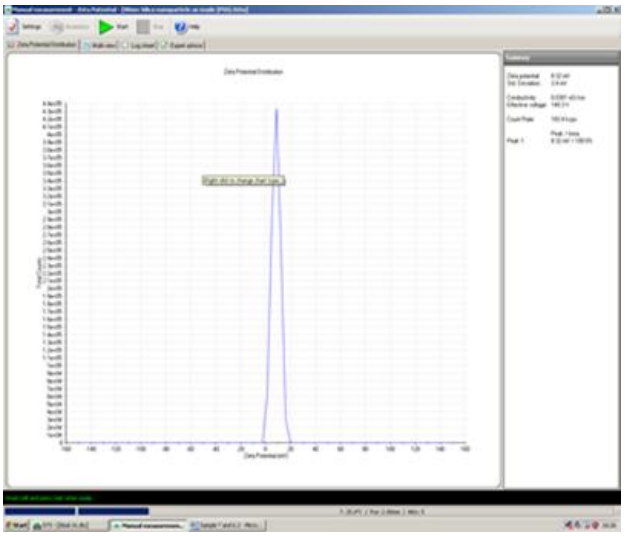

(d) Sample 8 (SBA-15) Zeta potential was 8.2 mV

Figure 3.9 (a, b, c, d): Shows the size, zeta potential measured by DLS for Samples 6 and 8 from (SBA-15) method. (a) Sample 6 (SBA-15): Size was around 623 nm. (b) Sample 6(SBA-15): Zeta potential was -27 mv. (c) Sample 8 (SBA-15): Size was 1681 nm. (d) Sample 8 (SBA-15): Zeta potential was 8.2 mV.

3.1.7 X-ray diffraction and FTIR

Using a potassium bromide (KBr) disc, the FTIR spectra of each mesoporous particle were obtained. This is a technique made in such a way that it is able to detect the template in the pores. With the aim of determining the proportion of the hydrogen, nitrogen, and carbon in each particle, the elemental analysis was done using CHN analyser (PE- 2400ll; Perkin Elmer). From Figure 3.10, below, of (SBA-15) sample, it can be seen that the template Pluronic P123 triblock copolymer has been removed.

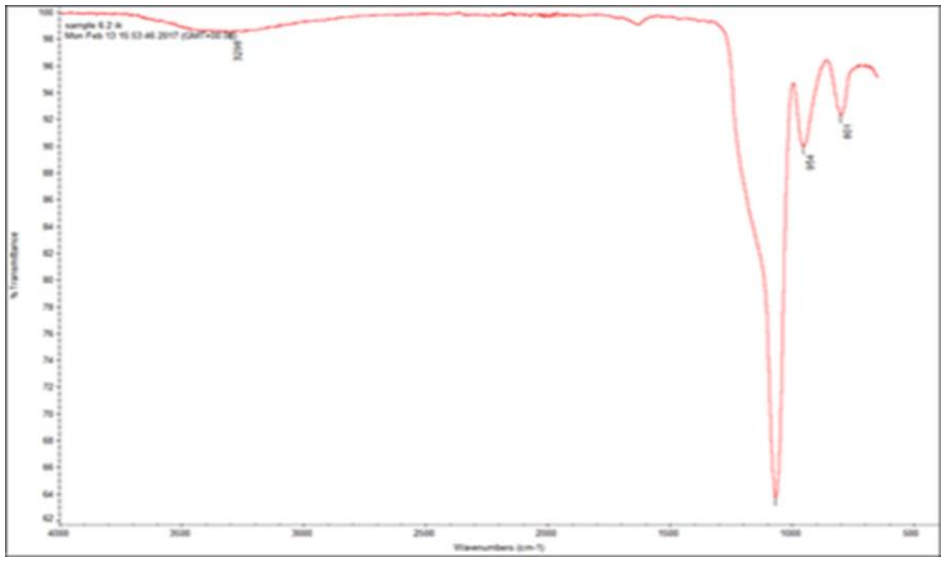

Figure 3.10: FTIR analysis of (SBA-15) sample to confirm the removal of the Pluronic P123 template. This method designed to detect the template within the pores. Elemental analysis was performed to determine the percentage of carbon, hydrogen and nitrogen on each particle using a CHN analyser (PE- 2400ll; Perkin Elmer). The graph shows that the template (Pluronic P123 triblock copolymer) has been removed.

From 0.3° to 70° 2θ, an analysis of the X-ray diffraction samples was done. A test kit obtained from Cambrex was used for conducting an endotoxin assay. This was done by mixing samples with the chromogenic substrate reagent and LAL reagent over a 16-minute incubation, and 408 nm was the reading of the absorbance. Figure 3.11, below, representing the results for (SBA-15) sample, indicates that it is possible for X-rays diffraction to access the structural and morphological data of the nanomaterials to conform the holes or pores in the NPs.

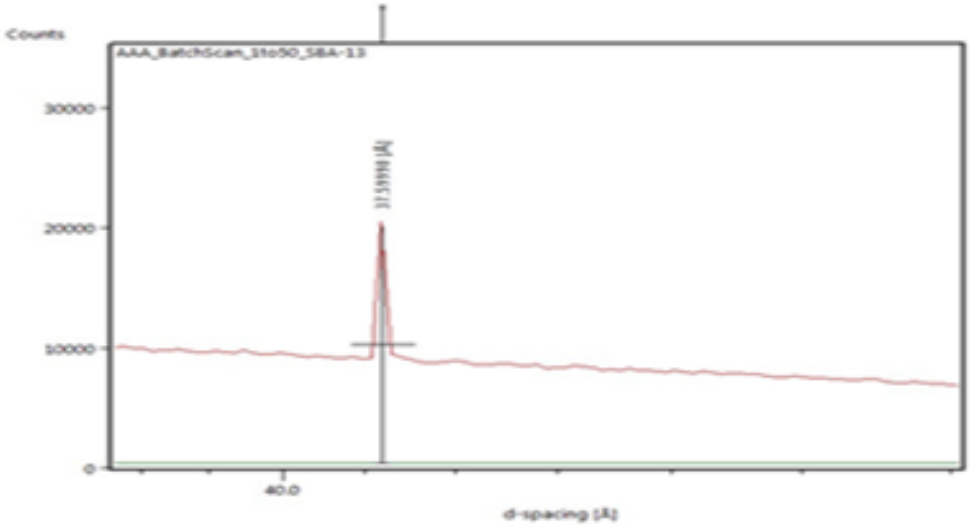

Figure 3.11: Shows that the X-rays diffraction of (SBA-15) sample. This method was used to confirm the holes and pores in the NPs sample.The graph of sample (SBA-15) shows that the X-rays diffraction can access the morphological and structural information of the nanomaterials to confirm that there are pores or holes in the NPs.

3.1.8 Release study of IGF-1 loaded into MSNPs

3.1.9 IGF-1 3D Structure

The Protein Homology/analogy Recognition Engine V 2.0 was used to determine the 3D dimension and structure of IGF-1, (Phyre2,http://www.sbg.bio.ic.ac.uk/phyre2/html/page.cgi?id=index). With the aim of making sure that the IGF-1 will be captured inside the pores, the IGF-1's affinity to MSNPs was evaluated and the MSNP's pore sizes were measured (Basyuni et al., 2018). From the Phyre2 engine analysis, it can be seen that the highest IGF-1 3D dimensions for X, Y, and Z are 3.3, 4.0, and 3.4 nm respectively. From this data, the SAB-15 stability for our project is confirmed, not just based on the fact that the sizes of the pores are big enough to absorb the IGF-1 but because they also have a big surface area this permits adequate amounts of IGF-1 to be loaded.

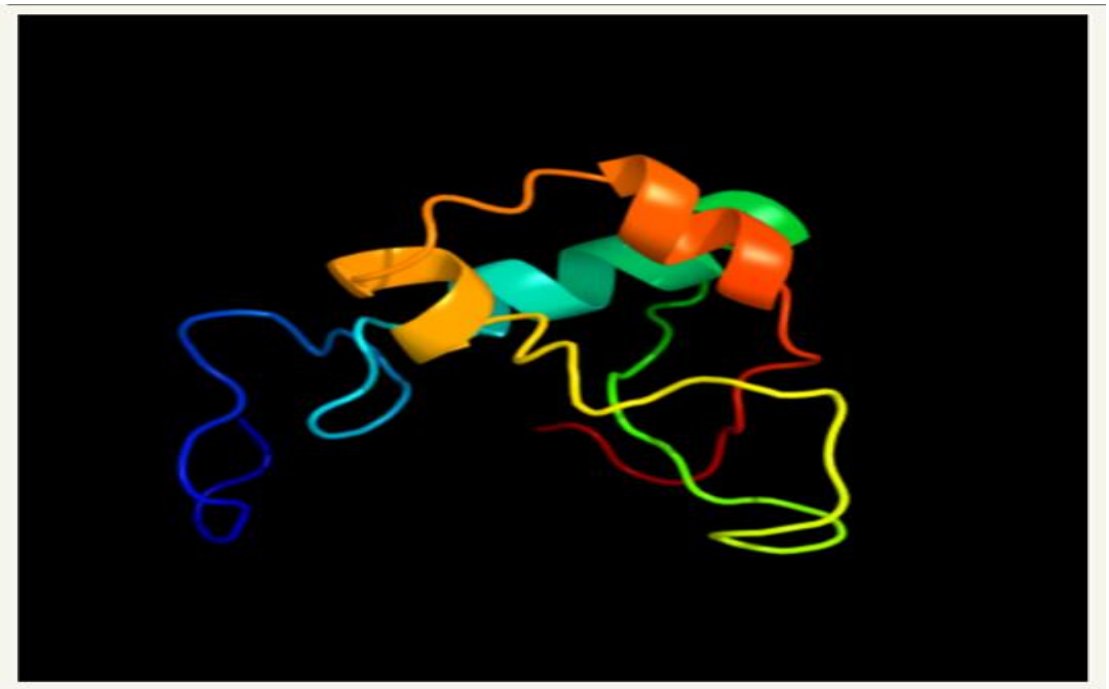

Figure 3.12: Phyre2 engine analysis for IGF-1 3-D dimensions. This indicates that the highest 3D dimensions (X; Y & Z) of IGF-1 are 3.3, 4.0, and 3.4 nm, respectively.

The surface of the MSNPs is positively charged, permitting for the electrostatical adsorption of negatively charged IGF-1 (0-100µg/ml) into the nanoparticles' pores. When the drug is loaded into the nanoparticles, controlled pore diffusion is used to regulate the release. So, the IGF-1 protein should be uploading for 4 hours with 72 hours required to determine the time course of the IGF-1 release. At intervals (2hrs, 6hrs, 22hrs, 48hrs & 72hrs), the sample was centrifuged, and the supernatant's fluorescence was measured with the aim of estimating the discharge of the labelled IGF-488 from the MSN.

The following experiment was conducted three times. Nanoparticles measuring 1.5mg were added to PBS measuring 1ml, and a rotator was used to mix these together for 15 minutes. IGF-1 was then added together with 13 µl of DyLight 488 NHS Ester. After a four hours, when the labelled IGF-1 was measured to determine the loaded quantity of IGF-1, it was noted that only 8.1µg of the labelled IGF-1 was inside the nanoparticles. Results also showed that the release was at 0.75µg after two hours. However, no release was noted at higher intervals (6hrs, 22hrs, 48hrs & 72hrs).

Based on the reason above, we attempted to gradually reduce the concentration of IGF-1 so that it ended up being 22.5 µg/ml with only 2.6 µl of the dye added. From the results, it was noted that 10.6µg/ml was uploaded after four hours. However, the discharge differs slightly between 2 and 72 hours. Detailed results are presented in Table **3.1.**

Table 3.1: Fluorescence measurement of the uploading and release study results

Uploading & Release	**First reading**	**Second reading**	**Mean average reading**	**Concentration µg/ml**
Uploading after 4hrs	377	373	375	11.9
Release 2hrs	221	232	226	-0.00
Release 6hrs	256	268	262	0.11
Release 22hrs	287	275	281	0.17
Release 48hrs	271	271	271	0.14
Release 72hrs	268	263	265	0.12

The result for the past experiment showed that around 50 percent of the IGF-1 concentration was uploaded after four hours. It was noted that the discharge was slightly different from 2 to 72 hours. Therefore, nanoparticles measuring 0.75 mg were added to PBS measuring 1ml, and a rotator was used to mix them together for 15 minutes. Following this, 12.5µL of IGF-1 was incorporated into the mix (NP+PBS+IGF). After mixing them together, the substances were placed in a rotator for four hours. This was followed by centrifuging the mixture for five minutes at speeds of 6000rpm, and the supernatant was measured. The result showed that (10.7µg/ml), which is around 85 percent of IGF-1 concertation was uploaded inside the NPs after 4 hours. A 100 hour period is used to determine the time course of the IGF-1 discharge. At intervals of 2hrs, 4 hrs, 8hrs, 25hrs, 50hrs and 75hrs, 100hrs the sample was centrifuged. This was followed by measuring the supernatant's fluorescence so that the IGF-1 discharge from the MSNP could be estimated. The results of this experiment are presented in Figure 3.14. These results show that from zero to eight hours, the discharge of the IGF-1 loaded to the nanoparticles was at a rate of 10-15 ng/ml. From 25 hours and above, an increase in the discharge to 48 ng/ml was noted. A further increase was recorded in 100 hours: 60 ng/ml.

Table 3.2: shows the fluorescence measurement of study release standard curve results.

Standard Curve	**First reading**	**Second reading**	**Mean average reading**	**Concentration µg /ml**
A	0	0	0	0
B	316	319	318	0.625
C	561	613	587	1.25
D	107	106	106	2.5
E	198	190	194	5
F	346	330	338	10
G	612	593	602	20

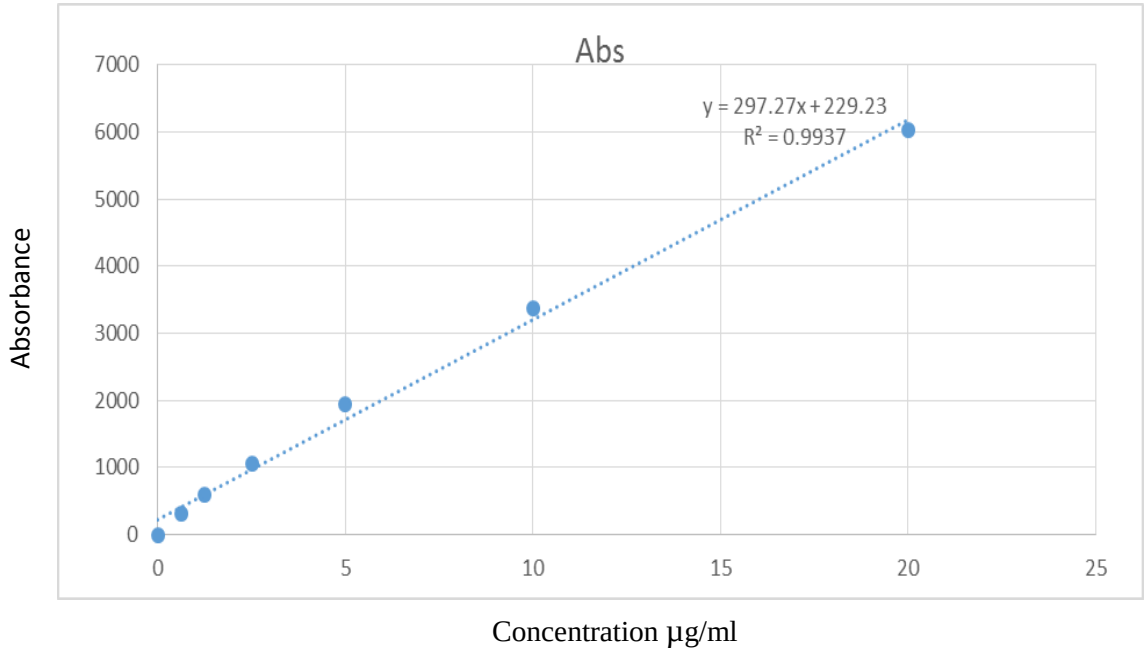

Figure 3.13: Shows the chart of the study's release standard curve Fluorescence measurement.

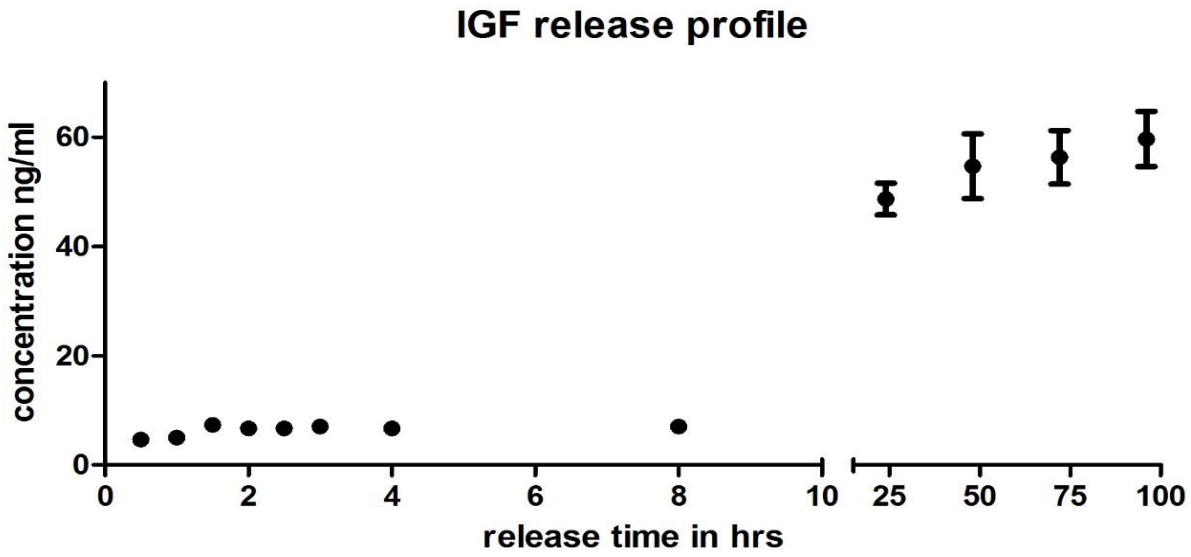

Figure 3.14: Shows the loaded IGF-1 release profile. From zero to eight hours, the release was between 10 and 15 ng/ml from the MSNP. After 25 hours, the release of IGF-1 increased to 48 ng/ml and continued to increase to 60 ng/ml in 100 hours.

3.1.10 MSNPs cytotoxicity and Biodegradation

It is important that MSNPs that will be employed as a drug delivery system (DDS) show that they have very low or no proliferative or cytotoxic effects on the cells that are targeted. It is for this reason that in initial essays, we scrutinised the MSNPs' impact on cell proliferation and apoptosis. Results showed that cells that were cultured with MSNPs, MCM-41 and SBA-15, indicated matching levels of death and S-phase entry to untreated controls. Before the nanoparticles are used in tissue culture, clinical environment, or animal models, it is important to determine cytotoxicity. From the flow cytometry analysis, it was noted that the data between untreated and treated SBA-15 cells was non-significant after three days in culture. SBA-15 treated cells with varying concentrations of SBA-15 MSNPs (200 µg, 400 µg and 800 µg) produced 12%, 10%, and 9% dead cells respectively. From the untreated cells, 10 percent of dead cells were recorded, which matches the results of the cells that were treated.

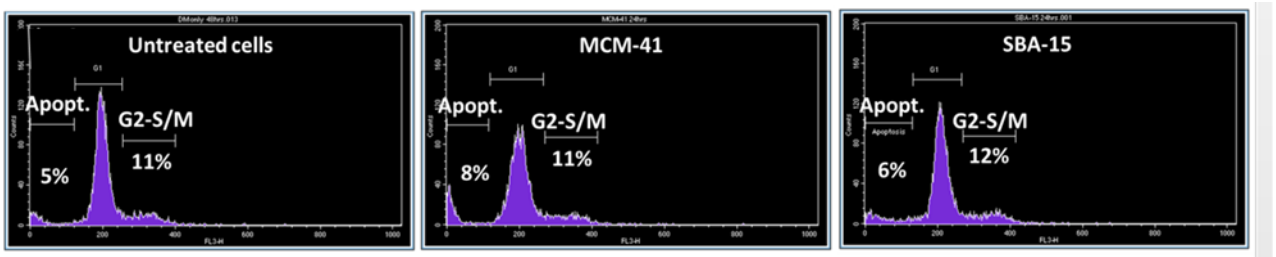

Figure 3.15: Shows cells cultured with MSNPs (MCM-41 and SBA-15). These cells revealed equivalent levels of cell death and S-phase entry to untreated controls.

3.1.11 Analysing SEM to confirm NPs biodegradability

To evaluate biodegradation, SBA-15 MSNPs and MCM-41 was cultured only in DM for 14 days. From the results, it was indicated that there is a limited degree of biodegradation, irrespective of the concentration of NPs.

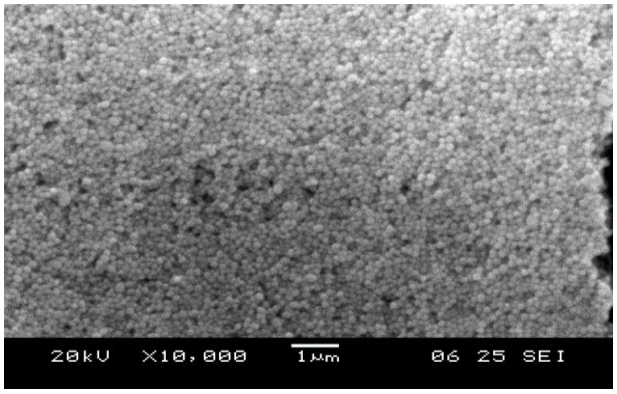

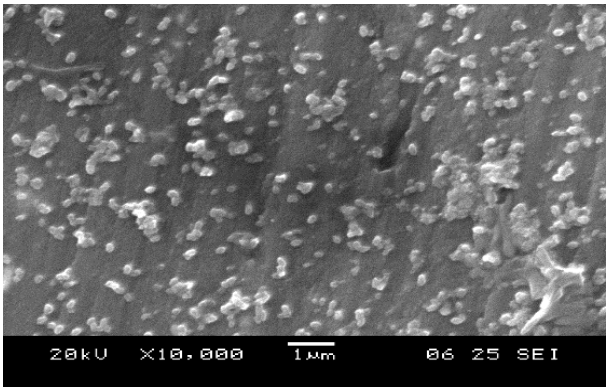

(a) Sample1 MCM-41 after the first week of incubation **(b)** Sample 6 SBA-15 after the first week of incubation

Figure 3.16 (a, b): Illustrates the biodegradability following Week 1 of incubation with DM.

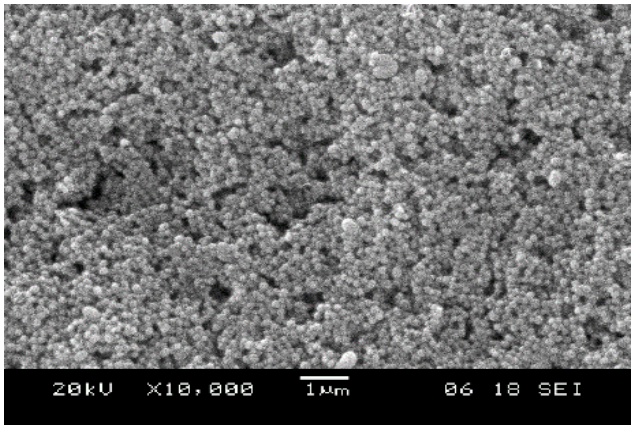

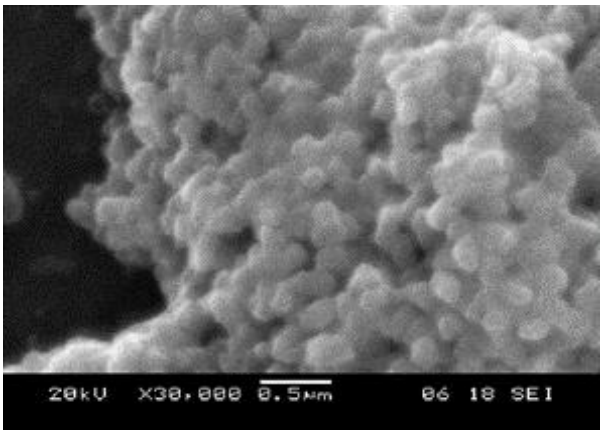

(a) Sample 1 MCM-41 after the second week of incubation (b) Sample 6 SBA-15 after the second week of incubation

Figure 3.17 (a, b): Illustrates the biodegradability after Week 2 of incubation with DM.

Figure 3.18 (a, b, c), below, shows the SEM analysis of Sample 6 (SBA-15). The images indicate the biodegradability following three months of incubation with methanol/water in varying temperatures. This is an exercise aimed at conforming the optimal condition to keep our NPs for extended periods. The results show a slight difference. However, it can be concluded that the best conditions can be obtained by keeping the sample in menthol at room temperature.

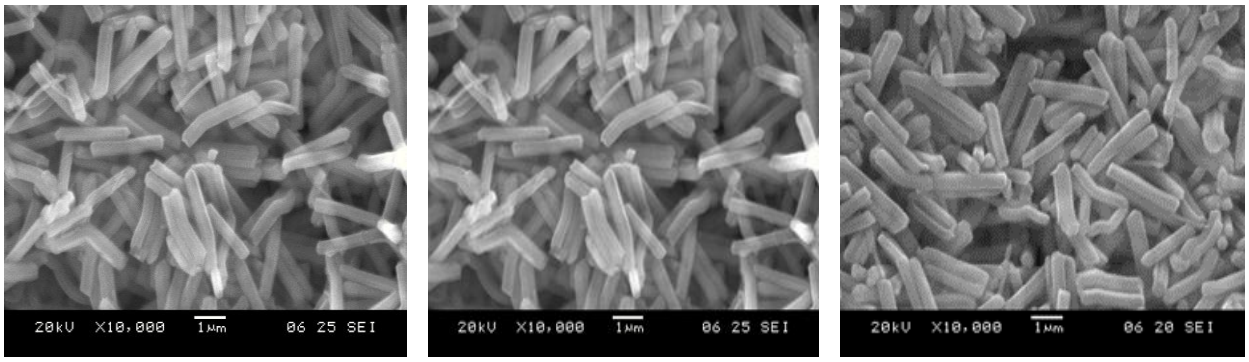

(a) Kept with methanol in -20C **(b) kept with water at -20C** **(c) kept with methanol at RT**

Figure 3.18 (a, b, c): Illustrates SEM analysis of Sample 6 (SBA-15) biodegradability after three months incubation with methanol/water in varying temperatures to confirm the optimal condition to keep NPs without any variations in their stability.

3.2 Discussion

In this chapter, a definition of the stability and toxicity of MSNPs was completed and confirmed that, the SBA-15 mesoporous silica nanoparticles are better at retaining IGF-1. Over the past years, MSNPs and skeletal muscle have been managed separately. However, it has been gradually realised that the use of nanotechnology as a novel method of delivering drugs is required. This is the idea that was applied in this study which examines how the proliferation skeletal muscle stem cell is affected by MSNPs (Mamaeva et al., 2013). The use of this method is driven by the aim of this research which is to obtain a comprehension of the effects MSNPs on the myoblast proliferation of the human skeletal muscle. The eventual objective behind these efforts is to develop a system for the treatment of skeletal muscle cell using IGF-1. It also aims to grow IGF-1 bioactivity periods through a safe and effective delivery mechanism that uses MSNPs to reduce the wasting of skeletal muscle and other linked conditions.

With regards to cytotoxicity, the nanoparticles shape and size, together with MSNPs concentrations, have a vital role to play. There is confirmation that a decrease in the size of particles corresponds with an increase in cytotoxic effects (Pasold et al., 2015). An analysis of available research shows that there are not many studies focusing on the effect of nanoparticles formed from numerous sources of cell proliferation and function. The studies become even fewer when one considers the effect of nanoparticle size and shape on cellular proliferation and function. Conclusions have shown that nanoparticles and cells collaboration could be a result of the shape of particles. In this regard, it has been noted that nanoparticles that have an aspect ratio that is minor influence proliferation and function to a lesser measure, a situation that is opposite to the nanoparticles that have an aspect ratio which is bigger (Huang et al., 2010). The reason behind the scenario discussed in the above paragraph is that the nanoparticles employed in this research are rod-shaped, and those MSNPs have been seen to be easily absorbed through the endocytosis. This is a situation that differs when one looks at alternative nanoparticles with shapes that are different. It is likely that this will have an impact on the cell's viability and function in addition to their proliferation (Gupta & Gupta, 2005). Even though nanoparticles that are spherical in shape are not likely to be easily endocytosed by cells, they still can have an effect on the proliferation and function of cells through circulating in the blood for extended periods as a lesser level when comparison is made to nanoparticles that are rod-shaped (Huang et al., 2010). As a result, it has been noted that nanoparticles that are spherical in shape tend to be more biocompatible and deliver more appropriate delivery of blood when working together with nanoparticles that are long rod-shaped and small rod-shaped (Huang et al., 2011; Qi et al., 1998).

It has been shown that the size of MSNP impacts the proliferation of cells (Huang et al., 2010). The development of cellular signalling is altered in connection with the size of nanoparticles. It is for this reason that a size range of between 2 and 200 nm could affect the SkMC proliferation and viability. Nevertheless, the most noticeable impacts are emphasised in the size range of MSNP between 40 and 50 nm (Jiang et al., 2008). Other research has come to the conclusion that for a nanoparticle size of 50 nm, there is a confirmed cells uptake which leads to cell function distribution and repressed proliferation (Lu et al., 2009). When the oxide nanoparticle pore size is large (for instance, 200nm), the impact on cell proliferation is low because this lessens cellular uptake. On the other hand, when the size of the pores is smaller (for instance 50nm), there could be a constraint in the growth of lung fibroblast cells, a situation which decreases the viability of such cells. In lung fibroblast cells, size showed the biggest effect, constraining the growth of cells and lessening their viability (Limbach et al., 2005). From the data, it can also be noted that the MSNP pore construction has an effect on cell proliferation. For instance, the supreme interface with SkMC was noted in the absorbent construction in that it is long-term controlled, a situation that upset proliferation and prompted apoptosis (Lin & Haynes, 2010).

The use of MSNPs in the treatment of cells in relation to injury, wasting, and other disorders like cancer is vital because they can function as a way of delivering drugs that is safe. This makes it possible to deliver anti-cancer drugs that are toxic, like doxorubicin (DOX). (Zhu et al., 2011; Kempen et al., 2015). It has been concluded from studies that DOX shows fluorescence, while the presence of apoptosis is noted in situations where nanoparticles deliver DOX to the site of the tumour (Lee et al., 2011). Added to this, it has been shown by some studies that nanotechnology could be a useful solution in therapy because it could have the capacity to convey other molecules like protein, antibodies, peptides, and plasmids (Lim et al., 2012).

Nanoparticles could be valuable when it comes to delivering drugs based on DNA. Hence, such drugs tend to have a short-half life, which means that cells do not freely embrace them as a result of their negative charge. Added to this, they have reduced nuclear access, together with their levels of translation and transcription. This situation results from intracellular degradation following cellular uptake (Mamaeva et al., 2013). The role of nanoparticles is to maintain the required particles which are important for the delivery of genes. At the present moment, the delivery of genes depends on viral vector use (Kempen et al., 2015). There is now knowledge to the effect that plasmids are not just uploaded into SBA-15's mesopores. However, research conclusions have shown nanoparticles enclosed with the common gene transfection agent polyethyleneimine (PEI) and produced a cationic surface to which the DNA and siRNA concepts were enclosed (Xia et al., 2009). The hosts are minute membrane-resistant proteins which are delivered into cells inside a transmembrane carrier which is

efficient and has huge pores (Slowing, Trewyn & Lin, 2007). Hence, macromolecules can be delivered through nanoparticle-based methods in addition to small drug molecules (Slowing et al., 2008).

3.3 Conclusions

From the results presented in this study, a decision was made to use SBA-15 mesoporous silica nanoparticles for my project because they have a big pore size and surface area which permits adequate amounts of IGF-1 easily. It can be inferred that the SBA-15 can be employed for purposes of controlling the discharge of IGF-1 in new systems of delivery, which is used to boost IGF-1 bioactivity. With the development of nanotechnology applications in the medical field, it is vital to directly separate and advance contributions useful to public health.

Chapter 4: Biological activity of IGF-1 loaded into the Mesoporus Nanoparticals

4.0 Background

4.0.0 Introduction

The human insulin-like growth factor-1 (IGF-1) gene introduces numerous, assorted mRNA transcripts via an amalgamation of several transcription instigation sites, alternative splicing, and distinct polyadenylation signals. Such IGF-1 mRNA transcripts provide coding for numerous isoforms of the original peptide of IGF-1 (IGF-1Ea, IGF-1Eb and IGF-1Ec or MGF in human skeletal muscle) that also experience alteration following translation. Focus in the effect of IGF-1 isoforms and differential expressing in the regulation of the hypertrophy and regeneration of muscle fibre following damage and mechanical overloading has been growing. One of the eye-catching developments in the framework of the IGF-1 autocrine/paracrine actions is the identifying a locally expressed, loading- or damage-sensitive IGF-1 isoform in skeletal muscle (Philippou A et al., 2007). The idea is that the competing procedures of cellular proliferation and differentiation, together with the escalation in the synthesis of protein needed for hypertrophic adaptation or repair of damaged muscle are controlled by differential expression and by specific roles played by IGF-1 isoforms (Philippou et al., 2007).

The loss of skeletal muscle as a result of ageing, ischemia, degeneration of motor neurons, heart failure, and cancer is a grave condition which has no effective cure at the moment however exercise and nutritional intervention could help for instance, modern research recommends that substantial physical exercise offers an outstanding motivation concerning the re-establishment of SkMC, and exercise has also been documented that growth factors show more significantly diverse expressions of proliferation throughout the following muscle repair and subsequent hypertrophy than normal (Armakolas et al., 2016). IGF-1 has an important role to play in the maintenance and repair of the muscle (Song YH, et al., 2013). From pre-clinical studies, it has been concluded that IGF-1 has the effect of boosting muscle strength and mass, lessening degradation, and constraining the protracted and extreme inflammatory process which results from toxin injury. It has been shown to have the effect of boosting satellite cells' proliferation potential (Song YH, et al., 2013). Also, IGF-1 has proved to be a robust neurotrophic factor, redeeming neurons from apoptosis and facilitating neuronal myelination and growth. Added to this, IGF-1's signalling pathway plays a profound role in the expansion of cancer. Hence, efforts to prompt this pathway for the purposes of therapy are currently progressing. A comprehension of the instruction and function of IGF-1 structure is going to be vital for both basic and clinical applications (Bentov & Werner, 2013). This is an issue that can be resolved by the selection of suitable peptides of isoforms, and then creating targeted delivery methods (Song YH, et al., 2013).

4.0.1 Aims

This study aims to use IGF-1 to create a treatment solution for the skeletal muscle cell. It will also seek to expand IGF-1 bioactivity duration through a safe and effective system for delivering drugs through nanotechnology to proficiently distribute IGF-1 to skeletal muscle cells with the aim of lessening skeletal muscle wasting and other conditions linked to it. This aim will be realised through the following objectives.

1. Optimising the concentration of IGF-1 to be employed in skeletal muscle cell culture to maintain cell viability and growth
2. Examining the properties of IGF-1 with MSNPs on the proliferation of skeletal muscle, its existence, differentiation, and metabolism

4.1 Results

4.1.0 Impact of IGF-1 on skeletal muscle myoblasts (C25)

For a period of 24 hours, C25 was grown in a plate with six wells at a density of $1.5x10^5$ cell/ml. DM was used to treat the cells after 24 hours. A comparison of the IGF-1 concentrations that follow compared with DM treatment only: 10 ng, 20 ng, 40 ng, 80 ng and 160 ng (this concentration was doubled each time to see the effect of IGF-1 on the cells and the significant difference between them). The treatment using DM only was used as a negative control so that the impact of IGF-1 on differentiation and proliferation could be validated. At a period of 96 hours following IGF-1 and DM cell treatment, morphological studies were done. The aim was to see if the IGF-1 had an influence on the C25 myoblast differentiation or proliferation. The images of the cell treatments where taken at 96 hours using a live cell imaging system microscope (Leica DM I6000 B). A magnification x20 and scale of 100 µm was used in capturing all images. For all the treatment schedules, the morphological differentiation and proliferation were evaluated across microscopic fields (in each microscopic view). C25, which was treated with DM only, showed myotubes with normal differentiation (Figure 4.0A). Relative to the myoblast proliferation, the myotube formation was dominant at 96 hours. In those cells were 10 ng IGF-1 was the treatment (Figure 4.0B), the results indicated myotubes that dominated the observed fields. On this basis, it could be said that the presence of differentiation decreases proliferation. The proliferation ratio was highlighted using the proliferation marker Ki67. It is concluded that this mark was low in instances where the concentration of IGF-1 was also low.

The second concentration used for IGF-1 was 20 ng and the results, just like 10 ng IGF-1, indicated that large differentiation myotubes dominated the microscopic fields, while the Ki67 marker was seldom detected (Figure 4.0C). For IGF-1 40 ng, the same results were observed with regards to proliferation and differentiation. In this instance, low Ki67 was noted for differentiated myotubes (Figure 4.0D). With the aim of measuring the substantial variation in myotube differentiation between various IGF-1 concentrations, the myotube area, fusion index, and aspect ratio were quantified. The experiments were repeated several times and five images were used for each treatment to calculate the averages for myotube area, fusion index and aspect ratio. From these calculations, substantial differences were noted in the area of myotubes at 96 hours between the negative control and IGF-1 in low concentrations in C25 cell treatment (control= 53% vs. 10 ng IGF-1= 77.4% (p =9.96), and 20 ng IGF-1 = 75.2%). Nonetheless, it is noted that at 40 ng IGF-1, the value of the myotube area what marginally lower (at 56.2%). A substantial variance was noted (p = 0.31) (Figure 4.3). Added to this, there were significant differences for various concentrations when one looks at the fusion index as presented in percentage. In this case, the negative controls value was 71.6% while the 10 ng IGF-

1fusion index was 82.4% with a substantial variance to the control (p = 0.006). For 20 ng IGF-1, the value was 80.6% and no significant difference was noted (p = 0.007) (Figure 4.4). An analysis of the aspect ratio at 96 hours indicates a slight difference. In that case, 3 represents the negative control. For 10 ng IGF-1, the value was 4.6 (p = 0.01), 20 ng IGF-1 had a value of 4 (p = 0.14), and 40 ng IGF-1was 2.4 (p = 0.02) (Figure 4.5).

When the concentration of IGF-1 was high, it was observed that proliferation happened without differentiation. While proliferation was noted when concentrations of IGF-1 were 80 ng and 160 ng, extremely small or no amounts of myotubes were identified. However, it was noted that there was cell growth. As can be seen in the images, the marker of proliferation, Ki67, was noted more in instances when concentrations were higher in the presence of proliferation (Figure 4.1). With the aim of measuring the growth of cells, fusion index, myotube area, and aspect ratio where quantified. The results showed that there were substantial variances in myotube differentiation when compared to the negative control. When IGF-1 concentrations were high, significant differences were presented by myotube area in contrast with the negative control. From the results, it can be noted that the myotube area, when the treatment area is 80 ng IGF-1, stands at 20.2% (p = 9.50E-05). For area 160 ng IGF-1 (p = 0.0001), the value is 17.4% (Figure 4.3). There were significant differences noted in the fusion index measurement: 80 ng IGF-1 delivered a result of 34.8% (p = 2.75E-05) and 160 ng IGF-1 brings up a fusion index of 32.2% (p = 0.0008) (Figure 4.4). For the aspect ratio, significant differences were also observed: 80 ng IGF-1 showed a result of 0.8 (p = 0.005) and 160 ng IGF-1 was 0.9 (p = 0.0041) (Figure 4.5).

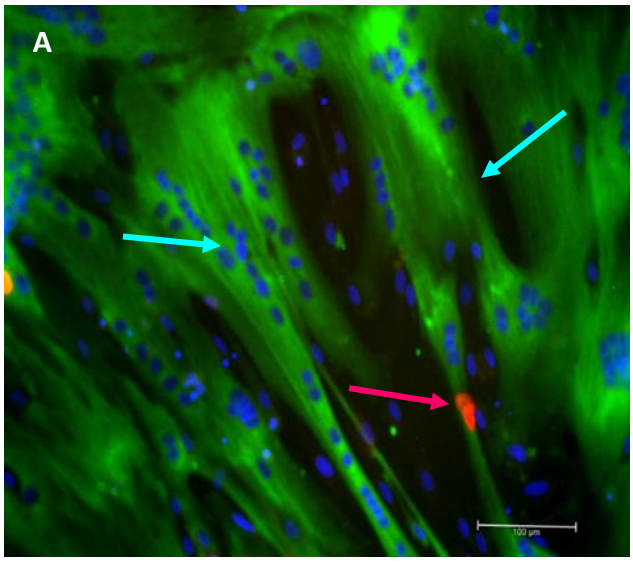

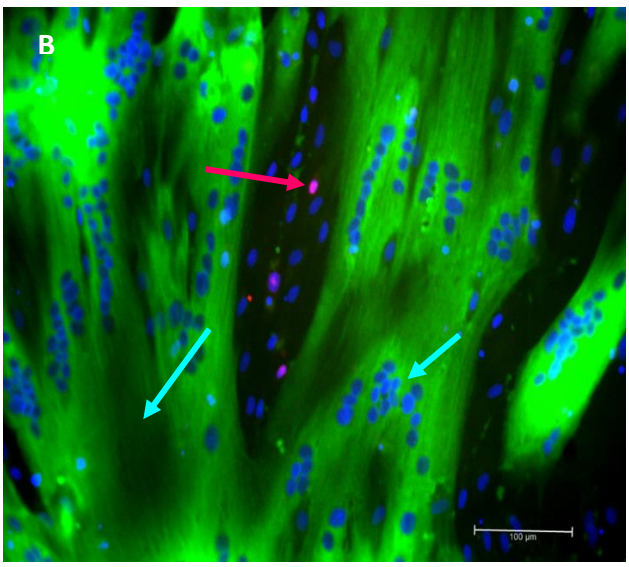

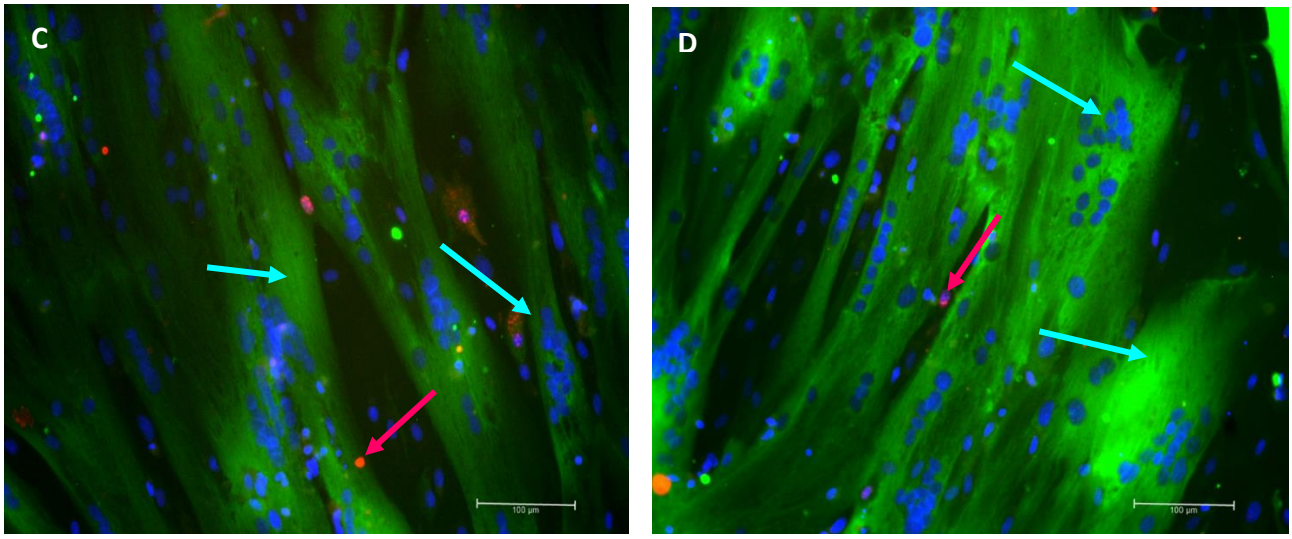

Figure 4.0: Representing low concentration IGF-1 cell treatment. From the images, it can be seen that the differentiation of C25 in DM occurred at 96 hours; (A) C25 differentiated in DM (negative control); (B) C25 treated with 10 ng IGF-1; (C) C25 treated with 20 ng IGF-1; and (D) C25 treated with 40 ng IGF-1. MHC, Ki67, and DAPI were employed for the purpose of staining all images. The proliferation marker is indicated using the pink arrow while the MHC-stained myotube is shown using the blue arrows, with numerous nuclei inside stained with DAPI (blue). A magnification x20, n=5 and scale of 100 µm scale was used when capturing all the images.

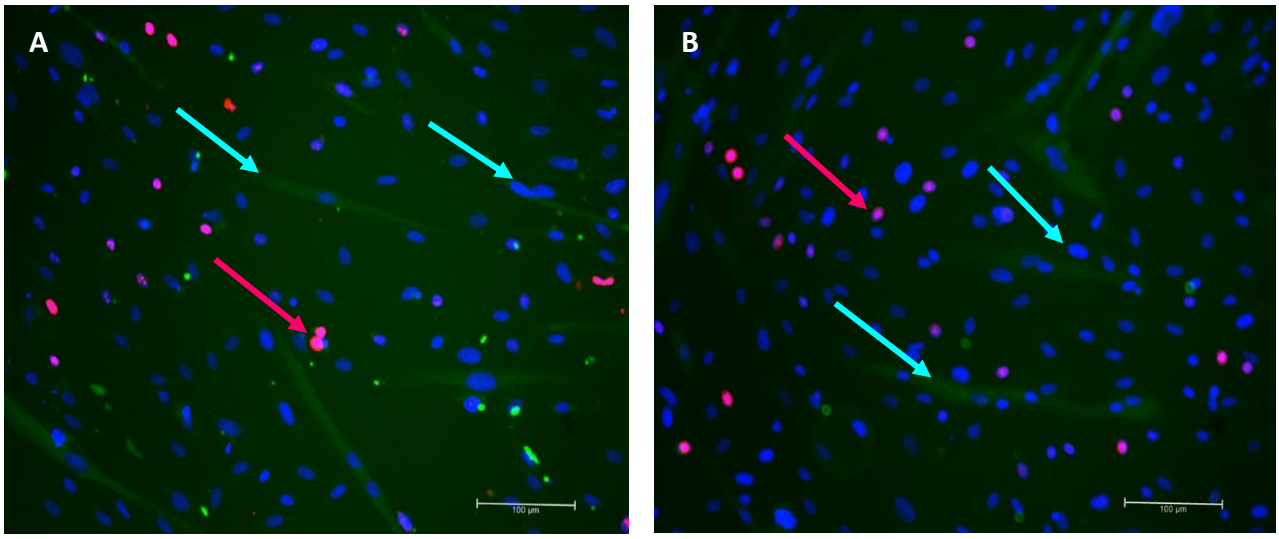

Figure 4.1: Illustrates treatment of cells with IGF-1 in high concentration. From the images, results for high IGF-1 concentration and DM-treated C25. Image A shows results for 80 ng IGF-1-treated C25 and B shows the results for 160 ng IGF-1-treated C25. MHC, Ki67, and DAPI are used for staining the images. The proliferation marker Ki67 is indicated by the pink arrows (red dots), while the MHC-stained myotube size is indicated by the blue arrows and the DAPI-stained nuclei (blue). A magnification of x20, n=5 and a scale of 100 µm was used when capturing all the images.

4.1.1 Impact of IGF-1 and MSNPs on skeletal muscle myoblasts (C25)

When the cells were treated with 0.75 mg/ml SBA-15 (MSNPs), it can be seen that the nanoparticle did penetrate the myotube. Nonetheless, it is also noted that there were no substantial differences observed with regard to differentiation. It is for this reason that large and clear myotubes can be seen (Figure 4.2A), with the quantity of the red dots (Ki67) being small. When compared to the negative control, it can be noted that the myotube area percentage was a little higher at 54% ($p = 1.73$). At 71.2%, the fusion index was a little lower, showing no significant difference ($p = 0.83$). An aspect ratio of 2.8 ($p = 0.74$) was also slightly lower (Figure 4.5).

Nonetheless, 0.75 mg/ml MSNPs and 10 ng IGF-1 was used to treat the cells; a higher level of differentiation could be seen (Figure 4.2B). For each condition, the fusion index, myotube area, and aspect ratio were calculated (Figures 4.3 -4.5). The results show distinct significant differences between the cells treated with IGF+ NP in low concentration and the control. The calculations indicate that the myotube area is higher than it is in the negative control. A proportion of 83.4% ($p =0.0001$) represents the myotube area, a significant difference. At 95.4% ($p = 0.0002$), it can be noted that the fusion index was also high. An aspect ratio of 5.6 is also higher than the negative controller with significant value ($p = 0.006$). Immunofluorescent images captured using primary antibody Ki67 with Texas Red®-X staining and DAPI nuclear counterstain, Alexa Fluor-488-MyHC were employed for the purpose of measuring the myotube area, fusion index, and aspect ratio.

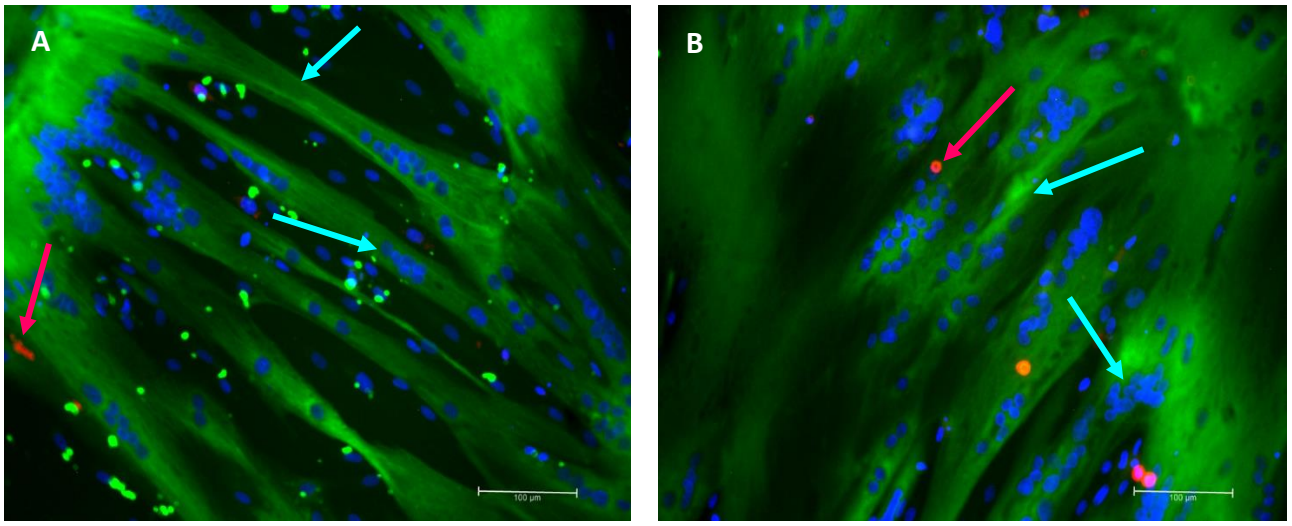

Figure 4.2: Illustrates treatment of cells with IGF-1 and MSNPs (SBA-15). Image A shows 0.75 mg/ml MSNPs (SBA-15)-treated C25 at 96 hours. Image B shows MSNPs (SBA-15) and 10 ng IGF-1-treated C25. MHC, Ki67, and DAPI are used for staining both images. The proliferation marker Ki67 is indicated by the pink arrows (red dots), while the MHC-stained myotube size is indicated by the blue arrows and the DAPI-stained nuclei (blue). A magnification of x20, n=5 and a scale of 100 µm was used when capturing all the images.

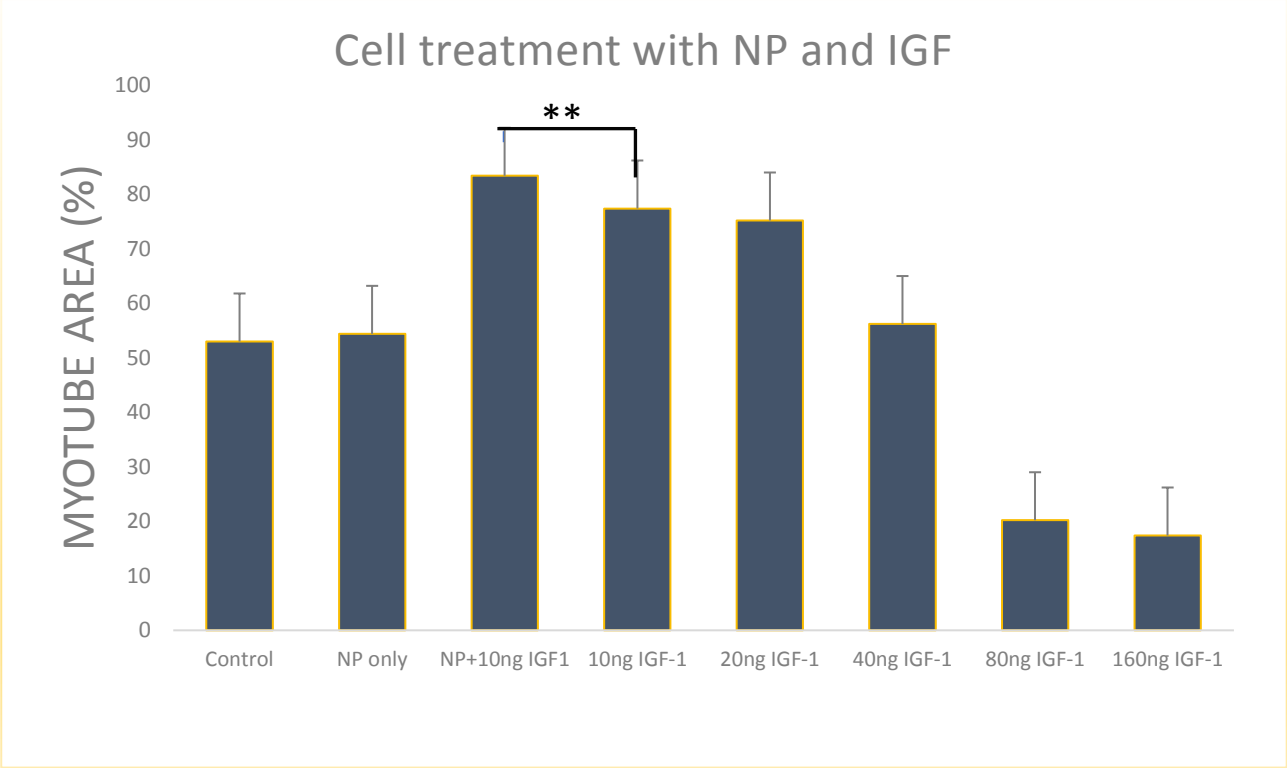

Figure 4.3: Presents a graph showing the myotube area as demonstrated in percentages in the cell treatment area for each condition with negative control included. For each condition a One-way ANOVA and Bonferroni's Multiple Comparison Test was performed. The graph shows that there is a significant difference between cells treated for each condition however, in this graph it compares and highlights the significant differences between cells treated with 10ng IGF-1 and cells treated with NPs +10ng IGf-1 only, which is (** denotes P<0.001).The calculation of the myotube area is done using these equations: (**total area of myotubes in a field) / (total area of the field) (x100).** n = 5 independent experiments.

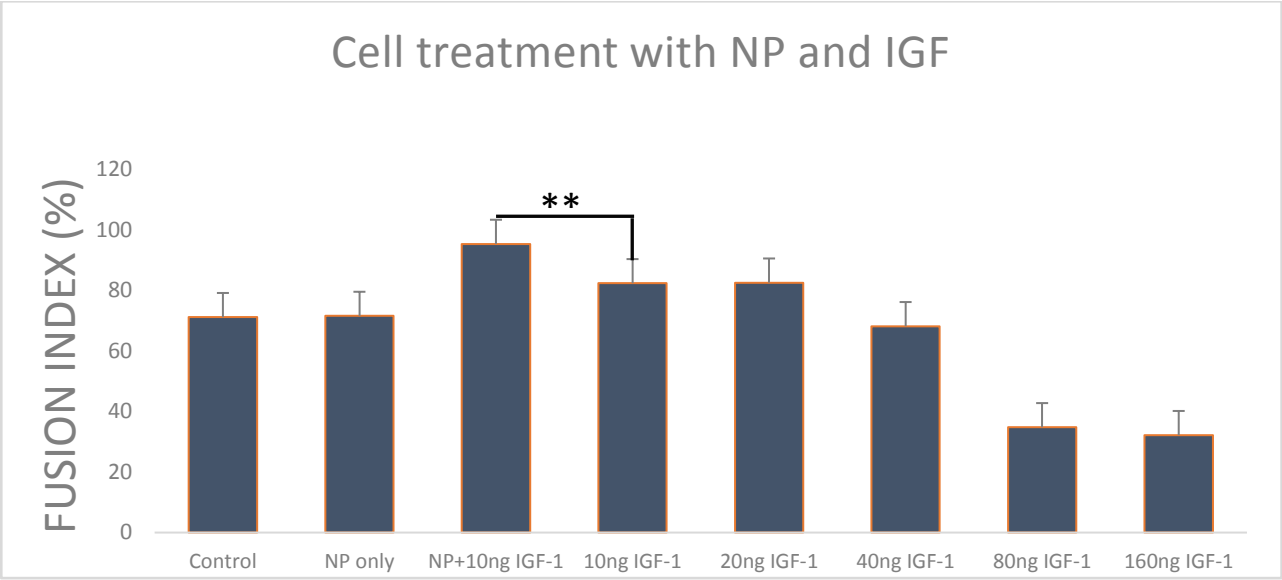

Figure 4.4: Illustrates the fusion index which is presented in percentages in the cell treatment for each condition, with the negative control included (DM only). Error bars are shown to represent ± SD. For each condition, a One-way ANOVA and Bonferroni's Multiple Comparison Test was performed.The graph shows that there is a significant difference between cells treated for each condition however, in this graph it compares and highlights the significant differences between cells treated with 10ng IGF-1 and cells treated with NPs+10ng IGf-1 only, which is (** denotes $P<0.001$).The computation of the fusion index was done as follows: **(total number of the nuclei in each myotube) / (total number of the nuclei in the field) (x100).** n =5 independent experiments.

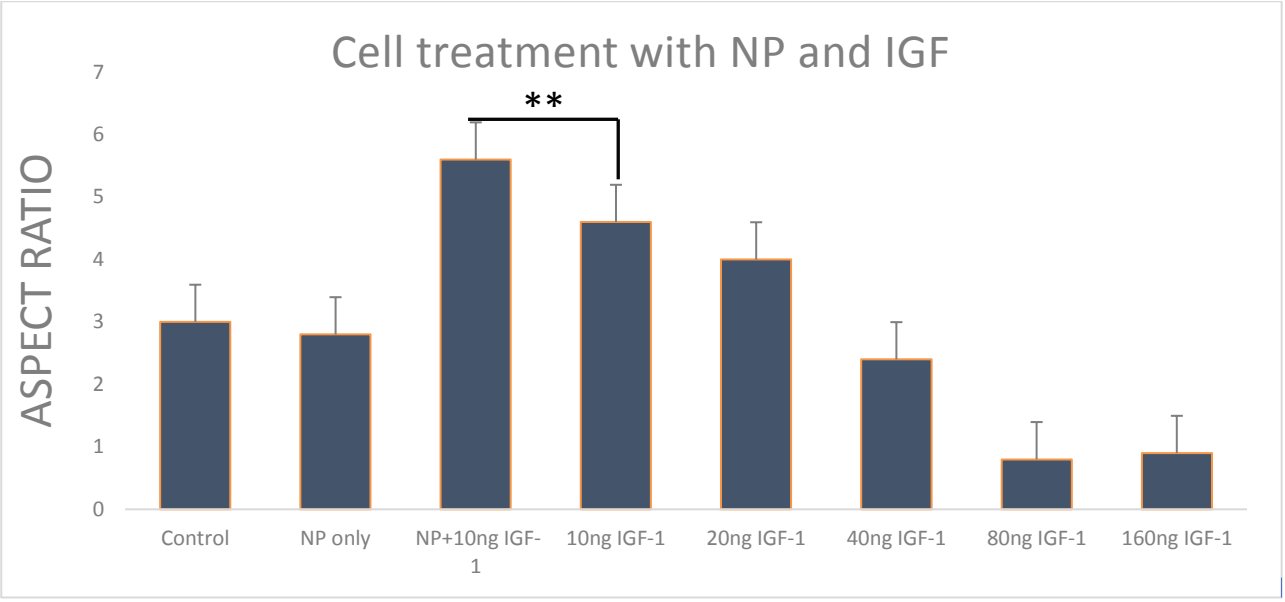

Figure 4.5: Graph representing the aspect ratio for each cell treatment condition, including negative control (DM only). Error bars are shown to represent ± SD. For each condition, a One-way ANOVA and Bonferroni's Multiple Comparison Test was performed. The graph shows that there is a significant difference between cells treated for each condition however, in this graph it compares and highlights the significant differences between cells treated with 10ng IGF-1 and cells treated with NPs +10ng IGf-1 only, which is (** denotes $P<0.001$). The calculation of the aspect ratio was done using the flowing equation: **(myotube length) / (myotube width).** n = 5 independent experiments.

4.1.2 Ki67 proliferation marker

The ratio of proliferation to differentiation is highlighted using the proliferation marker Ki67. The computation of the Ki67 numbers was obtained for each condition from the five images. This made it possible to compute the average quantity of Ki67 markers for each cell treatment. Hence, the significant difference was obtained using the T-test, and the standard deviation was computed for the purpose of attaining the significant differences. As can be seen in Figure 4.6, the average number for the negative controller is 2. For 10 ng IGF-1, the average number is 1.4, with no significant difference when compared to the negative control ($p = 0.2$). When 20 ng IGF-1 is used as the treatment, 1.8 becomes the average, and no significant differences were observed. The number for 40 ng IGF-1 was a little bit higher at 3 ($p = 0.14$). With regards to higher IGF-1 concentrations, significant differences can be noted as levels of proliferation were higher, and differentiation was lower. When treatment was done with 80 ng IGF-1, the average number was 11.4 ($p = 0.0005$). The average number dramatically escalated with 160 ng IGF-1 21.25 ($p = 0.001$). For this level of treatment, almost the whole field contained proliferated cells. For C25 treated only with 0.75 mg/ml SBA-15, the average number was 2.4, and there was a significant difference when compared to the control ($p = 0.0037$). For the cells treated with 10 ng IGF-1 and 0.75 mg/ml SBA-15, the observed average number was 1 ($p = 0.034$), considering that almost no Ki67 marker was observed because of the big dominance of differentiated myotubes.

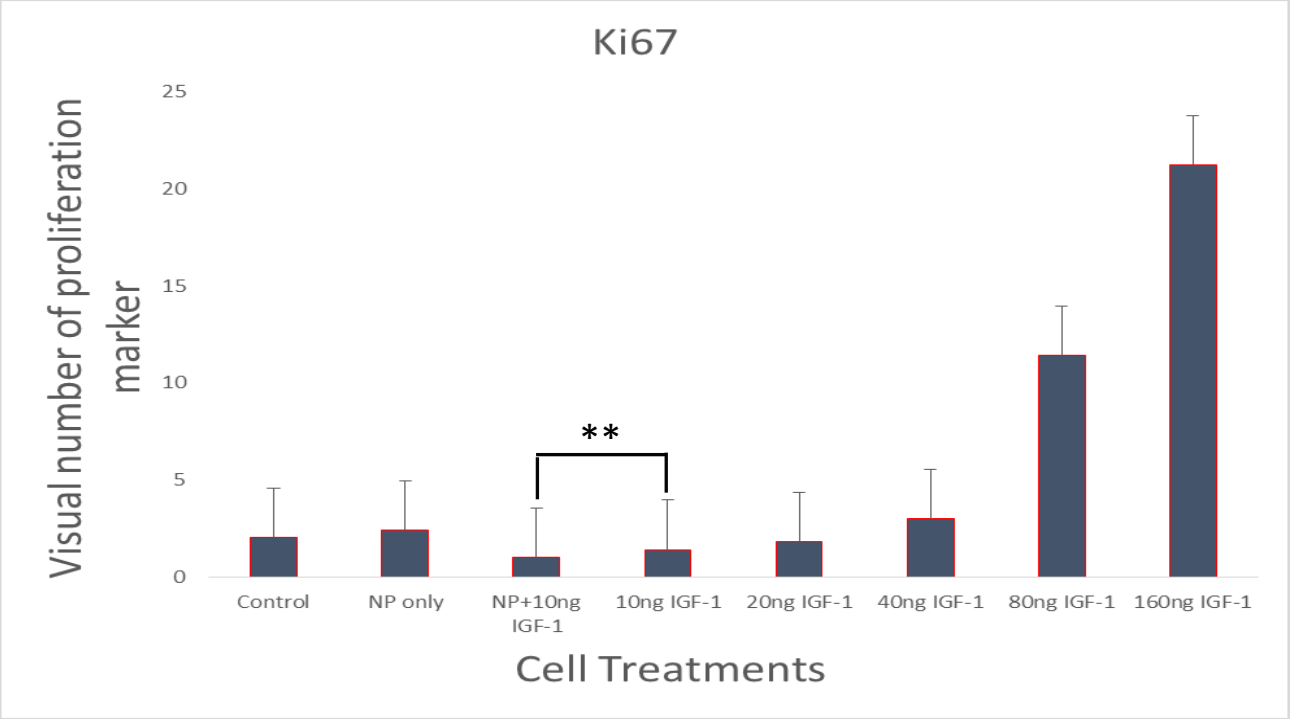

Figure 4.6: Presents the Ki67 markers. In the graph, each cell treatment condition, including the negative control (DM) is presented. Error bars are shown to represent ± SD. For each condition performed, the One-way ANOVA and Bonferroni's Multiple Comparison Test was performed. The graph shows that there is a significant difference between cells treated for each condition however, in this graph it compares and highlights the significant differences between cells treated with 10ng IGF-1 and cells treated with NPs+10ng IGf-1 only, (** denotes $P<0.001$).n = 5 independent experiments.

4.2 Discussion

In this chapter, optimising the concentration of IGF-1 was employed in skeletal muscle cell cultures to maintain cell viability and growth, as well as the impact of IGF-1 on differentiation and proliferation is validated at a period of 96 hours following IGF-1 and DM cell treatment, morphological studies. Notwithstanding the fact that there are several studies emphasising the role played by IGF-1 in the process of muscle repair, numerous studies have shown that there is a link in the differentiation process by activating the adipogenic and osteogenic genes expression pattern in mesenchymal stem cells. As human mesenchymal stem cells (hMSCs) are organised by IGF-1, there is a reduction of the expression of osteogenic genes and an increase in adipogenic genes. This is a process that allows for the adipogenic differentiation while inhibiting osteogenic differentiation, a situation linked directly with the healing of wounds. From studies, it has also been concluded that IGF-1 in neochondrogenesis facilitating the differentiation of rabbit MSCs regarding chondrocytes in the application of the PI3 K/AKT (Armakolas et al., 2016). As a result of the transforming growth factor 3 (TGF-3), in the hMSCs, chondrogenesis is triggered. Contemporary studies advise that IGF-1 has the ability to act in synergy with TGFβ-3 enclosed in silk fibroin scaffolds to embolden chondrogenic differentiation and chemotactic homing of hMSCs (Armakolas et al., 2016).

Depending on the concentration, there is a significant increase in TGFβ-3 (up to 2 times), in combination with IGF-1. It has also been observed that aggressive discharge of TGFβ-3 and enlarged collagen II facilitate the chondrogenesis of hMSCs. On the other hand, silk fibroin scaffolds with IGF-1 and TGFβ-3 made use of more CD29+/CD44+ cells and showed more extracellular matrix resembling cartilage and lower levels of fibrillary collagen in connection with TGFβ-3 adapted scaffolds. The research proposes that the IGF-1 concentration motivation is linked to the SkMC re-establishment. It has also been recognised that there is a link between hypertrophy and the proliferation expression (Armakolas et al., 2016; Tong et al., 2015; Jing et al., 2018).

The results produced by this study indicate that SkMC is significantly impacted by low concentration of IGF-1. Between the low concentration IGF-1 in C25 cell treatment and the negative control, there were significant differences noted in myotube area. In the meantime, with regards to myotube proliferation, myotube development was dominant. Results for 10 ng IGF-1 treated cells (Figure 4.0B) produced differentiated myotubes that had significant differences with regard to fusion index, myotube area, and aspect ratio with the C25 negative control. It is also illustrated by the IGF-1 release analysis that this was the most suitable concentration to be employed with regards to nanotechnology. Hence, it is seen as the most appropriate method for uploading nanoparticles. Notwithstanding the fact that 20 ng is not advisable for use in nanoparticle treatment, it indicated big differentiated

myotubes dominating the microscope fields while the Ki67 marker was hardly detected (Figure 4.0C). The same results were shown by IGF-1 40 ng with regards to proliferation and differentiation. Nonetheless, there were some significant differences noted. On this basis, it is not advisable to use IGF-1 40 ng in studies involving nanotechnology (Figure 4.0D). From the statistical analysis, it can be noted that there is no significant difference between IGF-1 concentrations of 10 ng and 20 ng. However, there are slightly lower significant differences with the IGF-1 40 ng concentration.

It has been recognised that IGF-1 overexpresses skeletal muscle cells at high concentrations. This is because proliferation seems to occur when there is no differentiation. This study analysed two IGF-1 high concentrations (80 ng and 160 ng). Both these concentrations indicated high proliferation. As a result of the absence of differentiation, myotubes were seldom observed. As can be seen from the images, the proliferation marker Ki67 was more noticeable when proliferation was higher, and proliferation was present (red dots) (Figure 4.1). As a result of the effect it has on cell expression, IGF-1 plays an important role in cancer where it has been linked to the facilitation of proliferation and an escalation of metastatic capacity in numerous cancers. In contexts of overexpression, IGF-1R or the insulin receptor's isoform A prompt some reaction. However, cancer cell proliferation is inhibited by their downregulation. IGF-1's oncogenic properties connection with cancer results in the development of antibodies when compared to IGF-1R and IGF-1, even though the effect is insufficient. This is due to the activation of downstream pathways (to a considerably more minor degree than IGF-1) when the anti-IGF-1R antibody binds to IGF-1R. For that role, targeting some main effects of the IGF-1R is considered based on their results in cancer when used together with anti-IGF-1R antibody or on its own (Armakolas et al., 2016).

The contributory role of other factors like the IGF-1Ec isoform has been proposed, more recent studies, to have a link to precancerous or cancerous conditions. It has been suggested that there is a link between IGF-1Ec expression and stage and grade in cancer. For instance, IGF-1Ec overexpression is connected to human prostate cancer (PCa) tissues and in prostatic intraepithelial neoplasia (PIN). Nonetheless, normal prostate tissue and prostatic epithelial cells have not been seen to have IGF-1Ec. Besides, unlike IGF-1, the exogenous controlling of artificial Pec, IGF-1Ec COO-terminal comprising the last 24 amino acids, which is lacking in IGF-1 that is mature, inspires PCa cell growth and triggers ERK1/2 phosphorylation without unsettling Akt phosphorylation.

Once INSR or IGF-1R is stopped, the result of PEc on PCa is maintained. This implies that the Ec peptide technique is implemented across GF-1R, INSR and IGF-1R/INSR hybrid receptors independent use. From reports on genetic overexpression, it can be noted that IGF-1 does have an effect on making muscle regeneration simpler after injury. This observation approves it as a molecule

with potential for use in the treatment of muscle injuries. On the other hand, IGF-1's short half-life is approximately 12 hours (Lammers et al., 1989) however, it was found to be 10–30 minutes in (Pan and Kastin , 2000; Hammers et al., 2012) together with potentially harmful systematic possession has lessened the beneficial presentation of the molecules. It was the aim of this report to appraise the curative potential of the delivery of IGF-1 in an environment that is safe and regulated, making use of appropriate IGF-1 concentration and a nanotechnology platform being used for drug delivery when treating skeletal muscle (Hammers et al., 2011). For this study, only 0.75 mg SBA-15 (MSNPs) was used for the treatment. The results indicated that nanoparticle was absorbed in the myotube. However, the presence of big clear myotubes indicated that there were no big differences noted with regards to differentiation (Figure 4.2A). This is indicated by the low quantity of red dots (Ki67). Considering the fact that a nanoparticle does not have the capability to deliver vital significant differences for cell treatment, it is important that IGF-1 plays the role of the cell treatment for muscle wasting and muscle injury. However, introducing IGF-1 is aimed at raising or facilitating chondrogenic differentiation since IGF-1 is a growth factor and has been employed to facilitate the link between chondrocytes to extracellular matrix proteins. It also controls prechondrocytes proliferation.

IGF-1 is an important contributor in preserving the reliability of cartilage and matrix production. However, when IGF-1 is overexpressed, it can trigger differentiation and hypertrophic mineralisation. It is on this basis that an organised and safe delivery of biomolecules across the process of recovery is important if adverse results are to be prevented. As is the case with other growth factors, IGF-1 has a short half-life. This implies the importance of closely managing them as opposed to systematically. For this study, it has been shown that the introduction of low concentrations of IGF-1 (10 ng), together with drug delivery SBA-15 at a concentration of 0.75 mg results in the upgrading of local, and constant delivery of IGF-1 to skeletal muscle cells. To achieve a long-term and organised local stimulation of cells when applied medically, MSNPs, together with growth factors, are employed in the delivery (Pasold et al., 2015).

For this experiment, huge differentiated myotubes were observed in morphological studies in addition to observation of myotubes in shorter time with this large size. For this study, the nanoparticles used were kept outside the SkMC (C25) cell membrane for targeting drug distribution to the cell membrane. Nonetheless, this study has shown that it is possible to adopt nanoparticles into the cells through endocytosis, and cell movement variations, resulting in reduced proliferation (Huang et al., 2010). A similar set of results to those of the experiment was produced in a study by Tsukahara and Haniu (2011). The results showed that IGF-1 and nanoparticles facilitated skeletal muscle myoblast differentiation while simultaneously inhibiting myogenic proliferation (Chen et al., 2012; Tsukahara & Haniu, 2011). The regulatory factors myogenin and MyoD regulate the transformation from

proliferating satellite cells to differentiated skeletal muscle cells (Yamane et al., 2000). An analysis of mesoporous silica-collagen hybrid nanoparticles cultured with skeletal muscle cells indicates an up-regulation in the expression of *myogenin* and *MyoD*, leading to augmented skeletal muscle cells differentiation into terminally differentiated myotubes that do not have the capacity to return to the cell cycle, leading to blocked myoblast proliferation (Chen et al., 2012).

4.3 Conclusion

From the results presented in this study, it can be noted that the optimal IGF-1 concentration that induce myoblasts differentiation for use with MSNPs is 10 ng. It is at this level that differentiation is boosted and proliferation reduced. When SBA-15 was introduced, differentiation was noted at 10 ng, 20 ng, and 40 ng. On the other hand, it has been noted from the study that high IGF-1 concentrations result in reduced differentiation as proliferation escalates. In high concentrations, Ki67 markers (red dots) were observed. This implies that Ki67 plays the role of a proliferation marker. For a drug delivery system that is efficient, it is a requirement that the MSNPs are biocompatible, possess skeletal muscle tissue specificity, and the release of the drug molecules if they are released are in a controlled fashion and this will ensure a concentration that is effective.

Chapter 5: Generation, Characterisation and Functional assessments of Neuromuscular Junction (NMJ) platform

5.0 Background

5.0.0 Introduction

The neuromuscular junction (NMJ) is a dedicated site that connects a motor neuron's axon's terminal to skeletal muscle. As the structure that makes it possible for a neuron to transmit a chemical or electrical signal to another neuron, the integrity of the NMJ is vital for moving the motor neuron signals which trigger the contraction of the skeletal muscle. The majority of diseases and the ageing of the skeletal muscle can be connected to the impairment in NMJ function and the connected wasting of the muscle (Liu & Chakkalakal, 2018). Neuromuscular Junctions also play the role of being a platform for the skeletal muscle and nerves to interact. It contains a presynaptic motor neuron terminal, a postsynaptic motor endplate, and a synaptic cleft. The structure for the formation and maintenance of NMJs relies on the back and forth molecular interface between the motor neuron and muscle (Zahavi et al., 2015).Co-dependent tissues motor neurons and skeletal muscle rely on each other for successful transmission/stimulation and trophic support (Delbono, 2003). Motor neurons and skeletal muscles synthesize IGF-1 (Delbono, 2003). The resulting IGF-1 signalling plays an important role in the formation of the neuromuscular junction as shown by Caroni and Becker (1992). Neuromuscular junctions become active as they form while at the same time motor neurons stop the production of GAPs (Caroni and Becker, 1992), which correlate highly with the skeletal muscle decreased production of maturational IGF-1. IGF-1 levels decrease as people age considering there is concomitant endplate loss and existing motor endplates decreased innervations (Messi and Delbono, 2003), which may make the transmission of impulses problematic. Age-related changes can be reversed successfully with overexpression of IGF-1 in skeletal muscles. The process can also sustain neuromuscular junction complexity successfully the required innervation and subsequent transmission of signal impulses (Messi and Delbono, 2003).

NMJ importance in NM disease has been shown in many studies on amyotrophic lateral sclerosis (ALS). Most research has shown that NMJ is one of the earliest yet detectable signs of the condition. There have been observations that NMJ insults are closely linked to the disease progression rather than the death or loss of MNs (Murray et al., 2008; Fischer et al., 2004; Gould et al., 2006). The degeneration of NMJ has been an important aspect in studying NM diseases that have not been thought of such as diabetes that is associated with many types of peripheral neuropathy as one of the commonest NM complications (Bril, 2014). Methods to study NMJs degeneration's contribution to

the aetiology of NM disease are non-existent. Most of the *in vivo* models that have been developed to study NM disease are animal models that are limited as they cannot replicate diseases in human beings adequately (van der Worp et al., 2010). *In vitro* models have a similar challenge as they use cells derived from animals (Haase, 2006; Prather et al., 2013). In addition, *in vitro* human SkMC monolayers NM models do not provide functional innervations necessary for the formation of NMJ and advanced muscle differentiation (Suuronen et al., 2004; Ashby et al., 1993; Wilson and Harris, 1993). The pathogenesis of NM disease can be enhanced by techniques that can successfully manipulate NMJs. Such methods must consider the importance of SkMC innervations and formation of NMJs in differentiation, maturation, and function of SkM. Such techniques may provide an important platform for testing potential NM disease therapies in human beings.

Mouse, rat, primary human myoblasts, human induced pluripotent stem cells (hiPSCs)-derived cells, human embryonic cells, and cross-species systems muscle co-culture models have been proposed as some of the best solutions to this challenge (Umbach et al., 2012; Arnold et al., 2012; Demestre et al., 2015; Guo et al., 2014; Harper et al., 2004). These proposed systems have the major challenge of inadequate experimental reproducibility due to the intricate culture system that needs neutrophiric and growth factors. Common culture media additions include animal serum, foetal calf serum, or foetal bovine serum (FBS) because they include y-globin and strong promoting driver (Ferruzza et al., 2012). However, there are serious ethical and scientific concerns for use of serum but it remains an important supplement of cell culture media (Brunner et al., 2010). In addition, there are technical disadvantages as the resident molecules increase the chances of contamination (Hadwe, 2009). At the same time, there are concerns that the serum collection process in animals makes them suffer, which raises ethical issues about their use (Riebeing et al., 2011). The concerns have made some researchers desist from using the approach. The division has had a negative impact as the number of studies is much less characterised by lower reproducibility.

These ethical concerns have led to the development of alternative chemical components for mammalian cell lines and primary cultures. Manufacturers must determine the appropriate medium formation, which is usually time consuming (Brunner et al., 2010). The serum used in classically established nerve-muscle co-culture systems (Giller et al., 1973; Nelson et al., 1993; Li et al., 2001; Daniels et al., 2000; Dutton et al., 1995) has indeterminate variables that arise because of the serum composition variation that leads to lower experimental reproducibility that may affect the experimental treatments on the system. These conditions make the addition of serum to a co-culture for the generation of NMJs *in vitro* impractical. Moreover, there are suggestions that serum in co-cultures may lead to retardation of MN myelation in *in vitro* systems (Rumsey et al., 2009).

5.0.1 Aims

Recently, our research group developed a novel entirely human NMJ platform using hESCs-derived neural progenitor cells (NPCs)-transfected with green fluorescent protein (GFP) and human myoblast. The aim of the current chapter was to use GFP transfected-NPCs (previously generated in our lab) and myoblasts to replicate Abd Al-Samid's model (Abd Al-Samid's et al., 2018), which was characterised using specific differentiation markers for motor neurons and myoblasts. To further verify that this NMJ model behaving physiological and muscle contraction is motor neuron-driven, NMJ model was manipulated using pharmacological drugs to pre- and post-synaptic NMJ agonist and antagonist drug (i.e. α-bungarotoxin & L-glutamic acid).

5.1 Results

5.1.0 Neural progenitors cells (NPCs) Expansion

Recently established an *in vitro* human co-culture (nerve-muscle) model in a *serum-free/neural growth factor-free defined medium* (Abd Al Samid et al., 2018). The model develops functional NMJs rapidly to elicit muscle contraction. The model is established using human embryonic stem cells (hESCs, shef3) derived NPCs and immortalised human myoblasts engineered. Neural progenitor cells (NPCs) derived from hESC differentiate into motor neuron in the co-culture myoblasts and are also named NPC passage 1(P1) that can be stored in liquid nitrogen to allow future studies. The cells can be passaged from P1 to P10 depending on the gestation period taken. Passage P1 or P2 being used extensively in many experiments throughout my PhD studies. They are usually removed from the liquid nitrogen a week before they can be used in a study. During this week, NPCs were cultured in laminin coated T25 flask with NEM media to induce proliferation to ensure that enough number of NPCs for the experiments were obtained. The cells that remained were cryopreserved in a 1 mL 90% fetal bovine serum (FBS) suspension and 10% Dimethyl sulfoxide (DMSO) (NPC P2). One cryovial taken from the liquid nitrogen was cultured in laminin coated T25 flask that included NEW media to start the proliferation process (Figure 5.0). Following the expansion of NPCs which are committed cells for motor neuron differentiation, their neural linage differentiation was confirmed using the Nestin-antibody specific marker for NPCs (Figure 5.1A). Some of the NPCs were transferred together with GFP-reporter lentivirus system (Figure 5.2). This step was followed by incubation of human myoblasts with GM in a period of 24 hours at 37°C within a 5% CO_2 environment in 6-well plates. Thereafter, there was a replacement of muscle differentiation media (co-culture media). The concentration of NPCs was 25 x 10^3/ml, which was incubated for up to 7 days at 37°C within 5% CO_2. After myogenic differentiation was initiated, the characteristics of functional motor units began to develop. This included myotube formation and axonal sprouting from the NPCs which subsequently formed NMJs along the myotubes (Figure 5.1B).

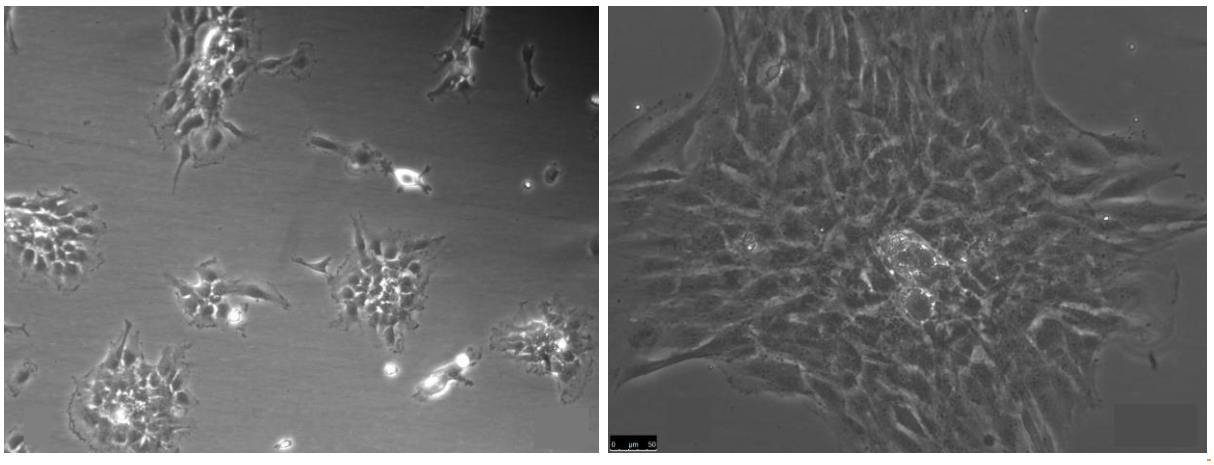

Figure 5.0: Neural progenitors cells (NPCs) Expansion. Neural progenitor cells expanding in suspension in NEM media, NPCs were observed at a Microscope Leica DMI6000B live. Image A 10X and image B 20X. Scale bar = 50 µm.

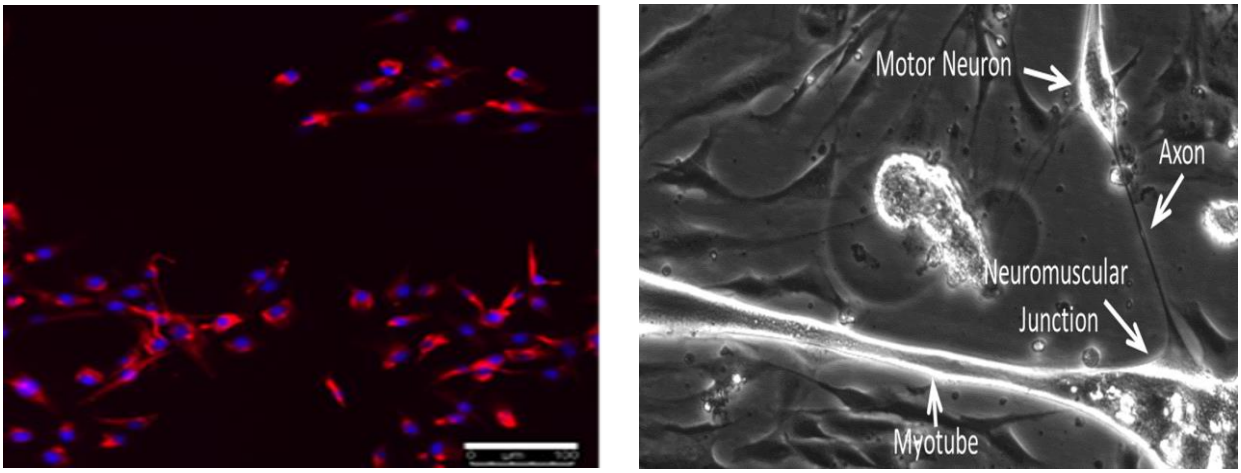

Figure 5.1: Representative images for neural progenitor cells identification. Image (A) immunohistochemistry staining for NPCs, using Nestin antibody (red) and DAPI for nucleus staining (blue). Scale bar =100µM. Image (B) representative of the MN and NMJ formation in co-culture showing an axon extended to contract a myotube. Scale bar = 50µM.

5.1.1 Morphology characterisation of the established NMJ platform

There was morphological co-culture assessment in day 1, 3, 5, and 7 after NPCs were plated with myoblasts using immunohistochemistry as shown in figure 5.2. Phalloidin (red), and nuclei with DAPI (blue), and NCPs transfected with GFP (green) were used to stain the myotubes. The fusion of myotubes was little after 24 hours as they showed multi and mono-nucleated myocytes' characteristics, which was an indication that differentiation was at the initial stage while NPCs did not show any differentiation signs such as neurite growth (Figure 5.2 day 1). The successful differentiation of NPCs leads to the sprouting of neurites and expansion over myotubes and myocytes in which more fusion was observed, which shows that there was multinucleated myotube formation (Figure 5.2 day 3). Obvious myocytes-to-myotube differentiation started and expansion of neurite growth expanded further in day five as shown in (Figure 5.2 day 5). Further expansion of neurite growth and progressive maturation of myotubes were observed in day seven (Figure 5.2 day 7). The neuronal axon terminals started having visible connections with the myotubes (Figure 5.2 day 7) while the first spontaneous contractions in individual myotubes were observed on the seventh day. These factors are an indication that immortalised human myoblasts were fully differentiated and innervated by cells that differentiated from the NPCs.

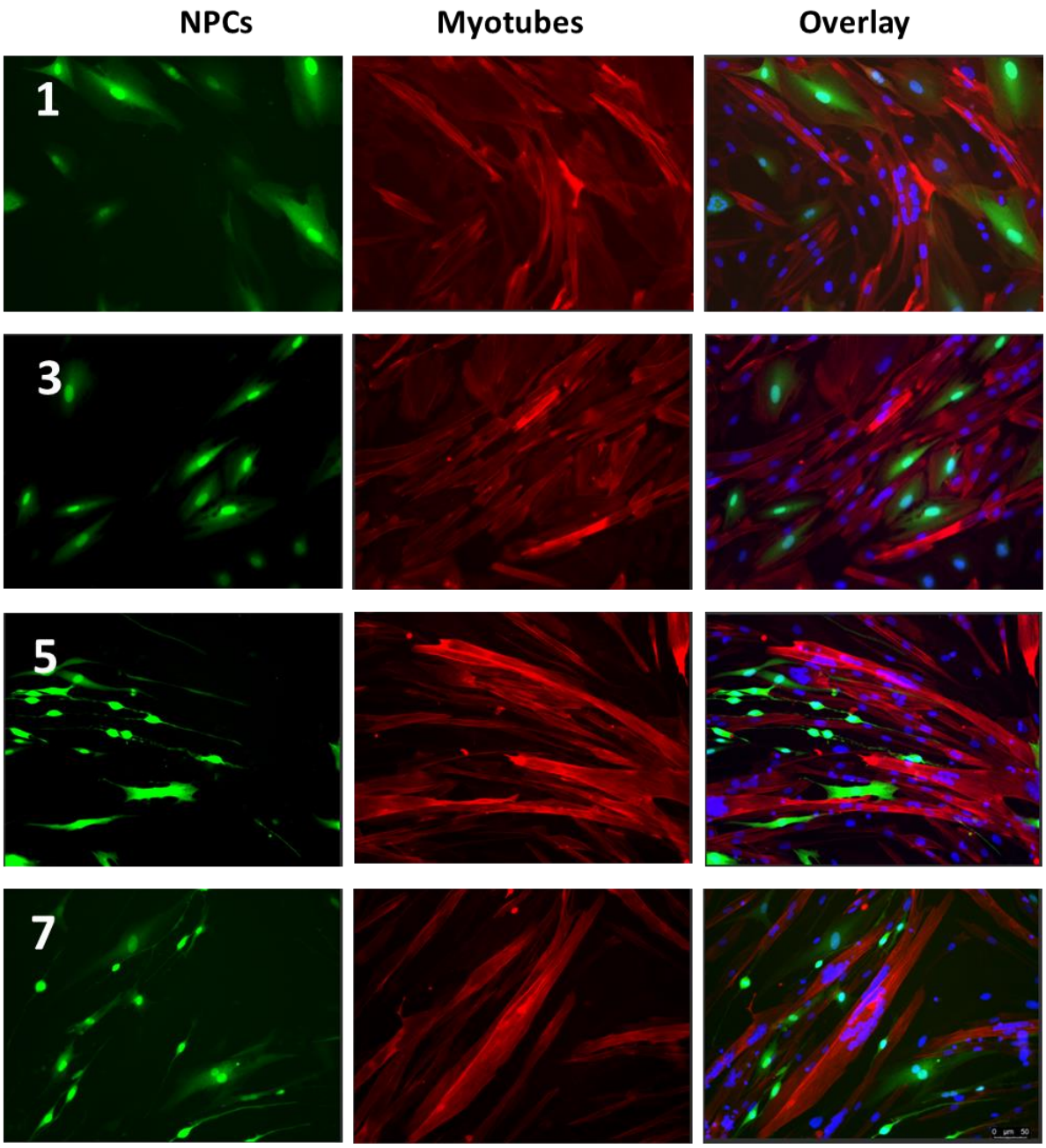

Figure 5.2: A representative images for the developing of NMJ model using NPCs-GFP and human myoblasts. This figure illustrates the differentiation of NCPs into mature motor neurons (left panel) and myoblasts into advanced differentiated myotubes (middle panel) and overlay (right panel) from day 1, 3, 5 and 7. The myotubes were stained for actin with phalloidin (red), differentiated motor neurons-GFP (green), and nuclei with DAPI (blue). n = 3 independent experiments. Scale bar = 50 μm.

5.1.2 Axonal growth measurements

Images were captured on days 1, 3, 5, and 7 to assess neurite growth in the co-culture (see section 2.1.23). NPC neurite elongation of the axonal length was measured using the Leica microscope micro-meter option. The neurite outgrowth increased from (32±3µM) in day one to (91±9µM) in day seven, which underscores that there was high motor neuron differentiation.

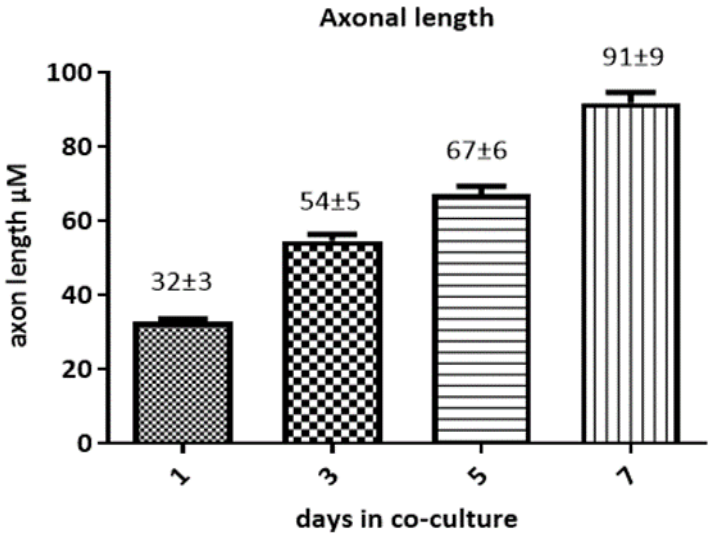

Figure 5.3: Neurite outgrowth in co-culture. This graph shows the axonal length in co-culture from day 1 to 7. Leica microscope measurement tool was used to assess the axon outgrowth, which increased with the time of the co-culture. n = 5 independent experiments.

5.1.3 Spontaneous Muscle contraction

Early contractions that do not have any external stimuli were observed in myotubes on the seventh day after the co-culture of NPCs with C25. Co-cultures with robust motor neuron differentiation innervated with the myoblasts to produce advanced and differentiated myotubes that had a form of contractile function when the atmospheric conditions were at 37°C with a 5% CO_2. (Figure 5.4) Functional motor units' characteristics developed after the initiation of myogenic differentiation. Some of the observations included myotube formation and axonal sprouting from the NPCs that lead to the formation of NMJs on the myotubes. Myotubes got spontaneous muscle contractions after the seven days without exogenous chemical and electrical stimuli (Figure 5.4). The force of the contractions made some myotubes to detach from the culture plate, which created large spaces in the co-culture. The myotubes cultured did not detach from the culture plate as they did not contract. These findings suggest that myotubes' contractions are single motor units that receive stimulation bursts from MNs. There were also some innervations points on myotubes in this stage. The distinction was the higher spontaneous contractile activity in myotubes co-cultured with motor neurons.

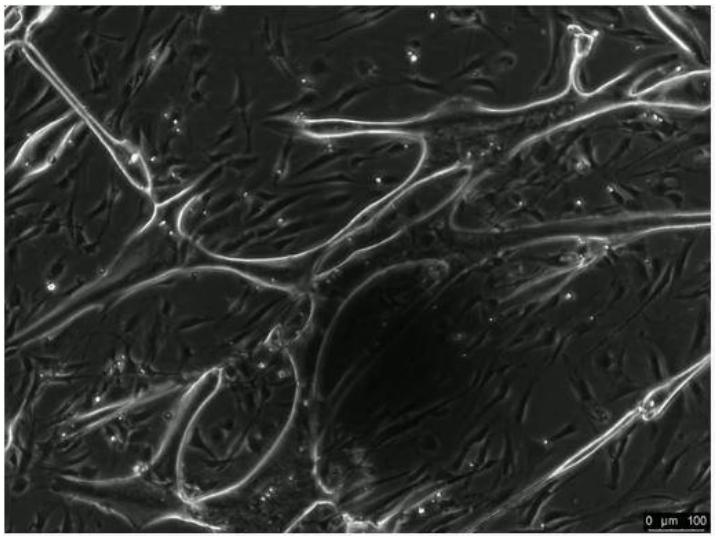

Figure 5.4: Phase contrast video micrograph of immortalised human myotube contractions at Day 7. Demonstrative video 1 of NPCs co-cultured in DM showing spontaneous contracting in serum, growth/neurotrophic factors, free media. Video captured at 24 frames per second. Scale bar =100 µm. (https://www.youtube.com/watch?v=FKsKA_abfL4&feature=youtu.be)

5.1.4 Characterisation of NMJ co-cultures

Assessment of motor neuron formation was completed on the seventh day using the βIII-tubulin motor neuron differentiation marker. Mature motor neurones have axons terminating on myotubes as shown in Fig. 5.5. The formation of cholinergic motor neurons was confirmed using acetyltransferase antibodies (ChAT, a key enzyme for acetylcholine biosynthesis), which is shown in green in Fig. 5.6 (Young et al., 2003). The two images (Fig. 5.5 & 5.6) show mature differentiated myotubes with the nuclei in the periphery.

NMJs usually have acetylcholine receptor (AChR) clusters along myotubes that were assessed using alpha-bungarotoxin (α-BTX) staining and can be identified as the red clusters as shown in Fig. 5.5 & 5.6. Motor neuron axons serve the myotubes with nerves that lead to the formation of NMJ as marked with α-BTX (red) (Young et al., 2003). Spontaneous myotube contractile activity was confirmed on the seventh day.

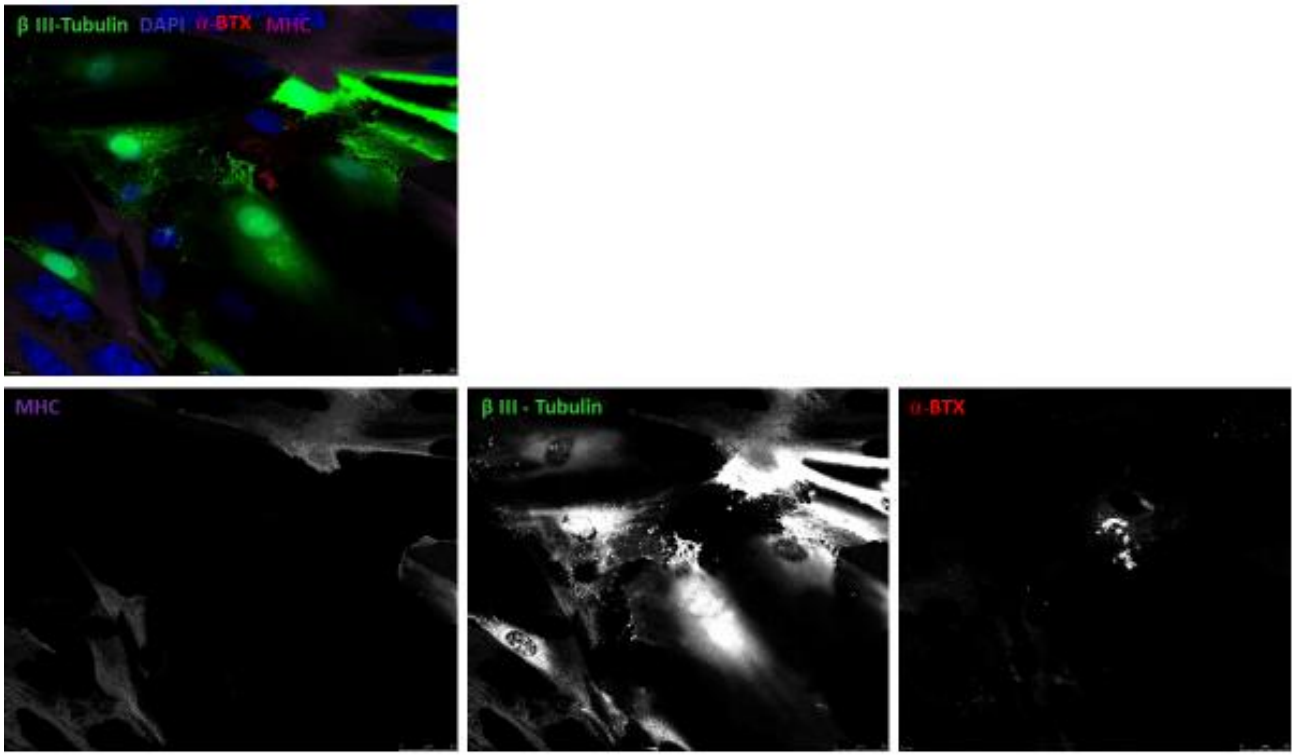

Figure 5.5: Characterisation of functional neuromuscular junction formation on Day 7. A representative image showing an individual motor neuron axon terminal interacting with an acetylcholine receptor cluster in culture. The co-cultures were stained for β-III-tubulin (green), α-bungarotoxin (BTX) (red), myosin heavy chain (MHC) (purple), and DAPI (blue). Scale bar =75 µm.

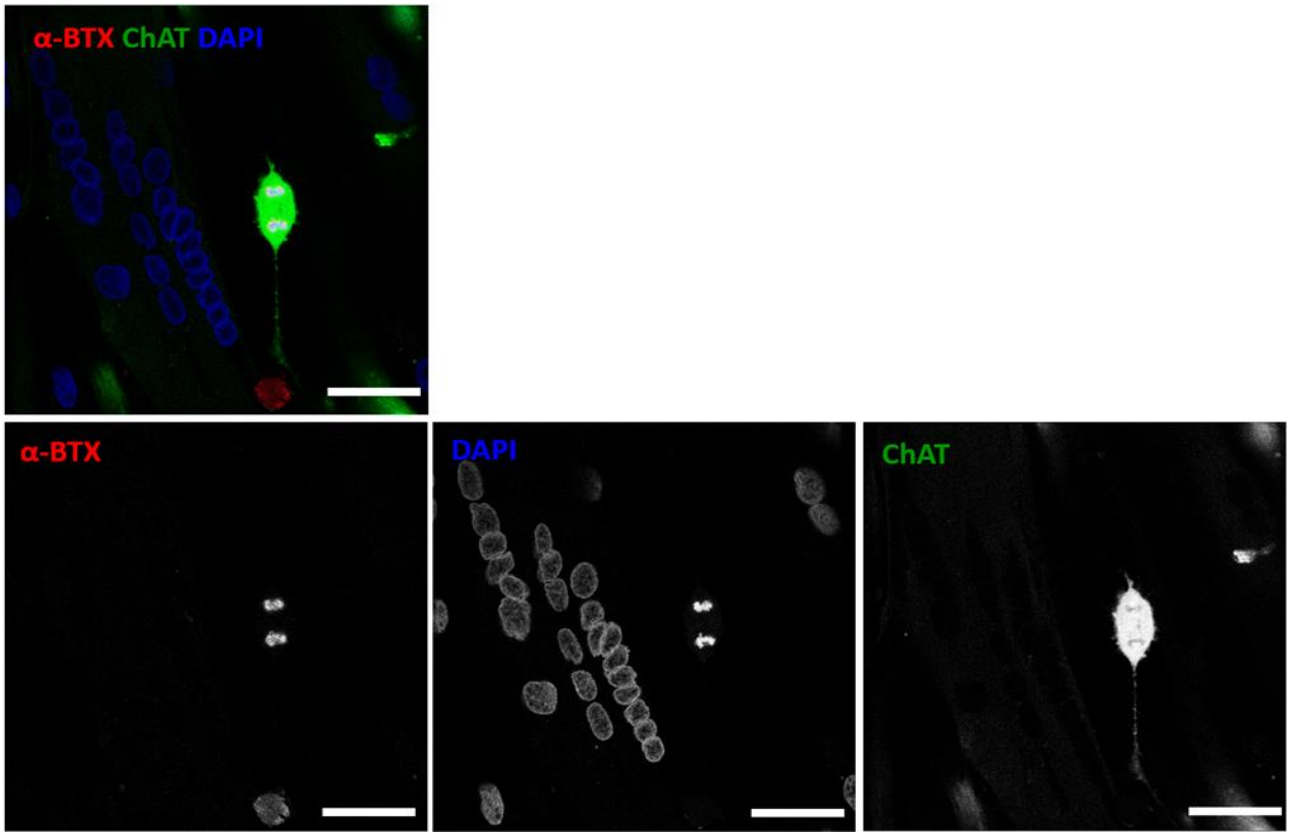

Figure 5.6: Characterisation of motor neuron formation on Day 7. A representative image showing the co-cultures were stained with ChAT (green), α-bungarotoxin (BTX) (red) and DAPI (blue). Scale bar = 75 µm.

5.1.5 Functional Assessment of NMJs with α-Bungarotoxin (α-BTX)

Myotube contraction cessation can be shown with the reversible and irreversible AChR inhibitors application such as bungarotoxin (Umbach et al.,2012; Guo et al., 2011). This study's experiments were done with C25 co-cultures to study the NMJs functional responses to biochemical intervention. The objective was to determine whether NMJs generated *in vitro* in the co-culture reflected the SkM paralysis observed *in vivo.* A dilution of 1:400 α-BTX (10nM) was added to the co-culture (Santhanam et al., 2018) to ensure the induction of postsynaptic AChRs permanent blockade. The most appropriate time to conduct it was the seventh day when peak spontaneous contraction frequency (CF) could be observed. The baseline CF was measured 30 seconds prior to the application of α-BTX, which showed that there were no significant differences in baselines CF between the positive (0.711 Hz ± 0.024) and negative controls (0.720 Hz ± 0.025), (P =0.42) before the treatment. Contraction of the myotubes stopped in the control and α-BTX-treated myotubes after the addition of treated and untreated diluent to the cultured cells. CF in the control decreased to 0.477 Hz ± 0.011 after fifteen minutes but there was no contraction of myotubes in co-cultures treated with α-BTX. The contraction in the untreated control was at 0.438 Hz ± 0.018 while no contraction was observed in the α-BTX after twenty minutes. The contractions in the control increased to 0.572 Hz ± 0.015 after 30 minutes but there was no activity in the α-BTX treated co-cultures. Further contraction occurred after 45 minutes (0.705 Hz ±0.014) and an hour 0.900 Hz ±0.014 in the controls while there were no contraction observations in the α-BTX treated cells. Control and BTX co-cultures were washed after which there was an addition of fresh DM at 1 hour and 35minutes which led to the cessation of contractions in the two. The two concentrations had similar contractions after 30 minutes with a baseline 30 minutes after washout (2 hours after the initial application of treatment) frequency of 0.633 Hz ± 0.008. A similar observation was made 24 hours after treatment with CF in the control being 0.606 Hz ± 0.12. There were no observations of contractile activity in the α-BTX treated co-cultures at these periods either.

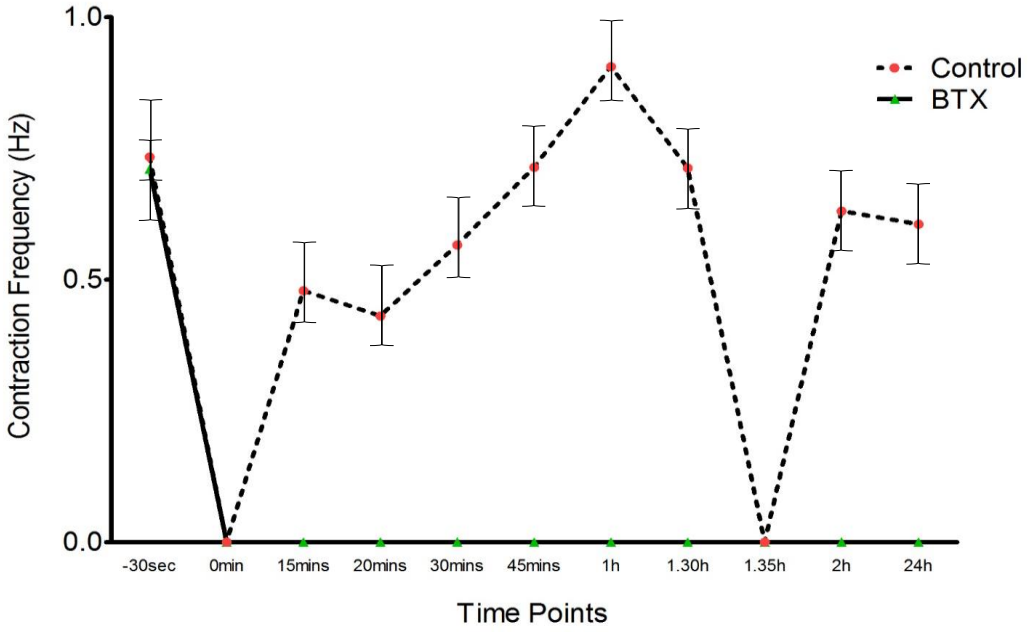

Figure 5.7: Assessment of the functional effects of 1:400 of 10nM α-Bungarotoxin (α-BTX) on co-cultured myotubes. A line graph comparing the contraction frequency (CF) of myotubes treated with α-BTX **and** untreated controls (There were no significant differences between them). The graph shows that the contractions had stopped completely in the myotubes treated with α-BTX and also stopped in the controls and α-BTX-treated myotubes at the time 0 and after wash at 1.35h. Data is representative of mean ±SD, n=10 independent experiments.

5.1.6 Functional Assessment of MNJs with L-Glutamic Acid

Past nerve-muscle co-culture models used in the application of excitatory neurotransmitters such as L-glutamate to stimulate MNs that result in contraction of myotubes have been used to demonstrate NMJs functional assessment. The experiment that followed aimed to show the impact of presynaptic agonist stimulation on MNs. The excitatory neurotransmitter glutamate, in the form of 400 µM L-glutamic acid (Smith et al., 2013) was used to assess the impact of L-Glut on the CF of co-cultured myotubes in the co-cultures (Figure 5.8). The CF baselines measurements were recorded 30 seconds before L-Glut application to the positive controls and untreated diluents to the negative controls in which there were no significant differences (0.749 Hz ± 0.003 vs 0.756 Hz ± 0.003, P = 0.148). The addition of treatment solutions to the culture leads to the cessation of contraction immediately after. The measurement of CF after 15 minutes after treatment application shows that the myotubes in the L-Glut treated cultures have a CF 0.106 Hz ± 0.003 ($P < 0.0001$), which was much higher compared to the controls (0.069 Hz ± 0.004). L-Glut treated co-cultures had a significantly higher CF of 1.463 Hz ± 0.033 compared to the control's 0.141 Hz ± 0.004. The CF of the myotubes was 0.780 Hz ± 0.014 in the controls after 30 minutes, which was an indication that it was the baseline. At the same time, the myotubes in the L-Glut treated cultures contracted at 2.305 Hz ± 0.033 with $P < 0.0001$, which is 1.5 Hz more than in the controls. The myotubes in the L-Glut co-culture had a CF of 0.690 Hz ± 0.018 while the controls had a CF of 0.700 Hz ± 0.014 after 45 minutes following treatment. The two cultures had CFs of (0.711 Hz ± 0.017 vs 0.775 Hz ± 0.004, P = 0.002) after one hour and (0.760 Hz ± 0.004 vs 0.803 Hz ± 0.006, $P < 0.0001$) after one and half hours. Washout and replacement of the DM after 1.35 hours after the first treatment led to the stoppage of the contractions in the two cultures. The two cultures had similar contractions 30 minutes after the washout (0.691 Hz ± 0.010 vs 0.735 Hz ± 0.005, P = 0.001) when compared to the baseline. The control and L-Glut treated cultures had similar CF of (0.750 Hz ± 0.004 vs 0.702 Hz ± 0.006), which was indicative of spontaneous activity compared to the baseline measurements.

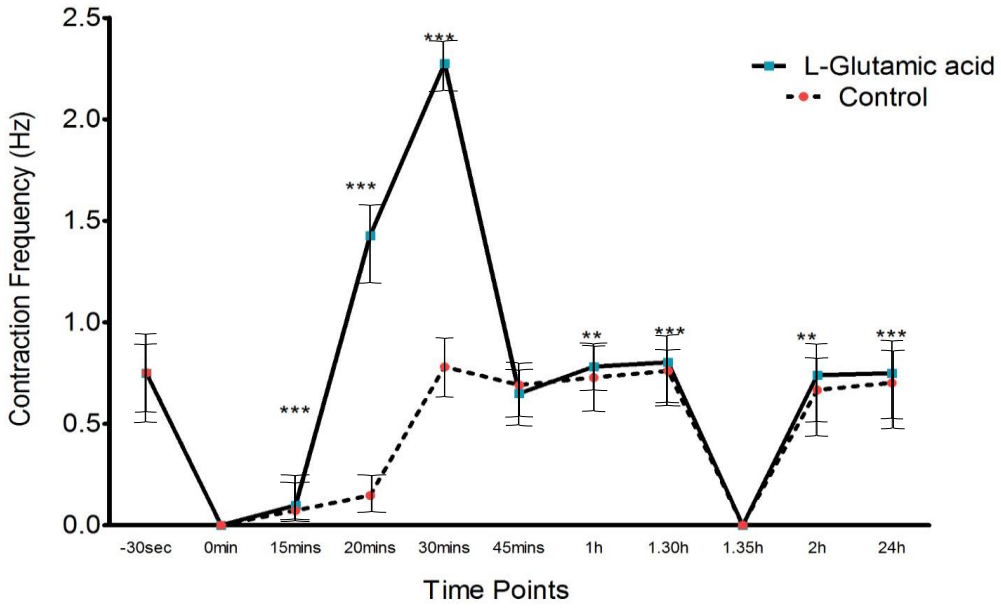

Figure 5.8: Assessment of the functional effects of 400 µM L-glutamic acid on co-cultured myotubes. A line graph comparing the contraction frequency of myotubes treated with L-glutamic acid and untreated controls.The graph shows that the contractions have significantly increased in the myotubes treated with the L-glutamic acid comparing with the controls. The contraction of the myotubes stopped in the controls and treated myotubes with L-glutamic acid at the time 0 and after wash at 1.35h. Data is presented as a mean, error bars signify ± SD. n = 10 independent experiments. There were significant differences between them ** denotes P<0.001*** denotes P < 0.0001.

5.2 Discussion

In this chapter, the generation, characterisation and functional assessments of neuromuscular junction were confirmed that in addition, the modulation of myotube contractile activity using the NMJs manipulation with presynaptic MN agonists and postsynaptic AChR antagonists was successful. Studying operational motor units is important in understanding the pathophysiological characteristics of NMJ disorders are common in major neurological diseases and older age. Recently, our research group developed a novel entirely human NMJ platform using hESCs-derived neural progenitor cells (NPCs)-transfected with green fluorescent protein (GFP) and human myoblast. The aim of the current chapter was to use GFP trafeceted-NPCs (previously generated in our lab) and myoblasts to replicate Abd Al-Samid's model (Abd Al Samid et al., 2018), which was characterised using specific differentiation markers for motor neurons and myoblasts. The importance of understanding the behaviour of neurons in human beings is underscored by the rejection of animal models. The explants and SkMCs cellular interaction would be better stipulated by replicating *in vivo* interactions (Zhang et al., 2015). Although some animal models could show similar physiological changes that lead to disease in human beings, they are avoided. *In vitro* human cell and tissue cultures would be much better in the analysis of physiological changes that can lead to the formation of disease. In addition, such studies are more relevant, cost effective, and faster compared to animal models that involve more stages that increase costs and time needed to achieve the desired results.

The use of the established functional nerve-muscle co-culture showed that there were muscle contractions after some time. Spontaneous differentiation of NPC nerve cells was in serum free media. The normal process involves platting NPCs on matrigel (50µl/cm2) to achieve orient terminal neural stem cell differentiation that can be observed in a period of four weeks. However, differentiation functional nerve muscle co-cultured as shown by Jasdeep occurred much faster with no additional regulation factors (Saini et al., 2019). Another similar human-based study with *in vitro* muscle co-culture had at least ten regulator factors, some of which included B27 and insulin growth factor (Guo et al., 2011) but there is a need for further categorisation and optimisation. The NPCs used in the study were from hESCs that differentiate in the order neuroepithelial stem cells, neural stem cells, and into NPCs. Neuroepithelial stem cells can differentiate into neurons, oligodendrocytes, and astrocytes. Confirming the NPCs stem cells was done using the nestin antibody, which is a specific marker for NPCs.

After the first contractions, the co-cultures were monitored every day and maintained with regular media changes to ensure that innervation and myotube maturation continued to achieve the desired level. The number of contraction per minute and an increase in the number of contracting myotube

was used to determine contraction frequency (CF). Large networks characterised by myotubes contracting in a systematic manner were observed by the seventh co-culture day (Figure 5.4). These findings suggest that myotube contractions were stimulated by MNs as a single motor unit. The co-culture system has more benefits in studying NM and muscle wasting disorders compared to traditional myoblast monoculture models. Moreover, the large nerve networks provide a better platform to determine what happens during disease development and progression. However, aneurally cultured human myotubes did not contract spontaneously in culture. On the contrary, innervated myotubes in the co-culture system showed contractile functionality stimulated endogenously (Feher, 2017).

The second objective of the experiment was to the physiological behaviour of NMJ and confirm that the spontaneous contractile activity of the myotubes was facilitated by MN signalling through NMJ. Therefore, NMJ assessment was done by analysing the myotube CF modulation while using agonist and antagonist pharmacological interventions that act on presynaptic MNs (L-Glut) or postsynaptically (α-BTX) on AChRs at the NMJ. The addition of α-BTX ion the co-cultures led to the immediate and permanent ceasure of spontaneous myotube contractions. Therefore, AChRs binding at NMJ motor endplate (MEP) with α-BTX inhibits Ach from binding with the postsynaptic receptors, which leads to the paralysis in the co-cultured innervated myotubes. There was indefinite immobilisation of myotube spontaneous activity despite being washed out and reverted to normal culture conditions after exposure to α-BTX. It was demonstrated that NMJs generated in the study's *in vitro* co-culture system was physiologically irreversible to competitive antagonist at the AChRs *in vivo* mammalian NMJ (Domet et al., 1995). Some studies have shown that receptors involved in muscle fiber membrane potential regulation through the nitric oxide synthase system (Urazaev et al., 1995), rather than signalling at the NMJ despite glutamate receptor detection in mammalian NMJs. It was shown that myotube contraction frequency increased significantly when there was implementation neuron-specific excitatory neurotransmitter L-Glut in the investigation of stimulation of associated neurons in co-cultures. MN impact stimulation with L-Glut on myotube CF was observed immediately, which made myotube contractions to increase significantly ($P < 0.0001$) between 15 and 20 minutes while there was a greater increase of 1.5 Hz after 30 minutes. The myotubes CF returned to normal in 45 minutes after the stimulation of MN with L-Glut. It is expected that SkMC membranes in mammals are stimulated through AChRs, which shows that there is a successful enhancement of myotube contractions in the co-cultures with the introduction of L-Glut, which is possibly achieved because of the increased Ach release from the MN cultured into the synaptic NMJs cleft.

5.3 Conclusion

In summary, entirely human NMJ was replicated in which myoblasts differentiated into myotubes while NPCs differentiated into MN sprouted axons and branched to form multiple NMJ innervation sites on the myotubes. It was also determined that spontaneous myotube contractions in the co-cultures were indeed driven by MN signalling through NMJs which was verified by responding physiologically in an appropriate manner to the drugs used in this study.

Chapter 6: Investigating the effects of slow release IGF-1 (IGF-1/NPs) on NMJ formation and function using human NMJ model

6.0 Background

6.0.0 Introduction

Previous chapters have shown how novel complete human nerve-muscle co-culture devoid of serum and trophic was established to induce spontaneous contractile activity in myotubes that have differentiated. The system's formation of neuromuscular junctions (NMJs) was underscored by the co-localisation of the axons and acetylcholine receptor (AChR) clusters. This chapter investigates the effects of IGF-1/NPs on the NMJ model formation and function. The study is guided by the researcher's findings that insulin-like growth factor 1 (IGF-1) can lead to the maturation and maintenance of neurons (Lewis et al, 1993). Another important finding was that some neurological disorders such as stroke may arise due to impaired IGF-1 signalling pathway (Lewis et al, 1993). IGF-1 action was mediated by type 1 IGF receptor (IGF-1R) binding proteins that regulate the bioavailability of the IGFs.

IGF-1 therapy has shown varying therapeutic outcomes in the treatment of motor neuron diseases such as amyotrophic lateral sclerosis, neuropathy, and peripheral nerve injury (Caroni and Becker, 1992). Functional repair of adult human beings central nervous system (CNS) is one of the major challenges in modern medicine. CNS traumatic injuries and neurodegenerative diseases usually lead to irreversible cognitive and/or motor functions loss as underscored by permanent disabilities (Dupraz et al., 2013). The main requirement to re-establish neural connections is the regeneration of the axonal and dendritic neurons to enhance normal CNS operations. The process through which axonal regeneration occurs is one of the major mechanisms of CNS development (Cui, 2006).

IGF-1 has an additional function of preventing choline acetyltransferase activity loss in embryonic spinal cord cultures and reducing programmed motor neurons death *in vivo* after spinal transaction or axotomy or normal development (Iwasaki and Ikeda, 1999). IGF-1 increased neuromuscular junctions' numbers and maintains the normal muscle morphology. However, positive nerve regeneration necessitates the local application of IGF-1, which is thought to be influenced by IGF-1 acting on Schwann cells in the treatment of nerve injuries (Iwasaki and Ikeda, 1999). Motor axons develop muscle targets that are important in the development of neuromuscular junctions (NMJs). The changes that occur during the maturation of incipient synapses at the nerve-muscle contact sites include clustering of acetylcholine receptors (AChRs) in the postsynaptic muscle membrane and

synaptic vesicles that store and release ACh accumulate within the presynaptic nerve terminal (Sanes and Lichtman, 2001). The changes at the two sites unsure that there is reliable synaptic transmission ate the NMJ and start the interaction with a muscle targets prevent the advancement of axon to trigger differentiation (Sanes and Lichtman, 2001).

6.0.1 Aims

The aim of this study is to examine how slow release of IGF-1 (IGF-1/NPs) affects NMJ formation and function. The human immortalized myoblasts and human embryonic stem cells (hESCs)-derived neural progenitor cells (NPCs) were used to study its concept to enhance NMJ model development and function.

6.1 Results

6.1.0 The effects of slow release IGF-1 on NMJ function (myotube contractions)

In the last chapter, NPCs were co-cultured with human immortalized myoblasts for 7 days in co-culture media (Figure 6.0) approved and used as a control. Therefore, the following experiments were performed to confirm the effects of slow release IGF-1 on NMJ function (myotube Contractions) for 7 days in co-culture media with adding NPs only (Figure 6.1), IGF-1 only (Figure 6.2), and slow release of IGF-1(IGF1/ NPs) (Figure 6.3). After the initiation of myogenic differentiation, functional motor units started to develop, including axonal sprouting from the NPCs formed along myotubes on NMJ and myotube formation. Myotubes were characterised by spontaneous muscle contractions without any exogenous chemical and electrical stimuli starting the seventh day (Figures 6.0, 6.1, 6.2 and 6.3).

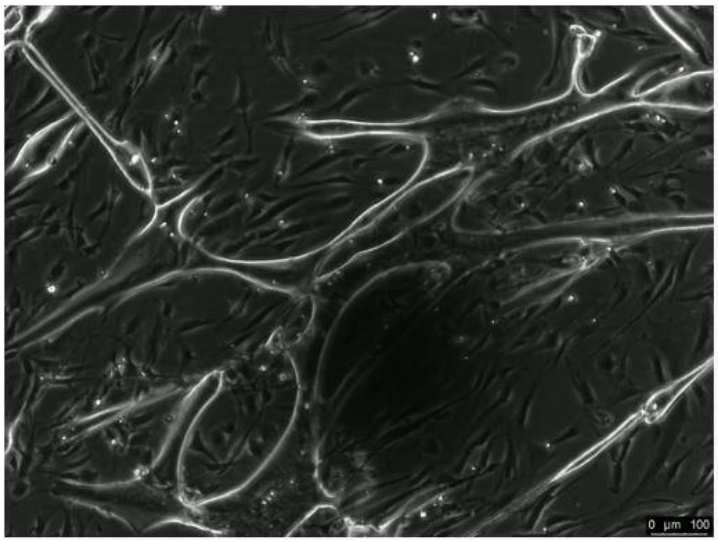

Figure 6.0: Phase contrast video1 micrograph of young immortalised human myotube contractions at Day 7. Illustrative video 1 of co-cultured in DM only spontaneously contracting as a network, devoid of serum, growth/neurotrophic factors, and external stimulus. Scale bar =100 µm. (https://www.youtube.com/watch?v=FKsKA_abfL4&feature=youtu.be)

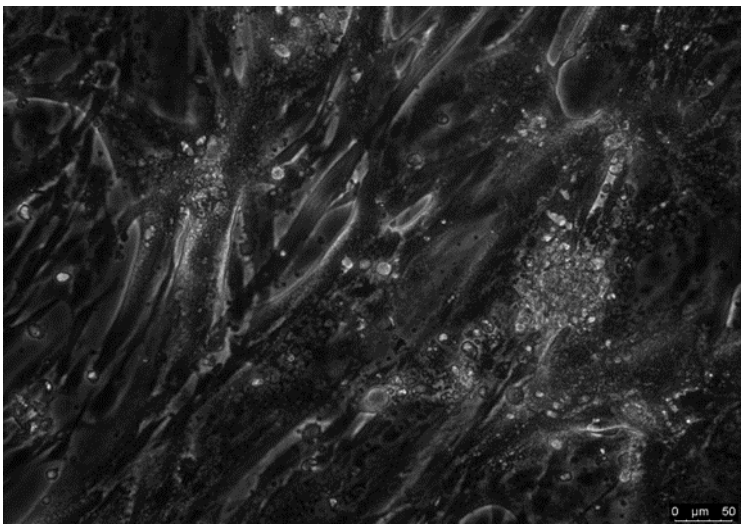

Figure 6.1: Phase contrast video 2 micrograph of human immortalised myotube contractions at Day 7. Illustrative video 2 of co-cultured treated with NPs spontaneously contracting as a network, devoid of serum, growth/neurotrophic factors, and external stimulus. Scale bar =50 µm. (https://www.youtube.com/watch?v=MkX4smWGRlk&feature=youtu.be)

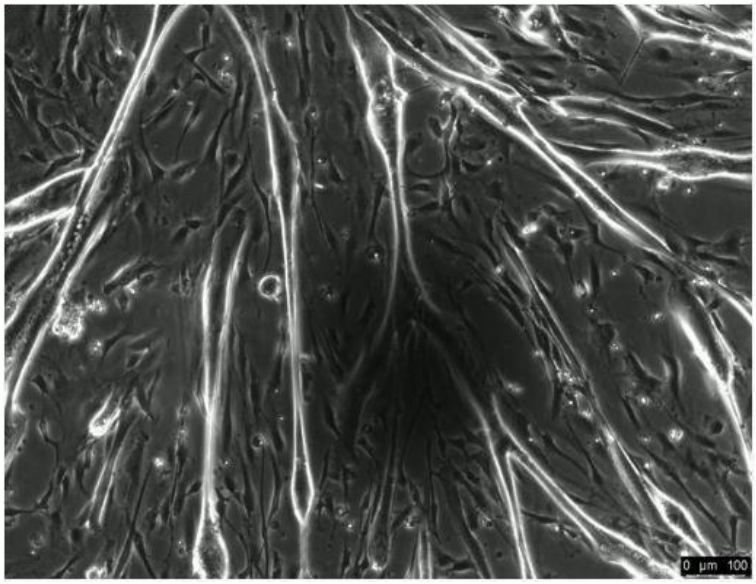

Figure 6.2: Phase contrast video 3 micrograph of human immortalised myotube contractions at Day 7. Illustrative video 3 of co-cultured treated with IGF-1 spontaneously contracting as a network, devoid of serum, growth/neurotrophic factors, and external stimulus. Scale bar = 100 µm. (https://www.youtube.com/watch?v=CN5luqbA_sU&feature=youtu.be)

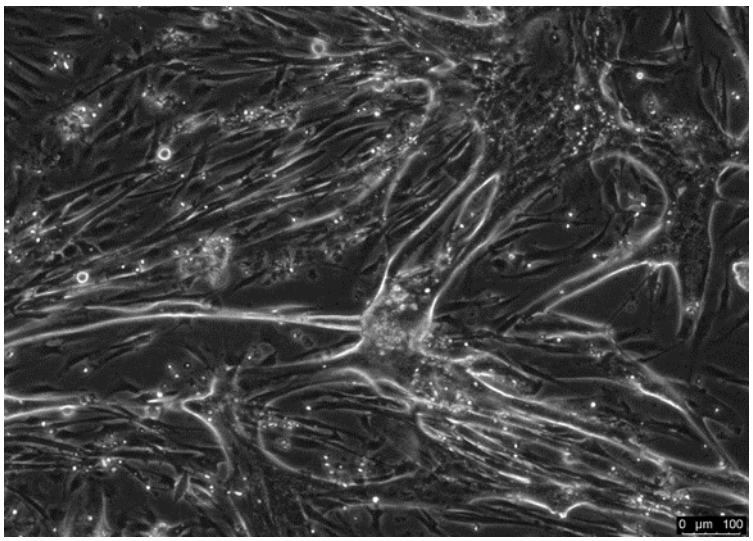

Figure 6.3: Phase contrast video 4 micrograph of human immortalised myotube contractions at Day 7. Illustrative video 4 of co-cultured treated with IGF-1/NPs spontaneously contracting as a network, devoid of serum, growth/neurotrophic factors, and external stimulus. Scale bar =100 µm. (https://www.youtube.com/watch?v=SN8PEzZMYlY&feature=youtu.be)

6.1.1 Contraction Frequency

To ensure optimal innervation of co-cultured myotubes, the efficiency of NPCs to induce contractions in the co-culture system with DM only was used as a control to compare against myotubes co-cultured with NPs only, IGF-1 only and IGF-1/NPs. Optimal innervation of myotubes was quantified by analysing Contraction Frequency (CF) every 24 hours post co-culture for 7 days, using live phase contrast microscopy to assess 20 random fields of view at x10 magnification. The results revealed no observable myotube contractions in either DM (control), NPs, IGF-1 or IGF-1/NPs co-cultured with myoblast after the first 48 hours. Following 6 days of co-culture, initiation of myotube contractions were observable in the DM, NPs, IGF-1 and IGF-1/NPs co-cultures, contracting at a frequency of DM (0.55 Hz ± 0.18), NPs (0.58 Hz ±0.20), IGF (0.69 Hz ± 0.28) and IGF/NPs (0.74 Hz ± 0.37). On day 7 the contractions were slightly higher in each condition for DM (0.59 Hz ±0.19), NPs (0.64 Hz ± 0.23), IGF-1 (0.81 Hz ± 0.33) however the contractions were witnessed and increased CF further in slow release IGF-1 co-culture (0.96 Hz ± 0.47), which was significant ($P < 0.0001$) (Figure 6.4). The findings confirmed co-cultured IGF-1/NPs are more efficient than the control DM, NPs and IGF-1 only.

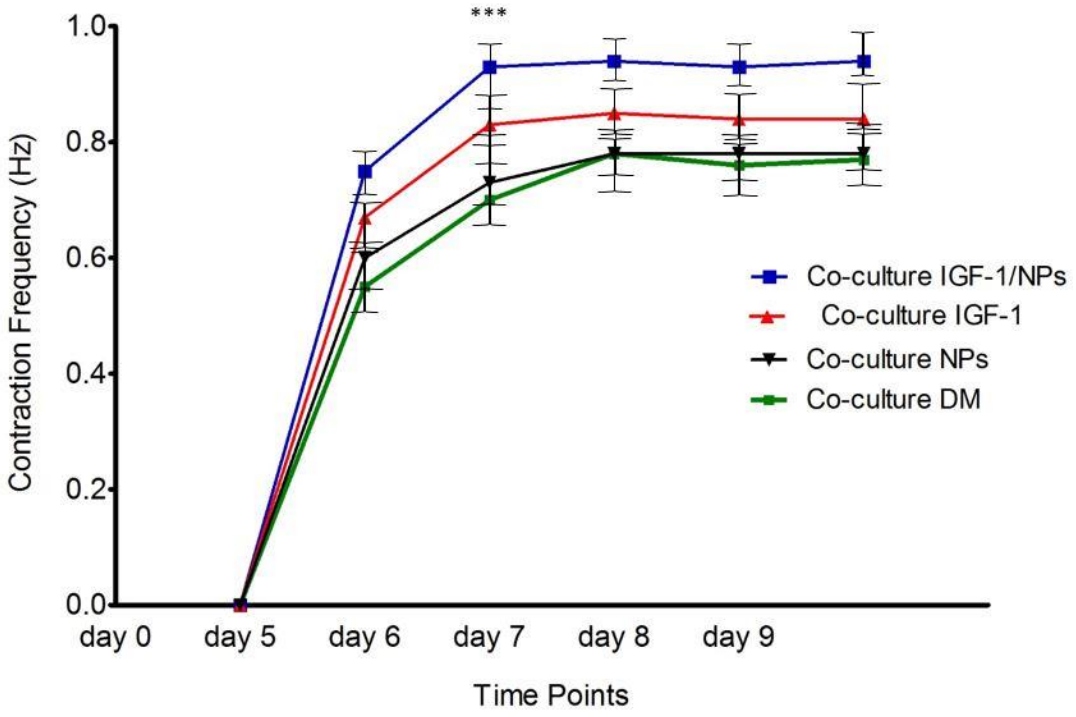

Figure 6.4: Contraction frequency of myotubes co-cultured with different co-culture conditions over 7 days. A line graph comparing the onset of myotube contractions and contraction frequency in young immortalised human myoblasts co-cultured with neural progenitors cells in differentiation media only (green line), NPs only (black line), IGF-1 only (red line) and IGF-1/NPs (blue line) suspension over 7 days.The contraction frequency started from day 6. Data presented as a mean, error bars signify ± SD. n = 6 independent experiments, *** denotes $P < 0.0001$.

6.1.2 Effects of IGF-1/NPs on motor neuron differentiation and axonal length

During embryonic development, motor axons grow to their muscle targets and establish neuromuscular junctions (NMJs) (Sanes and Lichtman, 2001). Investigations conducted in the future using this model could detect the main factors discharged from the muscle and nerve to coordinate axonal sprouting, localisation, and maintenance of NMJ (Jensen et al., 2009). Although One-Way ANOVA statistical text was used to analyse the data below, the main comparison focused on IGF-1 vs IGF-1/NPs. Therefore, the axonal length of differentiated motor neurons *in vitro* nerve-muscle co-culture treated with NPs, IGF-1 and IGF-1/NPs were measured over 7 days using Image J (see section 2.1.23 in the method and Figure 2.7). The degree of differentiation of motor neurons with regards to IGF-1 (12.5μg/ml) treatment, NPs (0.75 mg/ml) and IGF/NPs (12.5μg/ml + 0.75mg/ml) and DM as a control were stipulated using the measured axonal length (μM) at 24hr intervals. In the first set of analysis, the axonal length calculated on the first day was relatively different when compared to the differentiation measure obtained within 24 hours, which showed that there was no statistical significance. However, the axonal length of differentiated motor neurons was measured by using Bonferroni's multiple comparisons test at each time point over the 7 days of co-culture for all treatments. The results showed that the axonal length was increasing over 7 days in all treatment but the highest axonal length with a greatest significant difference was in the co-culture with IGF-1/NPs added ($P < 0.0001$), (Figures 6.5 – 6.12).

On the contrary, the axonal length calculated on day-7 showed high variance with remarkable increase of axonal length indicated by the white arrows in Figure (6.5, 6.7, 6.9 and 6.11). All treatments showed significant differences from day 1 to day 7, but the IGF-1/NPs showed the highest axonal length (228.6μM± 61.53) in day 7 when compared to the IGF-1 only and other treatments such as NPs and DM only. Lastly, the axonal length of differentiated motor neurons was measured at each treatment over the 7 days of co-culture. The result showed that the axonal length was increasing over the 7 day co- culture period with a greatest significant difference in DM adding IGF-1/NPs compared to other treatments. The mean for IGF-1/NPs was (228.6μM ± 61.53) compared to the control DM where the mean was (82.84μM ± 13.98), the NPs mean was (90.20μM ± 11.88) and when compared to the IGF-1 only, the mean was (158.8μM ±41.59). The IGF-1/NPs presented significant difference with P value <0.0001 (Figure 6.13), which underscores co-cultured IGF-1/NPs are more effectual than the IGF-1 only and other treatments.

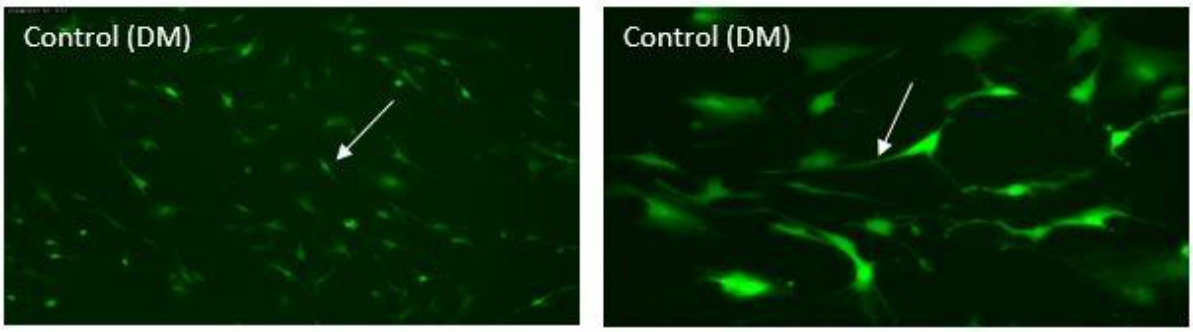

Figure 6.5: Shows the axonal growth in human myoblast co-cultured nerve cells for DM only at day 1 and 7. The image on the left displays the axonal growth at day one of culture. The image on the right displays the axonal growth at day seven of culture. Images were captured at x20 magnification. Scale bar = 50µm

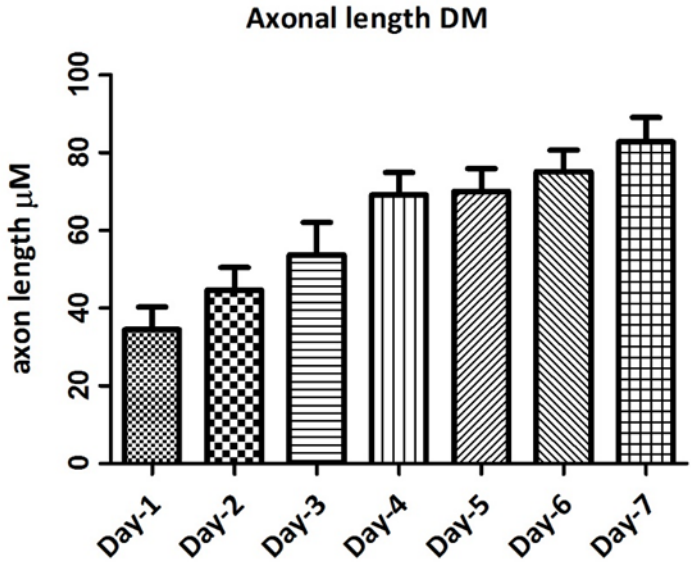

Figure 6.6: Quantitative analysis of axonal length in human myoblast co-cultured in DM over 7 days. This graph shows comparing the onset of axonal length in young immortalised human myoblasts co-cultured with neural progenitors cells in differentiation media only suspension over 7 days. Data presented as a mean, error bars signify ± SD. n = 4 independent experiments.

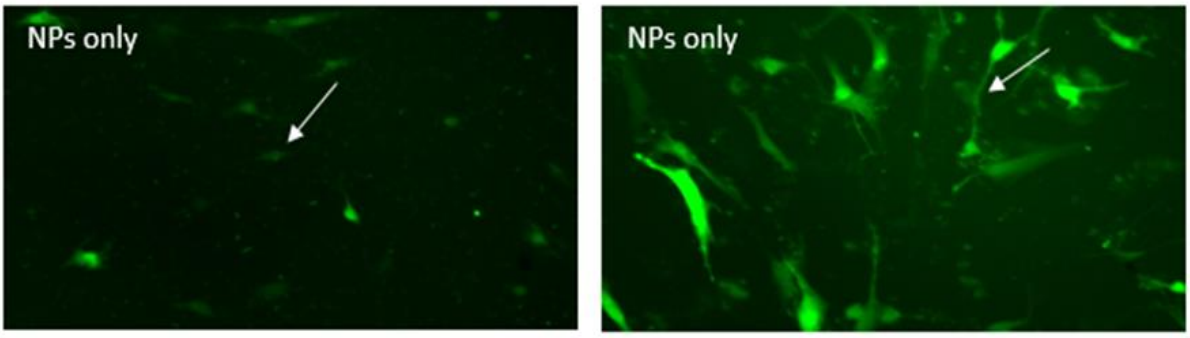

Figure 6.7: Shows the axonal growth in human myoblast co-cultured nerve cells for DM treated with NPs at day 1 and 7. The image on the left displays the axonal growth at day one of culture. The image on the right displays the axonal growth at day seven of culture. Images were captured at x20 magnification. Scale bar = 50µm

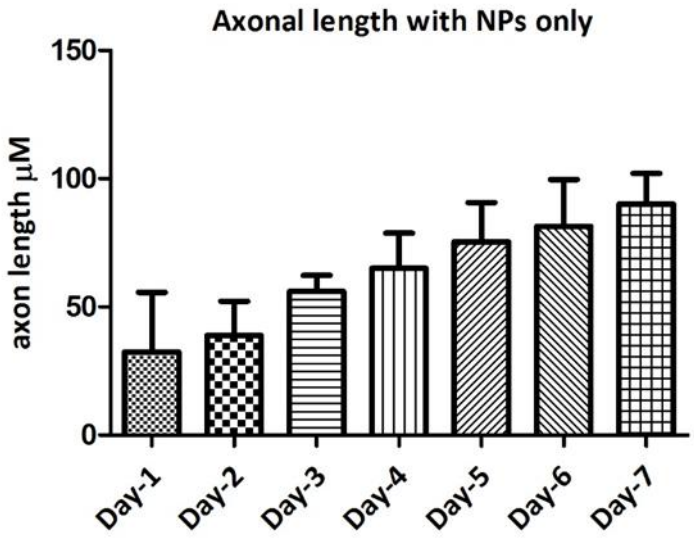

Figure 6.8: Quantitative analysis of axonal length in human myoblast co-cultured treated with NPs over 7 days. This graph shows comparing the onset of axonal length in young immortalised human myoblasts co-cultured with neural progenitors cells in differentiation media after treated with NPs suspension over 7 days. Data presented as a mean, error bars signify ± SD. n = 4 independent experiments.

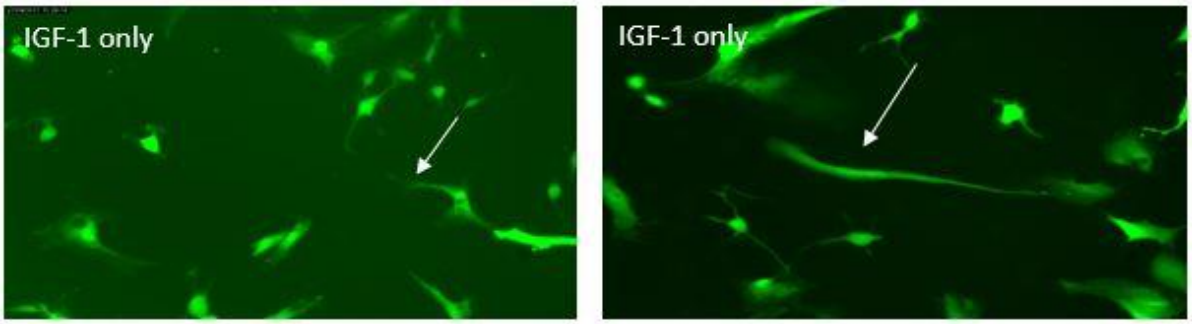

Figure 6.9: Shows the axonal growth in human myoblast co-cultured nerve cells for DM treated with IGF-1 at day 1 and 7. The image on the left displays the axonal growth at day one of culture. The image on the right displays the axonal growth at day seven of culture. Images were captured at x20 magnification. Scale bar = 50µm

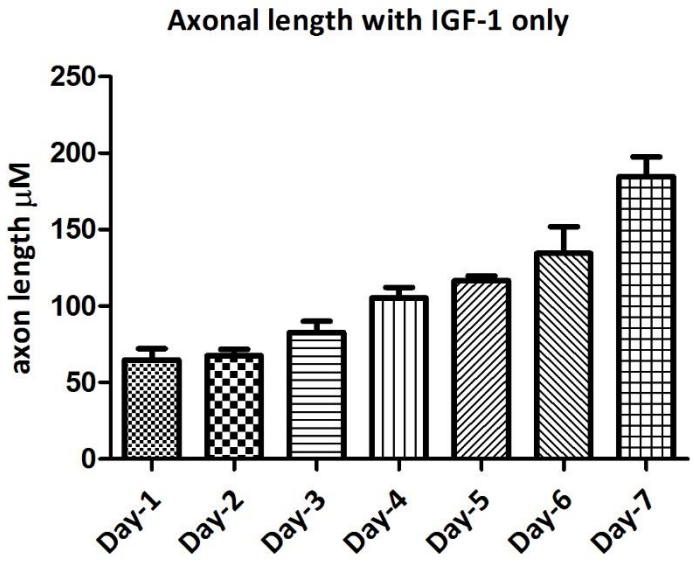

Figure 6.10: Quantitative analysis of axonal length in human myoblast co-cultured treated with IGF-1 only over 7 days. This graph shows comparing the onset of axonal length in young immortalised human myoblasts co-cultured with neural progenitors cells in differentiation media after treated with IGF-1 suspension over 7 days. Data presented as a mean, error bars signify ± SD. n = 4 independent experiments.

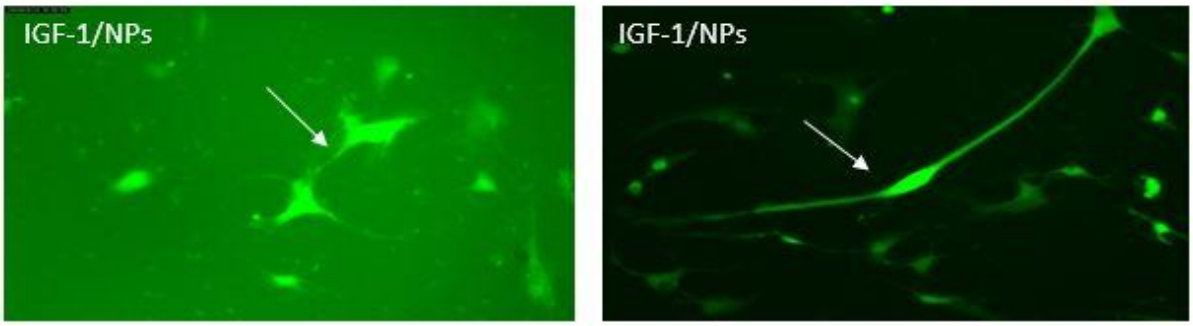

Figure 6.11: Shows the axonal growth in human myoblast co-cultured nerve cells for DM treated with IGF-1/NPs at day 1 and 7. The image on the left displays the axonal growth at day one of culture. The image on the right displays the axonal growth at day seven of culture. Images were captured at x20 magnification. Scale bar = 50µm

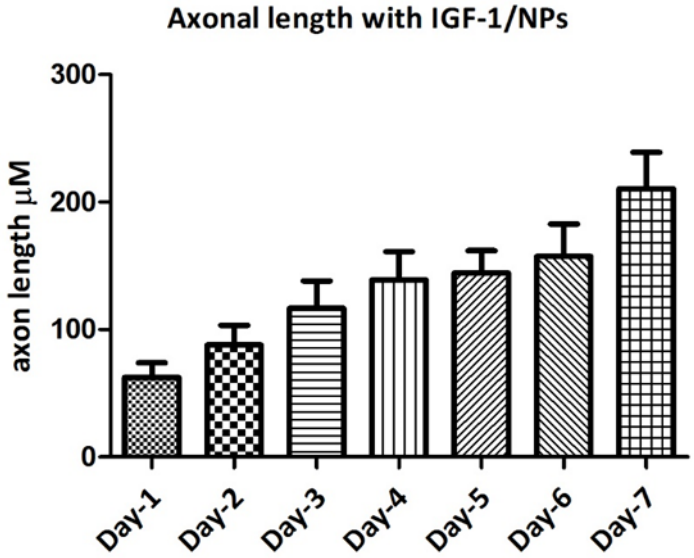

Figure 6.12: Quantitative analysis of axonal length in human myoblast co-cultured treated with IGF-1/NPs over 7 days. This graph shows comparing the onset of axonal length in young immortalised human myoblasts co-cultured with neural progenitors cells in differentiation media after treated with IGF-1/NPs suspension over 7 days. Data presented as a mean, error bars signify ± SD. n = 4 independent experiments.

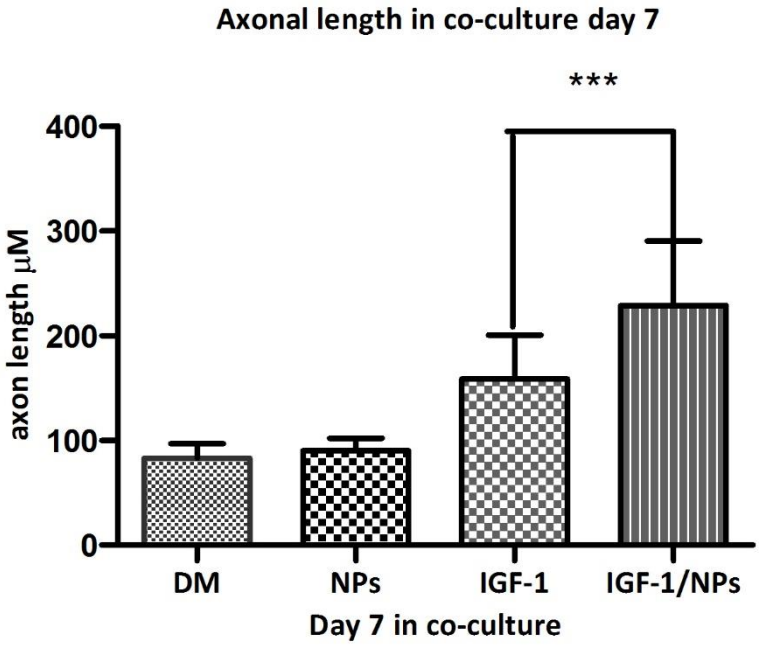

Figure 6.13: Quantitative analysis of axonal length comparisons between different co-culture conditions. This graph shows comparing the onset of axonal length in young immortalised human myoblasts co-cultured with neural progenitors cells in differentiation media after treated with NPs, IGF-1 and IGF-1/NPs suspension over 7 days. Data presented as a mean, error bars signify ± SD. n = 4 independent experiments. *** denotes $P < 0.0001$.

6.2 Discussion

The main finding of the generation, characterisation and functional assessments of neuromuscular junction (NMJ) platform study was consistent with the *in vitro* NMJ model discussed in the previous chapter. Therfore, the effects of slow release IGF-1 on NMJ formation and function were analysed, characterised and confirmed in this chapter. NPCs co-cultured with human immortalised C25 showed that cholinergic MNs co-localisation with differentiated myotubes that enhanced NMJs and myotubes interactions. Monitoring of the co-cultures was done every 24 hours after the first contractions were witnessed followed by maintenance with media regularly to enhance further innervation and maturation of myotubes. Co-cultures treated with slow release IGF-1 (IGF-1/NPs) showed higher myotube contraction frequency as defined by more contractions per minute and the higher number of myotubes. The myotubes were contracting systematically as large networks by the seventh co-culture day in figures 6.0, 6.1, 6.2 and 6.3), which affirmed that myotube contractions functioned as a single motor unit with MNs stimulation bursts. The IGF-1/NPs co-culture model has much more benefits compared to traditional myoblast monocultures in researching NM and muscle wasting disorders. The culture system's innervated myotube showed signs of endogenously stimulated contractile functionality (Feher, 2017). The study showed contraction frequency in myotubes co-cultured control DM only, adding NPs, IGF-1, and IGF-1/NPs individually in a period of seven days. A line graph has compared onset of myotube contractions and contraction frequency in a co-culture of young immortalised human myoblasts and neural progenitor cells while adding NPs, IGF-1, and IGF-1/NPs in a period of seven days. Initiation of myotube contractions was observed in all treatment cultures by the sixth day of co-culture but was slightly higher in different conditions. More contractions and CF increased significantly by the seventh day in IGF-1/NPs, which confirms that co-culture treated with slow release IGF-1(IGF-1/NPs) are much more enhanced compared to the IGF-1 due to its involvement in maturation and maintenance of neurons. IGF-1 signalling pathway has been determined to have an impact in the development of some neurological diseases such as stroke (Lewis et al, 1993). Motor axons usually grow muscle targets and establish neuromuscular junctions (NMJs) (Sanes and Lichtman, 2001). The future application of this model could help in detecting main factors discharged from nerves and muscles to coordinate axonal sprouting, maintenance of NMJ, and localisation (Jensen et al., 2009).

The use of the term "sprouting" has been controversial. Ramon and Cajal (1928) referred "The innervation of the peripheral stump of cut nerves (occurs) through the growth, across the scar, of nerve sprouts arising in the central stump." On the other hand, Liu and Chambers (1958) used "sprouting" to refer to growth that arises from an undamaged axon and maintains the growth of the central projections of *intact* dorsal root ganglion axons after adjoining roots injury. Repair neuron

programs are usually available for a short period after an injury and only remain effective if axons injured are provided a growth opportunity (Boyd and Gordon, 2003). Delayed reconstruction makes the growth associated genes to downregulate in which case the neurons die or become atrophic. The delay also leads to the impairment of the Schwann cell ability that usually supports regeneration (Sulaiman et al., 2002) and deterioration of denervated muscles (Boyd and Gordon, 2003). The axonal length of differentiated motor neurons *in vitro* nerve-muscle co-culture with human myoblast C25 treated with IGF-1, NPs, and IGF-1/NPs and measured in a seven day period. The measurement was completed using axonal length (μM) every day. The study found that the IGF-1/NPs had the highest axonal length and significant differences especially in the seventh day when compared to IGF-1 and other treatments. Although it had more effect on neuromuscular junctions, which confirms that they are more effective compared to IGF-1 and other treatments, the finding provides support to the bidirectional communication between the nerves and muscles that supports the formation of NMJ (Zahavi et al., 2015). The process is further enhanced by neural growth factors such as neurotrophic factors obtained from the brain and discharged by the muscle to ensure the formation, growth, and maturation of NMJ (Henderson et al., 1993; Funakoshi et al., 1995), which will be evaluated in the next chapter (7).

6.3 Conclusion

The data for this study demonstrated significant effects in morphology as observed in human immortalised myoblast co-cultured with NPCs over 7 days and especially in NMJs contraction and the axonal length of co-cultured motor neurons following treatment with IGF-1/NPs. The potent effect of the slow release of IGF-1 on the proliferation, differentiation, and survival of neurons make it good for studying treatment strategies for studies on axonal damage, demyelination, and neuronal death.

Chapter 7: Investigating the effects of Slow Release of IGF-1 on Bi-directional communications and soluble growth factors secretion during NMJ formation

7.0 Background

7.0.0 Introduction

Growth factors and neurotrophin occurring endogenously play an important role in the development, function, plasticity, survival, and death of neurons *in vivo* (Oppenheim 1991; Reichardt 2006). However, exogenous growth/neurotropic factors introduction in alternative nerve-muscle co-cultures (Guo et al., 2011; Guo et al., 2014; Das et al., 2007; Puttonen et al., 2015; Rumsey et al., 2009) can have a negative impact on drug screening and testing (Dugger et al., 2018). Therefore, there has been extensive research on the role of growth or neurotrophic factors play in the development and function of the nervous system. Some studies have indicated that the two play an important role in some cell populations such as SkMCs that has a perceived role in the expression of some growth factors, neurotrophins and cytokines. The finding indicates that SkMCs play an important role in neurotrophic signalling during formation, development, and innervation (Griesbeck et al., 1995; Gonzalez et al., 1999 ; Chevrel et al., 2006). IGF-1 is a possible trophic factor or a molecule that enhance the survival of cells for motor neurons and muscle fibers (Florini et al., 1996). Skeletal muscle IGF-1 has a target-derived neurotrophic impact on the survival of embryonic motor neurones (Neff et al., 1993) and innervation in muscles of aged animals (Messi & Delbono, 2003). Overexpression of IGF-1 improves motor neurone re-innervation in skeletal muscles after nerve injury (Rabinovsky et al., 2003). Further, the administration of IGF-1 improves re-innervation after nerve injury and hinders the death of motor neurone cell (Sjoberg & Kanje, 1989; Kanje et al., 1989; Li et al., 1994). The treatment of muscle mass and function loss as people age may be achieved using this system. Overexpression of IGF-1 reduces muscle loss associated with older age (Barton-Davis et al. 1998; Musaro et al. 2001). The process also plays an important role in maintaining skeletal muscle-specific force (Gonzalez ´ et al. 2003; Renganathan et al., 1998) and innervation of fibre in older mice. Higher levels of IGF-1 have target-derived trophic effects on mature muscle innervation and maintenance of neuromuscular junction's morphological integrity (Messi & Delbono, 2003; Barton-Davis et al., 1998). IGF-1 also regulates the genes involved in BDNF neurogenesis expression (Carro, 2001). IGF-1 binding proteins (IGFBPs) may improve or compromise IGF-1 activity depending on the cellular context (Murphy, 1998). IGFBPs during brain development studies (Green et al., 1994; Bondy and Lee, 1993) indicate that the proteins play a role in NSCs. Neutrophin-4 (NT-4) and Neutrophin-4 (NT-5) null mice studies have clear muscle development and function defects, which shows that NT-4/5 play a role in the differentiation of SkM fibre (Carrasco and English , 2003). Neurotrophin-3 (NT-3) has been

important in muscle spindles formation (Ernfors et al., 1994) and pathologies of dystrophic muscles common in altered nerve growth factor (NGF) (Capsoni et al., 2000). Studies on the expression of brain-derived neurotrophic factor (BDNF) have indicated that there are many physiological and pathological conditions that have an impact on SkMC expression of BDNF (Chevrel et al., 2006). Research with human subjects living with multiple sclerosis has shown that circulating BDNF can increase as individuals engage in more physical exercises (Ferris et al., 2007;Vega et al., 2006; Gold et al., 2003). It has also been shown that exercising at least two hours using equipment such as the ergometer bicycle has been used to induce BDNF mRNA production in SkM (Matthews et al., 2010). SkM neurotrophin concentrations are compromised in denervated SkMCs. Decreased expression of NT-3 and NGF mRNA and increased expression of BDNF mRNA in muscle had been revealed in studies involving diabetic mice (Fernyhough, Diemel, Hardy, et al., 1995; Ihara et al., 1996; Fernyhough, Diemel, Brewster, et al., 1995; Fernyhough et al., 1998; Fernyhough et al., 1996). Overexpression of glial cell line derived niurotrophic factor (GDNF) is SkM is characterised by hyper innervation NMJs because of the increased MN sprouting (Nguyen et al., 1998). Some studies have shown that GNDF can maintain cholinergic MNs during the aging process (Ulfhake et al., 2000) and ensure transient expression of GDNF at NMJs during embryonic myogenesis as seen *in vivo.* GDNF expression also increases denervated human SkM (Lie and Weis, 1998)

The human neural stem cells (NSCs) secrete IGF-1 that prolongs the lifespan of animals they are transplanted into by protecting dysfunctional motor neurons in amyotrophic lateral sclerosis models (Xu et al., 2006; Brain, 2007; Lu et al., 2003; Yan et al., 2004; Crigler et al., 2006). IGF-1 activates multiple downstream signal transduction pathways such as the transcription and epigenetic regulators that play a role in the regulation of expression genes during the neurogenesis process after binding to membrane receptors (Ming et al., 2011). Phosphatidylinositol 3-kinase (PI3K/Akt) and mitogen activated protein kinase/extracellular signal-regulated kinase (MEK/ERK) mediate these signalling pathways. The mechanisms allow sustainable neuron survival due to the good environment they provide (Pfrieger, 2009) for the proliferation and survival and differentiation of NSCs into motor neurons. NSCs secrete NT-3, GDNF, BDNF, and NGF that increase neuron survival *in vitro* and *in vivo* models (Glia, 2009; Park et al., 2008; Lu et al., 2003; Yan et al., 2004). Experiments in the previous chapter investigated the effects of slow release of IGF-1 on the functionality of NMJs in *in vitro* co-culture model. Myotube contractile activity successful modulation through the slow release of IGF-1 is an indication that *in vitro* NMJ system is physiologically consistent with the *in vivo* mammalian NMJ function as a response to IGF-1.

7.0.1 Aims

NMJ's interact with complex cytokines arrays and growth factors secreted by muscle and motor neurons to promote differentiation and the formation of NMJ and dictate their functions. This co-culture model is probably the first that involves the neural growth factors. Therefore, all the factors required for NMJ formation and maturation, myoblast and motor neurons differentiation were endogenously secreted in the co-cultures. Considering IGF-1 signalling pathways are important in neurogenesis and myogenesis regulation, the aim of the chapter is to evaluate the way in which slow release of IGF-1 affect the bi-directional communication that occurs between the muscle and the motor neuron as well as the co-culture microenvironment (endogenously secretion of neurotrophic factors such as BDNF, GDNF, IGF-1 and NT-3) in the process of NMJ formation. The hypothesis of the present study is that the growth factors that play an important role in enhancing the formation of NMJ are produced and secreted in co-culture cells as slow release IGF-1 avails a favourable regenerative microenvironment that can allow the formation of NMJ as well as the differentiation of neurons and myoblasts.

7.1 Results

7.1.0 Quantification of endogenously secreted Growth and Neurotrophic Factors

An ELISA-based microarray analysis of the growth/neurotrophic factor concentration followed by one way ANOVA statistical test was performed to determine whether the slow release of IGF-1 impacts the secretion of growth/neurotrophic factors in co-cultured conditions (co-culture only, co-culture with IGF-1, co- culture with NPs, and co- culture with IGF-1/NPs). Although the ANOVA test was conducted, the simplicity view of comparing NMJ treated with IGF-1 to those treated with IGF-1/NPs was undertaken as shown in the table below. Table 7.0 shows the quantified concentration of 40 growth/neurotrophic factors on the seventh day. The results indicate that four factors were significantly different ($P<0.05$) in varying co-culture conditions. BDNF, GDNF, IGF-1, and NT-3 (Figure 7.1) concentrations were very high in co-cultures that had been treated with IGF-1/NPs compared to those that had been treated with IGF-1 only.

Table 7.0: ELISA-based microarray analysis of growth and neurotrophic factor in supernatant collected from different co-culture treatments on day 7.

Growth factors	NMJ with IGF (pg/mL)	NMJ with IGF/NPs (pg/mL)	Fold change	*P* - value	Log-Log regression standard curve R^2
AR	4.03 ± 5.27	1.61 ± 1.87	0.4	0.26	0.987
BDNF	**43.4 ± 7.8**	**91.8 ± 18. 3**	2.1	**0.02***	**0.976**
bFGF	16.7 ± 7.5	5.7 ± 0.2	0.3	0.21	0.943
BMP-4	5.35 ± 3.6	12.9 ± 4.75	2.4	0.09	0.961
BMP-5	214.8 ± 244.6	400.3 ± 60.3	1.9	0.65	0.996
BMP-7	1.9 ± 2.76	3.7 ± 3.1	1.9	0.77	0.994
b-NGF	0.4 ± 0.5	0.24 ± 0.29	0.6	0.48	0.991
EGF R	39.2 ± 1.6	39.5 ± 1.08	1.0	0.8	0.995
EG-VEGF	0.3 ± 0.28	0.9 ± 0.56	3.0	0.35	0.986
FGF-4	13.65 ± 7.6	35 ± 15.49	2.6	0.68	0.997
FGF-7	1.53 ± .19	0	0	0.9	0.996
GDF-15	228.3 ± 6.9	260.5 ± 8.71	1.1	0.12	0.999
GDNF	**4.7 ± 1.02**	**7.51 ± 8.7**	1.6	**0.02***	**0.996**
GH	1.63 ± 0.95	5.81 ± 0.28	3.6	0.08	0.994
HB-EGF	0.38 ± 0.15	1.0 ± 0.14	2.6	0.15	0.971
HGF	68.25 ± 2.8	90.85 ± 33.2	1.3	0.79	0.991
IGFBP-1	2.73 ± 0.4	2.6 ± 0.98	1.0	0.9	0.997
IGFBP-2	1590.2 ± 765	1891 ± 945.01	1.2	0.11	0.999
IGFBP-3	911 ± 1480	1014 ± 783	1.1	0.23	0.988
IGFBP-4	1296 ± 319	1191 ± 11	0	0.54	0.999
IGFBP-6	1331.6 ± 161.6	948.9 ± 149.9	0.7	0.45	0.987
IGF-1	**84 ± 8.4**	**1848 ± 424.82**	22.0	**0.002****	**0.975**
Insulin	6438 ± 205	4796 ± 254	0	0.09	0.989
MCSF R	2.33 ± 1.58	4.21 ± 2.2	1.8	0.98	0.991
NGF R	144.1 ± 8.12	131.8 ± 0.91	0.9	0.38	0.987
NT-3	**1.4 ± .2**	**2.5 ± 0.4**	1.8	**0.0016****	**0.997**
NT-4	2.8 ± 0.5	3.4 ± 0.62	0	0.9	0.999
OPG	772 ± 37.7	852.7 ± 113.1	1.1	0.8	0.996
PDGF-AA	818 ± 812.7	828 ± 613.4	1.0	0.91	0.996
PlGF	137.3 ± 13	171.8 ± 29.89	1.3	0.07	0.987
SCF	1.3 ± 0.2	1.28 ± 0.7	1.0	0.99	0.996
SCF R	2.2 ± 0.2	1.66 ± 1.12	0.8	0.47	0.998
TGFa	0	0.01 ± 0.04	0	0.51	0.889
TGFb1	98.63 ± 197.3	15.71 ± 44.44	0.2	0.26	0.984
TGFb3	0.3 ± 0.6	0.21 ± 0.46	0.7	0.78	0.979
VEGF	60 ± 154.7	91.1 ± 105.9	1.5	0.8	0.963
VEGF R2	4.78 ± 6.74	1.96 ± 3.51	0.4	0.35	0.999
VEGF R3	4 ± 4.67	1.66 ± 1.92	0.4	0.23	0.991
VEGF-D	0.15 ± 0.24	0.13 ± 0.24	0.9	0.87	0.991

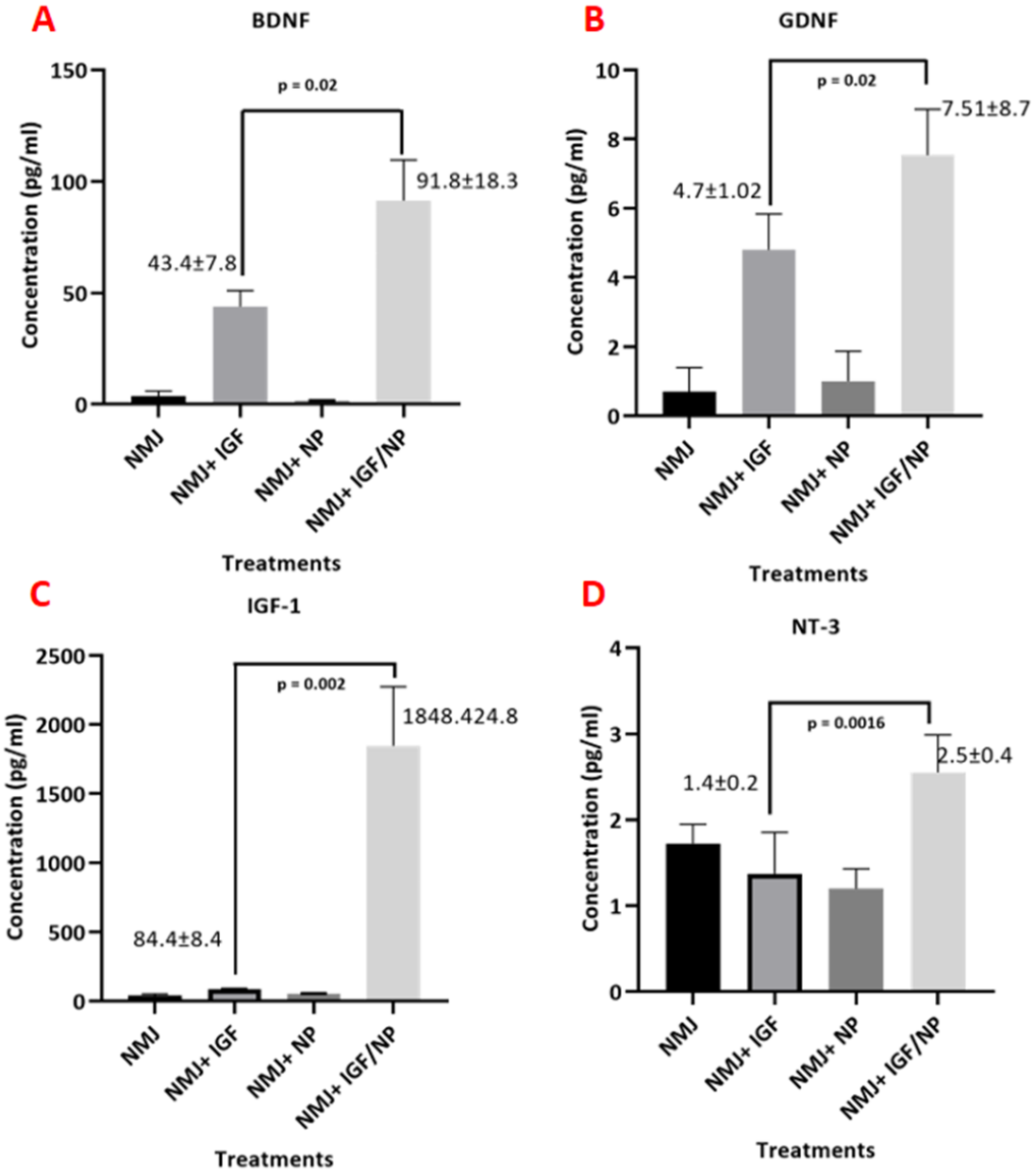

Figure 7.1: Trophic factor quantification and comparison between different co-culture conditions. The above Figures illustrate comparisons in the levels of the trophic factors between different co-culture treatments. Data is presented as a mean concentration of the trophic factor in each condition with error bars signifying ± SD. n=3 and represents the independent experiments/sample types from which the supernatant was collected. Four factors were significantly different, the BDNF P= 0.02*, GDNF P= 0.02*, IGF-1 P= 0.002** and NT-3 P= 0.0016**

7.2 Discussion

In this chapter it's determined and confirmed that the slow release of IGF-1 impacts the secretion of growth/neurotrophic factors in co-cultured conditions (co-culture only, co-culture with IGF-1, co-culture with NPs, and co- culture with IGF-1/NPs). The important IGF-1 growth factor plays a role in the regulation of muscle regeneration and neurogenesis. ELISA-based arrays was used in the quest to understand the way in which slow release IGF impacts the microenvironment that has soluble growth factors as well as differentiation factors and communication between muscle and motor neurons enhanced. The results were based on the comparison of quantitative measurement of 40 human growth factors and neutrophils produced endogenously in NMJ culture treated with IGF-1 *in vitro* and endogenously produced factors treated with IGF-1/NPs co-cultured myotubes. Microarray experiments were used to determine the growth factors' concentration to confirm that NMJs formation and development in co-culture systems were because of endogenous regulation of some growth or neurotrophic factors. The concentration of some of the factors like BDNF, GDNF, IGF-1, and NT-3 used in NMJ formation, MN maintenance, and myotube development was higher in IGF-1/NPs treated co-cultures compared to the IGF-1 only.

Motor neurons and skeletal muscles depend on each other for trophic support and synaptic stimulation and transmission (Aging Cell, 2003). IGF-1 (Aging Cell, 2003; LeRoith, 2008) and its receptors (Bedlack and Hardiman, 2009; Anastácio, 2006) are expressed by skeletal muscles and motor neurons, which underscores that the two cells communicate. Caroni and Becker (J Neurosci., 1992) found that IGF-1 plays a role in the formation of neuromuscular junction. Motor neurons usually stop the production of GAPs after the formation and action of the neuromuscular junctions (J Neurosci, 1992).

Data from the ELISA-based microarray indicated that BDNF levels increase significantly with slow release IGF-1 when compared to IGF-1 only (Figure 7.1A). IGF-1 that is involved in the expression of BDNF (McCusker et al., 2006) also enhances the regulation of BDNF-related neurogenesis (Pareja-Galeano et al., 2013). The injection of IGF-1 has the same effect as exercise-induced BDNF expression in the hippocampus that is later accumulated in brain cells (Pareja-Galeano et al., 2013). Studies that have focused on the role of BDNF in NMJs development have shown that SkM-derived BDNF plays a role in SkM innervation, MN survival, and the transmission of NMJ (Zhang and Poo, 2002; Yan et al., 1993). During embryonic development *in vivo,* high levels of BDNF are expressed by myoblasts and are gradually down regulated after NMJ and SkM fibre maturation (Griesbeck et al., 1995). Upregulation of BDNF led to synaptogenesis inhibition in the development of NMJs *in vitro.* These findings show that regulation of BDNF concentration endogenously in the presence of slow release IGF-1 co-culture system is instrumental in the formation and development of NMJs *in*

vivo. On the other hand, the inclusion of nerve exogenous BDNF in nerve-muscle co-culture systems (Das et al., 2010; Rumsey et al., 2010; Das et al., 2007; Guo et al., 2017; Guo et al., 2011; Guo et al., 2014; Puttonen et al., 2015; Vilmont et al., 2016; Smith et al., 2016) may not lead to robust formation of NMJ expected *in vitro* because of the unsuitable exogenous BDNF concentrations that prevent the maturation of NMJs (Song and Jin, 2015) .

IGF-1 slow release (IGF-1/NPs) increases GDNF levels unlike the cases in which a co-culture model is treated with IGF-1 only (Figure 7.1B). GDNF possibly provides postnatal motor neurons with neurotrophic or survival factors. A postnatal rat spinal cord slice model was used to evaluate whether there is interaction of IGF-1 and GDNF to increase the survival rate of motor neuron, the trophic effect on the activity of choline acetyltransferase (ChAT), and the possible impact they have on neurite growth (Bilak, 2001). The results show that there is a possibility that IGF-1 interact with GDNF to prevent chronic glutamate-mediated toxicity of the rat motor neurons while increasing their ChAT activity. It is important to note that IGF-1 does not enhance neurite growth in the model under study. These findings suggest that IGF-1 and GDNF interact and increase the chances of survival for the motor neuron.

This chapter's data shows that IGF-1 levels increased significantly in models in which the slow release of exogenous IGF-1 had been treated with IGF-1/NPs but such levels were not attained in cases in which treatment was done with IGF-1 only (Figure 7.1C). IGF-1 growth factor is thought to be an anabolic hormone that enhances growth throughout the human body and induces hypertrophic effects on SkM as it has been documented in muscle and animal cell culture models (Velloso, 2008). Muscle specific IGF-1 expression stabilises NMJs and enhances the survival of motor neurons (Dobrowolny et al., 2005). The injection of IGF-1 into SkM leads to the degeneration of MNs and NMJs that subsequently prevents age-related decline in mice (Payne et al., 2006). The concentration of IGFBP -1, -3, -4, -6 insulin-like growth factor binding proteins evaluated during microarray experiments with IGF-1 were higher in the co-cultures. The main function of IGFBPs is to serve as membrane transporter protein for IGF-1 as almost all IGF-1 bind to at least one of the seven members IGFBP Superfamily (Hwa et al., 1999). IGFBP-3 binds to ~80% of IGF-1 in circulation, which makes it the most common protein (Adachi et al., 2017). In addition, IGFBP was the most common in co-cultures and monocultures compared to the other IGFBPs in the microarray experiment. Studies show that IGFBPs has an impact by increasing the bioavailability of IGFs in circulation (Stewart et al., 1993). The upregulation of IGFBPs and IGF-1 confirms that ESCs and SkMCs in the co-culture system provides a favourable environment for the maturation of MN, differentiation of myofibres, and robust formation of NMJ *in vivo* formation.

The data in figure 7.1D show that there was a significant increase in NT-3 levels in co-culture systems treated with IGF-1/NPs compared to those treated with IGF-1 only. Studies on the effect of post traumatic IGF-1 administration on NT-3 in a focal unilateral penetrating brain injury showed that IGF-1 prevents the injury-induced changes in NT-3 and increases its concentration, which underscores that it can be used in repair and protective processes (Kazanis et al., 2004). The concentration of NT-3 also increased in the co-culture as compared to aneural myotube cultures. NT-3 also modulates synaptic function for the development and maintenance of NMJ presynaptic and postsynaptic apparatus (Belluardo et al., 2001; Gonzalez et al., 1999). Research on the early postnatal NMJ development and MN system deficient in mice models showed reduced somal size but the αMNs number were unaltered (Woolley et al., 1999). Additional research showed that there was less MEPs innervation by MNTs as well as a lower number of SkM fibres in NT-3 deficient mice at birth. The step that follows is a catastrophic postnatal loss of MNTs through postnatal development by the seventh day and full denervation of the muscles of the hindlimb that have no observable NMJ in the entire SkM endplate zones (Woolley et al., 2005). Further, haploinsufficiency-induced reductions in NT-3 in mice is characterised by MNT maturation, lower synaptic vesicle recycling, and reduced fibre diameter of SkM (Sheard et al., 2010). These findings may explain the data observed in the previous chapter which showed enhanced NMJ formation and function in co-culture treated with IGF/NPs compared to other treatments.

7.3 Conclusion

The report is an analysis of 40 human growth factors and neurotrophins concentration *in vitro* NMJ system. The higher concentrations of four factors involved in the development of MN, SkM and NMJ in a co-culture system with slow release IGF-1 were measured and showed that in terms of the higher concentrations of those four factors indicated, the NMJ platform observed *in vitro* behaved physiologically the same as *in vivo* conditions.

Chapter 8: General Discussion & Conclusions

8.0 Discussion

IGF-1 may have some impact on the proliferation, differentiation, and survival of muscle and neurons, which makes it a potential solution to diseases associated with the wasting of muscle conditions (Horst-Sikorska et al., 2013), ageing neuronal death and axonal damage, and MN diseases (Vincent et al., 2004). There have been attempts to apply IGF-1 in treatment of various conditions but only a few have included phase III human trials other than studies involving Amyotrophic Lateral Sclerosis (ALS). Injection of IGF-1 in ALS patients did not have any effects on them (Sorenson et al., 2008). Howe et al (2009) states that the negative impact may be because of low bioavailability of IGF-1 in brain parenchyma. Methods used to deliver IGF-1 have limited success due to the rapid depletion of local concentration, potency, bioavailability, and tissue response. The use of biodegradable polymeric systems leads to a localized and sustained growth factor that could address these challenges. IGF-1 is not enough to reverse muscle atrophy in all motor neuron degenerative diseases.

The main aim of this project was to develop a novel and simplified nerve-muscle co-culture with the addition of slow-release IGF-1 (IGF-1/NPs) system capable of generating functional *in vitro* NMJs, without the use of serum, growth, and/or neurotrophic factors. It provides a defined platform to investigate disease and disorders of the NM system through the examination of NMJ formation and functionality. In this report, a physical human motor unit platform produced by immortalised skeletal myoblasts and NPCs obtained from hESCs is described. Several objectives are behind the establishment of this unique platform. The fulfilment of this aim was first addressed through the optimisation size and shape of NPs. Therefore the first objective was to fabricate and characterise mesoporous nanoparticles (MSNPs). Experiments have also been done to determine the cellular uptake and cytotoxic influence of mesoporous particles on cells. As well as examining if the MSNPs' (MCM-41 and SBA-15) pore size was big enough to permit for loading IGF-1 into the MSNPs. Hence, to facilitate our suggested project, 19 samples of MCM-41 & SBA-15 monodispersed mesoporous silica particles were synthesised and conducted using the normal surfactant templating technique (Kresge et al. 1992). In Table 3.0, the characteristics of the NPs diameter, composition, porosity, and surface charge. Template molecule selection and reaction concentration conditions are the techniques employed in regulating the diameter and porosity. The application of configuration was done as soon as the particles were formed. This happened before acid extraction was used to remove the surfactant molecules, with the results being a well-organised and regular porous arrangement. With regards to cytotoxicity, the nanoparticles shape and size, together with MSNPs concentrations, have a vital role to play. There is confirmation that a decrease in the size of particles

corresponds with an increase in cytotoxic effects (Pasold et al., 2015). The eventual objective behind these efforts is to develop a system for the treatment of skeletal muscle cell using IGF-1. It also aims to increase IGF-1 bioactivity periods through a safe and effective delivery mechanism that uses MSNPs to reduce the wasting of skeletal muscle and other linked conditions. The second objective was to upload the IGF-1 in the mesoporous nanoparticles (MSNPs).Therefore the IGF-1 structure (3D structure) was studied first .The Protein Homology/analogy Recognition Engine V 2.0 was used to determine the 3D dimension and structure of IGF-1.With the aim of making sure that the IGF-1 will be captured inside the pores of NPs, the IGF-1's affinity to MSNPs was evaluated and the MSNP's pore sizes were measured. From the Phyre2 engine analysis, it can be seen that the highest IGF-1 3D dimensions for X, Y, and Z are 3.3nm, 4.0nm, and 3.4nm respectively (From this data and the information mentioned above, the two types of mesoporous silica particles were synthesised and fully characterised (MCM-41 and SBA-15) and then decided to use the SBA-15 stability for this project (which has been confirmed) because they have no cytotoxic effects on the cells and because the pore size of SBA-15 (5-9 nm) is big enough to absorb and fit the IGF-1 easily (3D dimention are: 3.3nm, 4.0nm, 3.4nm). In addition, they also have a big surface area which permits adequate amounts of IGF-1 to be loaded when its compared to MCM-41.

The following objective was to optimise the concentration of IGF-1 to be employed in skeletal muscle cell culture to maintain cell viability and growth while also examining the properties of IGF-1 with MSNPs (SBA-15) on the proliferation of skeletal muscle, its existence, differentiation, and metabolism. For a period of 24 hours, C25 was grown in a plate with six wells at a density of $1.5x10^5$ cell/ml. Differentiation media (DM) was used to treat the cells after 24 hours. A comparison of the IGF-1 concentrations that followed were compared with control DM only: 10 ng, 20 ng, 40 ng, 80 ng and 160 ng. The treatment using DM only was used as a negative control so that the impact of IGF-1 on differentiation and proliferation could be validated. At a period of 96 hours following IGF-1 and DM cell treatment, morphological studies were completed. Using DAPI, Ki67 (proliferation marker), and MHC (differentiation marker), together with immunohistochemistry, differentiation parameters were applied. The aim was to find out if the IGF-1 had an influence on the C25 myoblast differentiation or proliferation. The results confirmed that the optimal IGF-1 concentration for use with MSNPs is 10 ng. It is at this level that differentiation is boosted and proliferation reduced. When IGF-1/SBA-15 was introduced, differentiation was noted at 10 ng, 20 ng, and 40 ng. On the other hand, it has been noted from the study that high IGF-1 concentrations result in reduced differentiation as proliferation escalates. In high concentrations, Ki67 markers (red dots refer to the figure 4.1) were observed. This implies that Ki67 plays the role of a proliferation marker. For a drug delivery system that is efficient, it is a requirement that the MSNPs are biocompatible, possess skeletal muscle tissue specificity, and the release of the drug molecules are released in a controlled fashion. This will ensure

a concentration for IGF-1 (12.5µg/ml) and NPs (0.75mg) is effective. The next objective was to investigate the IGF-1 release from MSNPs (drug release study). The experiment was conducted three times and the concentration of IGF-1 used in these experiments was (12.5µg/ml) and the SBA-15 was (0.75 mg). The results of the experiments showed that around 85 percent of the IGF-1 concentration was uploaded inside the NPs after four hours. A 100 hour period is used to determine the time course of the IGF-1 discharge. At intervals of 2hrs, 4hrs, 8hrs, 25hrs, 50hrs and 75hrs and 100hrs, the sample was centrifuged. This was followed by measuring the supernatant's fluorescence so that the IGF-1 discharge from the MSNPs could be estimated. The result showed that from zero to eight hours, the discharge of the IGF-1 loaded to the nanoparticles was at a rate of 10-15 ng/ml. From 25 hours and above, an increase in the discharge to 48 ng/ml was noted. A further increase was recorded in 100 hours: 60 ng/ml. This outcome will establish and confirm the optimal concentration of IGF-1 is (12.5µg/ml) and SBA-15 is (0.75 mg), this refers to the drug release figure (3.14). As well as confirming that MSNPs can be used to boost IGF-1 bioactivity it can also be inferred that the SBA-15 mesoporous silica nanoparticles can be employed for purposes of controlling the discharge of IGF-1 in new systems of delivery. Moreover to be used in the treatment of muscle cells in relation to injury, wasting, ageing and other wasting disorders associated with diseases like diabetes and cancer which is vital because they can function as a way of delivering drugs that is safe. We recently established an *in vitro* human co-culture (nerve-muscle) model in a *serum-free/neural growth factor-free defined medium* (Abd Al Samid et al., 2018). The model develops functional NMJs rapidly to elicit muscle contraction. Neural progenitor cells (NPCs) from hESC differentiate into motor neuron in the co-culture myoblasts and are also named NPC passage 1(P1) that can be stored in liquid nitrogen to allow future studies. The objective was to conduct the generation and characterisation of the system with the aim of verifying the incidence of physiological NMJ formation. Before performing the co-culture characterisation, there were experiments done with the aim of determining the best time point, which would indicate that NMJ formation has reached maturity (Figure 5.5). For purposes of determining the mature formation of NMJ, peak contraction frequency was employed. The peak was observed to be seven days following the co-culture. Using antibodies for ChAT, the characterisation and identification, in the system, of Cholinergic MNs was done, revealing the interface between the systems myotubes and MNs. Such a significant finding is a reflection of NMJ noted *in vivo* ChAT are needed for the correct development and function of MN (Brandon et al., 2003; Misgeld et al., 2002). The assessment of motor neuron formation was done on the seventh day using the βIII-tubulin motor neuron differentiation marker. Mature motor neurones have axons terminating on myotubes as shown in Figure 5.5. The formation of cholinergic motor neurons was confirmed using acetyltransferase antibodies (ChAT, a key enzyme for acetylcholine biosynthesis), which is shown in green in Figure 5.6 (Young et al., 2003). NMJs usually have acetylcholine receptor (AChR)

clusters along myotubes that were assessed using alpha-bungarotoxin (α-BTX) staining and can be identified as the red clusters. Motor neuron axons serve the myotubes with nerves that lead to the formation of NMJ as marked with α-BTX (red) (Young et al., 2003). The skeletal muscle and neuron co-cultures were able to mature with no serum or neural growth factors cocktails being added. Within a period as short as six to seven days, the formation of myotube started being apparent, and the spontaneous myotube contractions were documented (Figure 5.4). When compared to previous studies where the myotube contractions and NMJ formation took 14 days (Vilmont et al., 2016), and sometimes as long as 20 to 25 days (Das et al., 2010) this can be considered quick. Studying operational motor units is important in understanding the pathophysiological characteristics of NMJ disorders common in major neurological diseases and older age.

Human cultures can be used to increase the chances of success in clinical practice. Most of the past cell culture models used cross-species cell types (Arnold et al., 2012; Guo et al., 2010) and had to be done with some growth factors (Demestre et al., 2015; Guo et al., 2011; Das et al., 2010; Guo et al., 2010). The present model deviated from these conventional methods and no adverse effects were observed. Therefore, all the necessary factors that promote nerve axonal spouting and NMJ formation in myotubes were availed to muscles and nerve cells. The interpretation of toxicity and pharmacological studies can be enhanced by the elimination of serum, the anonymous factor that may impact reproducibility (Rumsey et al., 2009). To confirm the physiological behaviour of NMJ and the spontaneous contractile activity of the myotubes by MN signalling through NMJ the NMJ assessment was completed by analysing the myotube CF modulation while using agonist and antagonist pharmacological interventions that act on presynaptic MNs (L-Glut) or postsynaptically (α-BTX) on AChRs at the NMJ. The results show that there is a successful enhancement of myotube contractions in the co-cultures with the introduction of L-Glut, which is possibly achieved because of the increased Ach release from the MN cultured into the synaptic NMJs cleft. In summary, entirely human NMJ was replicated in which myoblasts differentiated into myotubes while NPCs differentiated into MN sprouted axons and branched to form multiple NMJ innervation sites on the myotubes. It was also determined that spontaneous myotube contractions in the co-cultures were indeed driven by MN signalling through NMJs which was verified by responding physiologically in an appropriate manner to the drugs used in this study.

Consequently, the objective that followed was investigating the effects of IGF-1/NPs on NMJ model formation and function. In other studies it has been found that some neurological disorders such as stroke may arise due to impaired IGF-1 signalling pathway (Lewis et al, 1993). To ensure optimal innervation of co-cultured myotubes, the efficiency of NPCs to induce contractions in the co-culture system with DM only (Figure 6.0) approved and used as a control. Therefore, the experiments were

performed to confirm the effects of slow release IGF-1 on NMJ function (myotube contractions) for 7 days in co-culture media with adding NPs only (Figure 6.1), IGF-1 only (Figure 6.2), and slow release of IGF-1(IGF1/ NPs) (Figure 6.3). After the initiation of myogenic differentiation, functional motor units started to develop, including axonal sprouting from the NPCs formed along myotubes on NMJ and myotube formation. Myotubes were characterised by spontaneous muscle contractions without any exogenous chemical and electrical stimuli starting the seventh day. As well as the optimal innervation of myotubes was quantified by analysing Contraction Frequency (CF) every 24 hours post co-culture for 7 days, using live phase contrast microscopy to assess 20 random fields. The results revealed on day 7 that the contractions were slightly higher in each condition, however the contractions were witnessed and increased CF further in slow release IGF-1 co-culture, which was significant ($P < 0.0001$) (Figure 6.4). The findings confirmed co-cultured IGF-1/NPs are more efficient than the IGF-1 only and other conditions. A number of studies have showed that during development, motor neurons respond to IGF-1 with increased neurite outgrowth *in vitro* and *in vivo* models (Kissileff, and Van Itallie, 1982; Mulholland, 1992; Kimpinski, and Mearow, 2001). In addition the axonal length of differentiated motor neurons *in vitro* was measured at each treatment over the 7 days of co-culture. The result showed that the axonal length was increasing over the 7 day co- culture period with the greatest significant difference in DM adding IGF-1/NPs compared to other treatments. The mean for IGF-1/NPs was (228.6μM ± 61.53) compared to IGF-1 only, where the mean was (158.8μM ±41.59). The IGF-1/NPs presented significant difference <0.0001 (Figure 6.13), which underscores co-cultured IGF-1/NPs are more effectual than the IGF-1 only and other treatments. The potent effect of the slow release of IGF-1 on the proliferation, differentiation, and survival of neurons make it good for studying treatment strategies for studies on axonal damage, demyelination, and neuronal death (Lewis et al, 1993).

The process is further enhanced by neural growth factors such as neurotrophic factors obtained from the brain and discharged by the muscle to ensure the formation, growth, and maturation of NMJ (Henderson et al., 1993; Funakoshi et al., 1995). Therefore the last objective was to study the NMJ interact with complex cytokines arrays and growth factors secreted by muscle and motor neurons to promote differentiation and the formation of NMJ and dictate their functions. This co-culture model is probably the first that involves the neural growth factors. Hence, all the factors required for NMJ formation and maturation, myoblast and motor neurons differentiation were endogenously secreted. Considering IGF-1 signalling pathways are important in neurogenesis and myogenesis regulation, the aim was to evaluate the way in which slow release of IGF-1 affect the bi-directional communication that occurs between the muscle and the motor neuron as well as the co-culture microenvironment (endogenously secretion of neurotrophic factors such as BDNF, GDNF, NT-3 and IGF-1) in the

process of NMJ formation. The ELISA-based microarray analysis of the growth/neurotrophic factor concentration followed by one way ANOVA statistical test was performed to determine whether the slow release of IGF-1 impacts the secretion of growth/neurotrophic factors in co-cultured conditions (co-culture only, co-culture with IGF-1, co- culture with NPs, and co- culture with IGF-1/NPs). Table 7.0 shows the quantified concentration of 40 growth/neurotrophic factors on the seventh day. The results indicate that four factors were significantly different ($P<0.05$) in varying co-culture conditions. BDNF, GDNF, IGF-1, and NT-3 (Figure 7.1) concentrations were very high in co-cultures that had been treated with IGF-1/NPs compared to those that had been treated with IGF-1 only. The data from the ELISA-based microarray indicated that BDNF levels increase significantly with IGF-1/NPs when compared to IGF-1 only (Figure 7.1A). IGF-1 that is involved in the expression of BDNF (McCusker et al., 2006) also enhances the regulation of BDNF-related neurogenesis (Pareja-Galeano et al., 2013).The regulation of BDNF concentration endogenously in the presence of slow release IGF-1 co-culture system is instrumental in the formation and development of NMJs *in vivo* (Pareja-Galeano et al., 2013). IGF-1 slow release increases GDNF levels unlike the cases in which a co-culture model is treated with IGF-1 only (Figure 7.1B). GDNF possibly provides postnatal motor neurons with neurotrophic or survival factors. The results show that there is a possibility that IGF-1 interact with GDNF to prevent chronic glutamate-mediated toxicity of the rat motor neurons while increasing their ChAT activity. These findings suggest that IGF-1 and GDNF interact and increase the chances of survival for the motor neuron. The data in this study shows that IGF-1 levels increased significantly in models in which the slow release of exogenous IGF-1 had been treated with IGF-1/NPs but such levels were not attained in cases in which treatment was completed with IGF-1 only (Figure 7.1C). These findings suggest that IGF-1 and GDNF interact and increase the chances of survival for the motor neuron. Muscle specific IGF-1 expression stabilises NMJs and enhances the survival of motor neurons (Dobrowolny et al., 2005). The injection of IGF-1 into SkM leads to the degeneration of MNs and NMJs that subsequently prevents age-related decline in mice (Payne et al., 2006). The upregulation of IGFBPs and IGF-1 confirms that SCEs and SkMCs in the co-culture system provides a favourable environment for the maturation of MN, differentiation of myofibres, and robust formation of NMJ *in vivo* formation. The data in (Figure 7.1D) show that there was a significant increase in NT-3 levels in co-culture systems treated with IGF-1/NPs compared to those treated with IGF-1 only. Studies on the effect of post traumatic IGF-1 administration on NT-3 in a focal unilateral penetrating brain injury showed that IGF-1 prevents the injury-induced changes in NT-3 and increases its concentration, which underscores that it can be used in repair and protective processes (Kazanis et al., 2004).

Limitations & Future Directions: Despite the findings from this project, many concepts of nanotechnology in SkMCs treatments are still not completely understood and need further research. For an efficient drug delivery system, the MSNPs need to be biocompatible, have skeletal muscle tissue specificity and controlled release of the drug molecules to achieve an effective local concentration. After this, further research into the effects of MSNPs on human immortalised skeletal myoblasts (C25) proliferation and differentiation is necessary to further advance nanotechnology research towards a clinical stage for the development of a new drug delivery system for the treatment of skeletal muscle wasting. Future work could include studying the different cell treatments over a longer period of time as the experiment applied in this study was over 96 hours in monoculture and over 7 days in co-cultures. Other suggestions could be further examination of gene expression analysis in 3D constructs culture with and without motor neurons. This could be assisting in the development of 3D culture platforms for the study of diseases such as amyotrophic lateral sclerosis (ALS) (Richard and Maragakis, 2015). More research is still needed to elucidate SkMCs treatment with IGF-1 and nanoparticles in co-culture of human skeletal myoblasts and NPCs proliferation and differentiation, for better understanding of these drug delivery nanotechnology helps in cell treatment development and improvement of nanotechnology which can be translated into the clinical field. The additional tests that can be done in regard to this include immunohistochemical markers such as reverse transcriptase polymerase chain reaction (PCR), to identify motor-neuron specific markers (homebox) after RNA isolation and also for further studies to determine how motor neurons can be used to identify NMJs (Alves et al., 2015; Yi et al., 2018) and a triple co-culture method could be used to investigate the effect of these different cells on myoblast proliferation and differentiation. Results from this project fit with data from previous studies and confirm that the impact of results from this study can help in the future nanomedicine field. As the possibility of nanotechnology applications in medicine develops, it is significant to instantaneously distinguish and advance contributions useful to public health. A widespread range of modernisations in nanomedicine stand to influence nearly every medical specialty and expose novel ways to advance the quality and extend the duration of life. These improvements can be measured at both individual and population levels. Investigations determined by reformers through regulations such as engineering, biology, medicine, and public health should collaborate to accomplish greatest possible impression in health for individuals and populations. In addition, lack of knowledge concerning the potential health and safety associations of exposure to engineered nanomaterials must be continuously addressed and aggressively researched. Active and communally dependable research will drive nanomedicine as it plays a progressively fundamental and transformative role in medicine and public health in the 21st century.

8.1 Conclusion

In this project, 19 samples of MSNPs were completely synthesised and characterised with both techniques, the SBA-15 and MCM-41 to confirm the biodegradability, cytotoxicity and the correct NPs size to be employed for the uploading and release study. From the results presented in this study, a decision was made to use SBA-15 mesoporous silica nanoparticles for my project because they have a big pore size and surface area which permits adequate amounts of IGF-1 easily. It can be employed for purposes of controlling the discharge of IGF-1 in new systems of delivery, which is used to boost IGF-1 bioactivity. With the development of nanotechnology applications in the medical field, it is vital to directly separate and advance contributions useful to public health. As well as the results presented in this study, it also suggests that the best concentration of IGF-1 to be used with MSNPs is 10 ng, whereby differentiation is enhanced and proliferation is reduced. Differentiation was observed at 10 ng, 20 ng and 40 ng when SBA-15 was added. On the other hand, the study showed that a high concentration of IGF-1 reduces differentiation as proliferation is increased. Ki67 markers (red dots) were demonstrated clearly at high concentrations, thus Ki67 works as a proliferation marker. In addition, this project detailed the human immortalised myoblasts that were co-cultured with human embryonic stem cells (hESCs)-derived neural progenitor cells (NPCs). It was done in seven days in DM only as a control and by adding treatments such as NPs, IGF-1 and slow release of IGF-1 (IGF-1/NPs). The co-culture system does not have serum, growth, and neurotrophic factors yet they generate contractile myotubes, which is an indication that they have advanced differentiation that leads to the formation of NMJs that are functional and appropriate as is the case with *in vivo* conditions. Moreover the slow release of IGF-1 enhanced the bi-directional communications between motor neurons and muscle cells through the elevation of endogenously secreted essential neural growth factors providing a regenerative role for NMJ formation and function. The *in vitro* co-culture system can provide a platform for advanced research on the physiology of the skeletal muscle system and the formation and development of NMJ. The outcome of this project may provide a breakthrough approach to enable research in designing new therapeutic treatments using IGF-1 for muscle wasting and NMJ deterioration linked with ageing and diseases.

Chapter 9: References

9.0 References

Acernese, F., Agathos, M., Aiello, L., Allocca, A., Amato, A., Ansoldi, S., Antier, S., Arène, M., Arnaud, N., Ascenzi, S. and Astone, P., 2019. Increasing the astrophysical reach of the advanced virgo detector via the application of squeezed vacuum states of light. Physical Review Letters, 123(23), p.231108.

Adachi, Y., Nojima, M., Mori, M., Yamashita, K., Yamano, H.-O., Nakase, H., Endo, T., Wakai, K., Sakata, K. and Tamakoshi, A., 2017. 'Insulin-like growth factor-1, IGF binding protein-3, and the risk of esophageal cancer in a nested case-control study.' World journal of gastroenterology, 23(19) pp. 3488-3495.

Aging Cell. 2003 Feb; 2(1):21-9

Al-Shanti, N. and Aldahoodi, Z., 2006. Inhibition of alpha nascent polypeptide associated complex protein may induce proliferation, differentiation and enhance the cytotoxic activity of human CD8+ T cells. Journal of clinical immunology, 26(5), pp.457-464.

Anastácio, J.B.R., Pereira, C.L., Mestriner, R.G., de Souza Pagnussat, A., Netto, C.A. and Donadio, M.V.F. 2006. Análise morfométrica do corno anterior da medula espinal de ratos submetidos à isquemia focal e ao treinamento de habilidade do alcance. Revista da Graduação, 2(1).

Anuj, S.A., Gajera, H.P., Hirpara, D.G. and Golakiya, B.A., 2019. Bacterial membrane destabilization with cationic particles of nano-silver to combat efflux-mediated antibiotic resistance in Gram-negative bacteria. *Life sciences*, *230*, pp.178-187.

Aoyagi, T., Terracina, K.P., Raza, A., Matsubara, H. and Takabe, K., 2015. Cancer cachexia, mechanism and treatment. World journal of gastrointestinal oncology, 7(4), pp.17-29.

Argast, A. and Tennis III, C.F., 2004. A web resource for the study of alkali feldspars and perthitic textures using light microscopy, scanning electron microscopy and energy dispersive X-ray spectroscopy. Journal of geoscience education, 52(3), pp.213-217.

Argiles JM, Moore-Carrasco R, Fuster G, Busquets S, Lopez-Soriano FJ., 2003. Cancer cachexia: the molecular mechanisms. Int J Biochem Cell Biol. 35, pp.405-409.

Armakolas, N., Armakolas, A., Antonopoulos, A., Dimakakos, A., Stathaki, M. and Koutsilieris, M., 2016. The role of the IGF-1 Ec in myoskeletal system and osteosarcoma pathophysiology. Critical Reviews in Oncology/Hematology, 108, pp.137-145.

Arnold, A.-S., Christe, M. and Handschin, C., 2012. 'A Functional Motor Unit in the Culture Dish: Co-culture of Spinal Cord Explants and Muscle Cells.' Journal of Visualized Experiments: JoVE, (62), 04/12, p. 3616.

Armakolas, N., Dimakakos, A., Armakolas, A., Antonopoulos, A. and Koutsilieris, M., 2016. Possible role of the Ec peptide of IGF-1Ec in cartilage repair. Molecular medicine reports, 14(4), pp.3066-3072.

Ashby, P. R., Wilson, S. J. and Harris, A. J., 1993. 'Formation of primary and secondary myotubes in aneural muscles in the mouse mutant peroneal muscular atrophy.' Dev Biol, 156(2), Apr, pp. 519-528.

Bajekal, M., Osborne, V., Yar, M. and Meltzer, H., 2006. *Focus on health*. HMSO.

Barton-Davis, E.R., Shoturma, D.I., Musaro, A., Rosenthal, N. and Sweeney, H.L., 1998. Viral mediated expression of insulin-like growth factor I blocks the aging-related loss of skeletal muscle function. Proceedings of the national academy of sciences, 95(26), pp.15603-15607.

Baumgartner, R.N., Waters, D.L., Gallagher, D., Morley, J.E. and Garry, P.J., 1999. Predictors of skeletal muscle mass in elderly men and women. *Mechanisms of ageing and development*, *107*(2), pp.123-136.

Basso, J.C. and Suzuki, W.A., 2017. The effects of acute exercise on mood, cognition, neurophysiology, and neurochemical pathways: a review. *Brain Plasticity*, *2*(2), pp.127-152.

Basyuni, M., Wati, R., Sulistiyono, N., Hayati, R., Oku, H., Baba, S. and Sagami, H., 2018. Protein modelling of triterpene synthase genes from mangrove plants using Phyre2 and Swiss-model.

Bedlack, R. and Hardiman, O., 2009. ALSUntangled (ALSU): A scientific approach to off-label treatment options for people with ALS using tweets and twitters. Amyotroph Lateral Scler. 10(2): 63–73.

Belluardo, N., Westerblad, H., Mudo, G., Casabona, A., Bruton, J., Caniglia, G., Pastoris, O., Grassi, F. and Ibanez, C. F., 2001. 'Neuromuscular junction disassembly and muscle fatigue in mice lacking neurotrophin-4.' Mol Cell Neurosci, 18(1), Jul, pp. 56-67.

Bentov, I and Werner, H., 2013. 'Chapter 222 Insulin-like Growth Factor-1' Handbook of Biologically Active Peptides, *Elsevier*, pp. 1627-1632.

Bentzinger, C.F., Wang, Y.X. and Rudnicki, M.A., 2012. Building muscle: molecular regulation of myogenesis. *Cold Spring Harbor perspectives in biology*, *4*(2), p.a008342.

Berthomieu, C. and Hienerwadel, R., 2009. Fourier transform infrared (FTIR) spectroscopy. Photosynthesis research, 101(2), pp.157-170.

Berry, B.J., et al., 2015. Morphological and functional characterization of human induced pluripotent stem cell-derived neurons (iCell Neurons) in defined culture systems. Biotechnol Prog, 31(6), pp. 1613-22.

Bharti, C., Nagaich, U., Pal, A.K. and Gulati, N., 2015. Mesoporous silica nanoparticles in target drug delivery system: A review. International journal of pharmaceutical investigation, 5(3), p.124.

Biswal, B., Zerrin Yetkin, F., Haughton, V.M. and Hyde, J.S., 1995. Functional connectivity in the motor cortex of resting human brain using echo-planar MRI. Magnetic resonance in medicine, 34(4), pp.537-541.

Borasio, G.D., Robberecht, W., Leigh, P.N., Emile, J., Guiloff, R.J., Jerusalem, F., Silani, V., Vos, P.E., Wokke, J.H.J. and Dobbins, T., 1998. A placebo-controlled trial of insulin-like growth factor-I in amyotrophic lateral sclerosis. *Neurology*, *51*(2), pp.583-586.

Boyd, J.G., Gordon, T., 2003. Neurotrophic factors and their receptors in axonal regeneration and functional recovery after peripheral nerve injury. Molecular Neurobiology 27, 277–323.

Brack, A.S., Bildsoe, H. and Hughes, S.M., 2005. Evidence that satellite cell decrement contributes to preferential decline in nuclear number from large fibres during murine age-related muscle atrophy. *Journal of cell science*, *118*(20), pp.4813-4821.

Brack, A.S., Conboy, M.J., Roy, S., Lee, M., Kuo, C.J., Keller, C. and Rando, T.A., 2007. Increased Wnt signaling during aging alters muscle stem cell fate and increases fibrosis. *Science*, *317*(5839), pp.807-810.

Brain. 2007. 130(Pt 5):1289–1305.

Bril, V., 2014. 'Neuromuscular complications of diabetes mellitus.' Continuum (Minneap Minn), 20(3 Neurology of Systemic Disease), Jun, pp. 531-544.

Brunner, L.S., 2010. Brunner & Suddarth's textbook of medical-surgical nursing (Vol. 1). Lippincott Williams & Wilkins.

Buckingham, M., 2006. Myogenic progenitor cells and skeletal myogenesis in vertebrates. Current opinion in genetics & development, 16(5), pp.525-532.

Butler, K.S., Durfee, P.N., Theron, C., Ashley, C.E., Carnes, E.C. and Brinker, C.J., 2016. Protocells: modular mesoporous silica nanoparticle-supported lipid bilayers for drug delivery. *small*, *12*(16), pp.2173-2185.

Capsoni, S. and Cattaneo, A., 2006. On the molecular basis linking nerve growth factor (NGF) to Alzheimer's disease. Cellular and molecular neurobiology, 26(4-6), pp.617-631.

Carro, E., Trejo, J.L., Busiguina, S. and Torres-Aleman, I., 2001. Circulating insulin-like growth factor I mediates the protective effects of physical exercise against brain insults of different etiology and anatomy. Journal of Neuroscience, 21(15), pp.5678-5684.

Carrasco, D.I. and English, A.W., 2003. Neurotrophin 4/5 is required for the normal development of the slow muscle fiber phenotype in the rat soleus. Journal of experimental biology, 206(13), pp.2191-2200.

Caroni, P. and Becker, M., 1992. The downregulation of growth-associated proteins in motoneurons at the onset of synapse elimination is controlled by muscle activity and IGF1. Journal of Neuroscience, 12(10), pp.3849-3861.

Carosio, S., Berardinelli, M.G., Aucello, M. and Musaro, A., 2011. Impact of ageing on muscle cell regeneration. *Ageing research reviews*, *10*(1), pp.35-42.

Cha, D.M., Woo, S.J., Kim, H.J., Lee, C. and Park, K.H., 2013. Comparative analysis of aqueous humor cytokine levels between patients with exudative age-related macular degeneration and normal controls. *Investigative ophthalmology & visual science*, *54*(10), pp.7038-7044.

Cheetham, T.D., Connors, M., Clayton, K., Watts, A. and Dunger, D.B., 1997. The relationship between overnight GH levels and insulin concentrations in adolescents with insulin-dependent diabetes mellitus (IDDM) and the impact of recombinant human insulin-like growth factor I (rhIGF-I). *Clinical endocrinology*, *46*(4), pp.415-424.

Chen, J.C. and Goldhamer, D.J., 2003. Skeletal muscle stem cells. *Reproductive Biology and Endocrinology*, *1*(1), pp.1-7.

Chen, C., Lewis, S.K., Voigt, L., Fitzpatrick, A., Plymate, S.R. and Weiss, N.S., 2005. Prostate carcinoma incidence in relation to prediagnostic circulating levels of insulin-like growth factor I, insulin-like growth factor binding protein 3, and insulin. Cancer, 103(1), pp.76-84.

Chernausek, S.D., Backeljauw, P.F., Frane, J., Kuntze, J., Underwood, L.E. and GH Insensitivity Syndrome Collaborative Group, 2007. Long-term treatment with recombinant insulin-like growth factor (IGF)-I in children with severe IGF-1 deficiency due to growth hormone insensitivity. *The Journal of Clinical Endocrinology & Metabolism*, *92*(3), pp.902-910.

Chen, Y., Chen, H. and Shi, J., 2013. In vivo bio-safety evaluations and diagnostic/therapeutic applications of chemically designed mesoporous silica nanoparticles. Advanced Materials, 25(23), pp.3144-3176.

Chen, S., Chinnathambi, S., Shi, X., Osaka, A., Zhu, Y. and Hanagata, N., 2012. Fabrication of novel collagen-silica hybrid membranes with tailored biodegradation and strong cell contact guidance ability. Journal of Materials Chemistry, 22(41), pp.21885-21892.

Chevrel, G., Hohlfeld, R. and Sendtner, M., 2006. The role of neurotrophins in muscle under physiological and pathological conditions. Muscle & Nerve: Official Journal of the American Association of Electrodiagnostic Medicine, 33(4), pp.462-476.

Chin, M.H., Mason, M.J., Xie, W., Volinia, S., Singer, M., Peterson, C., Ambartsumyan, G., Aimiuwu, O., Richter, L., Zhang, J. and Khvorostov, I., 2009. Induced pluripotent stem cells and embryonic stem cells are distinguished by gene expression signatures. *Cell stem cell*, *5*(1), pp.111-123.

Clemmons, D.R., 2004. Role of insulin-like growth factor iin maintaining normal glucose homeostasis. Hormone research in paediatrics, 62(Suppl. 1), pp.77-82.

Coolican, S.A., Samuel, D.S., Ewton, D.Z., McWade, F.J. and Florini, J.R., 1997. The mitogenic and myogenic actions of insulin-like growth factors utilize distinct signaling pathways. Journal of Biological Chemistry, 272(10), pp.6653-6662. Glass, D.J., 2005.

Cox, E.P., O'Dwyer, N., Cook, R., Vetter, M., Cheng, H.L., Rooney, K. and O'Connor, H., 2016. Relationship between physical activity and cognitive function in apparently healthy young to middle-aged adults: a systematic review. *Journal of Science and Medicine in Sport*, *19*(8), pp.616-628.

Cormie, P., Galvão, D.A., Spry, N., Joseph, D., Chee, R., Taaffe, D.R., Chambers, S.K. and Newton, R.U., 2015. Can supervised exercise prevent treatment toxicity in patients with prostate cancer initiating androgen-deprivation therapy: a randomised controlled trial. *BJU international*, *115*(2), pp.256-266.

Coleman, N.R., O'Sullivan, N., Ryan, K.M., Crowley, T.A., Morris, M.A., Spalding, T.R., Steytler, D.C. and Holmes, J.D., 2001. Synthesis and characterization of dimensionally ordered semiconductor nanowires within mesoporous silica. *Journal of the American Chemical Society*, *123*(29), pp.7010-7016.

Crigler, L., Robey, R.C., Asawachaicharn, A., Gaupp, D. and Phinney, D.G., 2006. Human mesenchymal stem cell subpopulations express a variety of neuro-regulatory molecules and promote neuronal cell survival and neuritogenesis. Experimental neurology, 198(1), pp.54-64.

Cui Q., 2006. Actions of neurotrophic factors and their signaling pathways inneuronal survival and axonal regeneration. *Molecular Neurobiology, 33*, pp.155–179.

Daniels, M. P., Lowe, B. T., Shah, S., Ma, J., Samuelsson, S. J., Lugo, B., Parakh, T. and Uhm, C. S., 2000. 'Rodent nerve-muscle cell culture system for studies of neuromuscular junction development: refinements and applications.' Microsc Res Tech, 49(1), Apr 1, pp. 26-37.

Das M, Rumsey JW, Bhargava N, Stancescu M, Hickman JJ. A defined long-term in vitro tissue engineered model of neuromuscular junctions. Biomaterials. Jun 2010; 31(18):4880-4888.

Demestre, M., Orth, M., Föhr, K.J., Achberger, K., Ludolph, A.C., Liebau, S. and Böckers, T.M., 2015. Skeletal muscle hypertrophy and atrophy signaling pathways. The international journal of biochemistry & cell biology, 37(10), pp.1974-1984.

Demestre, M., Orth, M., Föhr, K. J., Achberger, K., Ludolph, A. C., Liebau, S. and Boeckers, T. M., 2015. 'Formation and characterisation of neuromuscular junctions between hiPSC derived motoneurons and myotubes.' Stem Cell Research, 15(2), pp. 328-336.

De Francesco, L., 2006. Towards the total synthesis of a potential M1 muscarinic agonist and study on regioselective cyclisations for the synthesis of highly substituted piperazinones. Cardiff University (United Kingdom).

Delbono, O., 2003. Neural control of aging skeletal muscle. Aging cell, 2(1), pp.21-29.

Denoth, J., Stüssi, E., Csucs, G. and Danuser, G., 2002. Single muscle fiber contraction is dictated by inter-sarcomere dynamics. *Journal of theoretical biology*, *216*(1), pp.101-122.

Dobrowolny, G., Giacinti, C., Pelosi, L., Nicoletti, C., Winn, N., Barberi, L., Molinaro, M., Rosenthal, N. and Musarò, A., 2005. 'Muscle expression of a local Igf-1 isoform protects motor neurons in an ALS mouse model.' The Journal of cell biology, 168(2) pp. 193-199.

Dodds, R. M., Roberts, H. C., Cooper, C. and Sayer, A. A., 2015. The Epidemiology of Sarcopenia. *Journal of Clin Densitom*, *18*(4), pp. 461-466.

Domet, M. A., Webb, C. E. and Wilson, D. F., 1995. 'Impact of alpha- bungarotoxin on tranmitter release at the neuromuscular-junction of the rat .' Neuroscience Letters, 199(1), Oct, pp. 49-52.

Dugger, S. A., Platt, A. and Goldstein, D. B., 2018. 'Drug development in the era of precision medicine.' Nature reviews. Drug discovery, 17(3) pp. 183-196.

Dumke, B.R. and Lees, S.J., 2011. Age-related impairment of T cell-induced skeletal muscle precursor cell function. *American Journal of Physiology-Cell Physiology*, *300*(6), pp.C1226-C1233.

Dupraz, S., Grassi, D., Karnas, D., Guil, A.F.N., Hicks, D. and Quiroga, S., 2013. The insulin-like growth factor 1 receptor is essential for axonal regeneration in adult central nervous system neurons. *PloS one*, *8*(1), p.e54462.

Dutton, E. K., Uhm, C. S., Samuelsson, S. J., Schaffner, A. E., Fitzgerald, S. C. and Daniels, M. P., 1995. 'Acetylcholine receptor aggregation at nerve-muscle contacts in mammalian cultures: induction by ventral spinal cord neurons is specific to axons.' J Neurosci, 15(11), Nov, pp. 7401-7416.

Erickson, K.I., Hillman, C.H. and Kramer, A.F., 2015. Physical activity, brain, and cognition. Current opinion in behavioral sciences, 4, pp.27-32.

Ernfors, P., Lee, K.F., Kucera, J. and Jaenisch, R., 1994. Lack of neurotrophin-3 leads to deficiencies in the peripheral nervous system and loss of limb proprioceptive afferents. Cell, 77(4), pp.503-512.

Feher, J., 2017. '3.6 - The Neuromuscular Junction and Excitation–Contraction Coupling.' In Quantitative Human Physiology (Second Edition). Boston: Academic Press, pp. 318-333.

Ferris, L.T., Williams, J.S. and Shen, C.L., 2007. The effect of acute exercise on serum brain-derived neurotrophic factor levels and cognitive function. Medicine and science in sports and exercise, 39(4), p.728.

Fernyhough, P., Maeda, K. and Tomlinson, D. R., 1996.'Brain-derived neurotrophic factor mRNA levels are up-regulated in hindlimb skeletal muscle of diabetic rats: effect of denervation.' Exp Neurol, 141(2), Oct, pp. 297-303.

Fernyhough, P., Diemel, L. T. and Tomlinson, D. R., 1998. 'Target tissue production and axonal transport of neurotrophin-3 are reduced in streptozotocin-diabetic rats.' Diabetologia, 41(3), Mar, pp. 300-306.

Fernyhough, P., Diemel, L. T., Brewster, W. J. and Tomlinson, D. R., 1995. 'Altered neurotrophin mRNA levels in peripheral nerve and skeletal muscle of experimentally diabetic rats.' J Neurochem, 64(3), Mar, pp. 1231-1237.

Fernyhough, P., Diemel, L. T., Hardy, J., Brewster, W. J., Mohiuddin, L. and Tomlinson, D. R., 1995. 'Human recombinant nerve growth factor replaces deficient neurotrophic support in the diabetic rat.' Eur J Neurosci, 7(5), May 1, pp. 1107-1110.

Ferruzza, S., Rossi, C., Scarino, M.L. and Sambuy, Y., 2012. A protocol for differentiation of human intestinal Caco-2 cells in asymmetric serum-containing medium. Toxicology in Vitro, 26(8), pp.1252-1255.

Fischer, L. R., Culver, D. G., Tennant, P., Davis, A. A., Wang, M., Castellano-Sanchez, A., Khan, J., Polak, M. A. and Glass, J. D., 2004. 'Amyotrophic lateral sclerosis is a distal axonopathy: evidence in mice and man.' Exp Neurol, 185(2), Feb, pp. 232-240.

Florini, J.R., Magri, K.A., Ewton, D.Z., James, P.L., Grindstaff, K and Rotwein, P.S., 1991. J Biol Chem, 266, pp. 15917-15923.

Frontera, W.R. and Ochala, J., 2015. Skeletal muscle: a brief review of structure and function. Calcified tissue international, 96(3), pp.183-195.

Funakoshi, H., Belluardo, N., Arenas, E., Yamamoto, Y., Casabona, A., Persson, H. and Ibanez, C.F., 1995. Muscle-derived neurotrophin-4 as an activity-dependent trophic signal for adult motor neurons. Science, 268(5216), pp.1495-1499.

Giri, S., Trewyn, B.G. and Lin, V.S., 2007. Mesoporous silica nanomaterial-based biotechnological and biomedical delivery systems.

Giller, E. L., Jr., Schrier, B. K., Shainberg, A., Fisk, H. R. and Nelson, P. G., 1973. 'Choline acetyltransferase activity is increased in combined cultures of spinal cord and muscle cells from mice.' Science, 182(4112), Nov 9, pp. 588-589.

Glia (Jan 2009). 57(1):13-23.

Gold, S.M., Schulz, K.H., Hartmann, S., Mladek, M., Lang, U.E., Hellweg, R., Reer, R., Braumann, K.M. and Heesen, C., 2003. Basal serum levels and reactivity of nerve growth factor and brain-derived neurotrophic factor to standardized acute exercise in multiple sclerosis and controls. Journal of neuroimmunology, 138(1-2), pp.99-105.

Gonzalez-Freire, M., de Cabo, R., Studenski, S.A. and Ferrucci, L., 2014. The neuromuscular junction: aging at the crossroad between nerves and muscle. Frontiers in aging neuroscience, 6, p.208.

Gonzalez-Freire, M., de Cabo, R., Studenski, S.A. and Ferrucci, L., 2014. The neuromuscular junction: aging at the crossroad between nerves and muscle. Frontiers in aging neuroscience, 6, p.208.

Gonzalez, M., Ruggiero, F. P., Chang, Q., Shi, Y. J., Rich, M. M., Kraner, S. and Balice-Gordon, R. J., 1999. 'Disruption of Trkb-mediated signaling induces disassembly of postsynaptic receptor clusters at neuromuscular junctions.' Neuron, 24(3), Nov, pp. 567-583.

Green, B.N., Jones, S.B., Streck, R.D., Wood, T.L., Rotwein, P. and Pintar, J.E., 1994. Distinct expression patterns of insulin-like growth factor binding proteins 2 and 5 during fetal and postnatal development. Endocrinology, 134(2), pp.954-962.

Griesbeck, O., Parsadanian, A. S., Sendtner, M. and Thoenen, H., 1995. 'Expression of neurotrophins in skeletal muscle: quantitative comparison and significance for motoneuron survival and maintenance of function.' J Neurosci Res, 42(1), Sep 1, pp. 21-33.

Gould, T. W., Buss, R. R., Vinsant, S., Prevette, D., Sun, W., Knudson, C. M., Milligan, C. E. and Oppenheim, R. W.,2006. 'Complete dissociation of motor neuron death from motor dysfunction by Bax deletion in a mouse model of ALS.' J Neurosci, 26(34), Aug 23, pp. 8774-8786.

Guo, X., Colon, A., Akanda, N., Spradling, S., Stancescu, M., Martin, C. and Hickman, J.J., 2017. Tissue engineering the mechanosensory circuit of the stretch reflex arc with human stem cells: sensory neuron innervation of intrafusal muscle fibers. Biomaterials, 122, pp.179-187.

Guo, X., Greene, K., Akanda, N., Smith, A.S., Stancescu, M., Lambert, S., Vandenburgh, H. and Hickman, J.J., 2014. In vitro differentiation of functional human skeletal myotubes in a defined system. Biomaterials science, 2(1), pp.131-138.

Guo, X., Gonzalez, M., Stancescu, M., Vandenburgh, H.H. and Hickman, J.J., 2011. Neuromuscular junction formation between human stem cell-derived motoneurons and human skeletal muscle in a defined system. Biomaterials, 32(36), pp.9602-9611.

Guo, X., Das, M., Rumsey, J., Gonzalez, M., Stancescu, M. and Hickman, J., 2010. Neuromuscular junction formation between human stem-cell-derived motoneurons and rat skeletal muscle in a defined system. Tissue Engineering Part C: Methods, 16(6), pp.1347-1355.

Gu, L., Hall, D.J., Qin, Z., Anglin, E., Joo, J., Mooney, D.J., Howell, S.B. and Sailor, M.J., 2013. In vivo time-gated fluorescence imaging with biodegradable luminescent porous silicon nanoparticles. Nature communications, 4(1), pp.1-7.

Gupta, A.K. and Gupta, M., 2005. Cytotoxicity suppression and cellular uptake enhancement of surface modified magnetic nanoparticles. Biomaterials, 26(13), pp.1565-1573.

Guo, X., Greene, K., Akanda, N., Smith, A., Stancescu, M., Lambert, S., Vandenburgh, H. and Hickman, J., 2014. 'In vitro Differentiation of Functional Human Skeletal Myotubes in a Defined System.' Biomater Sci, 2(1), Jan 1, pp. 131-138.

Happe, C.L., Tenerelli, K.P., Gromova, A.K., Kolb, F. and Engler, A.J., 2017. Mechanically Patterned neuromuscular junctions-in-a-dish have improved functional maturation. Molecular biology of the cell, 28(14), pp.1950-1958.

Harel NY, Strittmatter SM., 2006. Can regenerating axons recapitulate developmental guidance during recovery from spinal cord injury? Nat Rev Neuroscience, 7, pp. 603–616.

Hammers, D.W., Sarathy, A., Pham, C.B., Drinnan, C.T., Farrar, R.P. and Suggs, L.J., 2012. Controlled release of IGF-I from a biodegradable matrix improves functional recovery of skeletal muscle from ischemia/reperfusion. Biotechnology and bioengineering, 109(4), pp.1051-1059.

Haase, G., 2006. 'Motor Neuron Diseases: Cellular and Animal Models.' In Reviews in Cell Biology and Molecular Medicine. Wiley-VCH Verlag GmbH & Co. KGaA, Formation and characterisation of neuromuscular junctions between hiPSC derived motoneurons and myotubes. Stem cell research, 15(2), pp.328-336.

Harper, J. M., Krishnan, C., Darman, J. S., Deshpande, D. M., Peck, S., Shats, I., Backovic, S., Rothstein, J. D. and Kerr, D. A., 2004. 'Axonal growth of embryonic stem cell-derived motoneurons in vitro and in motoneuron-injured adult rats.' Proc Natl Acad Sci U S A, 101(18), May 4, pp. 7123-7128.

Hayes, 2020. https://www.investopedia.com/terms/b/bonferroni-test.

Henderson, C.E., Camu, W., Mettling, C., Gouin, A., Poulsen, K., Karihaloo, M., Ruilamas, J., Evans, T., McMahon, S.B., Armanini, M.P. and Berkemeier, L., 1993. Neurotrophins promote motor neuron survival and are present in embryonic limb bud. Nature, 363(6426), pp.266-270.

Hettler, S., Dries, M., Zeelen, J., Oster, M., Schröder, R.R. and Gerthsen, D., 2016. High-resolution transmission electron microscopy with an electrostatic Zach phase plate. *New Journal of Physics*, *18*(5), p.053005.

Horst-Sikorska, W., Dytfeld, J., Wawrzyniak, A., Marcinkowska, M., Michalak, M., Franek, E., Napiórkowska, L., Drwęska, N. and Słomski, R., 2013. Vitamin D receptor gene polymorphisms, bone mineral density and fractures in postmenopausal women with osteoporosis. Molecular biology reports, 40(1), pp.383-390.

Howe, C.L., Bergstrom, R.A. and Horazdovsky, B.F., 2009. Subcutaneous IGF-1 is not beneficial in 2-year ALS trial. Neurology, 73(15), pp.1247-1248.

Huang, X., Teng, X., Chen, D., Tang, F. and He, J., 2010. The effect of the shape of mesoporous silica nanoparticles on cellular uptake and cell function. Biomaterials, 31(3), pp.438-448.

Huang, X., Li, L., Liu, T., Hao, N., Liu, H., Chen, D. and Tang, F., 2011. The shape effect of mesoporous silica nanoparticles on biodistribution, clearance, and biocompatibility in vivo. ACS nano, 5(7), pp.5390-5399.

Hwa, V., Oh, Y. and Rosenfeld, R. G., 1999. 'The insulin-like growth factor-binding protein (IGFBP) superfamily.' Endocr Rev, 20(6), Dec, pp. 761-787.

Ihara, C., Shimatsu, A., Mizuta, H., Murabe, H., Nakamura, Y. and Nakao, K., 1996. 'Decreased neurotrophin-3 expression in skeletal muscles of streptozotocin-induced diabetic rats.' Neuropeptides, 30(4), Aug, pp. 309-312.

Iwasaki, Y. and Ikeda, K., 1999. Prevention by insulin-like growth factor-I and riluzole in motor neuron death after neonatal axotomy. Journal of the neurological sciences, 169(1-2), pp.148-155.

Izquierdo-Barba, I., Sousa, E., Doadrio, J.C., Doadrio, A.L., Pariente, J.P., Martínez, A., Babonneau, F. and Vallet-Regí, M., 2009. Influence of mesoporous structure type on the controlled delivery of drugs: release of ibuprofen from MCM-48, SBA-15 and functionalized SBA-15. Journal of sol-gel science and technology, 50(3), pp.421-429.

Jensen, J., Hyllner, J. and Björquist, P., 2009. Human embryonic stem cell technologies and drug discovery. Journal of cellular physiology, 219(3), pp.513-519.

Jiang, W., Kim, B.Y., Rutka, J.T. and Chan, W.C., 2008. Nanoparticle-mediated cellular response is size-dependent. Nature nanotechnology, 3(3), pp.145-150.

Jing, X., Ye, Y., Bao, Y., Zhang, J., Huang, J., Wang, R., Guo, J. and Guo, F., 2018. Mechano-growth factor protects against mechanical overload induced damage and promotes migration of growth plate chondrocytes through RhoA/YAP pathway. Experimental cell research, 366(2), pp.81-91.

J Neurosci. 1992 Oct; 12(10):3849-61.

Kalantarian, G., Ziamajidi, N., Mahjub, R., Goodarzi, M.T., Saidijam, M., Soleimani Asl, S. and Abbasalipourkabir, R., 2018. Effect of insulin–coated trimethyl chitosan nanoparticles on IGF-1, IGF-2, and apoptosis in the hippocampus of diabetic male rats. Restorative neurology and neuroscience, 36(4), pp.571-581.

Kanning, K.C., Kaplan, A. and Henderson, C.E., 2010. Motor neuron diversity in development and disease. Annual review of neuroscience, 33, pp.409-440.

Kazanis, I., Giannakopoulou, M., Philippidis, H. and Stylianopoulou, F., 2004. Alterations in IGF-1, BDNF and NT-3 levels following experimental brain trauma and the effect of IGF-1 administration. Experimental neurology, 186(2), pp.221-234.

Kempen, P.J., Greasley, S., Parker, K.A., Campbell, J.L., Chang, H.Y., Jones, J.R., Sinclair, R., Gambhir, S.S. and Jokerst, J.V., 2015. Theranostic mesoporous silica nanoparticles biodegrade after pro-survival drug delivery and ultrasound/magnetic resonance imaging of stem cells. Theranostics, 5(6), p.631.

Khan, R., Khan, S.U., Zaheer, R. and Khan, S., 2012, December. Future internet: the internet of things architecture, possible applications and key challenges. In 2012 10th international conference on frontiers of information technology (pp. 257-260).

Kimpinski, K. and Mearow, K., 2001. Neurite growth promotion by nerve growth factor and insulin-like growth factor-1 in cultured adult sensory neurons: role of phosphoinositide 3-kinase and mitogen activated protein kinase. Journal of neuroscience research, 63(6), pp.486-499.

Kim, M.J., Lee, B., Yang, K., Park, J., Jeon, S., Um, S.H., Kim, D.I., Im, S.G. and Cho, S.W., 2013. BMP-2 peptide-functionalized nanopatterned substrates for enhanced osteogenic differentiation of human mesenchymal stem cells. Biomaterials, 34(30), pp.7236-7246.

Kim, J., Cao, L., Shvartsman, D., Silva, E.A. and Mooney, D.J., 2011. Targeted delivery of nanoparticles to ischemic muscle for imaging and therapeutic angiogenesis. Nano letters, 11(2), pp.694-700.

.Kissileff, H.R. and Van Itallie, T.B., 1982. Physiology of the control of food intake. Annual review of nutrition, 2(1), pp.371-418.

Kresge, C.T., Leonowicz, M.E., Roth, W.J., Vartuli, J.C. and Beck, J.S., 1992. Ordered mesoporous molecular sieves synthesized by a liquid-crystal template mechanism. nature, 359(6397), pp.710-712.

Kurakhmaeva, K.B., Djindjikhashvili, I.A., Petrov, V.E., Balabanyan, V.U., Voronina, T.A., Trofimov, S.S., Kreuter, J., Gelperina, S., Begley, D. and Alyautdin, R.N., 2009. Brain targeting of nerve growth factor using poly (butyl cyanoacrylate) nanoparticles. Journal of drug targeting, 17(8), pp.564-574.

Lai, E.C., Felice, K.J., Festoff, B.W., Gawel, M.J., Gelinas, D.F., Kratz, R., Murphy, M.F., Natter, H.M., Norris, F.H. and Rudnicki, S.A., 1997. Effect of recombinant human insulin-like growth factor-I on progression of ALS: a placebo-controlled study. Neurology, 49(6), pp.1621-1630.

Lambooij, A.C., van Wely, K.H., Lindenbergh-Kortleve, D.J., Kuijpers, R.W., Kliffen, M. and Mooy, C.M., 2003. Insulin-like growth factor-I and its receptor in neovascular age-related macular degeneration. Investigative ophthalmology & visual science, 44(5), pp.2192-2198.

Lammers, R., Gray, A., Schlessinger, J. and Ullrich, A., 1989. Differential signalling potential of insulin-and IGF-1-receptor cytoplasmic domains. The EMBO journal, 8(5), pp.1369-1375.

Landmesser, L.T., 2001. The acquisition of motoneuron subtype identity and motor circuit formation. International Journal of Developmental Neuroscience, 19(2), pp.175-182.

Le Grand, F. and Rudnicki, M. A., 2007. Skeletal muscle satellite cells and adult myogenesis. Current opinion in cell biology, 19(6), pp. 628-633.

Leto, D. and Saltiel, A.R., 2012. Regulation of glucose transport by insulin: traffic control of GLUT4. Nature reviews Molecular cell biology, 13(6), pp.383-396.

Lee, S., Yun, H.S. and Kim, S.H., 2011. The comparative effects of mesoporous silica nanoparticles and colloidal silica on inflammation and apoptosis. Biomaterials, 32(35), pp.9434-9443.

LeRoith, D., 2008. Insulin-like growth factors and the brain. Endocrinology, 149(12), pp.5951-5951.

Lewis, M.E., Neff, N.T., Contreras, P.C., Stong, D.B., Oppenheim, R.W., Grebow, P.E. and Vaught, J.L., 1993. Insulin-like growth factor-I: potential for treatment of motor neuronal disorders. Experimental neurology, 124(1), pp.73-88.

Light, N. and Champion, A.E., 1984. Characterization of muscle epimysium, perimysium and endomysium collagens. Biochemical Journal, 219(3), pp.1017-1026.

Li, M., Du, C., Guo, N., Teng, Y., Meng, X., Sun, H., Li, S., Yu, P. and Galons, H., 2019. Composition design and medical application of liposomes. *European journal of medicinal chemistry*, *164*, pp.640-653.

Li, Y., Tan, Y., Ning, Z., Sun, S., Gao, Y. and Wang, P., 2011. Design and fabrication of fluorescein-labeled starch-based nanospheres. Carbohydrate polymers, 86(1), pp.291-295.

Li, L., Zeng, F., Li, W., Wang, Z., Liu, H., Peng, Y., Gu, Y., Song, J. and Liu, W., 2021. Nitrogen absorption behavior and mechanism of TiZrMnFe getter alloy. Vacuum, 183, p.109814.

Li, Z., Barnes, J.C., Bosoy, A., Stoddart, J.F. and Zink, J.I., 2012. Mesoporous silica nanoparticles in biomedical applications. Chemical Society Reviews, 41(7), pp.2590-2605.

Lie, D. C. and Weis, J., 1998. 'GDNF expression is increased in denervated human skeletal muscle.' Neurosci Lett, 250(2), Jul 3, pp. 87-90.

Li, M. X., Jia, M., Jiang, H., Dunlap, V. and Nelson, P. G., 2001. 'Opposing actions of protein kinase A and C mediate Hebbian synaptic plasticity.' Nat Neurosci, 4(9), Sep, pp. 871-872.

Limbach, L.K., Li, Y., Grass, R.N., Brunner, T.J., Hintermann, M.A., Muller, M., Gunther, D. and Stark, W.J., 2005. Oxide nanoparticle uptake in human lung fibroblasts: effects of particle size, agglomeration, and diffusion at low concentrations. Environmental science & technology, 39(23), pp.9370-9376.

Lim, J.S., Lee, K., Choi, J.N., Hwang, Y.K., Yun, M.Y., Kim, H.J., Won, Y.S., Kim, S.J., Kwon, H. and Huh, S., 2012. Intracellular protein delivery by hollow mesoporous silica capsules with a large surface hole. Nanotechnology, 23(8), p.085101.

Lin, Y.S. and Haynes, C.L., 2010. Impacts of mesoporous silica nanoparticle size, pore ordering, and pore integrity on hemolytic activity. Journal of the American Chemical Society, 132(13), pp.4834-4842.

Liu CN, Chambers WW., 1958. Intraspinal sprouting of dorsal root axons; development of new collaterals and preterminals following partial denervation of the spinal cord in the cat; 79 pp: 46–61.

Liu, W. and Chakkalakal, J.V., 2018. The composition, development, and regeneration of neuromuscular junctions. In Current topics in developmental biology (Vol. 126, pp. 99-124). Academic Press.

López, T., Basaldella, E.I., Ojeda, M.L., Manjarrez, J. and Alexander-Katz, R., 2006. Encapsulation of valproic acid and sodic phenytoin in ordered mesoporous SiO2 solids for the treatment of temporal lobe epilepsy. Optical Materials, 29(1), pp.75-81.

Low, S.P., Voelcker, N.H., Canham, L.T. and Williams, K.A., 2009. The biocompatibility of porous silicon in tissues of the eye. Biomaterials, 30(15), pp.2873-2880.

Lu, P., Jones, L.L., Snyder, E.Y. and Tuszynski, M.H., 2003. Neural stem cells constitutively secrete neurotrophic factors and promote extensive host axonal growth after spinal cord injury. Experimental neurology, 181(2), pp.115-129.

Luo X, Heidinger V, Picaud S, Lambrou G, Dreyfus H., 2001. Selective excitotoxic degeneration of adult pig retinal ganglion cells in vitro. Invest Ophthalmology Vis Science, 42, pp.1096–1106.

Lynch GS, Schertzer JD, Ryall JG., 2007. Therapeutic approaches for muscle wasting disorders. Pharmacol Ther. 113, pp.461-487.

Mamaeva, V., Sahlgren, C. and Lindén, M., 2013. Mesoporous silica nanoparticles in medicine—Recent advances. Advanced drug delivery reviews, 65(5), pp.689-702.

Mamchaoui, K., Trollet, C., Bigot, A., Negroni, E., Chaouch, S., Wolff, A., Kandalla, P.K., Marie, S., Di Santo, J., St Guily, J.L. and Muntoni, F., 2011. Immortalized pathological human myoblasts: towards a universal tool for the study of neuromuscular disorders. Skeletal muscle, 1(1), p.34.

Mantilla, C.B., Zhan, W.Z. and Sieck, G.C., 2004. Neurotrophins improve neuromuscular transmission in the adult rat diaphragm. Muscle & nerve, 29(3), pp.381-386.

Manzano, M. and Vallet-Regí, M., 2020. Mesoporous silica nanoparticles for drug delivery. *Advanced Functional Materials*, *30*(2), p.1902634.

Marzetti, E., Privitera, G., Simili, V., Wohlgemuth, S. E., Aulisa, L., Pahor, M. and Leeuwenburgh, C., 2010. Multiple pathways to the same end: mechanisms of myonuclear apoptosis in sarcopenia of aging. The Scientific World Journal, 10 pp. 340-349.

Matthews, E. and Hanna, M.G., 2010. Muscle channelopathies: does the predicted channel gating pore offer new treatment insights for hypokalaemic periodic paralysis?. The Journal of Physiology, 588(11), pp.1879-1886.

M Bilak, Andrea M Corse, Ralph W Kuncl, M., 2001. Additivity and potentiation of IGF-1 and GDNF in the complete rescue of postnatal motor neurons. Amyotrophic Lateral Sclerosis and Other Motor Neuron Disorders, 2(2), pp.83-91.

McComas, A.J., Fawcett, P.R.W., Campbell, M.J. and Sica, R.E.P., 1971. Electrophysiological estimation of the number of motor units within a human muscle. Journal of Neurology, Neurosurgery & Psychiatry, 34(2), pp.121-131.

McCusker, R.H., McCrea, K., Zunich, S., Dantzer, R., Broussard, S.R., Johnson, R.W. and Kelley, K.W., 2006. Insulin-like growth factor-I enhances the biological activity of brain-derived neurotrophic factor on cerebrocortical neurons. Journal of neuroimmunology, 179(1-2), pp.186-190.

McPhee, J.S., Hogrel, J.Y., Maier, A.B., Seppet, E., Seynnes, O.R., Sipilä, S., Bottinelli, R., Barnouin, Y., Bijlsma, A.Y., Gapeyeva, H. and Maden-Wilkinson, T.M., 2013. Physiological and functional evaluation of healthy young and older men and women: design of the European MyoAge study. Biogerontology, 14(3), pp.325-337.

Ming, G.L. and Song, H., 2011. Adult neurogenesis in the mammalian brain: significant answers and significant questions. Neuron, 70(4), pp.687-702.

Messi, M.L. and Delbono, O., 2003. Target-derived trophic effect on skeletal muscle innervation in senescent mice. Journal of Neuroscience, 23(4), pp.1351-1359.

Metzger, F., Sajid, W., Saenger, S., Staudenmaier, C., van der Poel, C., Sobottka, B., Schuler, A., Sawitzky, M., Poirier, R., Tuerck, D. and Schick, E., 2011. Separation of fast from slow anabolism by site-specific PEGylation of insulin-like growth factor I (IGF-1). Journal of Biological Chemistry, 286(22), pp.19501-19510.

Mishra, P., Pandey, C.M., Singh, U., Gupta, A., Sahu, C. and Keshri, A., 2019. Descriptive statistics and normality tests for statistical data. *Annals of cardiac anaesthesia*, *22*(1), p.67.

Mitchell, W.K., Atherton, P.J., Williams, J., Larvin, M., Lund, J.N. and Narici, M., 2012. Sarcopenia, dynapenia, and the impact of advancing age on human skeletal muscle size and strength; a quantitative review. Frontiers in physiology, 3, p.260.

Milner, L.D. and Landmesser, L.T., 1999. Cholinergic and GABAergic inputs drive patterned spontaneous motoneuron activity before target contact. Journal of Neuroscience, 19(8), pp.3007-3022.

Moore, G.E., 1965. Cramming more components onto integrated circuits.

Mouly, V., Aamiri, A., Perie, S., Mamchaoui, K., Barani, A., Bigot, A., Bouazza, B., Francois, V., Furling, D., Jacquemin, V. and Negroni, E., 2005. Myoblast transfer therapy: is there any light at the end of the tunnel?. Acta Myologica, 24(2), p.128.

Musarò, A., McCullagh, K., Paul, A., Houghton, L., Dobrowolny, G., Molinaro, M., Barton, E.R., Sweeney, H.L. and Rosenthal, N., 2001. Localized Igf-1 transgene expression sustains hypertrophy and regeneration in senescent skeletal muscle. Nature genetics, 27(2), pp.195-200.

Murray, L. M., Comley, L. H., Thomson, D., Parkinson, N., Talbot, K. and Gillingwater, T. H., 2008. 'Selective vulnerability of motor neurons and dissociation of pre- and post-synaptic pathology at the neuromuscular junction in mouse models of spinal muscular atrophy.' Hum Mol Genet, 17(7), Apr 1, pp. 949-962.

Mulholland, M.W., Romanchuk, G., Simeone, D.M. and Flowe, K., 1992. Stimulation of myenteric plexus neurite outgrowth by insulin and insulin-like growth factors I and II. Life sciences, 51(23), pp.1789-1796.

Neff, N.T., Prevette, D., Houenou, L.J., Lewis, M.E., Glicksman, M.A., Yin, Q.W. and Oppenheim, R.W., 1993. Insulin-like growth factors: Putative muscle-derived trophic agents that promote motoneuron survival. Journal of neurobiology, 24(12), pp.1578-1588.

Nelson, P. G., Fields, R. D., Yu, C. and Liu, Y., 1993. 'Synapse elimination from the mouse neuromuscular junction in vitro: a non-Hebbian activity-dependent process.' J Neurobiol, 24(11), Nov, pp. 1517-1530.

Nguyen, Q. T., Parsadanian, A. S., Snider, W. D. and Lichtman, J. W., 1998. 'Hyperinnervation of neuromuscular junctions caused by GDNF overexpression in muscle.' Science, 279(5357), Mar 13, pp. 1725-1729.

Norhasyimi Rahmat, A.Z.A. and Abdul Rahman, M., 2010. A review: Mesoporous Santa Barbara Amorphous-15, Ty pes, Synthesis and its applications towards biorefinery production American. J Appl Sci, 12, pp.1579-1586.

Office of Fair Trading, 2005.

Olawale A.R.Sulaiman, Catherine A.Munro, RajivMidha, Takeshi Matsuyama, Tessa Gordon, Abdulhakeem Al-Majed., 2002. Chronic Schwann cell denervation and the presence of a sensory nerve reduce motor axonal regeneration. Experimental Neurology.V176, Issue 2, Pp 342-354.

Oppenheim, R. W., 1991. 'Cell death during development of the nervous system.' Annu Rev Neurosci, 14 pp. 453-501.

Orlando, G., Balducci, S., Bazzucchi, I., Pugliese, G. and Sacchetti, M., 2016. Neuromuscular dysfunction in type 2 diabetes: underlying mechanisms and effect of resistance training. Diabetes/Metabolism Research and Reviews, 32(1), pp.40-50.

Pan, W. and Kastin, A.J., 2000. Interactions of IGF-1 with the blood-brain barrier in vivo and in situ. Neuroendocrinology, 72(3), pp.171-178.

Pang, A.L.Y., Martin, M.M., Martin, A.L. and Chan, W.Y., 2009. Molecular basis of diseases of the endocrine system. In Molecular Pathology (pp. 435-463). Academic Press.

Pang, A.L and Wai-Yee Chan, W.Y., 2010. Molecular Basis of Diseases of the Endocrine System. Essential Concepts in Molecular Pathology, Elsevier, pp. 289-307.

Parker, M. H., Seale, P. and Rudnicki, M. A., 2003. Looking back to the embryo: defining transcriptional networks in adult myogenesis. Nature Reviews Genetics, 4(7) pp. 497-507.

Park, H.J., Lee, P.H., Bang, O.Y., Lee, G. and Ahn, Y.H., 2008. Mesenchymal stem cells therapy exerts neuroprotection in a progressive animal model of Parkinson's disease. Journal of neurochemistry, 107(1), pp.141-151.

Pareja-Galeano, H., Brioche, T., Sanchis-Gomar, F., Montal, A., Jovaní, C., Martínez-Costa, C., Gomez-Cabrera, M.C. and Viña, J., 2013. Impact of exercise training on neuroplasticity-related growth factors in adolescents.

Pardridge, W.M., 2005. The blood-brain barrier: bottleneck in brain drug development. NeuroRx, 2(1), pp.3-14.

Pasold, J., Zander, K., Heskamp, B., Grüttner, C., Lüthen, F., Tischer, T., Jonitz-Heincke, A. and Bader, R., 2015. Positive impact of IGF-1-coupled nanoparticles on the differentiation potential of human chondrocytes cultured on collagen scaffolds. International journal of nanomedicine, 10, p.1131.

Payne, A. M., Zheng, Z., Messi, M. L., Milligan, C. E., Gonzalez, E. and Delbono, O., 2006. 'Motor neurone targeting of IGF-1 prevents specific force decline in ageing mouse muscle.' J Physiol, 570(Pt 2), Jan 15, pp. 283-294.

Pedersen, B.K., 2011. Muscles and their myokines. Journal of Experimental Biology, 214(2), pp.337-346.

Pedersen, B. K. and Toft, A. D., 2000. Effects of exercise on lymphocytes and cytokines. British journal of sports medicine, 34(4), pp. 246-251.

Pedersen, B.K. and Febbraio, M.A., 2008. Muscle as an endocrine organ: focus on muscle-derived interleukin-6. Physiological reviews.

Perkel, D., Naghi, J., Agarwal, M., Morrissey, R.P., Phan, A., Willix Jr, R.D. and Schwarz, E.R., 2012. The potential effects of IGF-1 and GH on patients with chronic heart failure. Journal of cardiovascular pharmacology and therapeutics, 17(1), pp.72-78.

Peruzzi, F., Prisco, M., Dews, M., Salomoni, P., Grassilli, E., Romano, G., Calabretta, B. and Baserga, R., 1999. Multiple signaling pathways of the insulin-like growth factor 1 receptor in protection from apoptosis. Molecular and cellular biology, 19(10), pp.7203-7215.

Petersen, R.C., Lopez, O., Armstrong, M.J., Getchius, T.S., Ganguli, M., Gloss, D., Gronseth, G.S., Marson, D., Pringsheim, T., Day, G.S. and Sager, M., 2018. Practice guideline update summary: Mild cognitive impairment: Report of the Guideline Development, Dissemination, and Implementation Subcommittee of the American Academy of Neurology. Neurology, 90(3), pp.126-135.

Pfrieger, F.W., 2009. Roles of glial cells in synapse development. Cellular and molecular life sciences, 66(13), pp.2037-2047.

Philippou, A., Halapas, A., Maridaki, M. and Koutsilieris, M., 2007. Type I insulin-like growth factor receptor signaling in skeletal muscle regeneration and hypertrophy. J Musculoskelet Neuronal Interact, 7(3), pp.208-218.

Philippou, A., Maridaki, M., Halapas, A. and Koutsilieris, M., 2007. The role of the insulin-like growth factor 1 (IGF-1) in skeletal muscle physiology. In Vivo, 21(1), pp.45-54.

Prather, R. S., Lorson, M., Ross, J. W., Whyte, J. J. and Walters, E., 2013. 'Genetically Engineered Pig Models for Human Diseases.' Annual review of animal biosciences, 1, 01/03, pp. 203-219.

Price, F. D., von Maltzahn, J., Bentzinger, C. F., Dumont, N. A., Yin, H., Chang, N. C., Wilson, D. H., Frenette, J. and Rudnicki, M. A., 2015. Corrigendum: Inhibition of JAK-STAT signaling stimulates adult satellite cell function. Nat Med, 21(4), p. 414.

Public Health England – Culture Collections, 2013.

Puttonen, K. A., Ruponen, M., Naumenko, N., Hovatta, O. H., Tavi, P. and Koistinaho, J., 2015. 'Generation of Functional Neuromuscular Junctions from Human Pluripotent Stem Cell Lines.' Frontiers in cellular neuroscience, 9 pp. 473-473.

Qi, L., Ma, J., Cheng, H. and Zhao, Z., 1998. Micrometer-sized mesoporous silica spheres grown under static conditions. Chemistry of materials, 10(6), pp.1623-1626.

Rabinovsky, E.D., Gelir, E., Gelir, S., Lui, H.U.I., Kattash, M., DeMayo, F.J., Shenaq, S.M. and Schwartz, R.J., 2003. Targeted expression of IGF-1 transgene to skeletal muscle accelerates muscle and motor neuron regeneration. The FASEB Journal, 17(1), pp.53-55.

Ramon y Cajal S., 1928. Degeneration and Regeneration of the Nervous System. London: Oxford University.

Rayment, I., Rypniewski, W.R., Schmidt-Base, K., Smith, R., Tomchick, D.R., Benning, M.M., Winkelmann, D.A., Wesenberg, G. and Holden, H.M., 1993. Three-dimensional structure of myosin subfragment-1: a molecular motor. *Science*, *261*(5117), pp.50-58.

Reilly, B.D. and Franklin, C.E., 2016. Prevention of muscle wasting and osteoporosis: the value of examining novel animal models. Journal of Experimental Biology, 219(17), pp.2582-2595.

Relaix, F. and Zammit, P. S., 2012. Satellite cells are essential for skeletal muscle regeneration: the cell on the edge returns centre stage. *Development*, *139*(16), pp. 2845-2856.

Ren, K., Crouzier, T., Roy, C. and Picart, C., 2008. Polyelectrolyte multilayer films of controlled stiffness modulate myoblast cell differentiation. *Advanced functional materials*, *18*(9), pp.1378-1389.

Reichinger, M., 2007. Poröse silicate mit hierarchischer porenstruktur: synthese von mikro-/mesoporösen MCM-41 und MCM-48 materialien aus zeolithischen baueinheiten des MFI-Gerüststrukturtyps. PhD. diss.

Reid, S.P., Tritsch, S.R., Kota, K., Chiang, C.Y., Dong, L., Kenny, T., Brueggemann, E.E., Ward, M.D., Cazares, L.H. and Bavari, S., 2015. Sphingosine kinase 2 is a chikungunya virus host factor co-localized with the viral replication complex. Emerging microbes & infections, 4(1), pp.1-9.

Reichardt, L. F., 2006. 'Neurotrophin-regulated signalling pathways.' Philosophical transactions of the Royal Society of London. Series B, Biological sciences, 361(1473) pp. 1545-1564.

Ricotti, L., Taccola, S., Bernardeschi, I., Pensabene, V., Dario, P. and Menciassi, A., 2011. Quantification of growth and differentiation of C2C12 skeletal muscle cells on PSS–PAH-based polyelectrolyte layer-by-layer nanofilms. *Biomedical Materials*, *6*(3), p.031001.

Richard, J.P. and Maragakis, N.J., 2015. Induced pluripotent stem cells from ALS patients for disease modeling. *Brain research*, *1607*, pp.15-25.

Riebe, C.J. and Wotjak, C.T., 2011. Endocannabinoids and stress. Stress, 14(4), pp.384-397.

Rodger Laurent., 2010. In the musculoskeletal system.

Rossi, F., Gianola, S. and Corvetti, L., 2007. Regulation of intrinsic neuronal properties for axon growth and regeneration. *Progress in neurobiology*, *81*(1), pp.1-28.

Rumsey JW, Das M, Stancescu M, Bott M, Fernandez-Valle C, Hickman JJ., Jul 2009. Node of Ranvier formation on motoneurons in vitro. Biomaterials. 30 (21):3567-3572.

Saboktakin, M., 2017. The biological and biomedical Nanoparticles applications. *Int J Mol Biol Open Access*, *2*(3), pp.76-87.

Sahoo, S.K. and Labhasetwar, V., 2003. Nanotech approaches to drug delivery and imaging. Drug discovery today, 8(24), pp.1112-1120.

Saini, J**.,** Faroni, A., Abd Al Samid, M., Reid, A. J., Lightfoot, A. P., Mamchaoui, K., Mouly, V., Butler-Browne, G., McPhee, J. S., Degens, H. and Al-Shanti, N. (2019) 'Simplified in vitro engineering of neuromuscular junctions between rat embryonic motoneurons and immortalized human skeletal muscle cells'.

Sanus, G.Z., Tanriverdi, T., Coskun, A., Hanimoglu, H., Is, M. and Uzan, M., 2007. Cerebrospinal fluid and serum levels of insulin-like growth factor-1 and insulin-like growth factor binding protein-3 in patients with severe head injury. ULUSAL TRAVMA VE ACIL CERRAHI DERGISI, 13(4), p.281.

Sanes, J.R. and Lichtman, J.W., 2001. Induction, assembly, maturation and maintenance of a postsynaptic apparatus. Nature Reviews Neuroscience, 2(11), pp.791-805.

Sakowski, S.A. and Feldman, E.L., 2012. Insulin-like growth factors in the peripheral nervous system. *Endocrinology and Metabolism Clinics*, *41*(2), pp.375-393.

Schuch, F.B., Deslandes, A.C., Stubbs, B., Gosmann, N.P., da Silva, C.T.B. and de Almeida Fleck, M.P., 2016. Neurobiological effects of exercise on major depressive disorder: a systematic review. Neuroscience & Biobehavioral Reviews, 61, pp.1-11.

Sheard, P. W., Bewick, G. S., Woolley, A. G., Shaw, J., Fisher, L., Fong, S. W. and Duxson, M. J., 2010. 'Investigation of neuromuscular abnormalities in neurotrophin-3-deficient mice.' European Journal of Neuroscience, 31(1), Jan, pp. 29-41.

Shefer, G., Van de Mark, D. P., Richardson, J. B. and Yablonka-Reuveni, Z., 2006. Satellite-cell pool size does matter: defining the myogenic potency of aging skeletal muscle. Dev Biol, 294(1), pp. 50-66.

Sherrington, C.S., 1925. Remarks on some aspects of reflex inhibition. Proceedings of the Royal Society of London. Series B, Containing Papers of a Biological Character, 97(686), pp. 519-545.

Siegel, A. L., Kuhlmann, P. K. and Cornelison, D. D., 2011. Muscle satellite cell proliferation and association: new insights from myofiber time-lapse imaging. Skelet Muscle, 1(1) p. 7.

Sigma-Aldrich, B. and Region, P.S.A., 2018. SIG MA-ALDRICH. Sigma, 302(H311), p.H331.

Silaghi, M.C., Chizallet, C. and Raybaud, P., 2014. Challenges on molecular aspects of dealumination and desilication of zeolites. Microporous and Mesoporous Materials, 191, pp.82-96.

Simionescu, A. and Pavlath, G. K., 2011. Molecular mechanisms of myoblast fusion across species. Adv Exp Med Biol, 713 pp. 113-135.

Slowing, I.I., Trewyn, B.G. and Lin, V.S.Y., 2007. Mesoporous silica nanoparticles for intracellular delivery of membrane-impermeable proteins. Journal of the American Chemical Society, 129(28), pp.8845-8849.

Slowing, I.I., Vivero-Escoto, J.L., Wu, C.W. and Lin, V.S.Y., 2008. Mesoporous silica nanoparticles as controlled release drug delivery and gene transfection carriers. Advanced drug delivery reviews, 60(11), pp.1278-1288.

Smith, A.S.T., Long, C.J., Pirozzi, K. and Hickman, J.J., 2013. A functional system for high-content screening of neuromuscular junctions in vitro. Technology, 1(01), pp.37-48.

Sjöberg, J. and Kanje, M., 1989. Insulin-like growth factor (IGF-1) as a stimulator of regeneration in the freeze-injured rat sciatic nerve. Brain research, 485(1), pp.102-108.

Song, Y.H., Song, J.L., Delafontaine, P. and Godard, M.P., 2013. The therapeutic potential of IGF-1 in skeletal muscle repair. Trends in Endocrinology & Metabolism, 24(6), pp.310-319.

Sosa, L., Dupraz, S., Laurino, L., Bollati, F., Bisbal, M., Cáceres, A., Pfenninger, K.H. and Quiroga, S., 2006. IGF-1 receptor is essential for the establishment of hippocampal neuronal polarity. Nature neuroscience, 9(8), pp.993-995.

Sorenson, E., Windbank, A.J., Mandrekar, J.N., Bamlet, W.R., Appel, S.H., Armon, C., Barkhaus, P.E., Bosch, P., Boylan, K., David, W.S. and Feldman, E., 2008. Subcutaneous IGF-1 is not beneficial in 2-year ALS trial. Neurology, 71(22), pp.1770-1775.

Song, W. and Jin, X. A., 2015. 'Brain-derived neurotrophic factor inhibits neuromuscular junction maturation in a cAMP-PKA-dependent way.' Neurosci Lett, 591, Mar 30, pp. 8-12.

Sousa-Victor, P., Garcia-Prat, L., Serrano, A. L., Perdiguero, E. and Munoz-Canoves, P., 2015. Muscle stem cell aging: regulation and rejuvenation. Trends Endocrinol Metab, 26(6), pp. 287-296.

Shi SH, Jan LY, Jan Y. N., 2003. Hippocampal neuronal polarity specified by spatially localized mPar3/mPar6 and PI 3-kinase activity. Cell, 112, pp. 63–75.

Stewart, C. E., Bates, P. C., Calder, T. A., Woodall, S. M. and Pell, J. M., 1993. 'Potentiation of insulin-like growth factor-I (IGF-1) activity by an antibody: supportive evidence for enhancement of IGF-1bioavailability in vivo by IGF binding proteins.' Endocrinology, 133(3), Sep, pp. 1462-1465.

Sullivan, K.A., Kim, B. and Feldman, E.L., 2008. Insulin-like growth factors in the peripheral nervous system. Endocrinology, 149(12), pp.5963-5971.

Suuronen, E. J., McLaughlin, C. R., Stys, P. K., Nakamura, M., Munger, R. and Griffith, M., 2004. 'Functional Innervation in Tissue Engineered Models for In Vitro Study and Testing Purposes.' Toxicological Sciences, 82(2) pp. 525-533.

Svanberg, E., Ohlsson, C., Kimball, S.R. and Lundholm, K., 2000. RhIGF-1/IGFBP-3 complex, but not free rhIGF-1, supports muscle protein biosynthesis in rats during semistarvation. European journal of clinical investigation, 30(5), pp.438-446.

Takahashi, T., Ishida, K., Itoh, K., Konishi, Y., Yagyu, K.I., Tominaga, A., Miyazaki, J.I. and Yamamoto, H., 2003. IGF-1 gene transfer by electroporation promotes regeneration in a muscle injury model. Gene therapy, 10(8), pp.612-620.

Tang, Q., Xu, Y., Wu, D. and Sun, Y., 2006. A study of carboxylic-modified mesoporous silica in controlled delivery for drug famotidine. Journal of Solid State Chemistry, 179(5), pp.1513-1520.

Tasciotti, E., Liu, X., Bhavane, R., Plant, K., Leonard, A.D., Price, B.K., Cheng, M.M.C., Decuzzi, P., Tour, J.M., Robertson, F. and Ferrari, M., 2008. Mesoporous silicon particles as a multistage delivery system for imaging and therapeutic applications. Nature nanotechnology, 3(3), pp.151-157.

Thomson, S.R., Wishart, T.M., Patani, R., Chandran, S. and Gillingwater, T.H., 2012. Using induced pluripotent stem cells (iPSC) to model human neuromuscular connectivity: promise or reality?. Journal of anatomy, 220(2), pp.122-130.

Tidball, J. G., 2005. Inflammatory processes in muscle injury and repair. Am J Physiol Regul Integr Comp Physiol, 288(2), pp.345-353.

Tong, S.Y., Davis, J.S., Eichenberger, E., Holland, T.L. and Fowler, V.G., 2015. Staphylococcus aureus infections: epidemiology, pathophysiology, clinical manifestations, and management. Clinical microbiology reviews, 28(3), pp.603-661.

Trewyn, B.G., Slowing, I.I., Giri, S., Chen, H.T. and Lin, V.S.Y., 2007. Synthesis and functionalization of a mesoporous silica nanoparticle based on the sol–gel process and applications in controlled release. Accounts of chemical research, 40(9), pp.846-853.

Tsukahara, T. and Haniu, H., 2011. Nanoparticle-mediated intracellular lipid accumulation during C2C12 cell differentiation. Biochemical and biophysical research communications, 406(4), pp.558-563.

Turner, N. J. and Badylak, S. F., 2012. Regeneration of skeletal muscle. Cell Tissue Res, 347(3) pp.759-774.

Ukmar, T., Maver, U., Planinšek, O., Kaučič, V., Gaberšček, M. and Godec, A., 2011. Understanding controlled drug release from mesoporous silicates: theory and experiment. Journal of Controlled Release, 155(3), pp.409-417.

Ulfhake, B., Bergman, E., Edstrom, E., Fundin, B. T., Johnson, H., Kullberg, S. and Ming, Y., 2000. 'Regulation of neurotrophin signaling in aging sensory and motoneurons: dissipation of target support?' Mol Neurobiol, 21(3), Jun, pp. 109-135.

Umbach, J. A., Adams, K. L., Gundersen, C. B. and Novitch, B. G., 2012. 'Functional Neuromuscular Junctions Formed by Embryonic Stem Cell-Derived Motor Neurons.' PLoS ONE, 7(5), p. e36049.

Ursø, B., Cope, D.L., Kalloo-Hosein, H.E., Hayward, A.C., Whitehead, J.P., O'Rahilly, S. and Siddle, K., 1999. Differences in signaling properties of the cytoplasmic domains of the insulin receptor and insulin-like growth factor receptor in 3T3-L1 adipocytes. *Journal of Biological Chemistry*, *274*(43), pp.30864-30873.

Urazaev, A. K., Magsumov, S. T., Poletayev, G. I., Nikolsky, E. E. and Vyskocil, F., 1995. 'Muscle NMDA receptors regulate the resting membrane potential through NO-synthase.' Physiol Res, 44(3) pp. 205-208.

Vallet-Regi, M., Izquierdo-Barba, I. and Colilla, M., 2012. Structure and functionalization of mesoporous bioceramics for bone tissue regeneration and local drug delivery. *Philosophical Transactions of the Royal Society A: Mathematical, Physical and Engineering Sciences*, *370*(1963), pp.1400-1421.

Vallet-Regı, M., Doadrio, J.C., Doadrio, A.L., Izquierdo-Barba, I. and Pérez-Pariente, J., 2004. Hexagonal ordered mesoporous material as a matrix for the controlled release of amoxicillin. Solid State Ionics, 172(1-4), pp.435-439.

Vallet-Regi, M., Ramila, A., Del Real, R.P. and Pérez-Pariente, J., 2001. A new property of MCM-41: drug delivery system. Chemistry of Materials, 13(2), pp.308-311.

Vallet-Regí, M., Balas, F. and Arcos, D., 2007. Mesoporous materials for drug delivery. Angewandte Chemie International Edition, 46(40), pp.7548-7558.

Van der Worp, H.B., Howells, D.W., Sena, E.S., Porritt, M.J., Rewell, S., O'Collins, V. and Macleod, M.R., 2010. Can animal models of disease reliably inform human studies?. PLoS med, 7(3), p.e1000245.

Vavsari, V.F., Ziarani, G.M. and Badiei, A., 2015. The role of SBA-15 in drug delivery. RSC advances, 5(111), pp.91686-91707.

van der Worp, H. B., Howells, D. W., Sena, E. S., Porritt, M. J., Rewell, S., O'Collins, V. and Macleod, M. R., 2010. 'Can animal models of disease reliably inform human studies?' PLoS Med, 7(3), Mar 30, p. e1000245.

Vega, S.R., Strüder, H.K., Wahrmann, B.V., Schmidt, A., Bloch, W. and Hollmann, W., 2006. Acute BDNF and cortisol response to low intensity exercise and following ramp incremental exercise to exhaustion in humans. Brain research, 1121(1), pp.59-65.

Velloso, C. P., 2008. 'Regulation of muscle mass by growth hormone and IGF-1.' British journal of pharmacology, 154(3) pp. 557-568.

Vergani, L., Di Giulio, A.M., Losa, M., Rossoni, G., Muller, E.E. and Gorio, A., 1998. Systemic administration of insulin-like growth factor decreases motor neuron cell death and promotes muscle reinnervation. Journal of neuroscience research, 54(6), pp.840-847.

Villegas, M.R., Baeza, A., Noureddine, A., Durfee, P.N., Butler, K.S., Agola, J.O., Brinker, C.J. and Vallet-Regí, M., 2018. Multifunctional protocells for enhanced penetration in 3D extracellular tumoral matrices. *Chemistry of Materials*, *30*(1), pp.112-120.

Vilmont, V., Cadot, B., Ouanounou, G. and Gomes, E.R., 2016. A system for studying mechanisms of neuromuscular junction development and maintenance. Development, 143(13), pp.2464-2477.

Vincent, A.M., Mobley, B.C., Hiller, A. and Feldman, E.L., 2004. IGF-1 prevents glutamate-induced motor neuron programmed cell death. Neurobiology of disease, 16(2), pp.407-416.

Wang, Y., Zhao, Q., Han, N., Bai, L., Li, J., Liu, J., Che, E., Hu, L., Zhang, Q., Jiang, T. and Wang, S., 2015. Mesoporous silica nanoparticles in drug delivery and biomedical applications. Nanomedicine: Nanotechnology, Biology and Medicine, 11(2), pp.313-327.

Webster, C. and Blau, H.M., 1990. Accelerated age-related decline in replicative life-span of Duchenne muscular dystrophy myoblasts: implications for cell and gene therapy. Somatic cell and molecular genetics, 16(6), pp.557-565.

Wellisz, T., Armstrong, J.K., Cambridge, J., An, Y.H., Wen, X., Hill, C.M. and Fisher, T.C., 2008. The effects of a soluble polymer and bone wax on sternal healing in an animal model. *The Annals of thoracic surgery*, *85*(5), pp.1776-1780.

Wilson, S. J. and Harris, A. J., 1993. 'Formation of myotubes in aneural rat muscles.' Dev Biol, 156(2), Apr, pp. 509-518.

Woolley, A., Sheard, P., Dodds, K. and Duxson, M., 1999. 'Alpha motoneurons are present in normal numbers but with reduced soma size in neurotrophin-3 knockout mice.' Neurosci Lett, 272(2), Sep 10, pp. 107-110.

Wu, H., Xiong, W.C. and Mei, L., 2010. To build a synapse: signalling pathways in neuromuscular junction assembly. Development, 137(7), pp.1017-1033.

Xia, T., Kovochich, M., Liong, M., Meng, H., Kabehie, S., George, S., Zink, J.I. and Nel, A.E., 2009. Polyethyleneimine coating enhances the cellular uptake of mesoporous silica nanoparticles and allows safe delivery of siRNA and DNA constructs. ACS nano, 3(10), pp.3273-3286.

Xu, L., Yan, J., Chen, D., Welsh, A.M., Hazel, T., Johe, K., Hatfield, G. and Koliatsos, V.E., 2006. Human neural stem cell grafts ameliorate motor neuron disease in SOD-1 transgenic rats. Transplantation, 82(7), pp.865-875.

Yakar, S., Rosen, C.J., Beamer, W.G., Ackert-Bicknell, C.L., Wu, Y., Liu, J.L., Ooi, G.T., Setser, J., Frystyk, J., Boisclair, Y.R. and LeRoith, D., 2002. Circulating levels of IGF-1 directly regulate bone growth and density. The Journal of clinical investigation, 110(6), pp.771-781.

Yamane, A., Ohnuki, Y. and Saeki, Y., 2000. Delayed embryonic development of mouse masseter muscle correlates with delayed MyoD family expression. Journal of dental research, 79(12), pp.1933-1936.

Yan, J., Welsh, A.M., Bora, S.H., Snyder, E.Y. and Koliatsos, V.E., 2004. Differentiation and tropic/trophic effects of exogenous neural precursors in the adult spinal cord. Journal of Comparative Neurology, 480(1), pp.101-114.

Yang, P., Gai, S. and Lin, J., 2012. Functionalized mesoporous silica materials for controlled drug delivery. Chemical Society Reviews, 41(9), pp.3679-3698.

Yin, D., Sleight, B., Alvey, C., Hansson, A.G. and Bello, A., 2013. Pharmacokinetics and Pharmacodynamics of Figitumumab, a Monoclonal Antibody Targeting the Insulin-Like Growth Factor 1 Receptor, in Healthy Participants. The Journal of Clinical Pharmacology, 53(1), pp.21-28.

Yin, H., Price, F. and Rudnicki, M. A., 2013. Satellite cells and the muscle stem cell niche. Physiol Rev, 93(1), pp.23-67.

Young, H. S., Herbette, L. G. and Skita, V., 2003. 'Alpha-bungarotoxin binding to acetylcholine receptor membranes studied by low angle X-ray diffraction.' Biophys J, 85(2), Aug, pp. 943-953.

Zahavi, E.E., Ionescu, A., Gluska, S., Gradus, T., Ben-Yaakov, K. and Perlson, E., 2015. A compartmentalized microfluidic neuromuscular co-culture system reveals spatial aspects of GDNF functions. Journal of cell science, 128(6), pp.1241-1252.

Zanou, N. and Gailly, P., 2013. Skeletal muscle hypertrophy and regeneration: interplay between the myogenic regulatory factors (MRFs) and insulin-like growth factors (IGFs) pathways. *Cellular and Molecular Life Sciences*, *70*(21), pp.4117-4130.

Zhang, L., Gu, F.X., Chan, J.M., Wang, A.Z., Langer, R.S. and Farokhzad, O.C., 2008. Nanoparticles in medicine: therapeutic applications and developments. Clinical pharmacology & therapeutics, 83(5), pp.761-769.

Zheng, H., Huang, Z. and Che, S., 2012. Mesostructured chitosan–silica hybrid as a biodegradable carrier for a pH-responsive drug delivery system. Dalton Transactions, 41(16), pp.5038-5044.

Zhou, C., Wu, L., Ni, F., Ji, W., Wu, J. and Zhang, H., 2014. Critical illness polyneuropathy and myopathy: a systematic review. Neural regeneration research, 9(1), p.101.
Zhu, Y., Fang, Y., Borchardt, L. and Kaskel, S., 2011. PEGylated hollow mesoporous silica nanoparticles as potential drug delivery vehicles. Microporous and Mesoporous Materials, 141(1-3), pp.199-206.